25
21/7/89 JS (2)

DN: 660-

DE89 1 / 32043 - - T26 - Vol. 1

DOCUMENT NO. 87SDS4213
MAY 1988

GE Astro Space

FINAL SAFETY ANALYSIS REPORT FOR THE GALILEO MISSION

VOLUME I
REFERENCE DESIGN DOCUMENT

GENERAL PURPOSE HEAT SOURCE
RADIOISOTOPE THERMOELECTRIC GENERATOR
PROGRAM
CONTRACT DE-AC01-79ET32043

PREPARED FOR
U.S. DEPARTMENT OF ENERGY

DISCLAIMER

LEGIBILITY NOTICE

A major purpose of the Technical Information Center is to provide the broadest possible dissemination of information contained in DOE's Research and Development Reports to business, industry, the academic community, and federal, state, and local governments. Non-DOE originated information is also disseminated by the Technical Information Center to support ongoing DOE programs.

Although large portions of this report are not reproducible, it is being made available only in paper copy form to facilitate the availability of those parts of the document which are legible. Copies may be obtained from the National Technical Information Service. Authorized recipients may obtain a copy directly from the Department of Energy's Technical Information Center.

DOE/ET/32043--T26-Vol.1

DE89 007268

DOCUMENT NO. 87SDS4213
MAY 1988

FINAL SAFETY ANALYSIS REPORT FOR THE GALILEO MISSION

VOLUME I
REFERENCE DESIGN DOCUMENT

GENERAL PURPOSE HEAT SOURCE
RADIOISOTOPE THERMOELECTRIC GENERATOR
PROGRAM
CONTRACT DE-AC01-79ET32043

PREPARED FOR
U.S. DEPARTMENT OF ENERGY

ASTRO-SPACE DIVISION
SPACECRAFT OPERATIONS
Valley Forge Space Center
P.O. Box 8555 Philadelphia, PA 19101

This Final Safety Analysis Report was prepared by the General Electric Company under Contract De-AC01-79ET-32043 with the U.S. Department of Energy.

INTRODUCTION

The Final Safety Analysis Report (FSAR) consists of three volumes which are related to the safety analysis of the Galileo mission:

Volume I	Reference Design Document
Volume II	Accident Model Document
Volume III	Nuclear Risk Analysis Document

An Executive Summary pertaining to Volumes I and II is also provided.

The Galileo mission uses nuclear power sources called Radioisotope Thermoelectric Generators (RTGs) to provide the spacecraft's primary electrical power. Because these generators contain nuclear material, a Safety Analysis Report (SAR) is required. A preliminary SAR and an updated SAR were previously issued that provided an evolving status report on the safety analysis. Prior to the Space Shuttle Challenger accident in January, 1986, a Final Safety Analysis Report (FSAR) was issued to provide the results of the latest analyses and safety tests on the General Purpose Heat Source (GPHS) RTG available at that time. That FSAR thus presented the final safety evaluation which was to initiate the concluding activities in the process to obtain flight approval for the Galileo and Ulysses missions, the launch of Galileo being anticipated in May, 1987. As a result of the Challenger accident, the launch dates for both missions were later rescheduled for November 1989 and October 1990, respectively. The Challenger accident and the shortly following Titan 34D-9 accident (although unrelated missions) prompted an intensive effort by NASA to reevaluate the vehicle failure modes and associated accident environments that they had previously provided for use in the GPHS-RTG safety evaluation for Galileo and Ulysses. The decision was made by agreement between the DOE and the NASA to have a revised safety evaluation and report (FSAR) prepared on the basis of these revised vehicle accidents and environments. The results of this latest revised safety evaluation are presented in this document (Galileo FSAR).

Volume I, this document, provides the background design information required to understand the analyses presented in Volumes II and III. It contains descriptions of the RTGs, the Galileo spacecraft, the Space Shuttle, the Inertial Upper Stage (IUS), the trajectory and flight characteristics including flight contingency modes, and the launch site. There are two appendices in Volume I which provide detailed material properties for the RTG.

Volume II describes the effect of the postulated launch vehicle accidents on the nuclear heat source modules contained in the RTGs. Volume III assesses the risks (if any) associated with these postulated accidents.

TABLE OF CONTENTS

TABLE OF CONTENTS (Cont'd)

LIST OF ILLUSTRATIONS

LIST OF ILLUSTRATIONS (Cont'd)

LIST OF ILLUSTRATIONS (Cont'd)

LIST OF ILLUSTRATIONS (Cont'd)

LIST OF TABLES

BLANK

ACRONYMS

ACS	Attitude Control System
AFSCF	Air Force Satellite Control Facility
AFWL	Air Force Weapons Laboratory
AKA	Active Keel Actuator
AMD	Accident Model Document
AOA	Abort-Once-Around
AOCS	Attitude and Orbit Control System
APL/JHU	Applied Physics Laboratory/Johns Hopkins University
APU	Auxiliary Power Unit
ASE	Airborne Support Equipment
ATO	Abort-To-Orbit
$BKNO_3$	Boron Potassium Nitrate
BOL	Beginning-of-Life
BOM	Beginning-of-Mission
CBCF	Carbon Bonded Carbon Fiber
CBGS	Confinement-by-the-Ground-Surface
CBM	Confinement-by-the-Missile
CCAFS	Cape Canaveral Air Force Station
CCU	Central Control Unit
CCVAPS	Computer Controlled Vent and Pressurization System
CD	Command Destruct
CDC	Confined Detonating Cord
CIL	Orbiter Critical Items List
CIU	Communications Interface Unit
COE	Center-of-Explosion
CTU	Central Terminal Unit
CU	Control Unit
CVS	Clad Vent Set
DCU	Digital Computer Unit
DKR	Detra-Kemp-Riddell
DMS	Data Management System
DOE	Department of Energy
DOF	Degrees-of-Freedom

ACRONYMS (Cont'd)

DSN	Deep Space Network
DSU	Data Storage Unit
DUFTAS	Dual Failure Tolerant Arm/Safe Sequencer
DVT	Development Verification Test
ECLSS	Environmental Control and Life Support System
ECT	Early Compatibility Test
EEC	Extendable Exit Cone
EED	Electro Explosive Device
EOD	Earth Orbit Decay
EOM	End-of-Mission
ESS	Equipment Support Section
ET	External Tank
FAST	Failure/Abort Sequence Tree
FC	Fueled Clad
FFC	Flat Faced Cylinder
FSAR	Final Safety Analysis Report
FWD	Forward
FWPF	Fine Weave Pierced Fabric
GIS	Graphite Impact Shell
GM	Galileo Mission
GMV	Gas Management Valve
GPHS	General Purpose Heat Source
HGA	High Gain Antenna
HSA	Heat Source Assembly
HTPB	Hydrogen Terminated Polybutadiene
IIP	Instantaneous Impact Point
IMG	Inertial Measurement Group
INSRP	Interagency Nuclear Safety Review Panel
IRU	Inertial Reference Unit
IUS	Inertial Upper Stage
JPL	Jet Propulsion Laboratory
KSC	Kennedy Space Center
LANL	Los Alamos National Laboratory

ACRONYMS (Cont'd)

LGA	Low Gain Antenna
LH_2	Liquid Hydrogen
Li/SO_2	Lithium/Sulfur Dioxide
LOX	Liquid Oxygen
MECO	Main Engine Cutoff
MES	Main Engine Start
MLI	Multilayer Insulation
MMH	Monomethyl Hydrazine
NASA	National Aeronautics and Space Administration
NIT	Nominal Impact Test
NRAD	Nuclear Risk Analysis Document
N_2H_4	Hydrazine
OMS	Orbital Maneuvering Subsystem
OTA	Ordnance Train Assembly
PCM	Pulse Code Modulation
PCP	Power Control Panel
PCU	Pyro Control Unit
PDU	Power Distribution Unit
PPE	Purge Purification Equipment
PRD	Pressure Relief Device
PTA	Propellant Tank Assembly
RCE	Reaction Control Equipment
RCIU	Remote Control Interface Unit
RCS	Reaction Control System
RDD	Reference Design Document
REM	Rocket Engine Module
RFDU	Radio Frequency Distribution Unit
RIMU	Redundant Inertial Measurement Unit
RM	Redundancy Management
RMU	Remote Multiplex Unit
RPM	Revolutions Per Minute
RTD	Resistance Temperature Detectors
RTG	Radioisotope Thermoelectric Generator

ACRONYMS (Cont'd)

RTLS	Return-To-Launch-Site
RTU	Remote Terminal Unit
S&A	Safe and Arm
SC	Spacecraft
SCU	Sequence Control Unit
SCU	Signal Conditioning Unit
SEU	System Electronic Unit
SGLS	Space Ground Link Subsystem
SiGe	Silicon-Germanium
SiMo	Silicon-Molydenum
SiO_2	Silicon Dioxide
SIU	Servo Inverter Unit
SIU	Signal Interface Unit
S-L	Sibulkin-Lees
SMAB	Solid Motor Assembly Building
SMDC	Shielded Mild Detonating Cord
SO	Superorbital
SPH	Spherical
SR	Structural Release
SRB	Solid Rocket Booster
SSME	Space Shuttle Main Engine
STS	Space Transportation System
SVT	Safety Verification Test
TAA	Trans Atlantic Abort
TCC	Transparent Conductive Coating
TCM	Trajectory Correction Maneuver
TDRSS	Tracking and Data Relay Satellite System
TPS	Thermal Protection System
TVC	Thrust Vector Control
TWTA	Travelling Wave Tube Amplifier
USAR	Updated Safety Analysis Report
VPF	Vertical Processing Facility
W/O	Without
γ_{min}	Minimum-Gamma Reentry Angle

SECTION 1

NUCLEAR POWER SYSTEM

1.1 GENERAL DESCRIPTION

The GPHS-RTG is a radioisotope fueled, thermoelectric generator consisting of two major components - the General Purpose Heat Source (GPHS) and the Converter. A conceptual drawing of the RTG is presented in Figure 1-1, which shows a cutaway portion of the Converter to illustrate its internal construction and the position of the GPHS modules.

The nuclear heat source for the GPHS-RTG is a stacked column of eighteen individual GPHS modules. An expanded view of a portion of this heat source is shown in Figure 1-2. Table 1-1 also lists the salient features of the heat source and its fuel loading. Each module primarily consists of an aeroshell, two Graphite Impact Shells (GIS), and four Fueled Clads (FC). Each FC consists of a fuel pellet of plutonium-238 in the form of the oxide PuO_2 encased in an iridium shell which serves to contain the fuel. Two of these FC's, separated by a graphite floating membrane, are then encased in a GIS which provides the primary resistance to mechanical impact loads. The graphite aeroshell, which serves as the module's primary structural element and ablator, provides protection for two graphite impact shells. Each GIS is separated from the aeroshell by a graphite insulator.

The converter consists of the outer case, which is actively cooled during launch (until the IUS is deployed in orbit) and is the main support structure for the thermoelements as well as the GPHS; the axial and mid-span heat source supports; the thermoelectric elements; multifoil insulation packet and internal frame; and the gas management system. Five hundred seventy-two thermoelectric couples convert decay heat from the fuel directly into electrical energy. These couples are supported in a cantilever fashion from the aluminum outer case; the couples support the insulation packet. The heat source support system provides preload to the GPHS to enable the RTG to withstand the launch and ascent dynamic environment and to prevent separation of the GPHS modules. The gas management system consists of a pressure relief device (PRD) and a gas management valve (GMV) which in conjunction with the pressure tight converter case are used to maintain the desired internal environment of the generator. This system maintains an inert gas environment to allow partial power operation on the launch pad. Full power operation in space is achieved after venting the inert gas through the PRD. The GMV is a manually actuated valve required for pressure maintenance of the generator during ground storage.

1.2 DESIGN REQUIREMENTS

1.2.1 HEAT SOURCE

Major design constraints placed upon the heat source are dictated by safety considerations. The safety philosophy adhered to for the GPHS-RTG design is that immobilization of the plutonium fuel shall be assured to the maximum extent possible during all mission phases including ground handling, transportation, launch, ascent, and temporary orbit and during unplanned

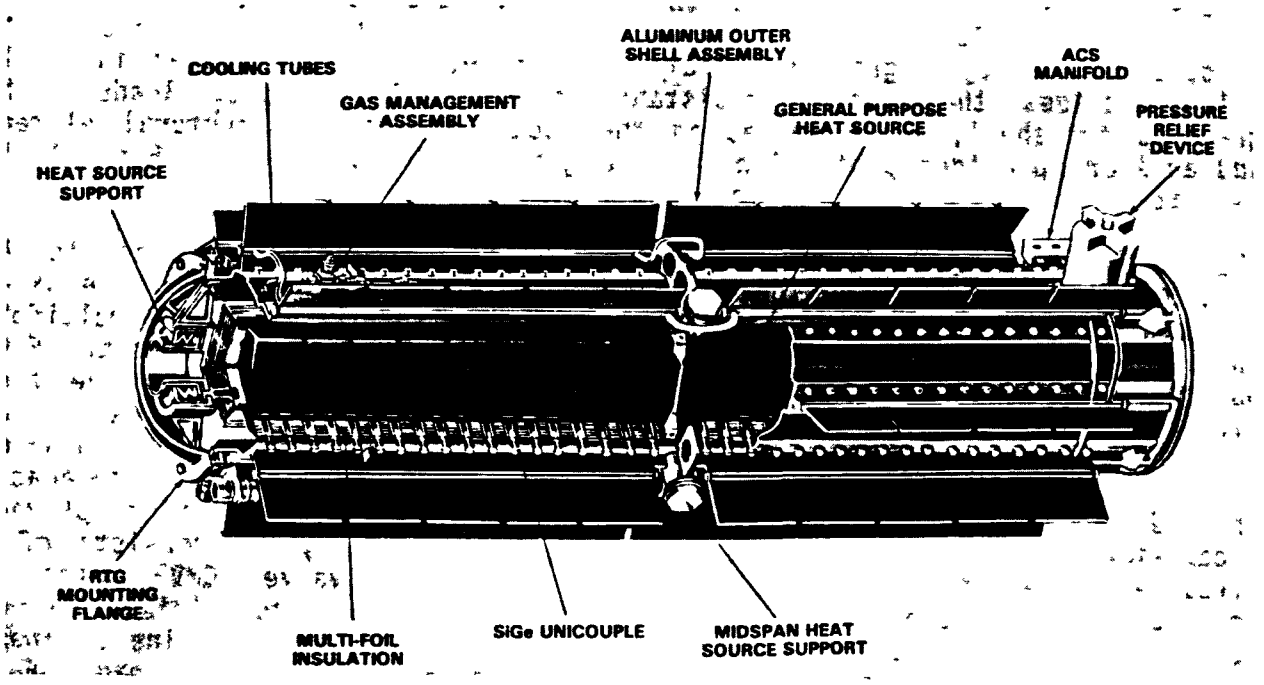

Figure 1-1. GPHS-RTG

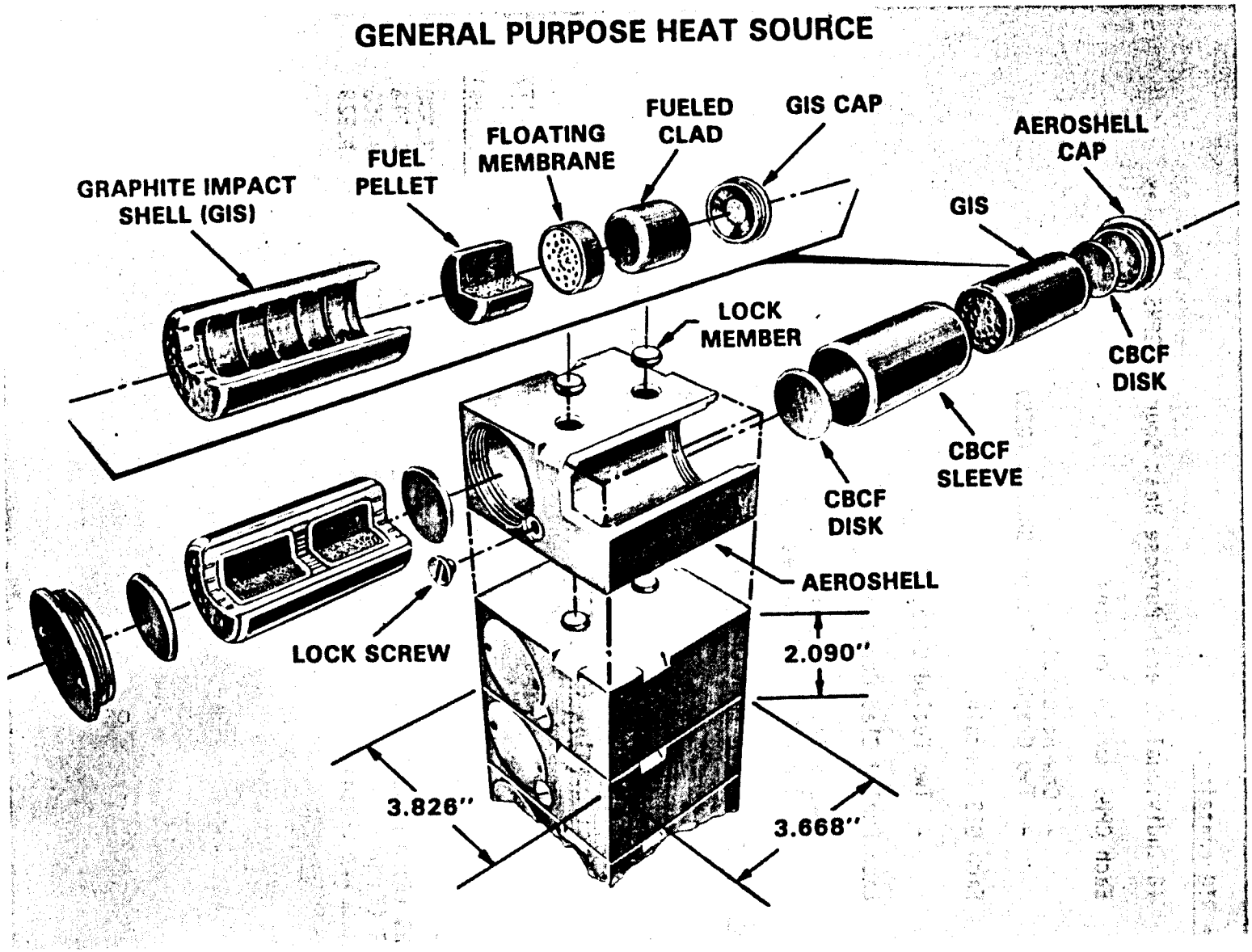

Figure 1-2. General Purpose Heat Source

Table 1-1. RTG Heat Source Components and Fuel Loading

1. One RTG contains:

   - 18 Individual General Purpose Heat Source (GPHS) Modules
   - Each GPHS Module Contains
     - One Aeroshell
     - Two Graphite Impact Shells (GIS)
   - Each GIS Contains
     - Two Fueled Clads
   - Each Fueled Clad Contains
     - One Iridium Shell
     - One PuO_2 Fuel Pellet

2. Total Components Within One RTG

   - GPHS 18
   - GIS 36
   - Fueled Clads 72
   - Fuel Pellets 72

3. RTG BOL Fuel Loading (One RTG)
   (based on Nov 89 launch)

	PUO_2 (Grams)	Thermal Power (Watts)	Activity Level (Curies)
RTG	11,030	4,197	132,200
GPHS (Each Module)	612	233	7,344
GIS (Each)	306	116.6	3,672
Fueled Clads (Each)	153	58.3	1,836

events such as reentry, impact, and post-impact situations. Techniques of physical containment, immobilization mechanisms and inherent fuel form characteristics, including combinations of these, are incorporated into the GPHS design to assure that plutonium immobilization periods will be maximized with respect to the active life of the fuel. A summary of the safety objectives applicable to normal, accident, and post-accident situations is as follows:

1. Preclude the release of fuel and the dissemination thereof, especially in the form of biologically significant, respirable particles.

2. Minimize biospheric contamination, particularly on populated land masses.

3. Maximize long-term immobilization following postulated accidents.

1.2.2 RADIOISOTOPE THERMOELECTRIC GENERATOR

The initial design specifications for the GPHS-RTG were as follows:

• RTG Power Output*	285 watts (BOM) 250 watts (minimum at EOM)
• Operation Life	40,000 hours after launch
• Weight	123.5 pounds
• Output Voltage	28-30 Volts
• Envelope	~18 in. diameter x ~45 in. long
• Hot Junction Temperature	1000°C
• Fuel	PPO ($83.5 \pm 1\%$ $^{238}PuO_2$)
• Thermoelectric Material	SiGe
• Magnetic Field	~30 nano tesla (30×10^{-5} Gauss) at 1 meter
• On Pad	30 day unattended capability
• Storage Life	3 year ground storage
• Auxiliary Cooling	Remove $\geq$ 3500 watts with an average sink temp. of 25°C and an inlet coolant temp. of 30°C.

*The values projected to the November 1989 launch date are:
281 watts (BOM)
238 watts (EOM)

1.3 RADIOISOTOPE FUEL

1.3.1 TYPE OF FUEL

The radioisotope fuel material is an isotopic mixture of plutonium in the form of the dioxide, PuO_2, containing 83.5 ± 1% $^{238}PuO_2$. The physical form of the fuel is in multiple, basically cylindrical shaped, solid ceramics pellets. The pellets have an average diameter of 2.753 ± 0.025 cm (1.084 ± 0.010 inch) and an average length of 2.756 ± 0.038 cm (1.085 ± 0.015 inch). Geometric density of the fuel is 9.60 g-cm^{-3}, and with a specific thermal power of 0.40 W-g^{-1}, the corresponding power density is 3.84 W-cm^{-3}. The half life of the plutonium-238 isotope is 87.8 years.

1.3.2 QUANTITY OF FUEL

Each fuel pellet contains an initial thermal inventory of 62.5 ± 1.5 watts. A total of 72 pellets provides a nominal thermal power of 4410 (+54/-0) watts for the GPHS. This GPHS power requires 11.03 Kg (24.26 pounds) of PuO_2 and, corresponding to this total loading, a quantity of 9.21 Kg (20.26 lb) of $^{238}PuO_2$. The $^{238}PuO_2$ activity is 1.322 x 10^5 curies per heat source based on a November 1989 launch.

The reduction of thermal power is approximately 0.8 percent per year due to alpha decay based on the half life.

1.3.3 PROPERTIES

The physical, thermal, and chemical properties of the radioisotope fuel are summarized in Appendix A.

1.3.4 NUCLEAR CRITICALITY

Table A-1 in Appendix A indicates that the minimum critical mass for $^{238}PuO_2$ (actually an isotopic mixture with approximately 83.5% ^{238}Pu and the balance other plutonium content) is on the order of 23 kg (9 kW thermal) unreflected; the fully reflected minimum critical mass is around 8.6 kg (3.4 kW thermal). The GPHS-RTG contains 11.03 kg (4.4 kW thermal) total PuO_2 (with 9.2 kg of $^{238}PuO_2$ constituting approximately 83.5% of total PuO_2). However, the PuO_2 in the GPHS-RTG could not credibly be formed, in an uncontrolled manner, into the compact spherical mass required to produce the critical configuration. Los Alamos National Laboratory has performed criticality analyses on the normal RTG configuration and on various configurations of the components of the GPHS heat source. The values in Table 1-2 summarize the results of the LANL analyses.

Variations in these configurations were analyzed in which spacing (i.e., rather than close packing) and water with lower density were investigated. In all of these variations, the resulting value of k (multiplication constant) was lower than for the configurations shown in Table 1-2.

Table 1-2. Multiplication Constant, k, for Various Heat Source Combinations

Assembly		Reflection	k
• Stack of 18 GPHS Modules (i.e., 1 RTG)		- None	.252 ± .003
• Stack of 18 GPHS Modules		- Fully dense water	.352 ± .004
• 4 Stacks in square array (closely packed)		- None	.391 ± .002
• 4 Stacks in square array separated by spacing as in shipping containers		- None	.258 ± .002
• 72 GPHS Modules, nearly cubical array		- Fully dense water	.627 ± .004
• GIS Arrays, closely packed		- Fully dense water and interstitial water	
- 4 x 4 x 2 1/2	(80 FCs)		.554 ± .004
- 5 x 4 x 2	(80 FCs)		.560 ± .005
- 6 x 6 x 2 1/2	(180 FCs)		.704 ± .005
- 7 x 7 x 3	(294 FCs)		.789 ± .005
- 9 x 9 x 4	(648 FCs)		.923 ± .005

It is clear from these results that the RTG is well below critical (k=1) both in its normal configuration and for storage and shipping. For mission accident related situations, the hypothetical arrays of modules or GIS's investigated show that k increases but remains subcritical. Even for a closely packed array of 9 x 9 x 4 GIS's (equivalent to 9 GPHS-RTG's) with fully dense water reflection, k is 0.923 which is still subcritical. LANL has not estimated the multiplication constant of bare fueled clads in closely packed arrays. However, the absence of the graphite members of the GPHS even with full water reflection would be expected to result in some decrease in the effective multiplication due to the change that would occur in the neutron energy spectrum and resulting neutron capture for fission. The LANL analysis, in addition, did not include the iridium clads in the analytical model which should be significantly conservative. Iridium is a strong neutron absorber in both the thermal and resonance energy regions.

1.4 HEAT SOURCE

1.4.1 CONFIGURATION

The isotope heat source consists of eighteen independent GPHS modules. A typical module is shown in Figure 1-3. The primary heat source element is the fueled clad (FC) which is a self-contained modular fuel element.

As described previously, four FC's are contained in each GPHS module. The modules are stacked into a single column. The relative motion of the GPHS modules is restricted by the heat source support system which provides axial compression to prevent separation of the modules and by locking members that minimize any relative lateral motion of the individual GPHS modules.

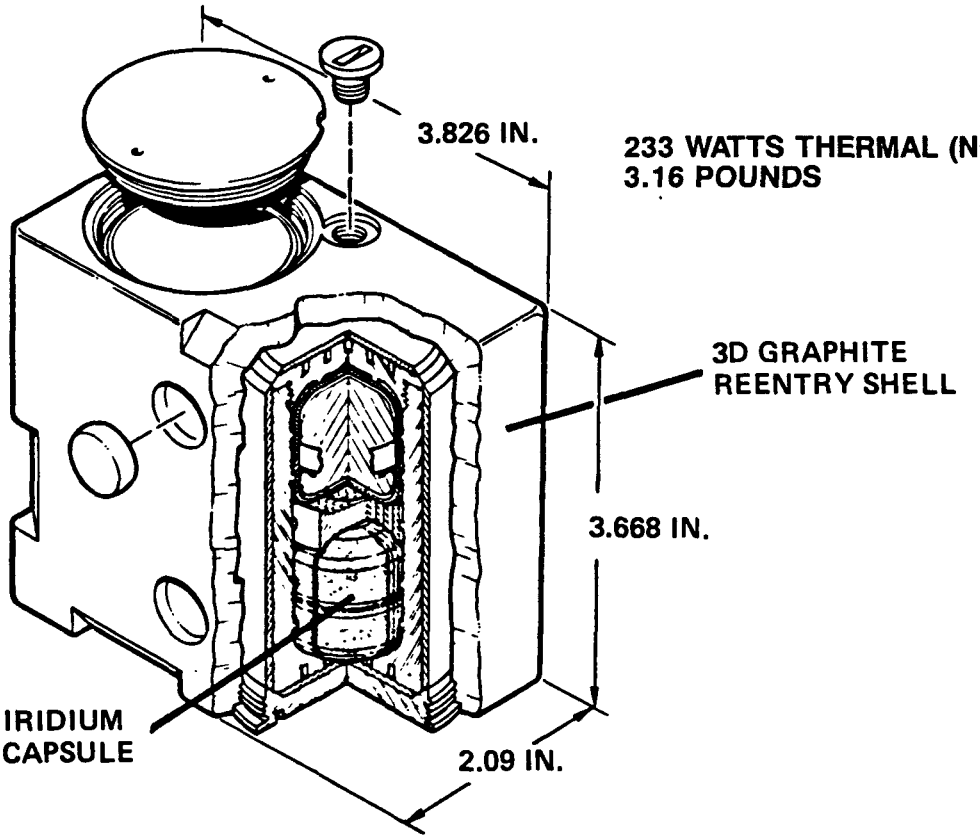

Figure 1-3. GPHS Design Description

1.4.2 MATERIALS AND WEIGHTS

A summary of the typical heat source components, materials, and their associated weights are presented in Table 1-3. Detailed descriptions of each of the GPHS components are given in Paragraph 1.4.3.

1.4.3 COMPONENT DESCRIPTION

1.4.3.1 Fueled Clad (FC)

The Fueled Clad (FC) is the basic GPHS fuel element. The FC is comprised of the PuO_2 fuel pellet and a Clad Vent Set (CVS) which includes the post impact containment shell (PICS), a weld shield, and a filter/vent subassembly. The FC is intended to provide post impact containment of the fuel for one year. The description of the fuel pellet is presented in Section 1.3.

1.4.3.1.1 Clad Vent Set (CVS)

The CVS consists of two welded, cup-like iridium sections which encapsulate the fuel pellet. These iridium cups have a minimum thickness of 0.022 inch. Each CVS is designed with the following: (1) a vent hole (0.0175 inch diameter) and vent hole filter subassembly which permits the helium gas to vent but prevents the release of particles from the interior of the CVS; (2) a decontamination cover which is welded over the vent hole to seal the CVS

Table 1-3. GPHS Components (18 Modules)

Component	Material	No. of Units Per Heat Source	Unit Weight (pounds)	Total Weight (pounds)
Fuel Pellet	PuO_2	72	0.456	32.832
Post Impact Shell	Iridium	72		
Impact Shell	FWPF-3D Graphite	36	0.200	7.200
Floating Member	FWPF-3D Graphite	36	0.015	0.540
Insulator	CBCF Graphite	36	0.0095	0.342
Aeroshell	FWPF-3D Graphite	18	0.887	15.966
Lock Members	FWPF-3D Graphite	32	0.003	0.096
Total GPHS Components				59.976

hermetically, thus permitting decontamination after fuel encapsulation; and (3) a weld shield, mounted on one cup of the set, to provide thermal protection to the fuel during closure welding and to prevent contamination of the weld by the fuel. When assembled, these components (the iridium cups, one with a vent hole, the vent hole filter subassembly, the decontamination cover, and the weld shield) comprise the CVS. All components of the CVS are made of iridium. The configuration of the cups and a sectional view of the assembly is shown in Figures 1-4 through 1-10, (dimensions shown on these figures are in millimeters).

Figure 1-11 shows the arrangement of the vent hole filter subassembly. The filter medium is a frit of iridium powder.

1.4.3.1.2 FC Assembly Procedures

The assembly of the FC entails the welding of the fuel pellet into a Clad Vent Set (with vent hole, vent hole filter assembly, decontamination cover, and weld shields already installed). The FC then undergoes a decontamination cycle to remove surface contamination from the iridium. Depending on the overall heat source assembly cycle, the FC will either be put into storage, or the decontamination cover will be opened and the FC will be installed in a graphite impact shell.

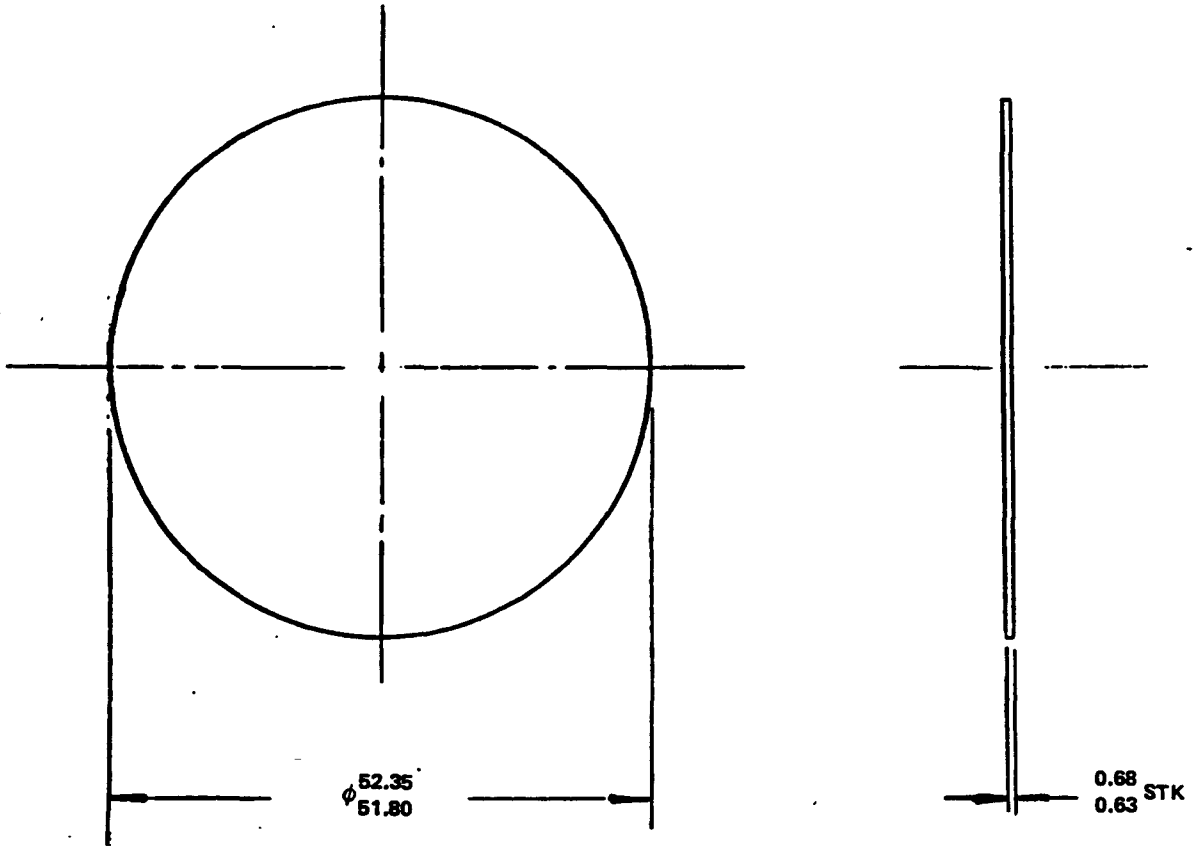

Figure 1-4. Iridium Blank

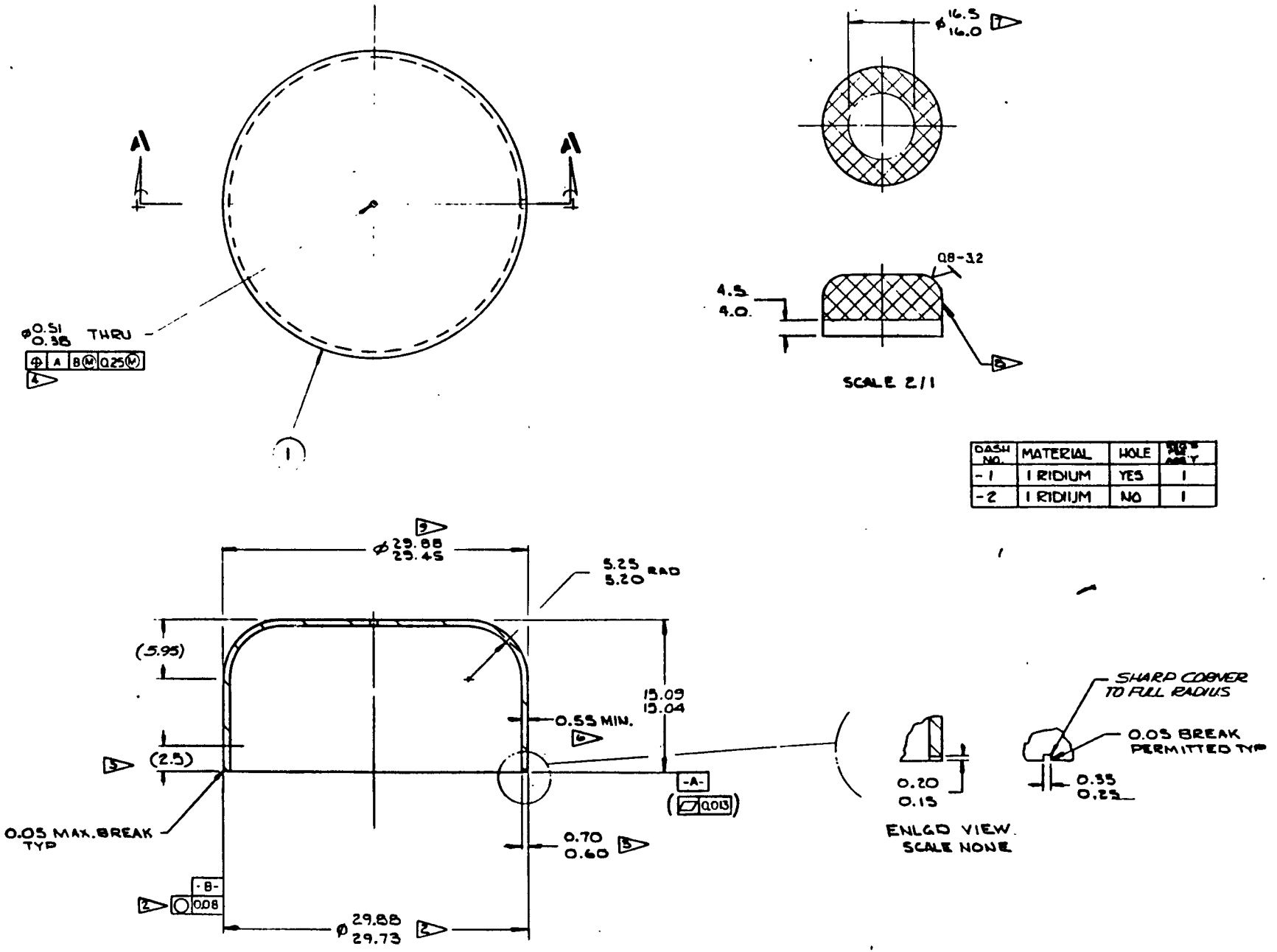

Figure 1-5. Iridium Cup

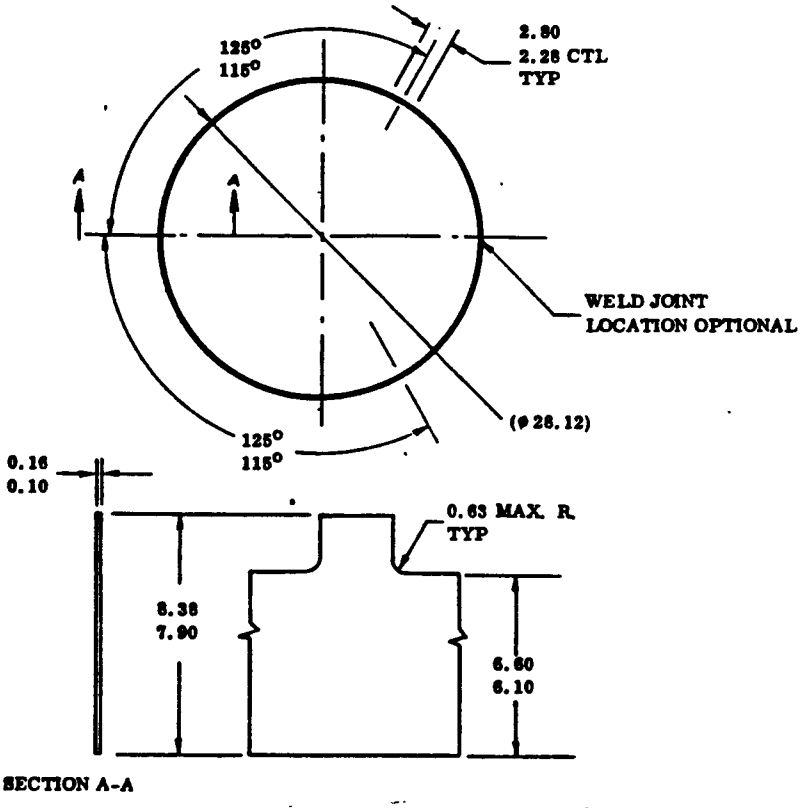

Figure 1-6. Weld Shield

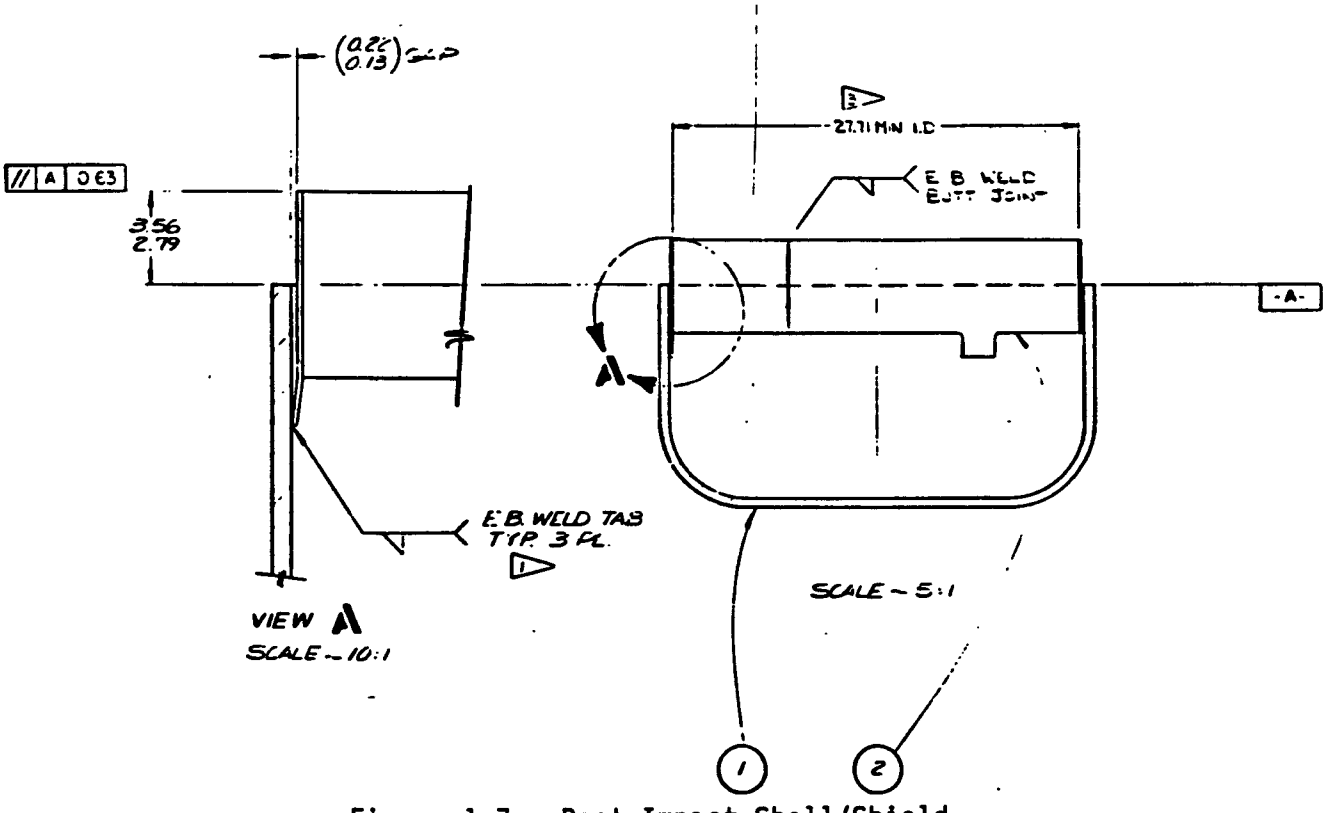

Figure 1-7. Post Impact Shell/Shield

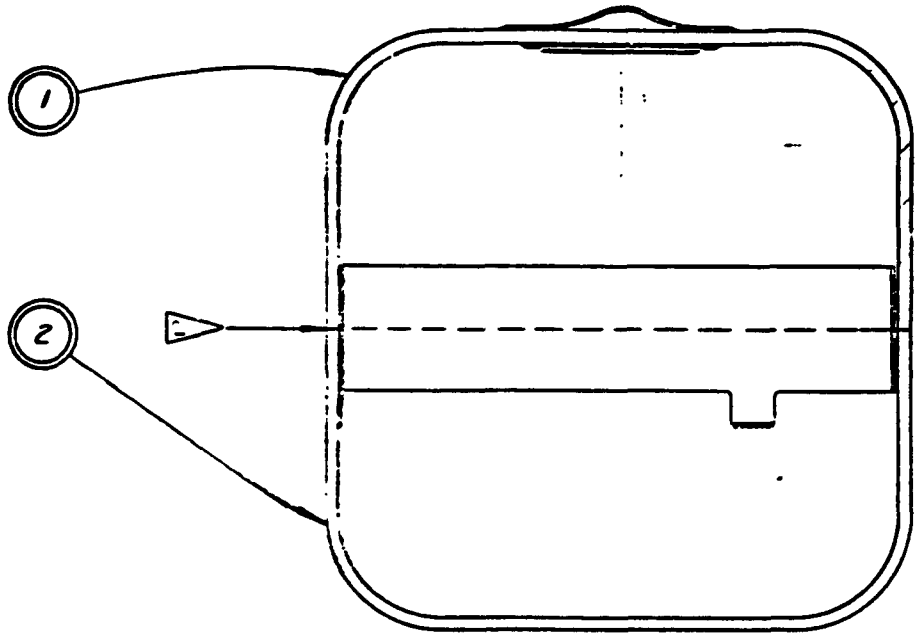

Figure 1-8. Clad Vent Set

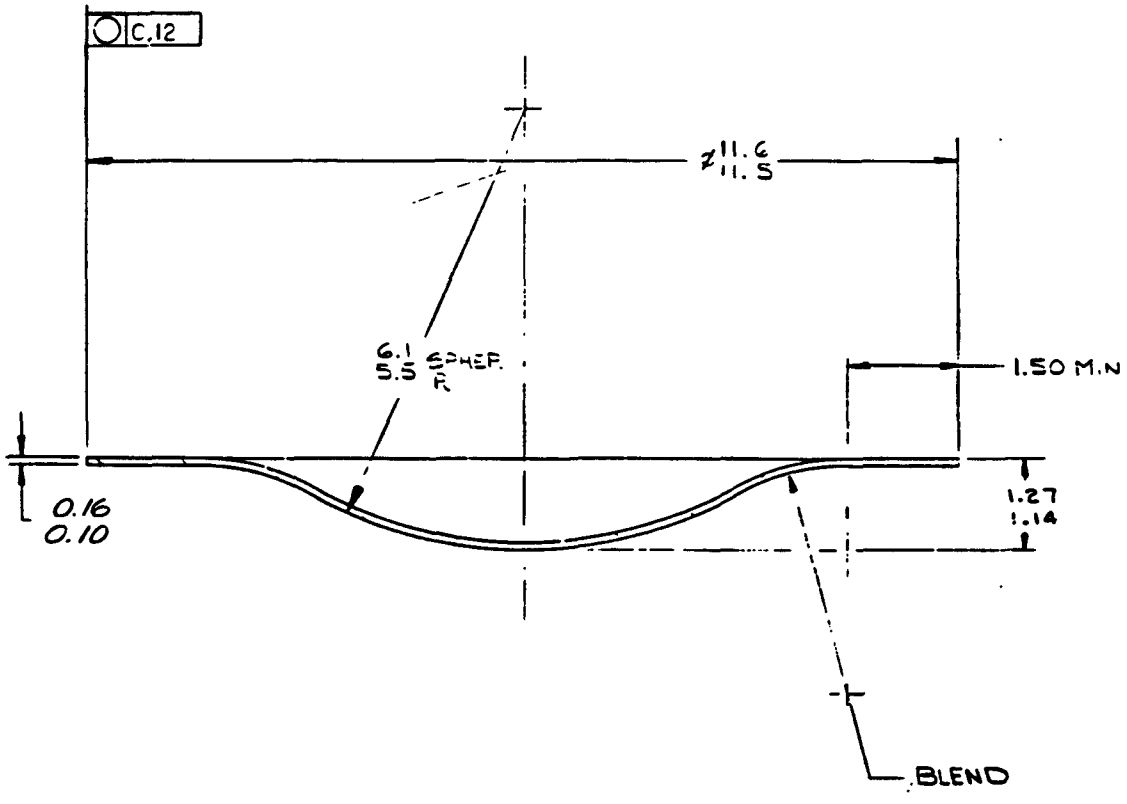

Figure 1-9. Decontamination Cover

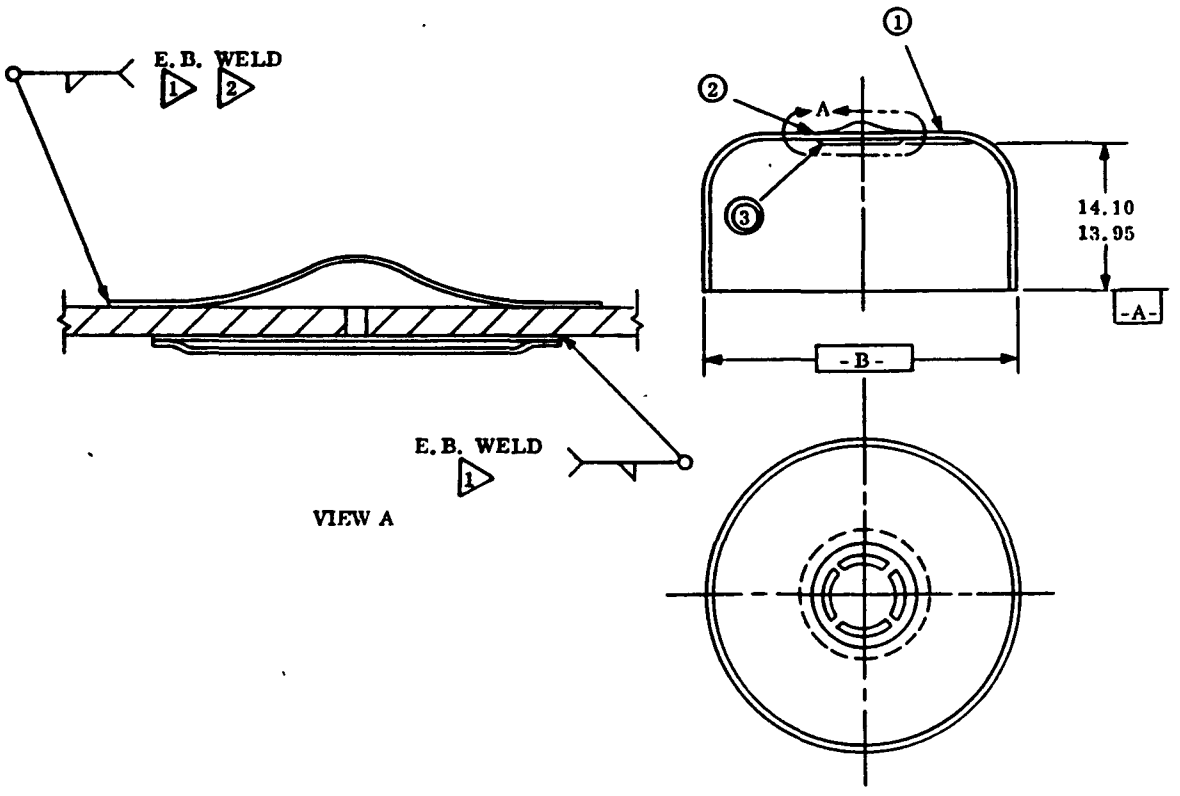

Figure 1-10. Post Impact Shell/Vent

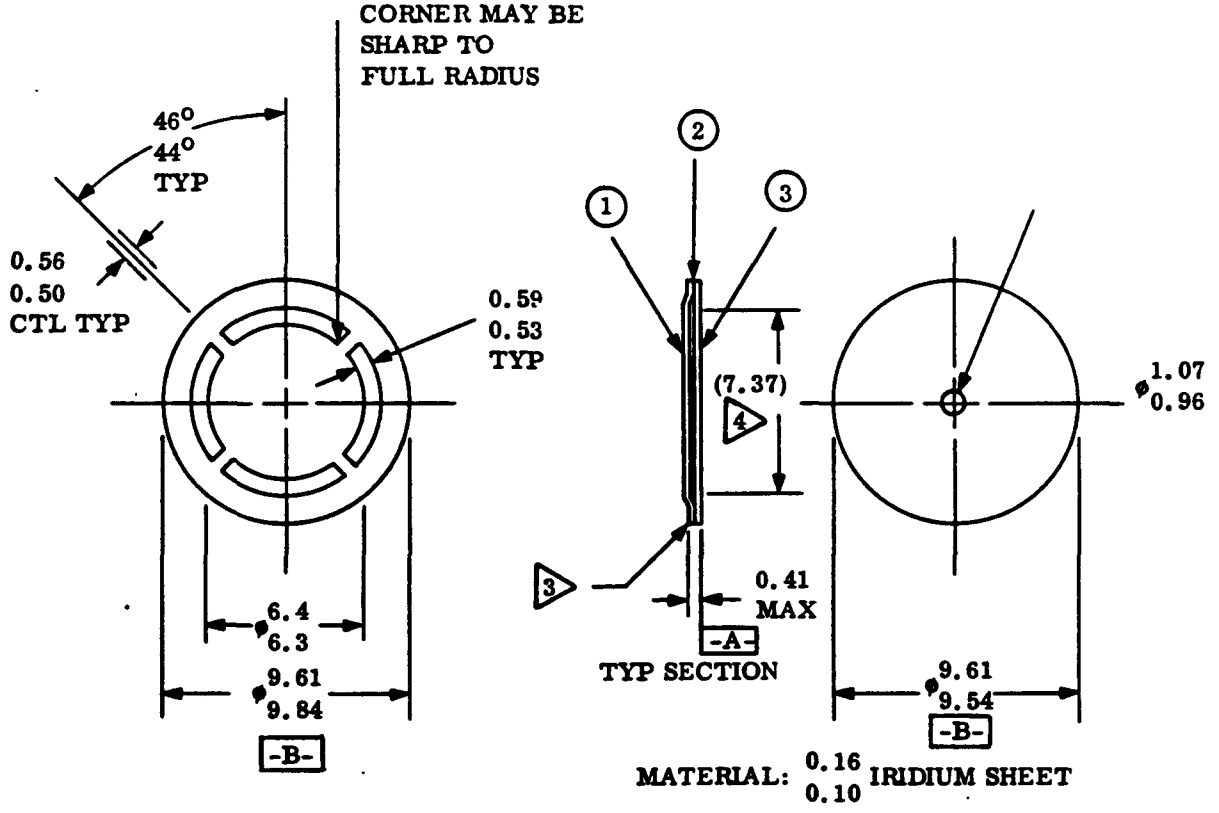

Figure 1-11. Vent Hole Filter Subassembly

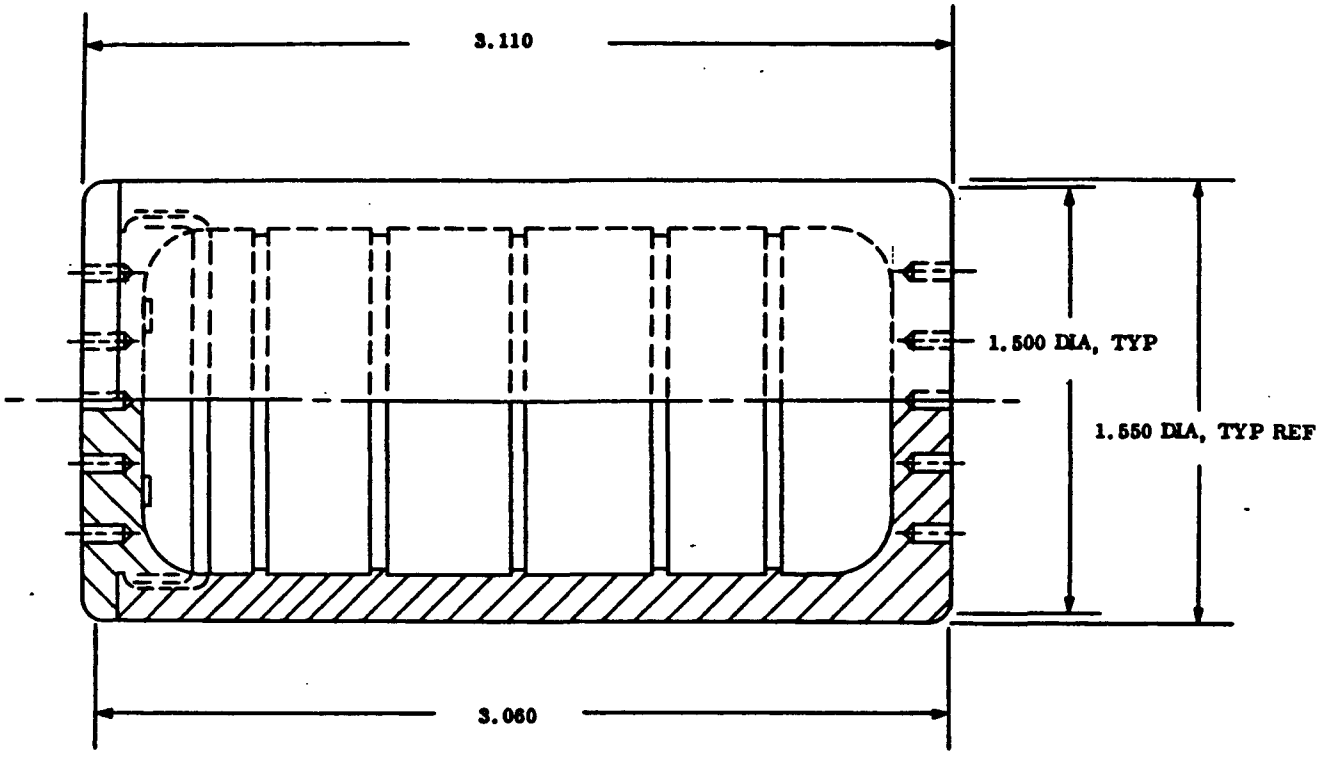

Figure 1-12. Graphite Impact Shell

1.4.3.2 Impact Shell

The Graphite Impact Shell (GIS) is designed to provide impact protection for two post impact shell assemblies under impact conditions associated with GPHS module terminal velocity. The two FC's in the GIS are separated by a floating membrane. Both the GIS and the floating members are constructed of fine weave pierced fabric (FWPF) graphite, which is described in Appendix B. The GIS consists of a body and a cap which are threaded to provide a means of retention of the cap. Figure 1-11 shows the configuration of the graphite impact shell. The GIS is cylindrical with lands and an outer diameter of approximately 3.937 cm (1.550 inches) and a length of 7.899 cm (3.110 inches).

1.4.3.3 Aeroshell

The aeroshells, in addition to acting as the primary structural members of the GPHS modules, are designed to protect two graphite impact shells (and therefore four FC's) from the severe aerothermodynamic environment that may be encountered during a postulated reentry. A CBCF graphite insulator that separates each GIS from the aeroshell provides additional thermal protection for the GIS. The aeroshells are 9.317 cm x 9.718 x 5.308 cm (3.668 inches x 3.826 inches x 2.090 inches) hexahedrons of FWPF graphite.

The aeroshells are designed to have threaded caps to hold each GIS in place. The configuration of a typical aeroshell is shown in Figure 1-13.

1.4.4 HEAT SOURCE ASSEMBLY

The assembly procedure for the General Purpose Heat Source is shown by Figure 1-13. An assembled FC as described in Paragraph 1.4.3.1.2 is inserted into a Graphite Impact Shell, followed by the floating membrane, and then another FC. The FC's are arranged such that their clad vent holes face the floating member. The GIS cap is then screwed onto the GIS. The GIS is inserted, cap first, into the CBCF sleeve which has previously been placed in the aeroshell. The threaded aeroshell cap is then put into place. This procedure is repeated for a second GIS to complete a single GPHS module. The individual modules are stacked with two locking members placed between each pair of GPHS modules.

1.4.5 MATERIALS PROPERTIES

The currently available physical and thermal properties of the GPHS materials are tabulated in Appendix B. A more complete listing of properties for the PuO_2 fuel is given in Appendix A.

1.4.6 AERODYNAMIC CHARACTERISTICS

Drop tests from a helicopter were conducted during the GPHS-RTG program to determine the terminal velocity of the GPHS Module (Reference 1-1). The average of nominal sea level terminal velocity was determined to be 165 feet per second with a corresponding drag coefficient of 1.01. The results from this test provide the best averaged value for the subsonic drag coefficient since they implicitly account for the subsonic motion of the module.

Detailed testing has recently been performed to determine both hypersonic and subsonic aerodynamic characteristics of the GPHS module. The hypersonic testing was performed at the NASA-Langley Research Center, and the subsonic testing at the National Research Council of Canada. The results of these tests are presented in Volume II, Appendix I.

1.5 CONVERTER

1.5.1 CONVERTER CONFIGURATION AND ASSEMBLY

The converter design, as shown in Figures 1-14 through 1-17, consists of an aluminum outer case with aluminum pressure domes, an active converter housing cooling system, heat source supports, thermoelectric Unicouple asssemblies attached to the outer shell, and the molybdenum/astroquartz multifoil insulation peripheral and end assemblies. A mounting flange with holes and barrel nuts for four bolts is provided at the inboard end of the outer shell for attachment of the RTG to the spacecraft. This arrangement is shown in Figure 1-18. Overall diameter of the converter is 42.16 cm (16.6 inches) and the length is 114.05 cm (44.9 inches). A gas management system mounted external to the outer shell is provided for charging the assembly with inert gas for ground operation and for venting the gas to space after launch.

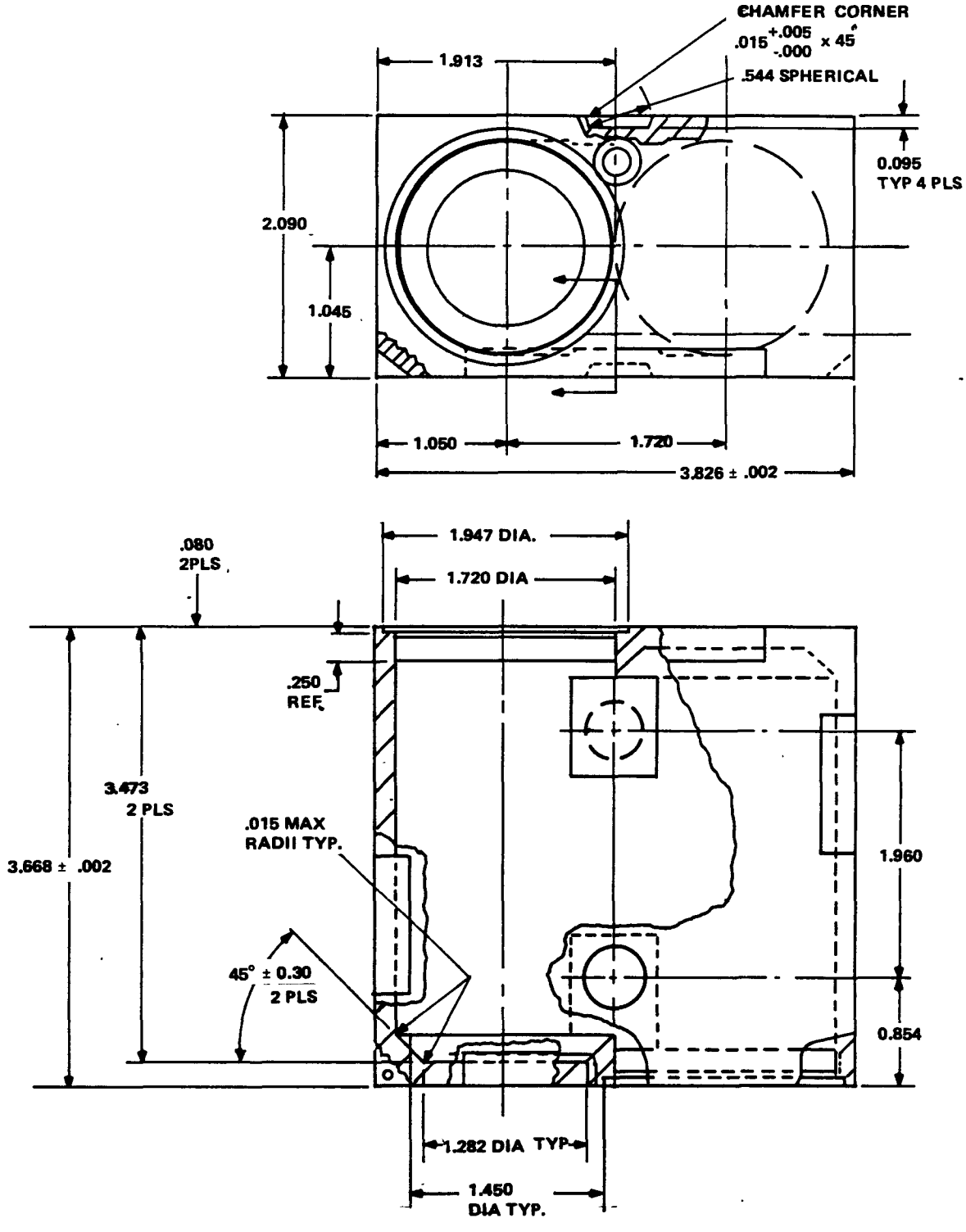

Figure 1-13. Aeroshell Body

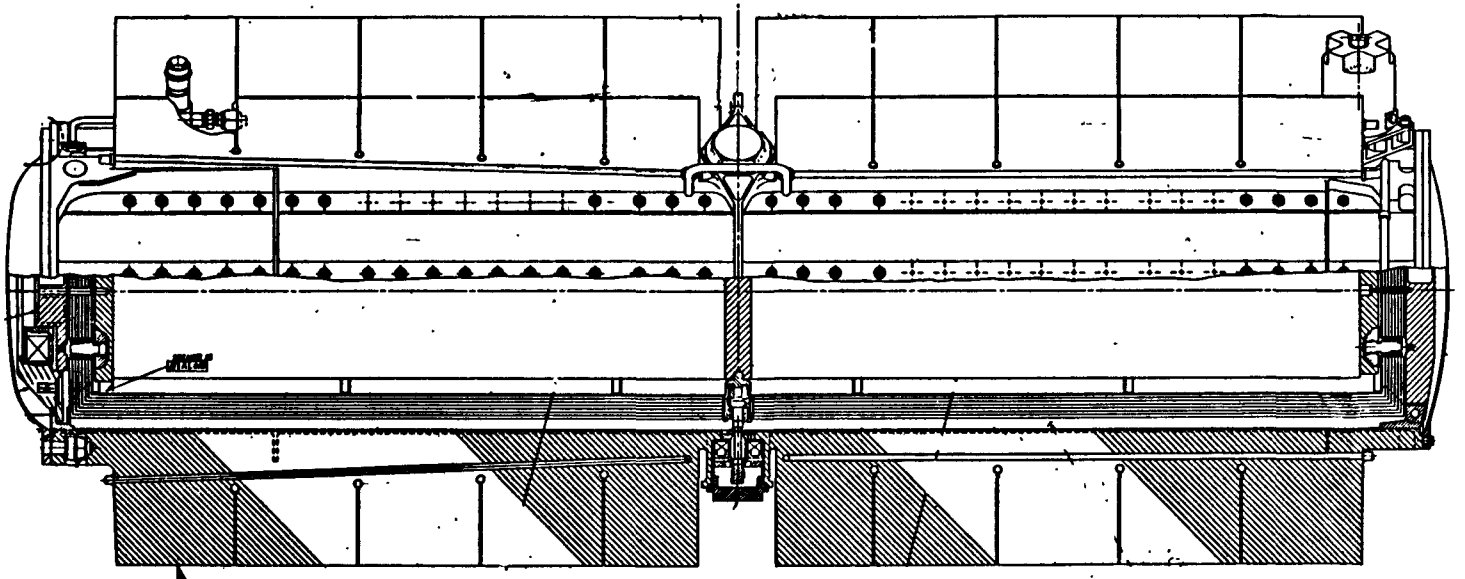

Figure 1-14. GPHS-RTG Assembly Profile

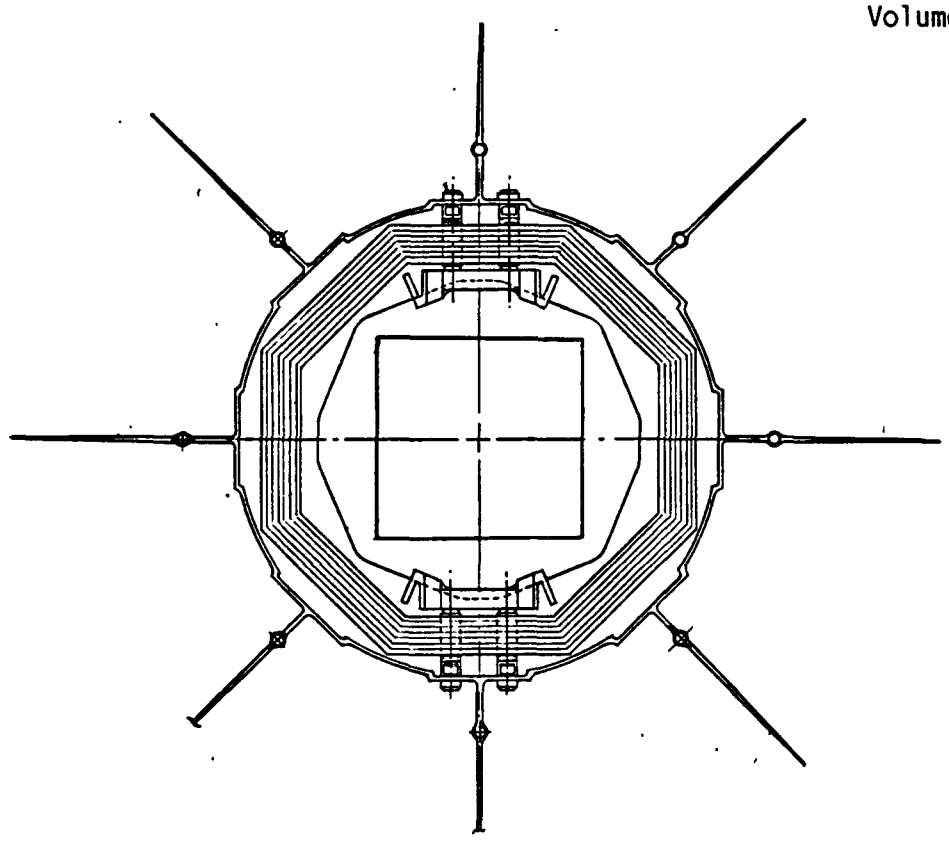

Figure 1-15. GPHS-RTG Assembly Section Through Thermopile

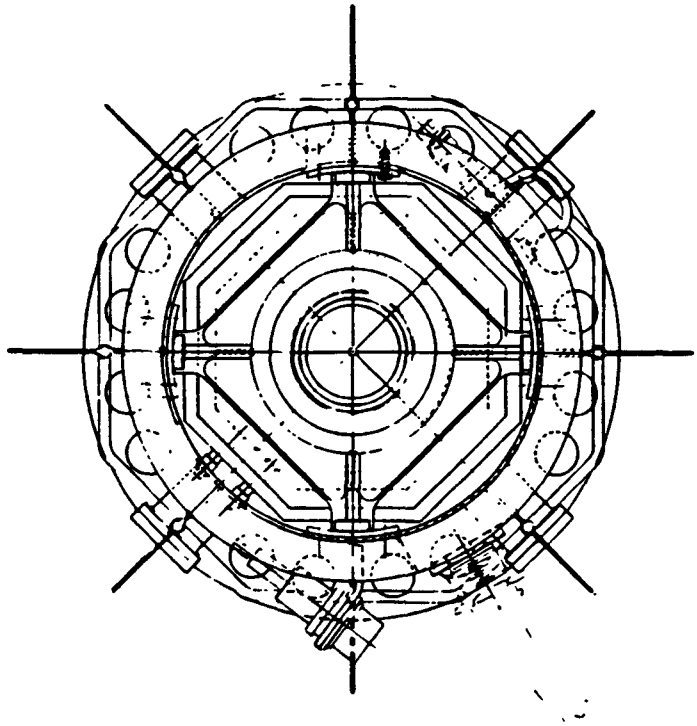

Figure 1-16. GPHS-RTG Assembly Inboard End View (Dome Removed)

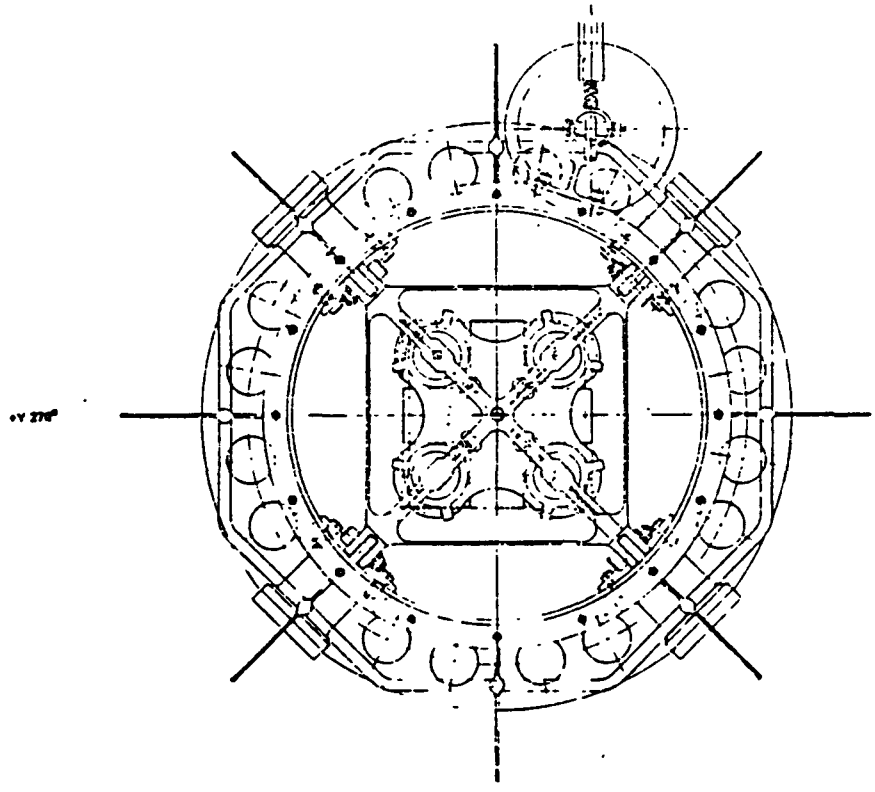

Figure 1-17. GPHS-RTG Assembly Outboard End View

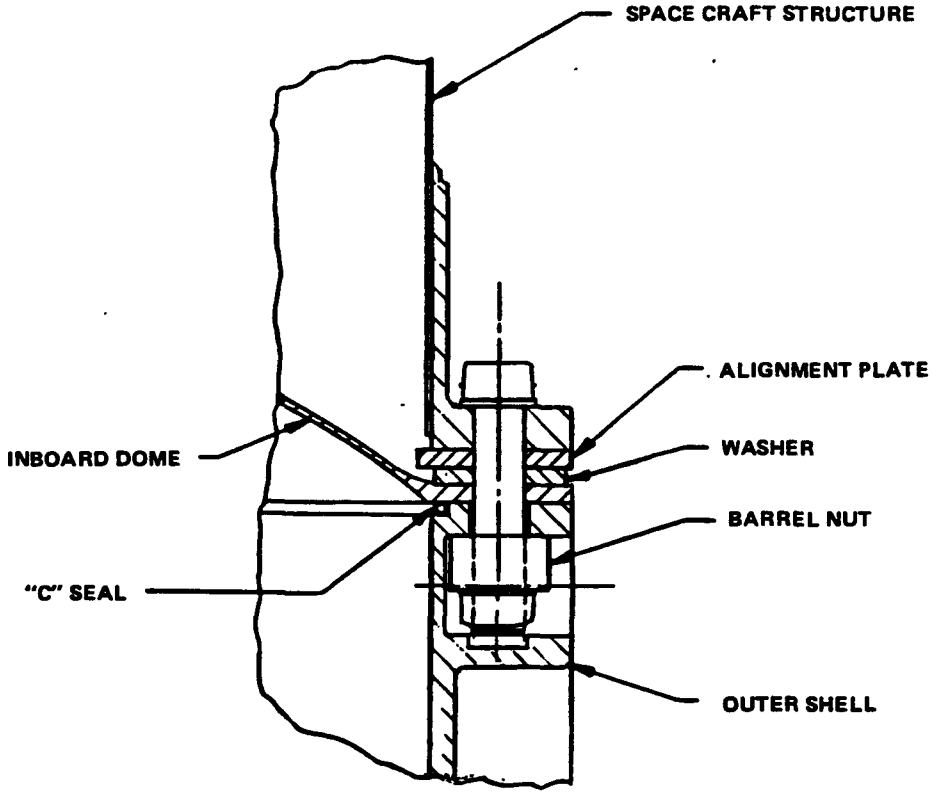

Figure 1-18. Spacecraft Mounting Attachment Joint

The aluminum outer shell is the primary structural member and is used for attachment to the spacecraft structure. The GPHS is supported as a column within the converter by the Heat Source Support System.

The Unicouples are attached directly to the outer shell by titanium screws engaging captive nut plates for each pair of couples. An electric power connector and a feed-through fitting for the gas management vent line are located on the outer shell. The pressure domes are retained by inconel bolts (24 for outboard dome, 20 for inboard dome plus 4 mounting bolts). Inconel C seals are used for the two domes, for each Unicouple attachment, for the gas management and power connector penetrations, and at the mid-span support penetrations to provide a sealed unit after assembly. The allowable leakage rates for each penetration are given in Table 1-4 while the sum of these allowable rates is compared with the allowable RTG pressure decay in Figure 1-19. An active cooling system is provided with cooling passages integral with the outer housing assembly fins in order to remove excess heat during certain ground operations and while the RTG's are aboard the Space Shuttle.

Table 1-4. C-Seal Leakage Rate

Penetration	Allowable Leakage* (std ccAr/sec)	No. of Seals	Total Leakage
Unicouple	6.3×10^{-6}	572	36.3×10^{-4}
PRD	5.4×10^{-6}	1	0.05×10^{-4}
Gas Management	8.3×10^{-6}	1	0.08×10^{-4}
Dome	3.4×10^{-4}	2	6.8×10^{-4}
Power Connector	1×10^{-4}	1	1.0×10^{-4}
Mid Span Support	1×10^{-4}	4	4.0×10^{-4}
48.23×10^{-4} std cc Ar/sec = 416 std cc Ar/Day $\approx$ 0.245 psi/day at 3 psi			
*Leakage rate specified at 3 psi differential pressure			

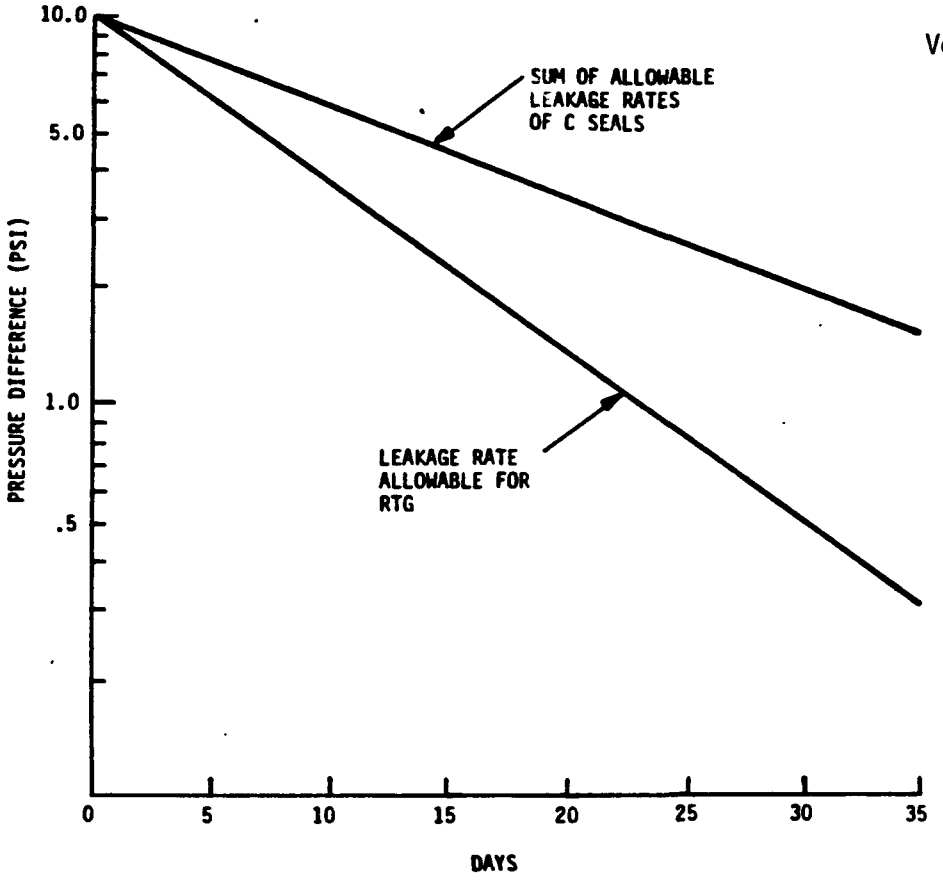

Figure 1-19. Allowable Pressure Decay

1.5.2 COMPONENT DESCRIPTION

1.5.2.1 Outer Housing Assembly

The converter outer housing assembly consists of the outer shell and upper and lower pressure domes. These elements are machined from 2219-T6 aluminum and have a nominal thickness of 0.060 inch. The use of aluminum ensures that, in the event of a postulated reentry, the housing will burn up and the GPHS modules will be released. The outer housing is designed to resist an anticipated launch load.

The housing is designed with eight tapered fins that are E-beam welded to longitudinal ribs and stub fins. Integral with these fins are cooling passages that are to provide for an active cooling system flow designed to remove at least 3500 watts with an average radiant sink temperature of 25°C and an inlet coolant temperature of 30°C. The pressure domes are spherical segments with no service penetrations. In order to enhance heat transfer, the outer housing assembly is coated externally with a GE silicone base paint which has a minimum emissivity of 0.90.

1.5.2.2 Thermocouples

The converter contains 572 thermocouples arranged in 16 circumferential columns. The couples are made in Unicouple assemblies as shown in Figure 1-20, and are individually bolted to the outer case. The Unicouple

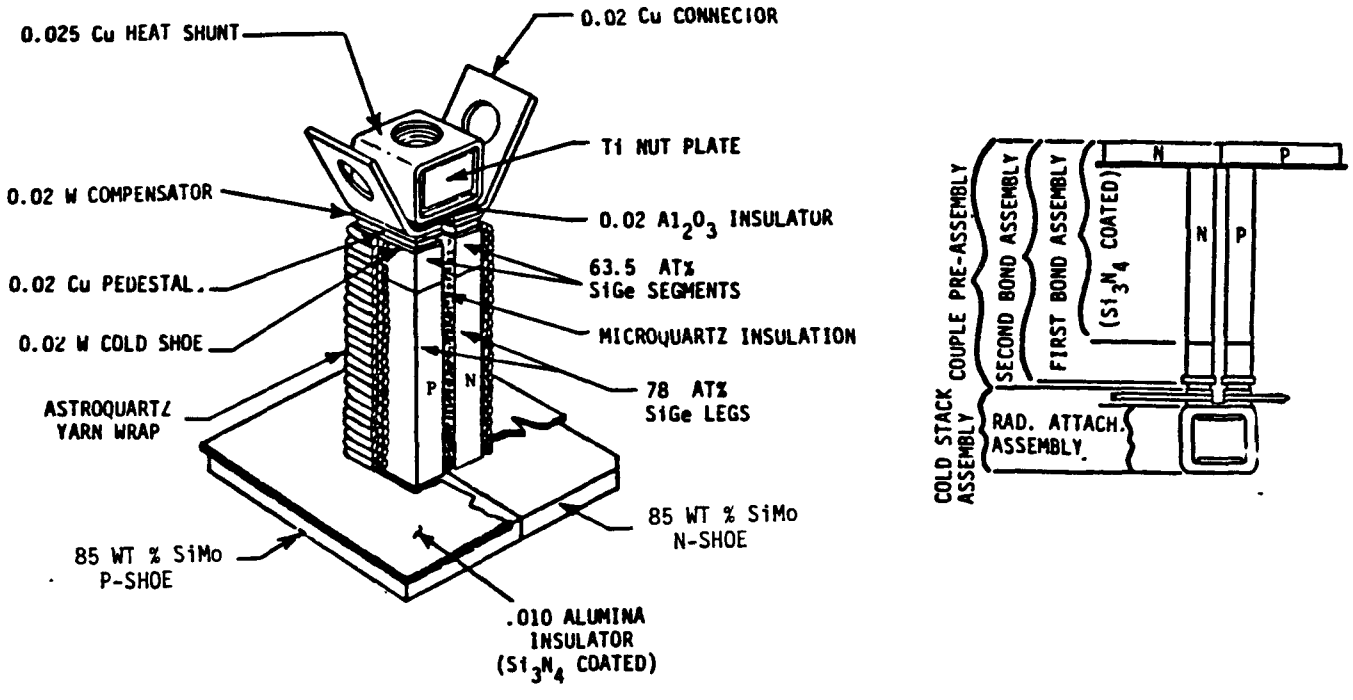

Figure 1-20. Silicon Germanium Unicouple

also contains the SiMo (85% w/o Si) hot shoe to which the SiGe thermocouple legs are bonded.

Two compositions of the SiGe alloy are used in the legs: 78 atomic percent Si for most of the length and a short segment of 63.5 atomic percent at the cold end of the couple. This lower Si content segment is used to provide better matching for thermal expansion of bond parts. The two SiGe legs of the couple and their corresponding sections of the hot shoe are doped to provide thermoelectric polarity; the N-type material is doped with phosphorous and the P-type with boron. The silicon alloy thermocouple is bonded to a cold stack assembly of tungsten, copper,and alumina parts, which separate the electrical and thermal currents. A silicon nitride coating in the 10,000 angstrom thickness range is applied to the thermocouple legs to retard silicon sublimation.

Electrical current is conducted between Unicouples by copper electrodes. These electrodes or straps are riveted together in the space between the inside of the outer case and the outside of the insulation system to form the thermopile electrical circuit. A two string, series-parallel, electric wiring circuit is used. This circuit permits continued operation in the event a thermocouple fails in either the open or short mode. The thermocouples are electrically insulated from the multifoil insulation by several layers of astroquartz yarn tightly wound around the two SiGe legs of each couple and by an alumina wafer beneath the hot shoe.

1.5.2.3 Insulation System

The thermopile insulation consists of an insulation canister and end caps composed of successive layers of 0.0003 inch molybdenum foil and astroquartz (SiO_2) cloth separators and a molybdenum frame. The canister has 572 rectangular perforations through which the thermocouples pass; the two end caps each have two perforations for the heat source support preload studs.

The lids are made of octagonal sheets of foil and separators of varying sizes folded in such a way that they form a cone with a stepped outer edge matting with the 8-sided thermopile insulation. Figure 1-21 shows these stepped corner joints which are packed with quartz felt to further minimize heat loss. The thermopile insulation shown in Figures 1-22 and 1-23, is made of staggered layers of 90 degree half-length sections laid on and folded over an inner molybdenum frame. This octagonal frame is constructed with eight longerons and six rings. Circumferential retaining bands are used at three axial positions around the quarter sections so that the assembled foil basket is self-supporting. The total insulation thickness is 0.70 inch with a total of 61 metallic layers in both the canister and lids. The entire insulation assembly is supported after installation in the case by the couples. The end caps are held in place by the titanium pressure plates of the heat source support system.

1.5.2.4 Heat Source Support System

The heat source support system consists of an upper and lower assembly and a mid-span support assembly.

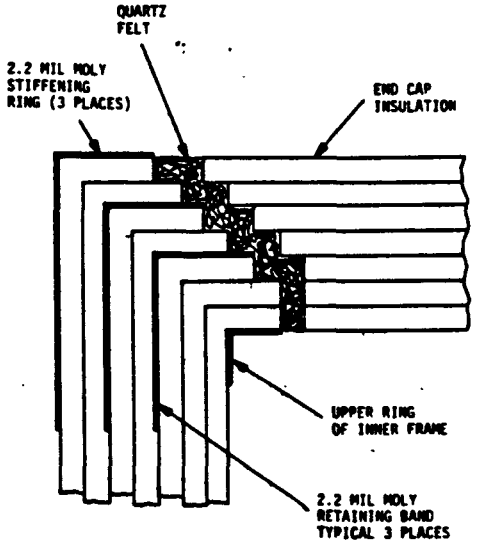

Figure 1-21. Thermopile Insulation Corner Detail

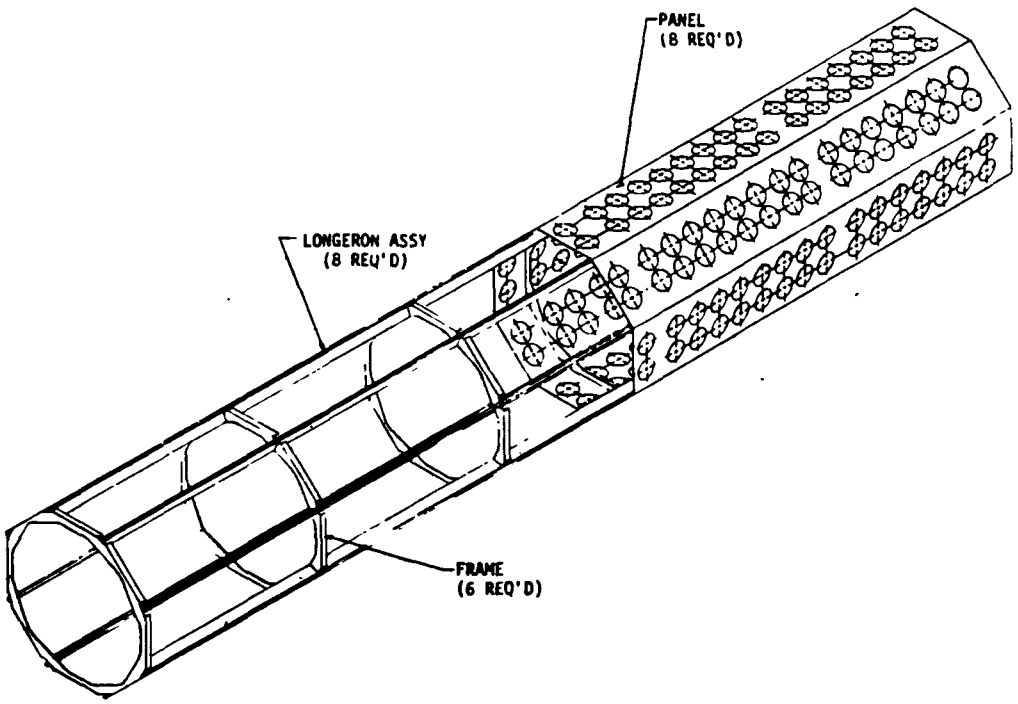

Figure 1-22. Thermopile Inner Frame Assembly

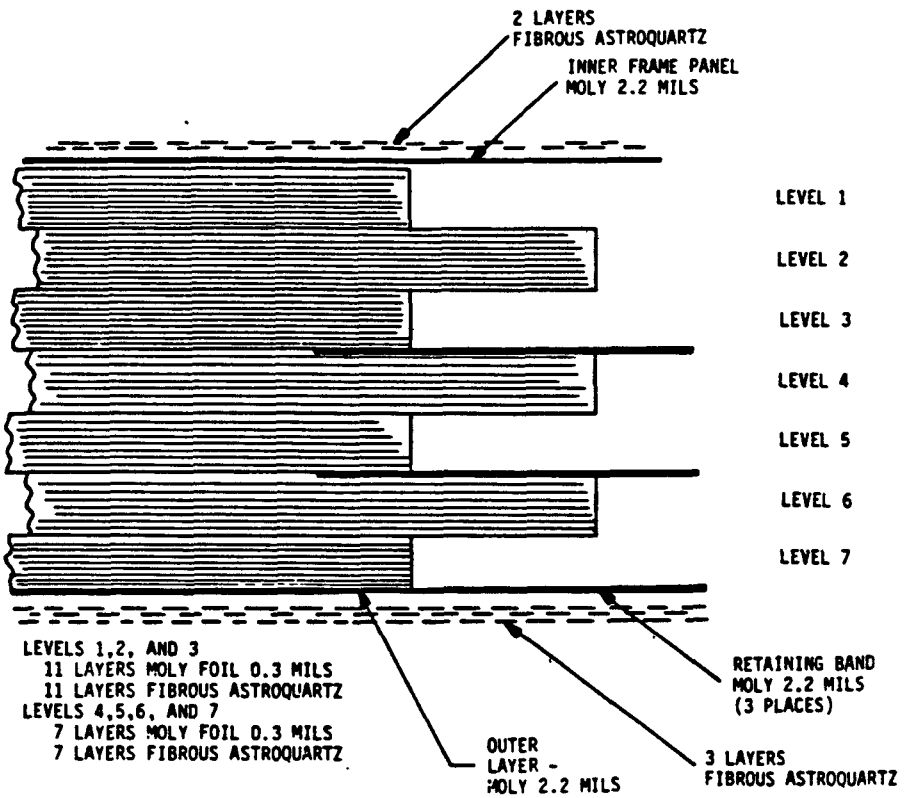

Figure 1-23. Thermopile Insulation

The upper and lower supports maintain an axial compression load on the GPHS in order to prevent separation of the individual GPHS modules. The mid span support shares the lateral loads while also reducing the required axial payload. The preload forces are adjusted and maintained by the support system through spring washer stack arrangements. The inboard, outboard, and mid-span support assemblies are shown in Figures 1-24, 1-25 and 1-26. In addition to being capable of supporting the GPHS during anticipated mission loads, the heat source support system is designed to maintain preload forces, allow thermal growth, and to minimize thermal losses.

1.5.2.5 Gas Management System

A gas management system is provided to maintain an inert gas atmosphere within the converter to protect the molybdenum foil and refractory materials during storage and ground operations at high temperatures. The converter is charged with inert gas after assembly and, for optimum operation in space, the gas is vented by the pressure relief device (PRD).

The gas management assembly consists of a fitting that penetrates the aluminum outer shell and a high temperature, hermetically sealed bellows. The feed-through fitting is made from stainless steel and uses an Inconel C-Seal and locknut to seal it hermetically to the aluminum case. The gas management valve is a manually operated, stainless steel, bellows type valve.

The PRD is designed to vent the internal inert gas from the converter upon actuation. The PRD is actuated by a nonexplosive device designed by the user. The PRD design consists of a spring-loaded lance contained in an aluminum housing. Upon actuation, the lance is driven through a 0.005 inch thick stainless steel diaphragm located in the outer shell wall.

1.5.3 MATERIALS AND WEIGHTS

A summary of the various converter components, materials and weights are presented in Table 1-5.

1.5.4 MATERIALS PROPERTIES

Material properties for the converter components are summarized in Appendix B.

1.5.5 RTG INSTRUMENTATION

The only flight instrumentation included on the GPHS-RTG will be three temperature sensors (i.e., RTD's - Resistance Temperature Detectors) per RTG. A fourth RTD is available for on-ground temperature monitoring.

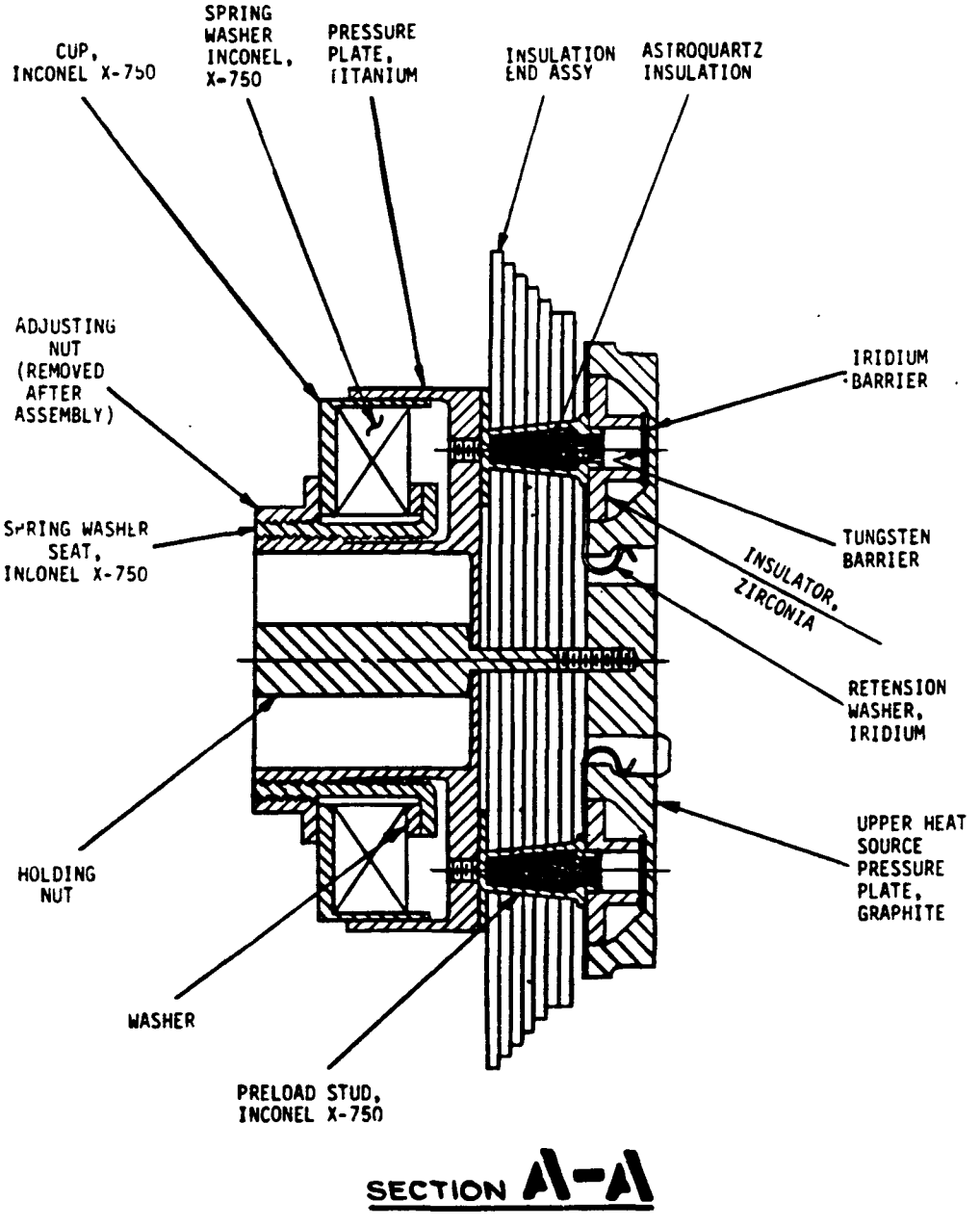

Figure 1-24. Inboard Heat Source Support Assembly

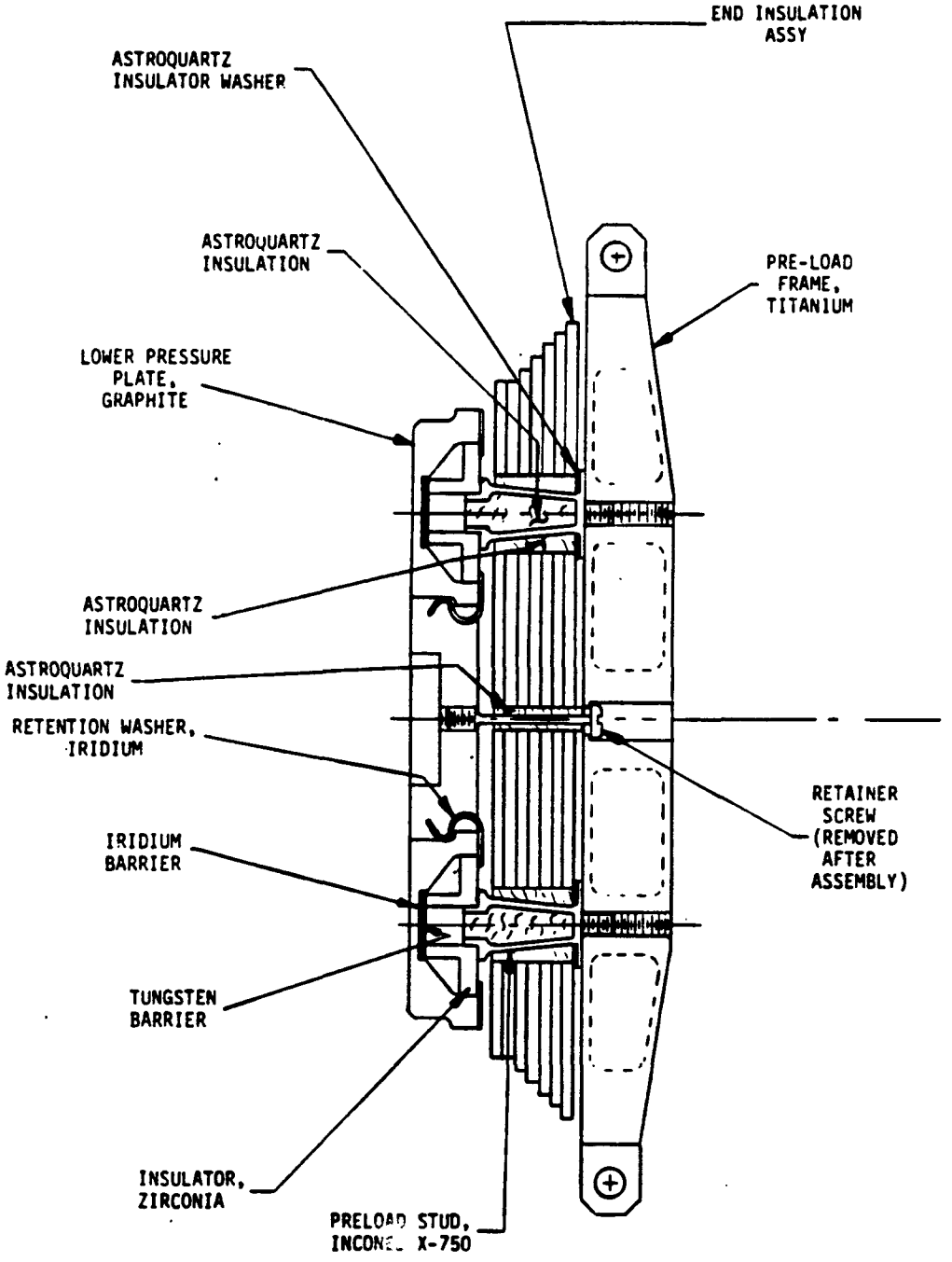

Figure 1-25. Outboard Heat Source Support Assembly

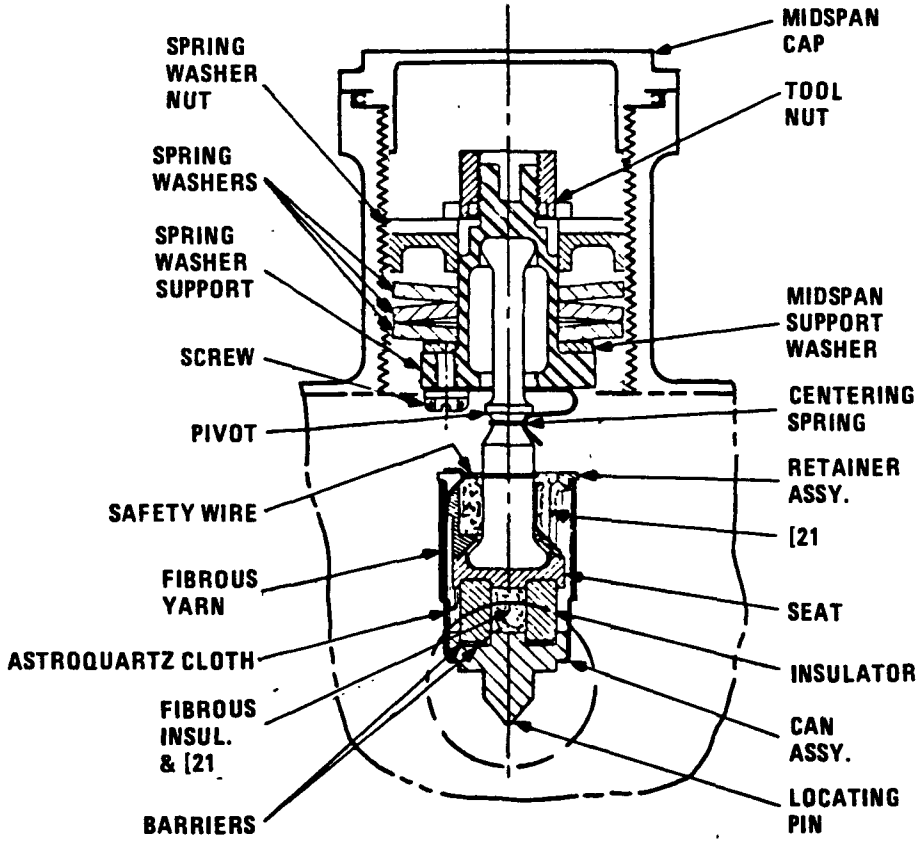

Figure 1-26. Mid-Span Support Assembly

Table 1-5. GPHS-RTG Converter Weights and Materials

Item	Material	Quantity	Weight (Pounds)
Housing			
Outer Shell w/Fins, Coating	2219-T6 A1	1	18.89
Aux. Cooling Tube Manifold	2219-T87	1	0.57
Nuts	IN A286	8	0.11
Converter			
T/E Unicouples	SiGe	572	11.90
T/E Sealing Screws	Ti-6A1-4V	572	1.54
T/E Spacers	Al_2O_3	572	0.64
Nut Plates	Ti 6A1-4V	286	0.84
Foil Insulation – T/P	Mo and Astroquartz	1	12.15
Insulation Frame Support	Mo	1	1.91
Power Connector	IN X-750	1	0.29
Gas Management Assembly	316L SS	1	0.36
Electrical Straps	Copper-OFHC	X	1.65
PRD	2219-T87 A1	1	0.94
Pressure Dome	2219-T87 A1	2	1.68
RTD Assembly	IN X-750	1	0.67
Misc. Hardware, Insul.	Numerous	X	1.24
Inner Frame Support Ass'y	Mo & Mo-Re	1	0.497
Heat Source Support Ass'y			
Outboard Support Ass'y			
Frame	Ti 6-2-4-2	1	0.91
End Cap. Insulation Ass'y	Mo and Astroquartz	1	0.64
Pressure Plate	FWPF Graphite	1	0.68
Stud Insulator	ZrO_2	4	0.27
Preload Stud	IN X-750	4	0.15
Latch	IN X-750	4	0.20
Misc. Hardware, Insul.	Numerous	X	0.144
Inboard Support Ass'y			
Frame	Ti 6-2-4-2	1	1.12
Pressure Plate	Ti 6-2-4-2	1	0.79
End Cap Insulation Ass'y	Mo and Astroquartz	1	0.58
Spring Washer	17-4-SS	3	1.13
Collar	Ti 6-2-4-2	1	0.15
Guide	IN X-750	1	0.37
Preload Stud	IN X-750	4	0.15
Pressure Plate	FWPF Graphite	1	0.49
Stud Insulator	ZrO_2	4	0.27
Latch	IN X-750	4	0.08
Misc. Hardware, Insul.	Numerous	X	0.104

Table 1-5. GPHS-RTG Converter Weights and Materials (Cont'd)

Item	Material	Quantity	Weight (Pounds)
Midspan Support Ass'y			
Cap	2219-T87 A1	4	0.24
Pivot	Rene 41	4	0.13
Support	IN X-750	4	0.25
Lock Nut	2219-T87 A1	4	0.11
Spring Washer Nut	IN X-750	4	0.24
Spring Washer	17-7 PH	12	0.04
Can Assembly	Ir	4	0.04
Locating Pin	FWPF Graphite	4	0.05
Misc. Hardware, Insul.	Numerous	X	0.396
Midspan Plate	FWPF Graphite	1	0.57
Total Converter and Housing			66.171

BLANK

SECTION 2.0

SPACECRAFT DESCRIPTIONS

2.1 RTG APPLICATIONS

This Safety Analysis Report applies specifically to the spacecraft system that utilizes the Radioisotope Thermoelectric Generator (RTG) to satisfy mission power requirements. The spacecraft described is for the Galileo mission, which is a deep space mission with long term data gathering power requirements. RTG safety hazards during launch and deployment are generally independent of the Spacecraft design, with the exception of how the RTG is mounted and how the Spacecraft might break up in the event of an accidental Earth reentry. Descriptions of the Spacecraft are provided as general information to support the safety analysis and to understand system design requirements and interfaces.

2.2 GALILEO SPACECRAFT DESCRIPTION

2.2.1 GENERAL DESCRIPTION

The Galileo Spacecraft is a 2500 Kg vehicle, which is designed to accomplish a scientific investigation of the planet Jupiter, its satellites, and its environments. The spacecraft basically consists of a Jovian planetary orbiter, an atmospheric probe, and self-contained control, command and data communication subsystems. Vehicle stowed and cruise configurations are shown in Figures 2-1 and 2-2.

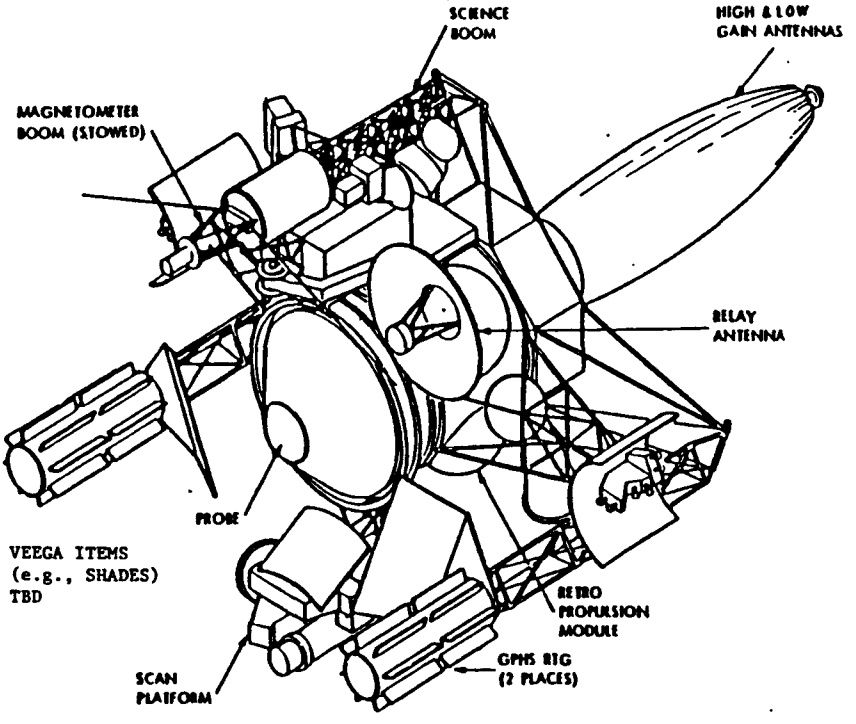

Figure 2-1. Galileo Spacecraft: Stowed Configuration

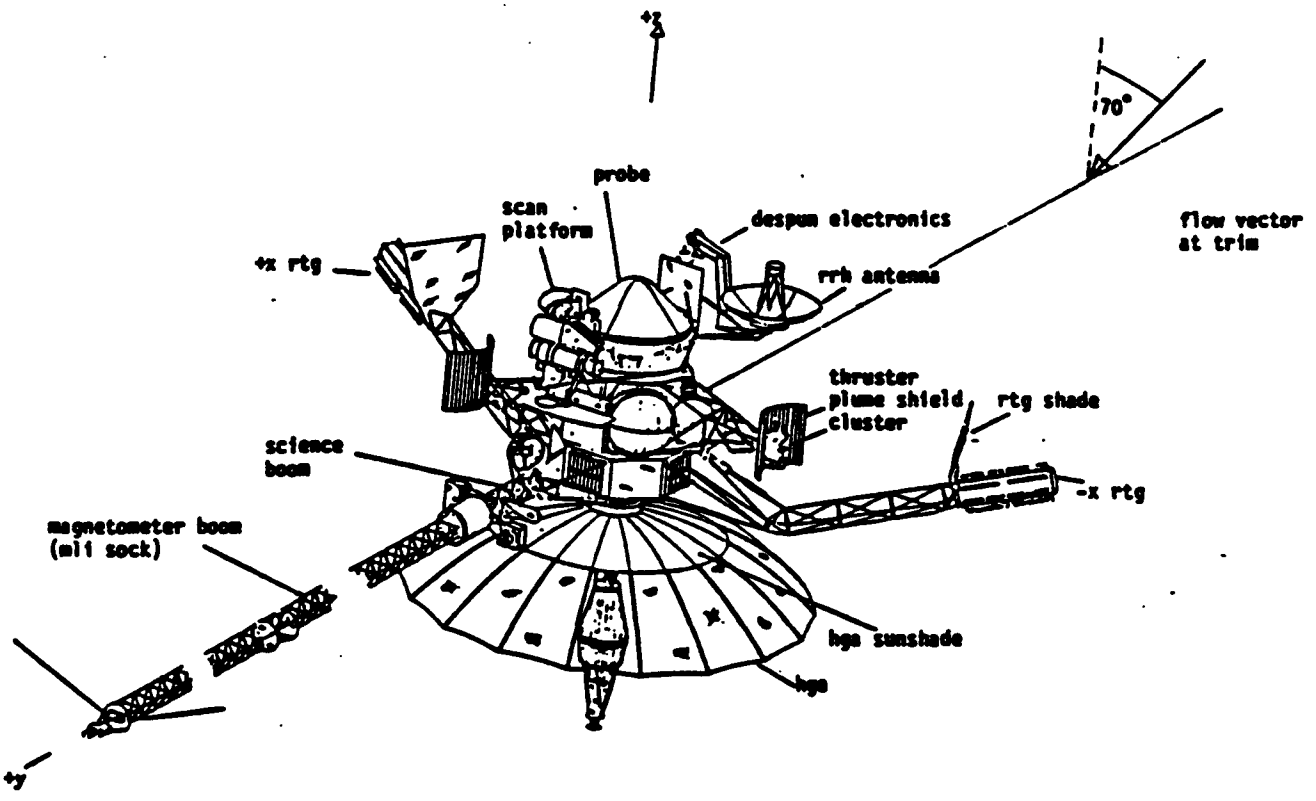

Figure 2-2. Galileo Spacecraft: Cruise Configuration

Following separation from the Inertial Upper Stage (IUS) and the achievement of the predetermined Earth escape trajectory, the spacecraft RTG, science, and magnetometer booms are deployed in the cruise configuration, and the spacecraft provides cruise control and status telemetry during the 2318-day trip to Jupiter including the two Earth flybys. The planetary orbiter and the atmospheric probe remain an integral unit until about five months before the arrival at Jupiter, when the probe goes on its own internal power just prior to separation from the Spacecraft. After releasing the probe, the spacecraft is configured for acquisition, storage, and retransmission of data from the probe. The Spacecraft command and control system is used to make trajectory adjustments during the cruise phase of the mission, to perform deflection maneuvers after the probe release, and to make correction and trim maneuvers for insertion into orbit around Jupiter.

2.2.2 MAJOR SPACECRAFT SUBSYSTEM

The major subsystems of the Galileo Spacecraft are separated into those relating to the planetary orbiter and to the atmospheric probe as follows:

Orbiter:
- Orbiter Communications Subsystem
- Command and Data Subsystems
- Attitude and Articulation Control Subsystem
- Power Subsystem (two GPHS-RTGs)
- Orbiter Pyrotechnic Subsystem
- Retropropulsion Subsystem

Probe: Probe Deceleration Module
Probe Descent Module

-Command and Data Subsystem
-Power Subsystem
-Communication Subsystem

Relay Radio Hardware

-Relay Receivers
-Relay Antenna

Note: The RTGs are attached to the Orbiter

The planetary orbiter is a dual spin spacecraft, as shown in Figure 2-2. Part of the spacecraft will be three-axis stabilized to provide a steady base for the remote-sensing instruments, which must be precisely pointed. The despun section carries its related electronics. The main portion of the orbiter will spin at three revolutions per minute to provide stability and to allow its instruments to continuously sweep the sky to make their measurements. The spun section contains both the high and low gain antennas, the retropropulsion module for all propulsion and attitude maneuvers, the RTGs for electrical power, and most of the electronics, command and data equipment, and science instruments. The despun section carries four remote sensing instruments including the solid state imaging system.

The Orbiter contains programmable computers that carry out its mission as a function of the commands received from Earth and from programs stored in its memories. In the absence of control commands from Earth the computers will carry out routine functions and will respond to on-board faults to maintain the spacecraft in a safe state.

The Galileo spacecraft will use a 4.8 meter diameter furlable antenna to communicate with Earth. A smaller (1 meter) relay antenna will ride on the despun section of the orbiter to receive data from the atmospheric probe for relay to Earth.

Additional, more detailed subsystem descriptions of the planetary orbiter may be found in Reference 2-1.

The Galileo Probe is designed to carry a science instrument payload to Jupiter for the exploration of its atmosphere and magnetosphere by a combination of in-situ measurements and remote observations. In addition to the complement of science instruments, the Galileo Probe System consists of a deceleration module, which provides thermal protection during entry into the atmosphere, and a descent module, which houses and controls the instruments. An adapter which mounts the Probe to the Galileo Orbiter and an Orbiter-mounted Relay Radio data receiver subsystem are also provided with the Probe System. The Probe internal arrangement is shown in Figure 2-3. The probe sequence of events from Orbiter separation through entry is shown in Figure 2-4.

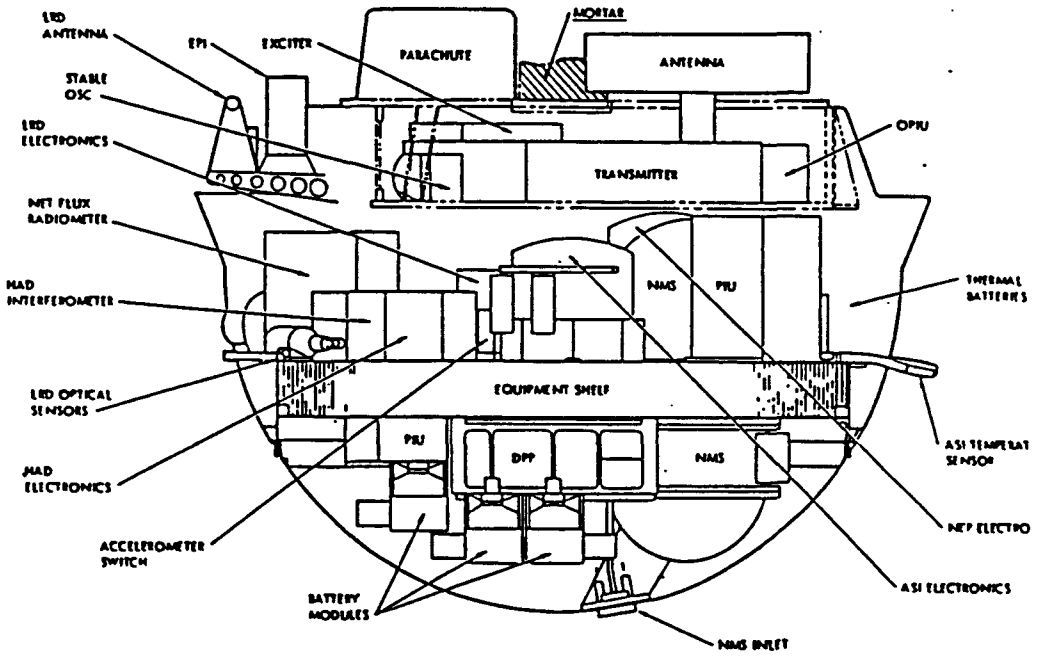

Figure 2-3. Galileo Probe Descent Module

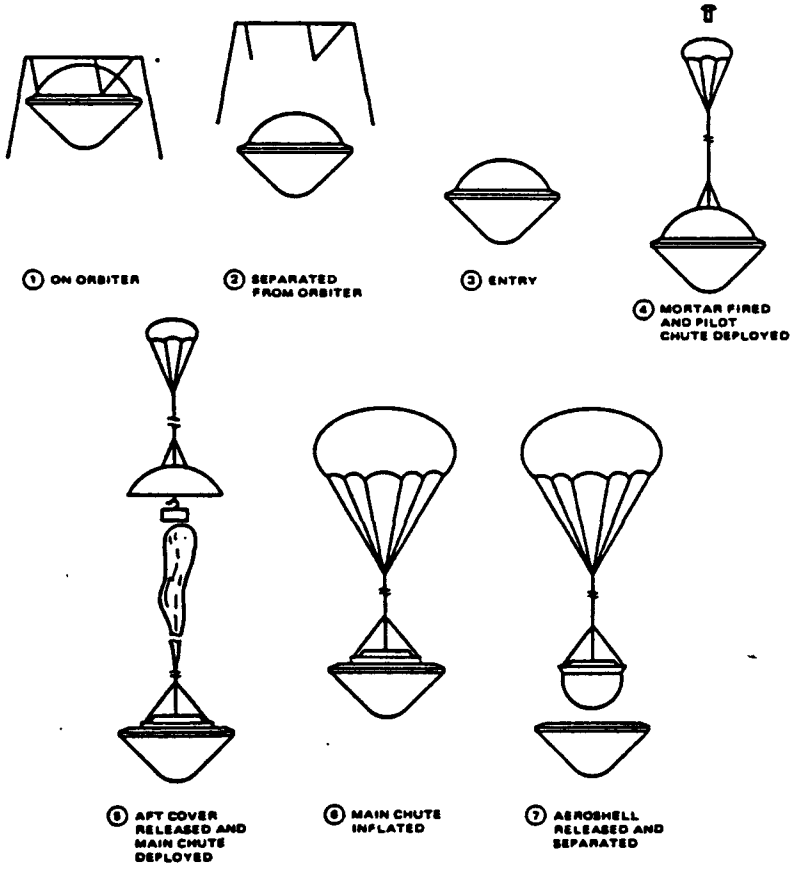

Figure 2-4. Galileo Probe System

The deceleration module consists of a conical forward aeroshell, a hemispherical aft cover, a two-stage parachute system and a thermal control system. A carbon phenolic ablative heat shield is bonded to the conical aeroshell. The aft cover provides thermal protection with a phenolic nylon shield. The main parachute is deployed by a mortar ejected pilot chute. Thermal control of the probe is provided by multi-layer mylar insulation blankets, a complement of internally mounted 1-watt radiosotope heaters (RHUs), and partial gold taping of the full body nose to adjust heat loss through the unblanketed portion of the heatshield.

The descent module, which supports the instrument payload and engineering units, consists of a main equipment shelf, and aft compartment, aerodynamic fairings, thermal blankets, electrical harness and various structural elements.

The scientific payload package consists of six (6) scientific instruments, three of which have sensors mounted external to the descent module and three of which have inlets to admit atmospheric samples. The instruments require 72 watts of electrical power and a total of six (6) serial digital, six (6) analog, and eight (8) bi-level telemetry channels to receive discrete commands and transmit data. Additional information on the purpose and description of each instrument is found in Reference 2-1.

The power subsystem provides power distribution to the subsystem units and science instruments, and a power interface with the orbiter. The primary Probe power source is the Li-SO_2 battery made up of three 13-cell modules with a total capacity of 21.6 ampere-hours. Two thermal batteries provide energy for pyrotechnic initiation.

The command and data handling subsystem consists of the DCP, the PCU, and four acceleration switches (two redundant pairs). The DCP is a redundant micro-controller-based processor which provides and controls all system command, telemetry, data storage, and timing functions. The PCU provides 46 current-limited squib driver outputs to all of the redundant pyrotechnic initiators, except those which are internal to the NMS. The acceleration switches initiate the descent sequence and provide a backup to turn on the Probe in the event of coast timer malfunction.

The communications subsystem provides two L-Band channels, each comprising an exciter, a power amplifier and an ultrastable oscillator or a standard, thermally controlled oscillation, respectively. Both channels are transmitted through a dual-feed, crossed-dipole antenna.

The communication link to the Orbiter is closed by the Relay Radio Hardware (RRH). The Orbiter mounted RRH consists of two receivers, ultra stable oscillators, and an antenna. Each receiver is designed to acquire, coherently track, and demodulate the Probe signals as well as provide radio science and engineering data. The RRH antenna is mounted on the Orbiter despun section on a deployable mechanism for storage at launch and for pointing during Probe descent.

BLANK

SECTION 3.0

LAUNCH VEHICLE

3.1 GENERAL DESCRIPTION

The launch vehicle for the Galileo Mission consists of two main components, the Space Shuttle and the Inertial Upper Stage (IUS), designed to boost the spacecraft into an Earth-escape trajectory. The Space Shuttle along with the tracking and communications relay satellites, the Kennedy Space Center and Jet Propulsion Laboratory control centers, the Goddard Space Flight Center, and the worldwide space tracking and data network form the Space Transportation System (STS). The description of the IUS used for this mission is presented in Section 4.0 of the RDD.

3.2 SPACE SHUTTLE

The basic mission of the Space Shuttle is to be a space transport carrying payloads into space and returning to Earth for another load. The Shuttle consists of the Orbiter, the external tank (ET), and the solid rocket boosters (SRBs). The arrangement of these components is shown in Figures 3-1 through 3-4.

Figure 3-5 shows the basic mission cycle for the Space Shuttle. It starts with the launch of the Shuttle vehicle (with the SRB's and Orbiter main engines firing). After approximately two minutes, (about 23 miles altitude), the SRBs are jettisoned and fall back to Earth for recovery. After approximately eight minutes of flight (before the Orbiter attains orbit), the main engines are shut down and the ET is separated and falls back to Earth. The orbital maneuvering engines thrust the Orbiter into orbit. For these missions the orbital operations include ejecting the IUS with spacecraft from the Orbiter. The Orbiter would return subsequently to Earth to be made ready for its next flight.

3.2.1 MAIN ENGINES

The main propulsion subsystem of the Orbiter consists of three Space Shuttle main engines (SSME) which burn for approximately eight minutes from just before lift-off until slightly before attaining orbit. The SSMEs are reusable, high performance, liquid propellant rocket engines with variable thrust. The propellants, LH_2 (fuel) and LOX (oxidizer), are carried in the external tank (ET). Each engine weighs about 2860 kilograms (6300 pounds) and has a rated thrust of 1.67 million Newtons (375,000 pounds) at sea level and 2.09 million Newtons (470,000 pounds) in vacuum. The nozzle is gimbaled with hydraulic actuators for steering.

3.2.2 SOLID ROCKET BOOSTERS

The signals to ignite the two solid rocket boosters (SRB's) and release the holddown bolts will be sent at T-0. The initiation of these signals is dependent upon normal operation of the SSMEs with at least 90 percent of rated thrust. The simultaneous operation of the SRBs and the main engines, which

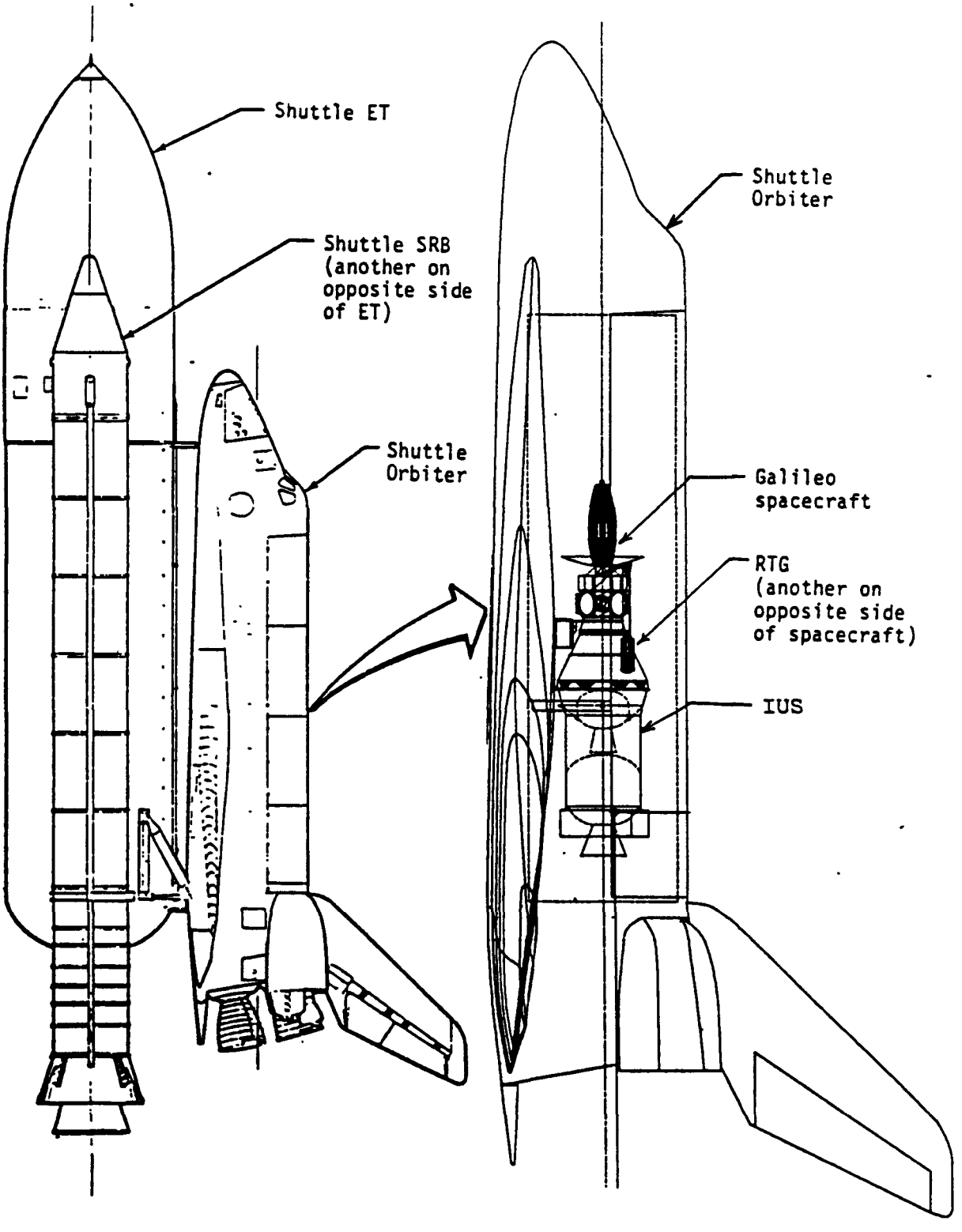

Figure 3-1. Galileo Launch Configuration

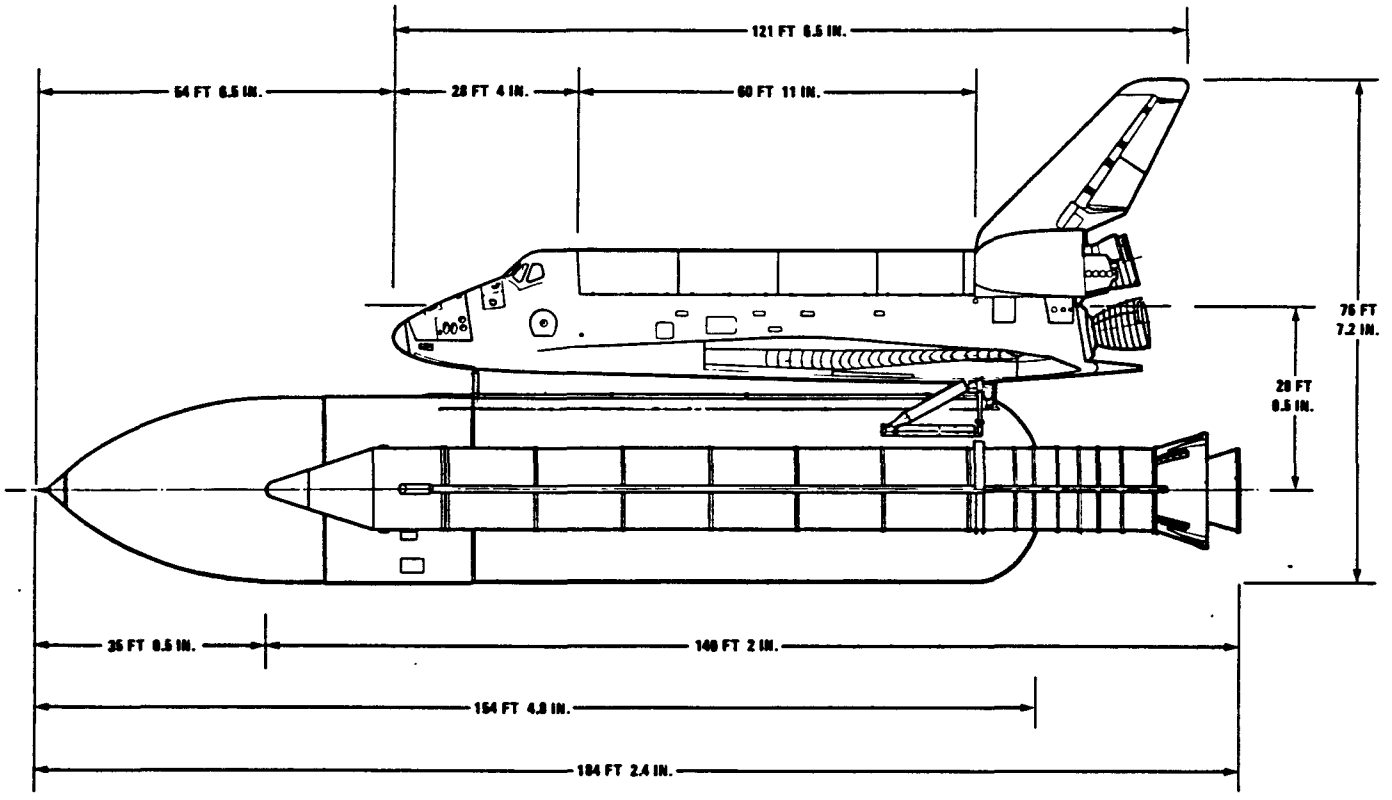

Figure 3-2. Shuttle Vehicle, Side View

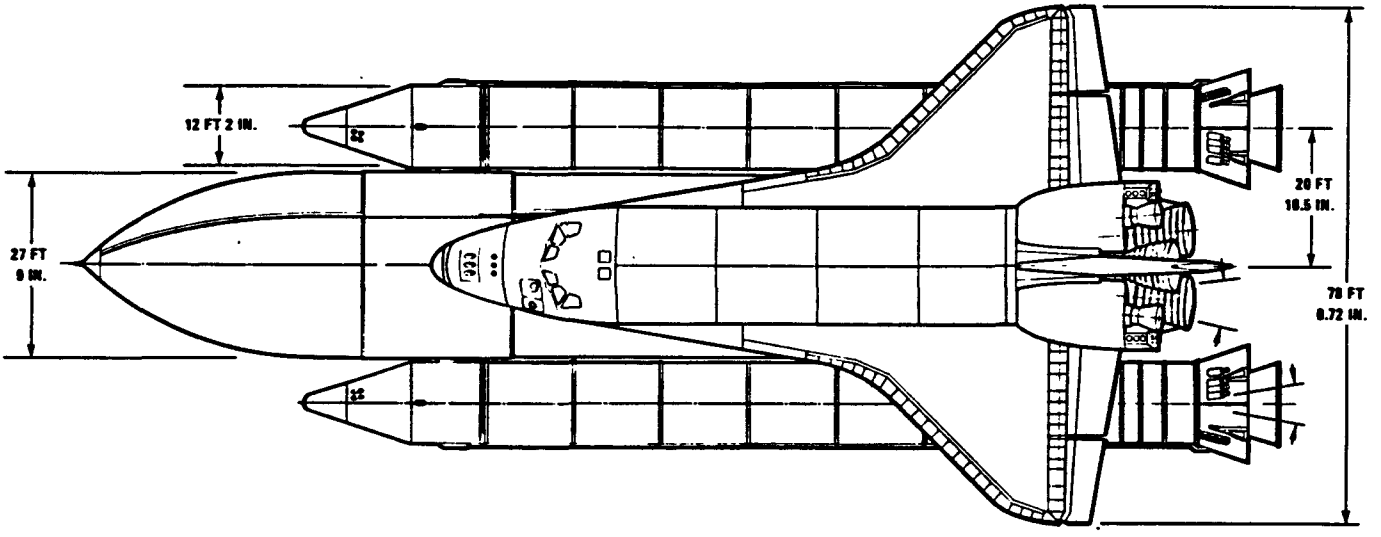

Figure 3-3. Shuttle Vehicle, Top View

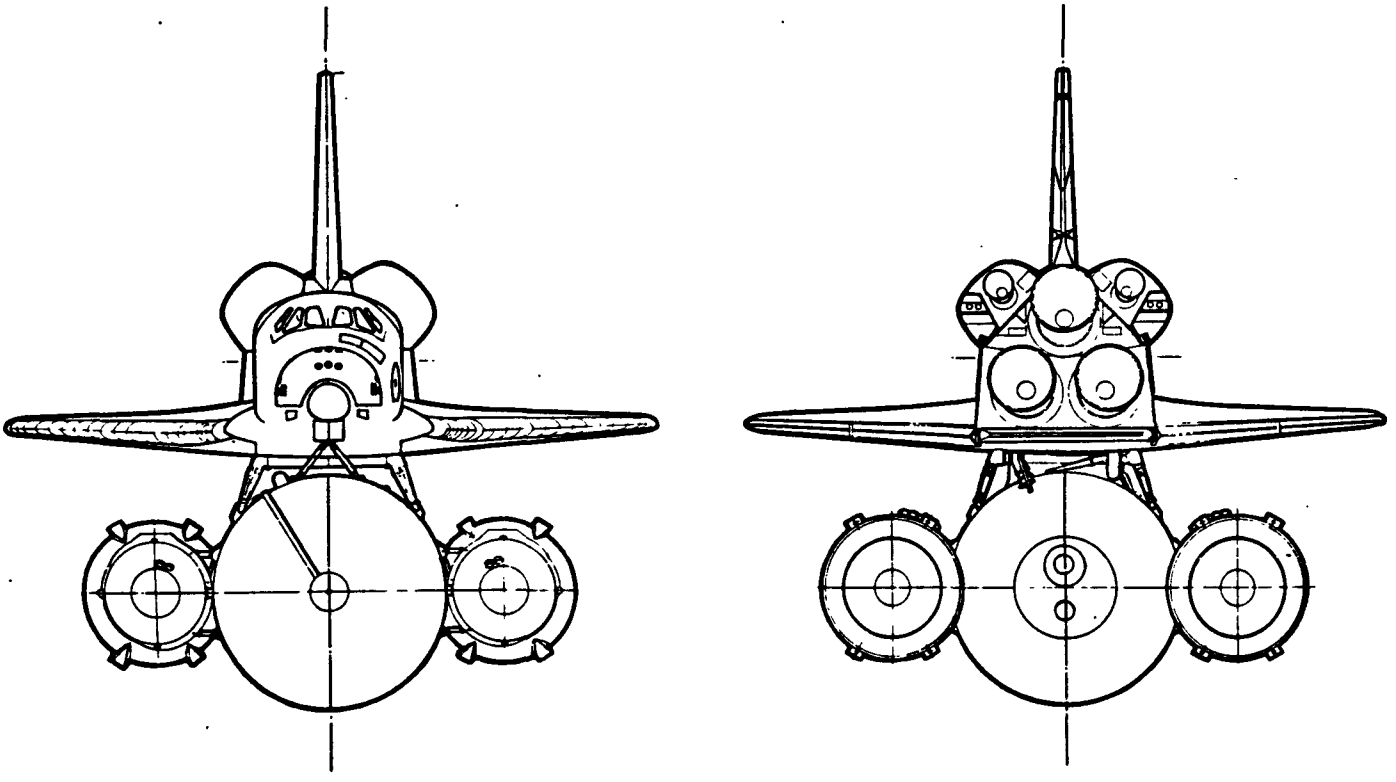

Figure 3-4. Shuttle Vehicle, Front and Back Views

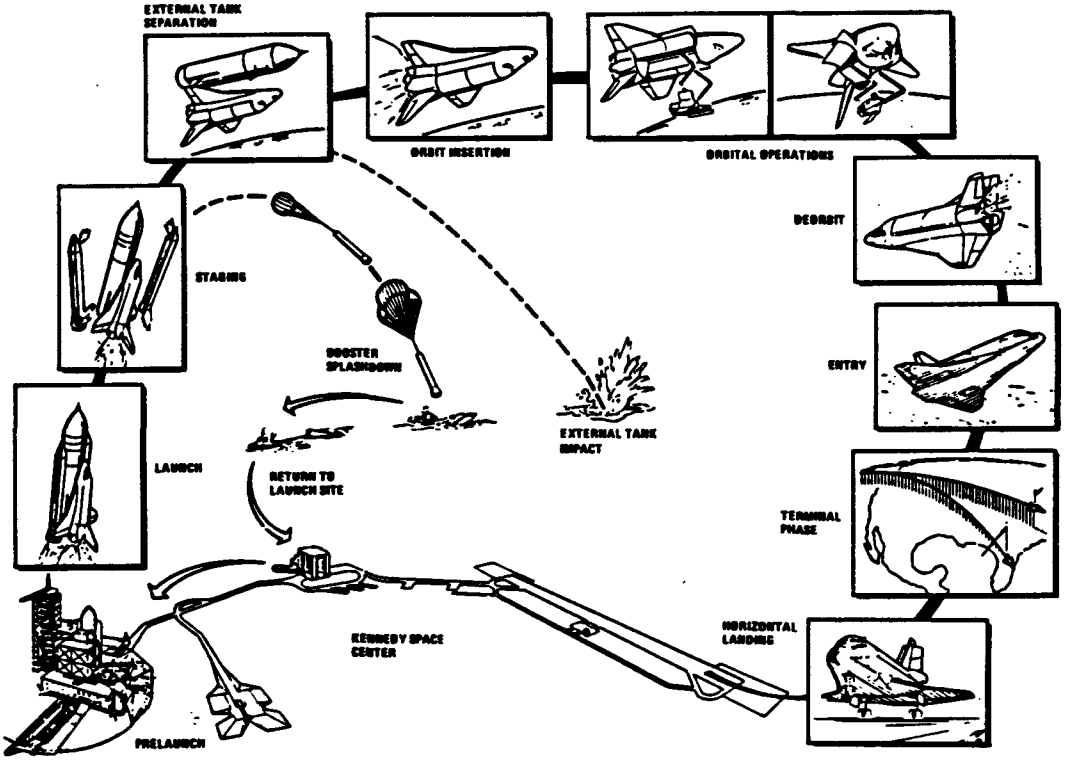

Figure 3-5. Basic Mission Cycle for Shuttle

are started in sequence about 6.6 seconds before lift-off, will cause lift-off to occur.

Each SRB provides 12.9 million Newtons (2.9 million pounds) of thrust at sea level and contains 505,000 kg (1.11 million pounds) of propellant. The propellant is a composite type solid propellant formulated of polybutadiene acrylic acid-a-crylonitrile terpolymer binder, ammonium perchlorate, and aluminum powder with a small amount of iron oxide added as a burning rate catalyst. The nozzle of the SRB is gimbaled with hydraulic actuators for steering.

Figures 3-6 and 3-7 show the SRB's components and overall construction.

3.2.3 ORBITAL MANEUVERING SUBSYSTEM

The orbital maneuvering subsystem (OMS) includes two engines, located in pods at the top of the aft fuselage on either side of the vertical tail. The arrangement of these OMS pods is shown in Figure 3-8.

These engines provide thrust for carrying the Orbiter into orbit after the main engines are shut down, for maneuvering while in orbit, and for providing retrothrust to retard the Orbiter out of orbit for reentry. The rated (vacuum) thrust of each engine is 26,700 Newtons (6000 pounds). The fuel is monomethylhydrazine (MMH), and the oxidizer is nitrogen tetroxide (N_2O_4). The nozzles are gimbaled for steering with electromechanical actuators.

3.2.4 ORBITER REACTION CONTROL SYSTEM

The reaction control system (RCS) includes 44 thrusters (38 primary, 6 vernier) for attitude control and three-axis translation during orbit insertion, on-orbit, and entry phase of the Orbiter flight. The RCS propellants are MMH and N_2O_4. The thrust (in vacuum) is 3870 Newtons (870 pounds) for each primary thruster and 107 Newtons (24 pounds) for each vernier thruster.

3.2.5 EXTERNAL TANK

The external tank (ET) supplies the Orbiter main propulsion system with liquid hydrogen (LH_2) and liquid oxygen (LOX). The ET contain 703,000 kilograms (1.55 million pounds) of usable propellant for main engines at lift-off. At main engine cutoff (MECO), the ET is separated from the Orbiter before orbital velocity is achieved. The ET then proceeds on a ballistic reentry for a safe impact in the ocean. Figure 3-9 shows the ET construction.

3.2.6 RTGs LOCATION WITHIN SHUTTLE CARGO BAY

Presented in Figures 3-10 and 3-11 are views of the RTGs used in the Galileo spacecraft as they will be located within the Shuttle cargo bay in their launch configuration. Figure 3-10 shows the horizontal plane (X_O) within the cargo bay in which the mid-span points of the two RTGs for the Galileo spacecraft are located. Figure 3-11 is a view of that plane showing the Y_O and Z_O coordinates for those RTGs.

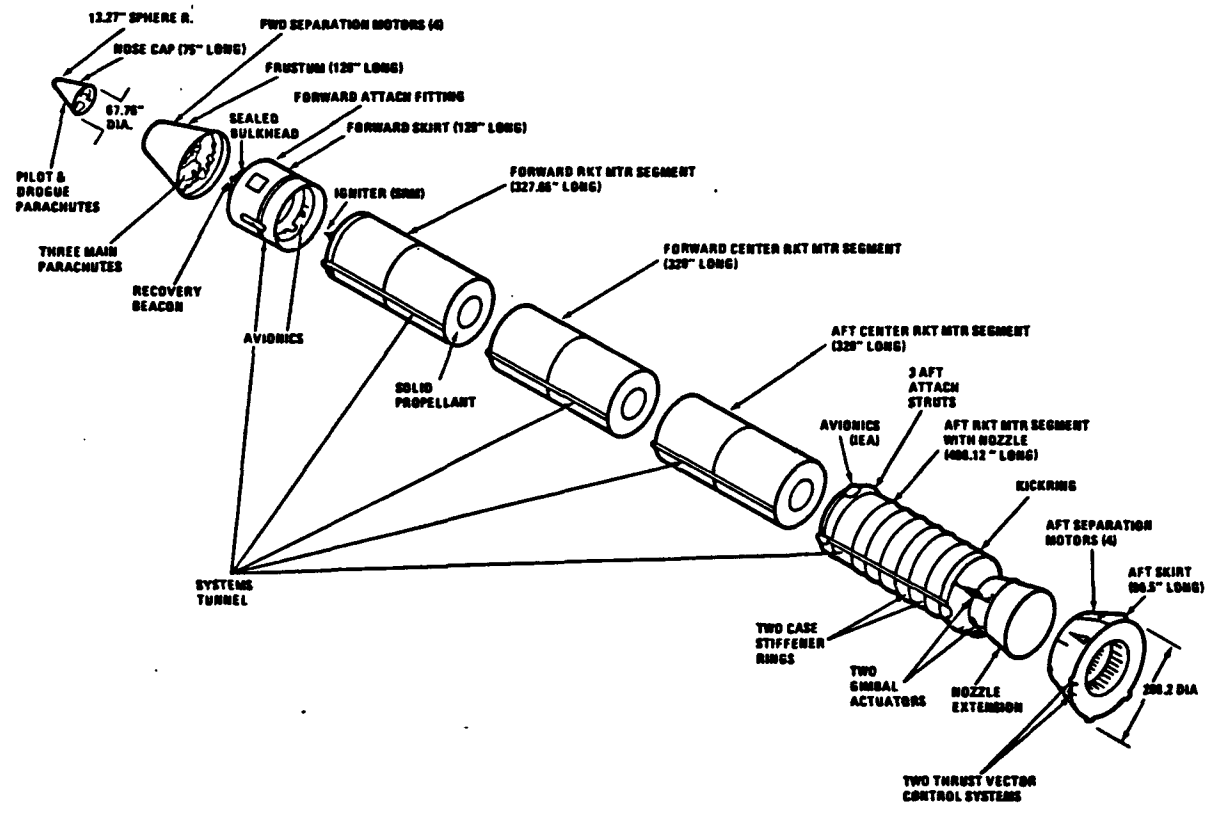

Figure 3-6. Solid Rocket Booster Parts

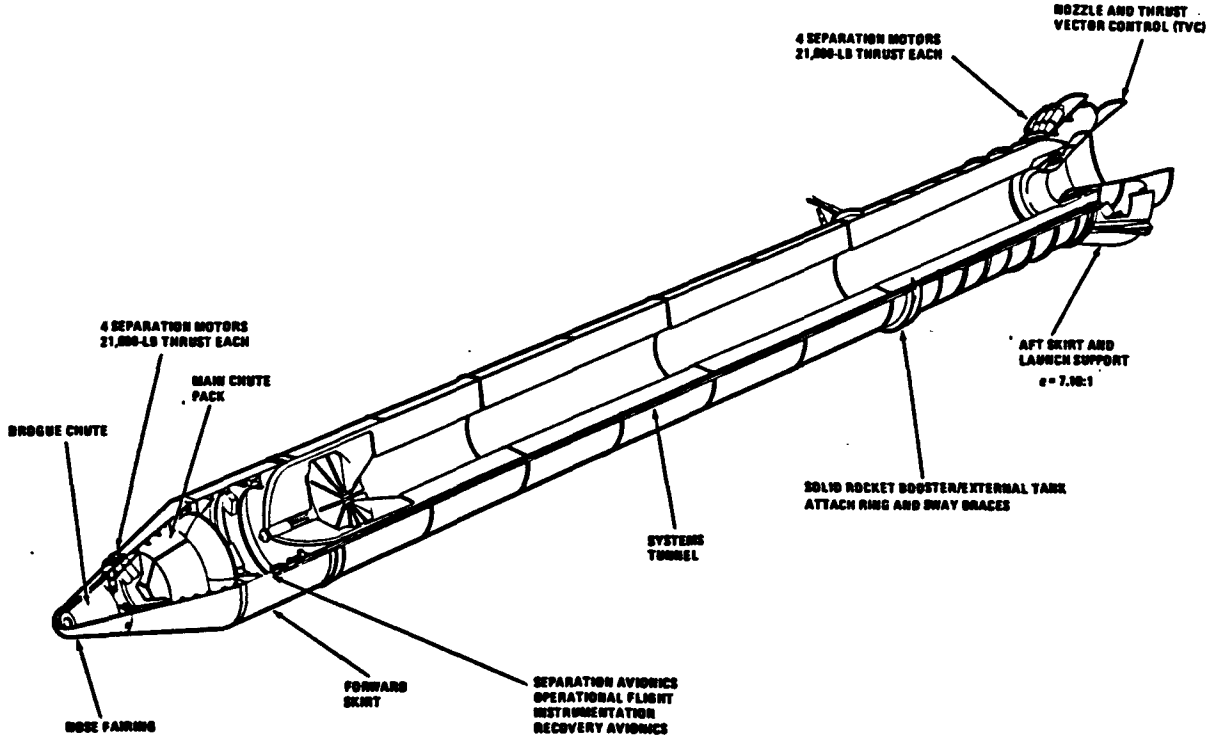

Figure 3-7. Shuttle Solid Rocket Booster

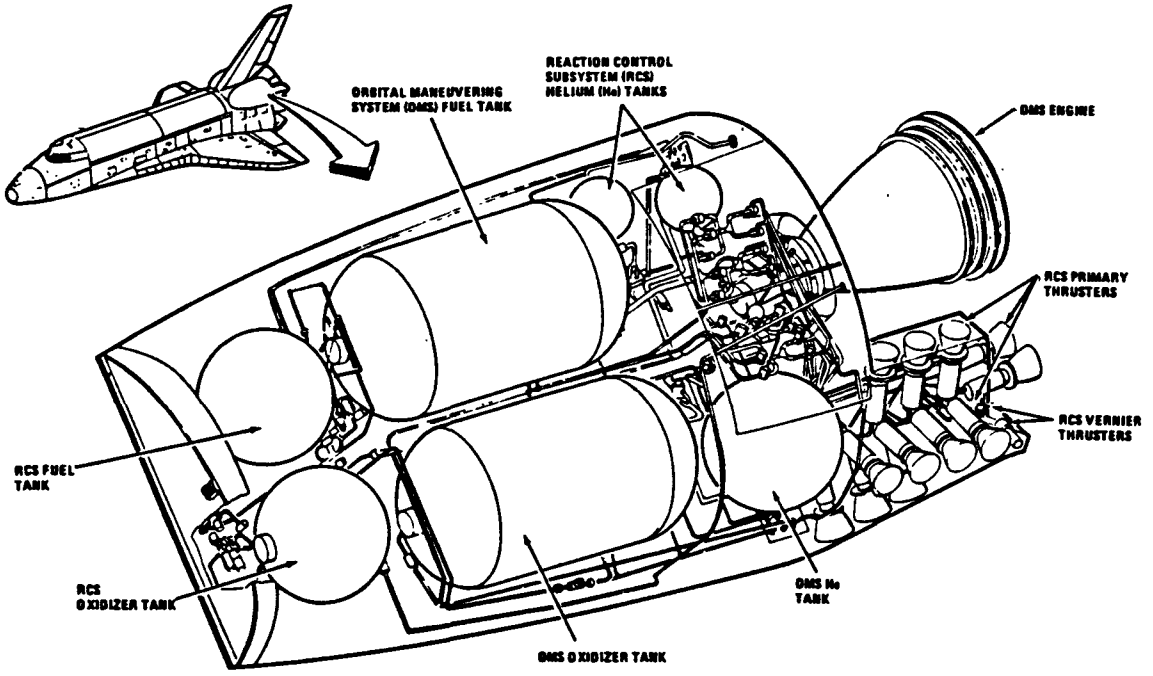

Figure 3-8. Orbital Maneuvering Subsystem Engine POD

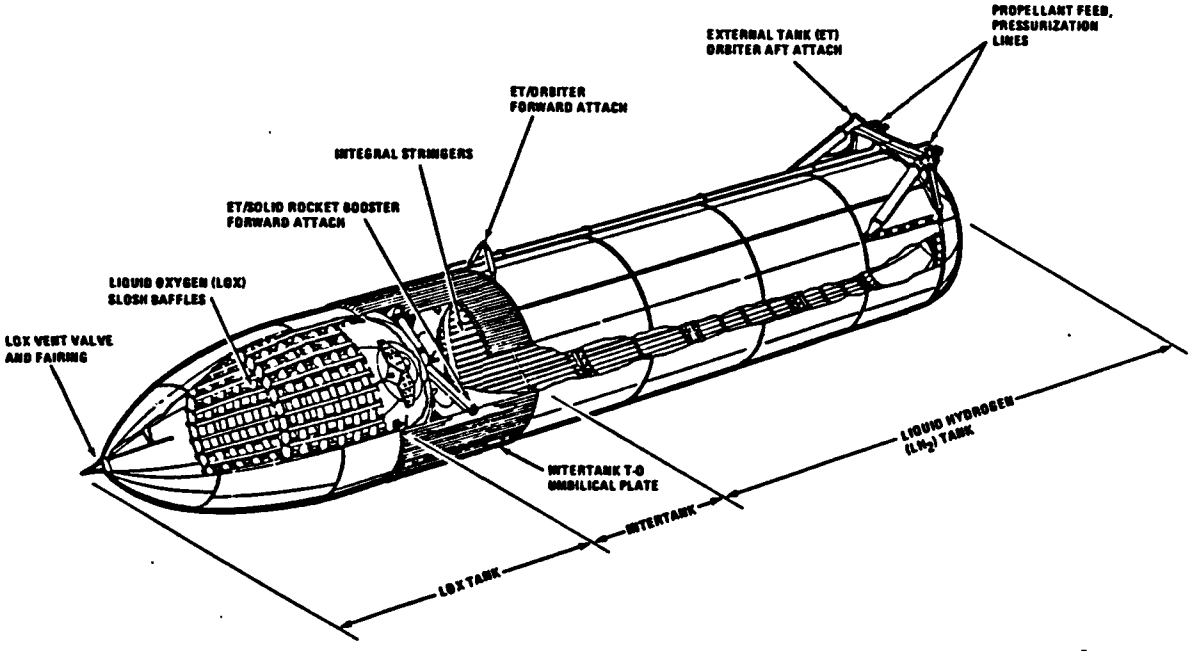

Figure 3-9. Shuttle External Tank

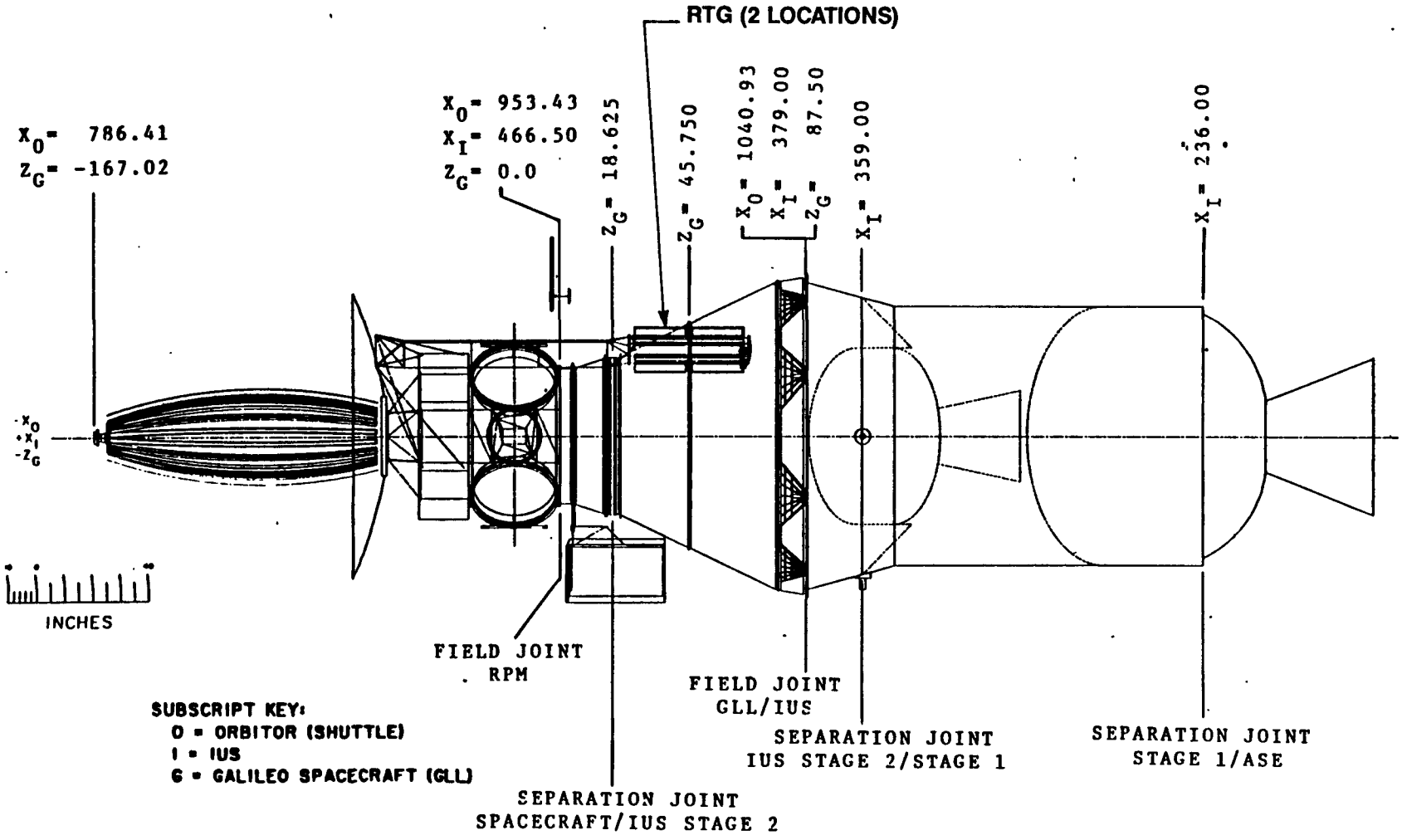

Figure 3-10. Galileo/IUS Configuration

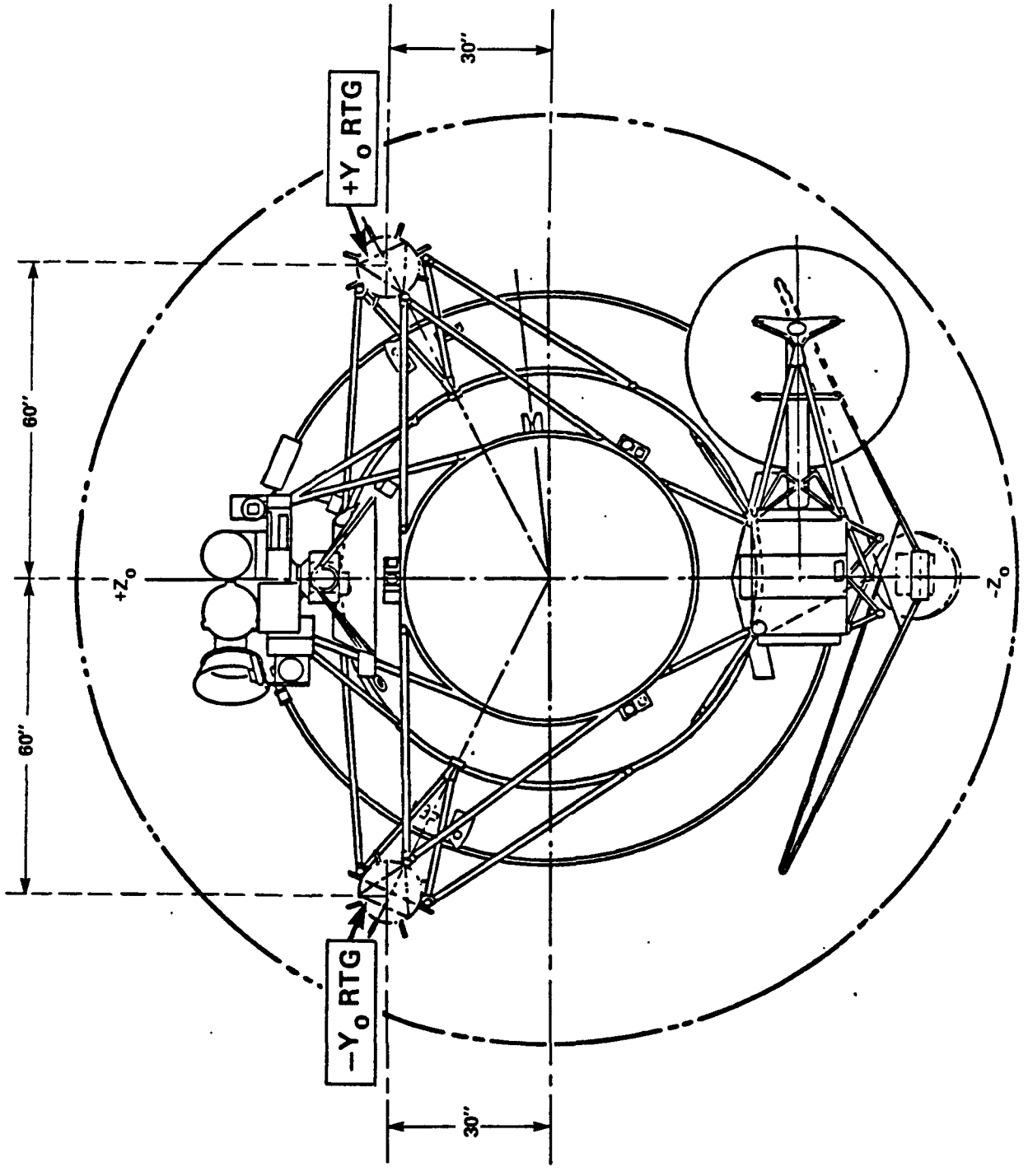

Figure 3-11. Mid-Span Locations of the $+Y_O$ and $-Y_O$ GPHS-RTGs on the Galileo Spacecraft

BLANK

SECTION 4.0

INERTIAL UPPER STAGE DESCRIPTION

4.1 GENERAL DESCRIPTION

The IUS vehicle is shown in Figure 4-1. The basic two-stage vehicle is 16.4 feet long, 7.6 feet in diameter in the cylindrical section, flaring to 9.5 feet at the forward end. The vehicle consists of two stages. The first stage includes the interstage structure, the large solid rocket motor and avionics that are only required prior to staging. The second stage has a smaller solid rocket motor and the equipment support section which houses the majority of vehicle avionics.

Major subsystems of IUS avionics are inertial guidance and navigation subsystem; a data management subsystem (DMS) to perform all computation, signal conditioning, data processing and formatting associated with the navigation, guidance control, and data management functions; a telemetry, tracking, and command subsystem for the communication function; and an electrical power subsystem. Vehicle attitude is controlled by gimbaled rocket nozzles during solid rocket burn and by hydrazine-fueled reaction control thrusters during coast flight. Navigation, guidance, and control functions are implemented by means of algorithms programmed in the digital computers of the DMS. Figure 4-2 is a simplified block diagram of the avionics system.

In addition to the IUS vehicle, airborne support equipment (ASE) is required to provide the mechanical and electrical interfaces between the IUS and the Orbiter.

The IUS employs the following subsystems:

IUS Structure,
Thermal Control,
Propulsion,
Reaction Control,
Guidance and Navigation,
Telemetry, Tracking and Command,
Electrical Power,
Data Management,
Thrust Vector Control,
Software,
Redundancy Management
Airborne Support Equipment
RTG Cooling.

A summary of each subsystem functions is included in the following paragraphs.

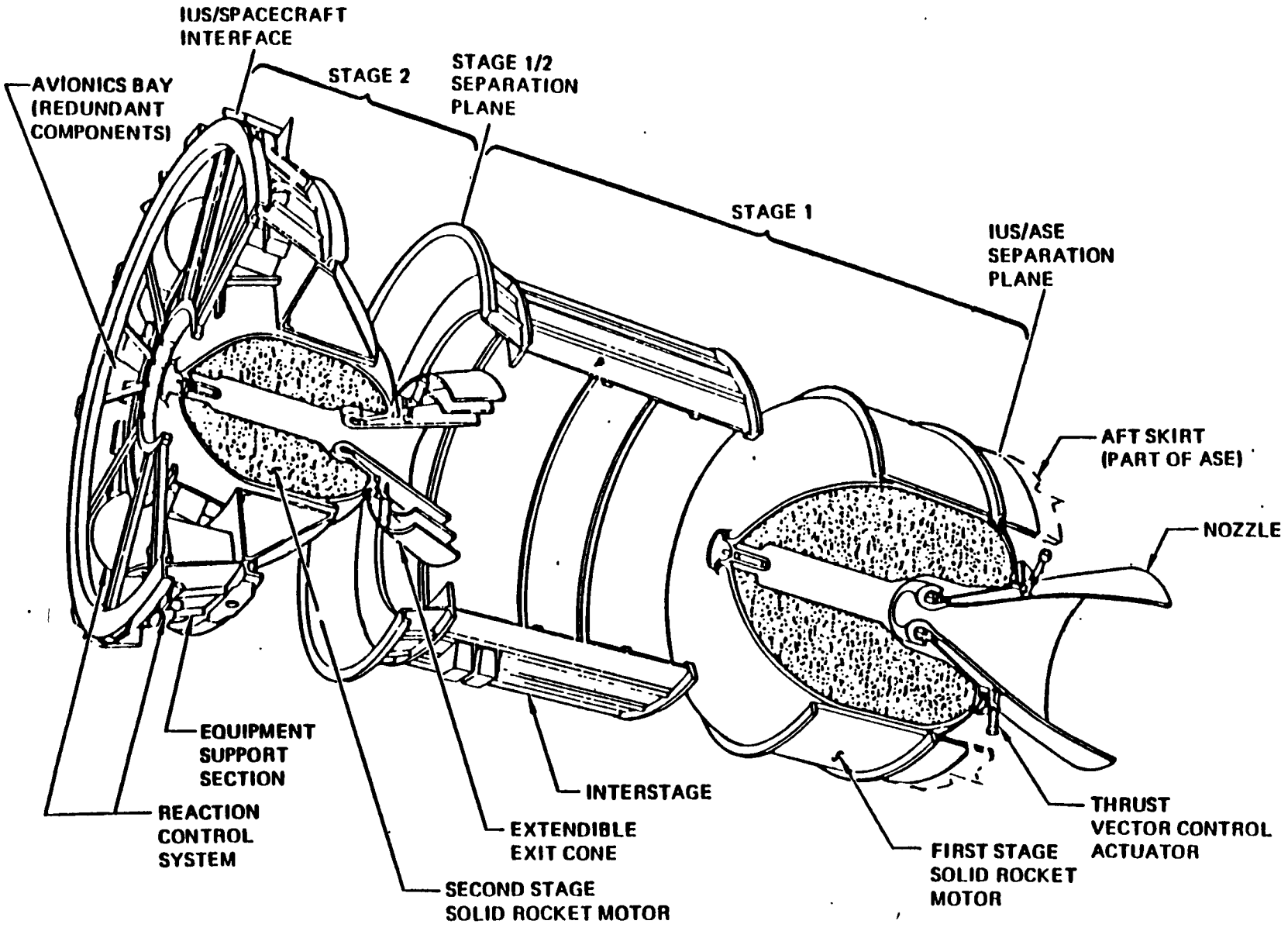

Figure 4-1. Two-Stage IUS Vehicle

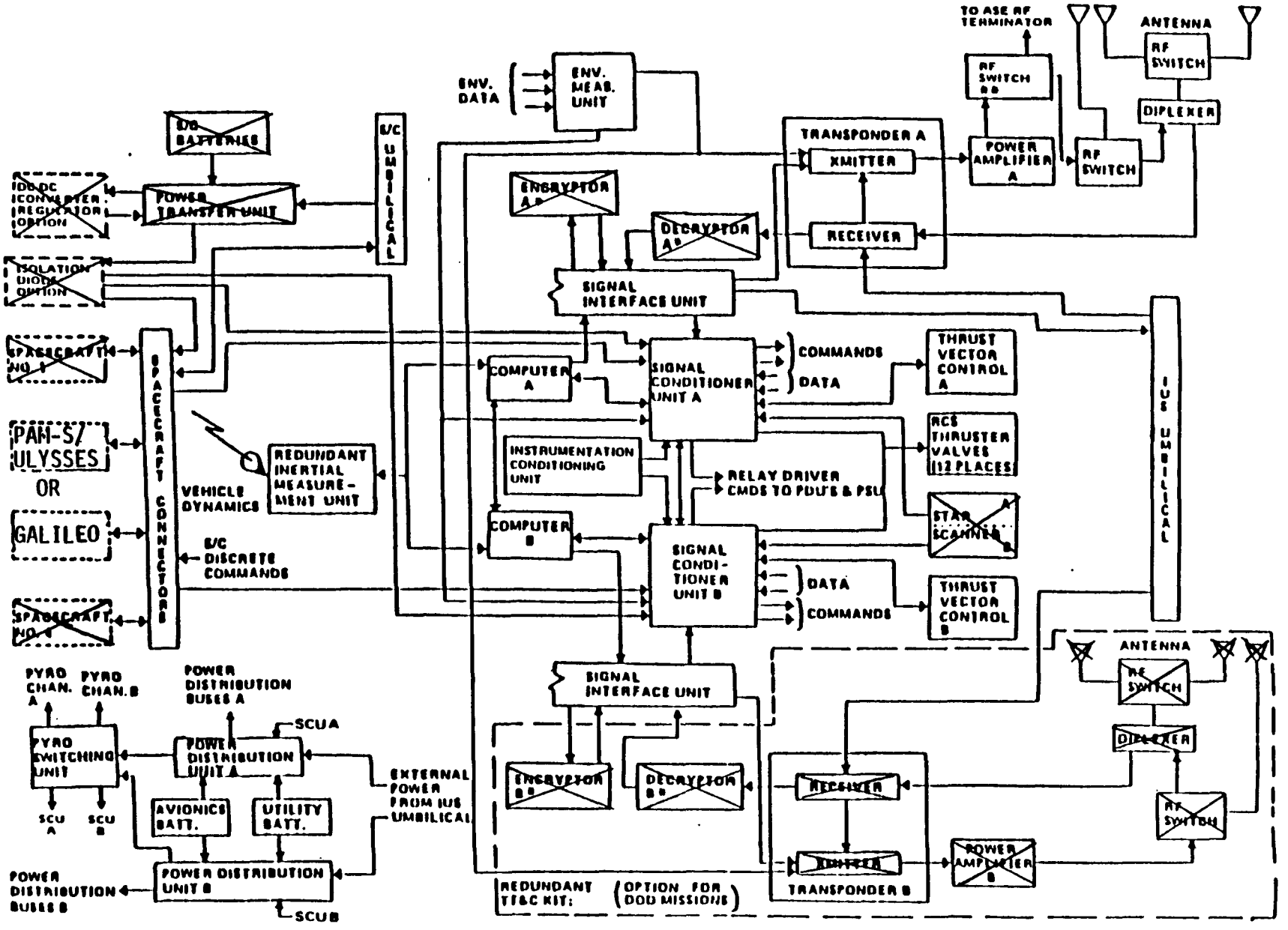

Note: Planetary configuration shown

Figure 4-2. IUS Avionics System Block Diagram

4.2 IUS VEHICLE

4.2.1 IUS STRUCTURE

The major structural assemblies for the two-stage vehicle are shown in Figure 4-3 and include the equipment support section (ESS), the interstage and the aft shirt. The ESS structure includes a 20 inch long external conical section of aluminum skin/stringer/longeron construction, a support cone for the stage 2 motor and internal framing to support the avionics and cabling. Three panels located on the outside of the ESS provide access to the internal avionics. The spacecraft is attached to the forward ESS ring via an adapter. The interstage is attached to the aft end of the ESS with eight separation bolts and serves as the separation plane between the first and second stages. The interstage is constructed of aluminum skin with external stringers and longerons and internal ring frames. The first stage batteries and stage 1 motor safe and arm devices are mounted on the outside of the interstage. The aft end of the interstage bolts directly to the forward end of the stage 1 motor. An aft shirt provides the structural interface and separation joint between the vehicle and the ASE. The skirt is considered part of the ASE and bolts directly to the aft ring of the stage 1 motor. Separation is accomplished by a contained linear charge which runs around the circumference of the aft skirt.

4.2.2 THERMAL CONTROL

The thermal control subsystem comprises active and passive elements. Heaters are used on reaction control subsystem components, batteries and the redundant inertial measurement unit. Passive thermal control is achieved by selective application of exterior coatings, blanket insulation and thermal isolators.

4.2.3 PROPULSION SUBSYSTEM

The propulsion subsystem includes the following components:

Safe and Arm (S&A) Devices,
Ordnance Train Assemblies (OTA),
Solid Rocket Motors (SRM),
Extendible Exit Cones (EEC) (SRM-2 only).

The propulsion subsystem (Figure 4-4) provides the primary IUS vehicle propulsion and consists of two solid rocket motors (SRMs), each with a vectorable nozzle and an independent redundant motor ignition system. Refer to Table 4-1 for SRM leading particulars. Following deployment from the Orbiter, the two first stage S&A devices are armed, and the first stage SRM is ignited. Following the first stage burn, the vehicle performs a vernier velocity correction maneuver with the reaction control system (RCS) to compensate for SRM total impulse dispersions. After coasting, the expended first stage SRM and the interstage are separated from the second stage. The two second stage S&A devices are armed, and the second stage SRM is ignited. Following second stage burn, a second RCS vernier correction is made, and spacecraft separation is performed.

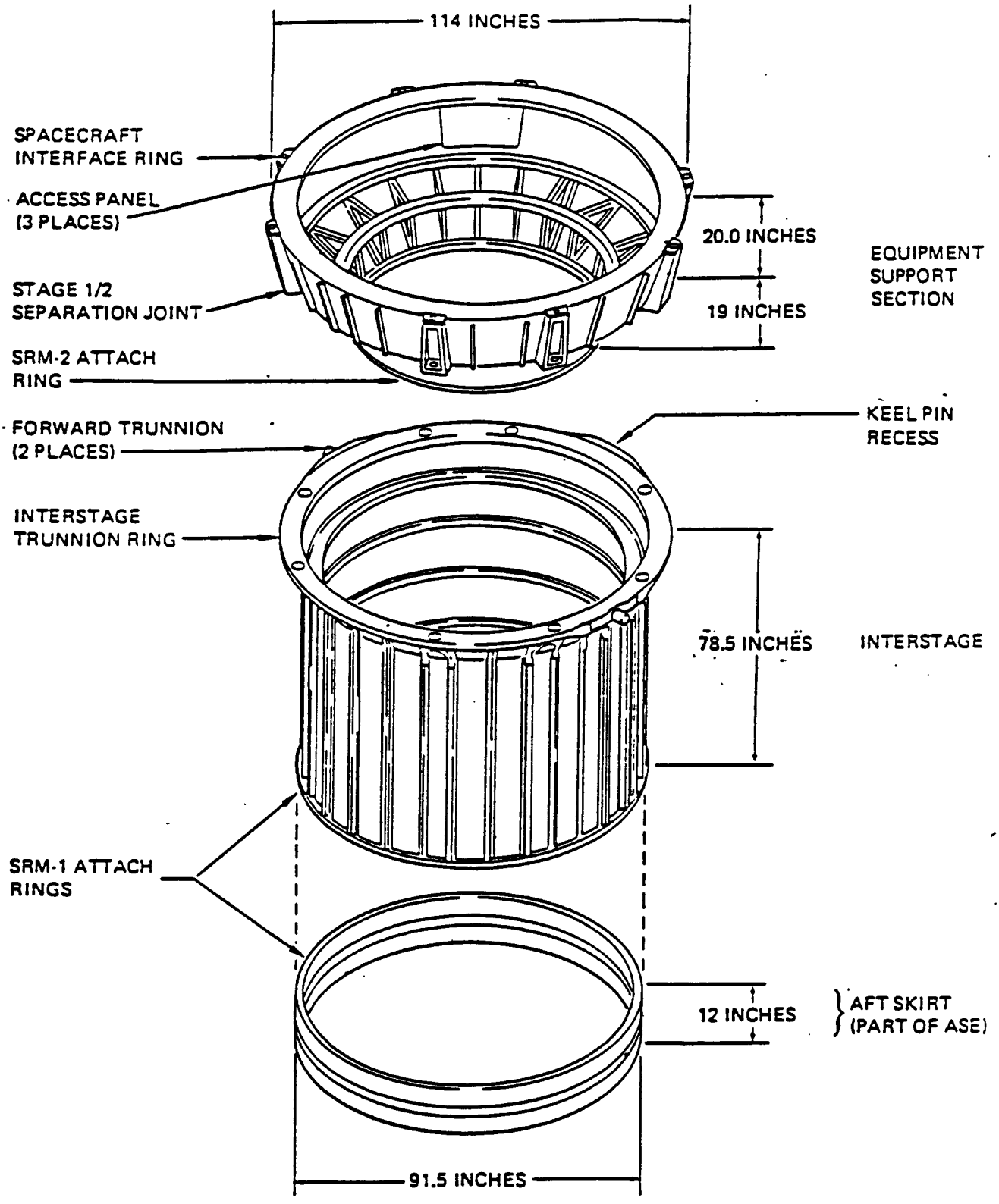

Figure 4-3. IUS Vehicle Structure

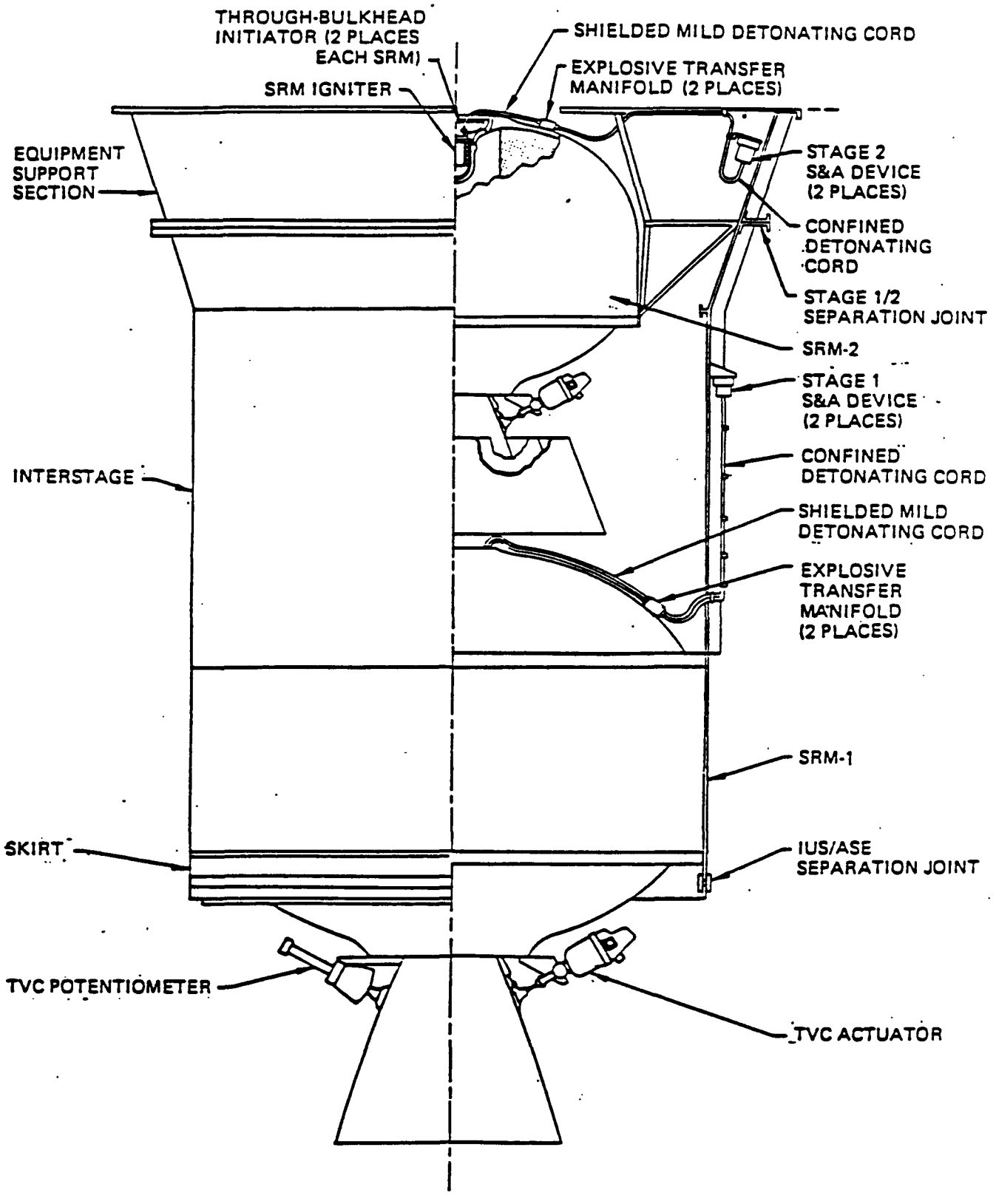

Figure 4-4. IUS Propulsion Subsystem

Table 4-1. SRM Leading Particulars

SRM DESCRIPTION AND PERFORMANCE	SRM-1	SRM-2	
		WITH EEC	WITHOUT EEC
Motor Description:			
Overall length, in.	124	77.98 (Stowed) 117.85 (Extended)	74.2
Case diameter, in.	92.0	63.3	63.3
Total loaded weight, lb. m.	22,907	6689	6598
Propellant weight, lb. m.			
Onload motor (Note 2)	21,580	6059	6059
Full load motor	21,400	6000	6000
Offload motor (max. offload)	10,700	3000	3000
Igniter propellant weight, lb.	3.8	1.8	1.8
Nozzle length, in.	59.3	36.68 (Stowed) 76.55 (Extended)	32.9
Nozzle throat diameter, in.	6.480	4.207	4.207
TVC capability, deg.	4° Max	7° Max	7° Max
Motor Performance (16°C):			
Duration time, sec. (Note 3)	149.2	109.3	109.3
Average pressure, psia	621.8	564.3	564.3
Maximum pressure, psia	838.6	797.1	797.1
Average thrust, lb. f.	42190.7	16742.3	15945.8
Maximum thrust, lb. f.	57483.6	23664.0	22538.3
Average expansion ratio	57.53	161.63	44.02
Average effective ISP, sec.	293.3	301.2	286.9
Total Impulse, lb. sec.	6292237	1829868	1742811

Note 1: Total loaded weight, nozzle throat diameter and motor performance data is applicable to motors with the baseline propellant load configuration:

SRM-1 - Full load (100%) propellant
SRM-2 - Onload (101%) propellant

Note 2: "Onload" motors are motors machined with a "skin cut" which removes the minimum amount of propellant necessary to insure ignition. These motors, in contrast to the other motors, are machined to a dimension instead of a weight and the propellant weight shown is a nominal weight. This propellant load provides maximum motor performance and is the baseline load for SRM-2 motors and is an option available on certain SRM-1 motors. Onload motors will be used for planetary missions.

Note 3: Duration time is defined as the time from the ignition signal until the burn area equals zero.

Each solid rocket motor is provided with a redundant ignition system comprising two safe and arm devices, a dual path explosive transfer assembly, two through-bulkhead-initiators, and a single motor igniter. The motor ignition S&A devices are armed by computer command via the respective power distribution unit (PDU) just prior to issue of the fire signal. Fire signals are issued simultaneously by both computers via the pyro switching unit (PSU) to the dual detonators in each S&A device. The explosive output of each detonator is conducted by lengths of confined detonating cord (CDC), explosive transfer manifolds, and lengths of shielded mild detonating cord (SMDC) to the through-bulkhead-initiators installed in the motor igniter. The through-bulkhead-initiators propagate the detonation impulse across a pressure bulkhead to initiate the motor igniter. The two explosive transfer manifolds are inert blocks that provide a "Y" junction where the dual CDCs converge to a single SMDC.

All IUS solid rocket motors are of similar construction and materials but are provided in two sizes, large and small, with variable propellant loads available to satisfy mission requirements. The large rocket motor (SRM-1) (Figure 4-5) is 92 inches in diameter, has a vectorable nozzle, and is used as the first stage motor on all IUS vehicles. The small rocket motor (SRM-2) (Figure 4-6) is 63 inches in diameter, has a vectorable nozzle with extendible exit cones (EEC), and is used as the second stage motor. Major design differences between the solid rocket motors are tabulated in Table 4-1. Each solid rocket motor consists of an igniter, a loaded motor case, and a vectorable nozzle assembly.

An SRM igniter is installed in the forward dome of each SRM (see Figures 4-5 and 4-6) and initiates the burning of the rocket motor propellant grain upon receipt of detonation impulse through one or both of the through-bulkhead-initiators. The igniter used on large rocket motors is of the same design as the igniter used on the small rocket motors, differing only in size. The igniter consists of an insulated aluminum propellant case and mounting adapter, an intermediate charge and a propellant cartridge. The igniter is attached to the forward motor dome by a threaded retaining ring and becomes an integral part of the rocket motor pressure vessel. The igniter is initiated by a detonation impulse transmitted through either or both of the through-bulkhead-initiators. The initiators ignite the intermediate charge composed of boron potassium nitrite (BKNO3) pellets. The resulting hot gases pass through holes in the pellet retainer plate and ignite the main igniter propellant charge which discharges hot gases out three exhaust nozzles to ignite the rocket motor propellant grain.

The motor case is constructed of filament-wound, epoxy-bonded Kevlar fibers and is insulated with rubber. The propellant used in all motors is cast in a tubular grain and consists of hydroxy-terminated polybutadiene (HTPB) binder (14 percent), aluminum (18 percent) and ammonium perchlorate (68 percent). After propellant casting, the center cavity of all motors is machined at the manufacturer's facility to provide the required propellant load. On motors requiring maximum performance, the propellant is "skin cut" which removes only the minimum amount of propellant necessary to insure good ignition. These skin cut motors are designated "onload" motors and are machined to a dimension instead of to a weight. This "onload" is the basic propellant configuration

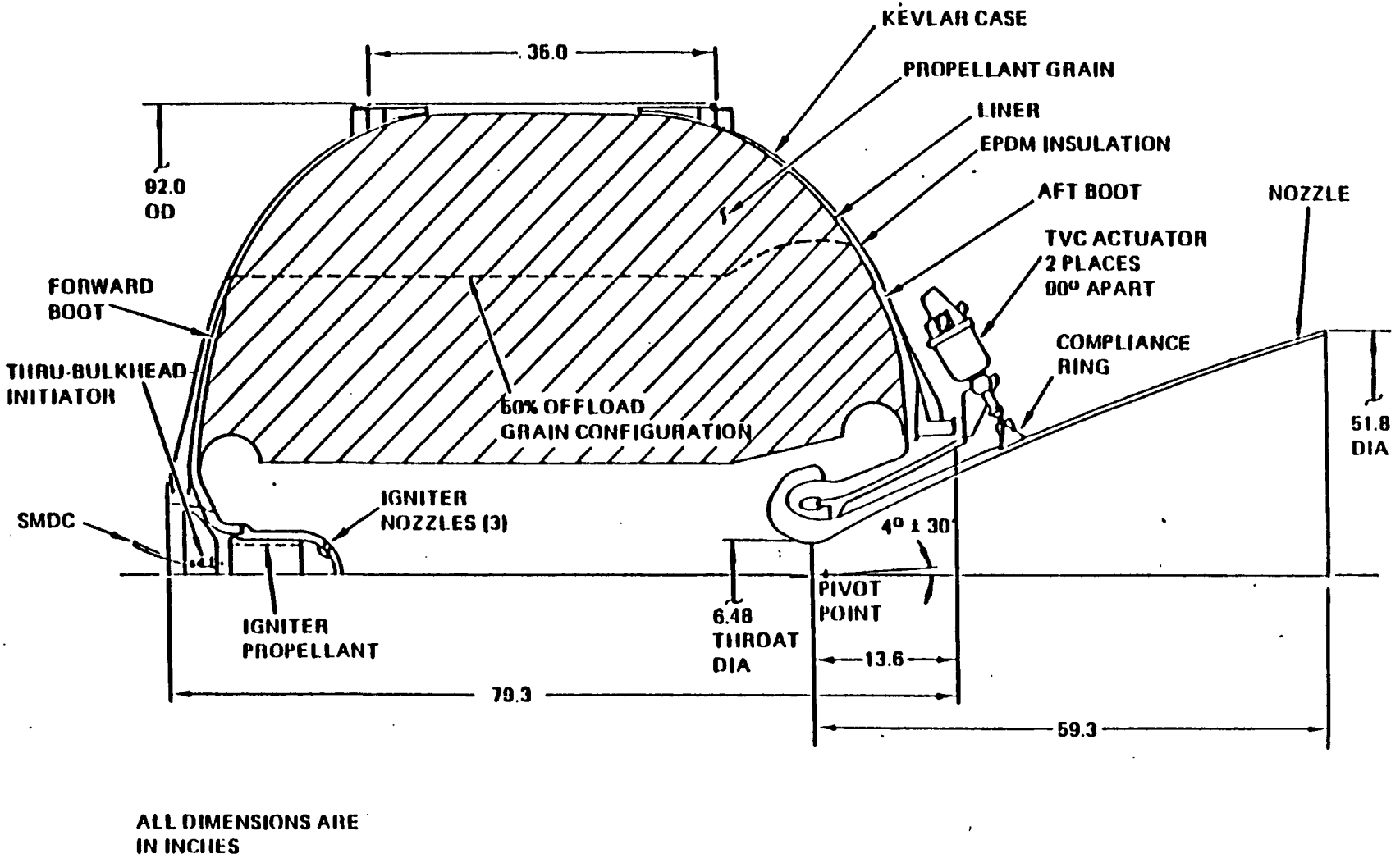

Figure 4-5. Solid Rocket Motor SRM-1

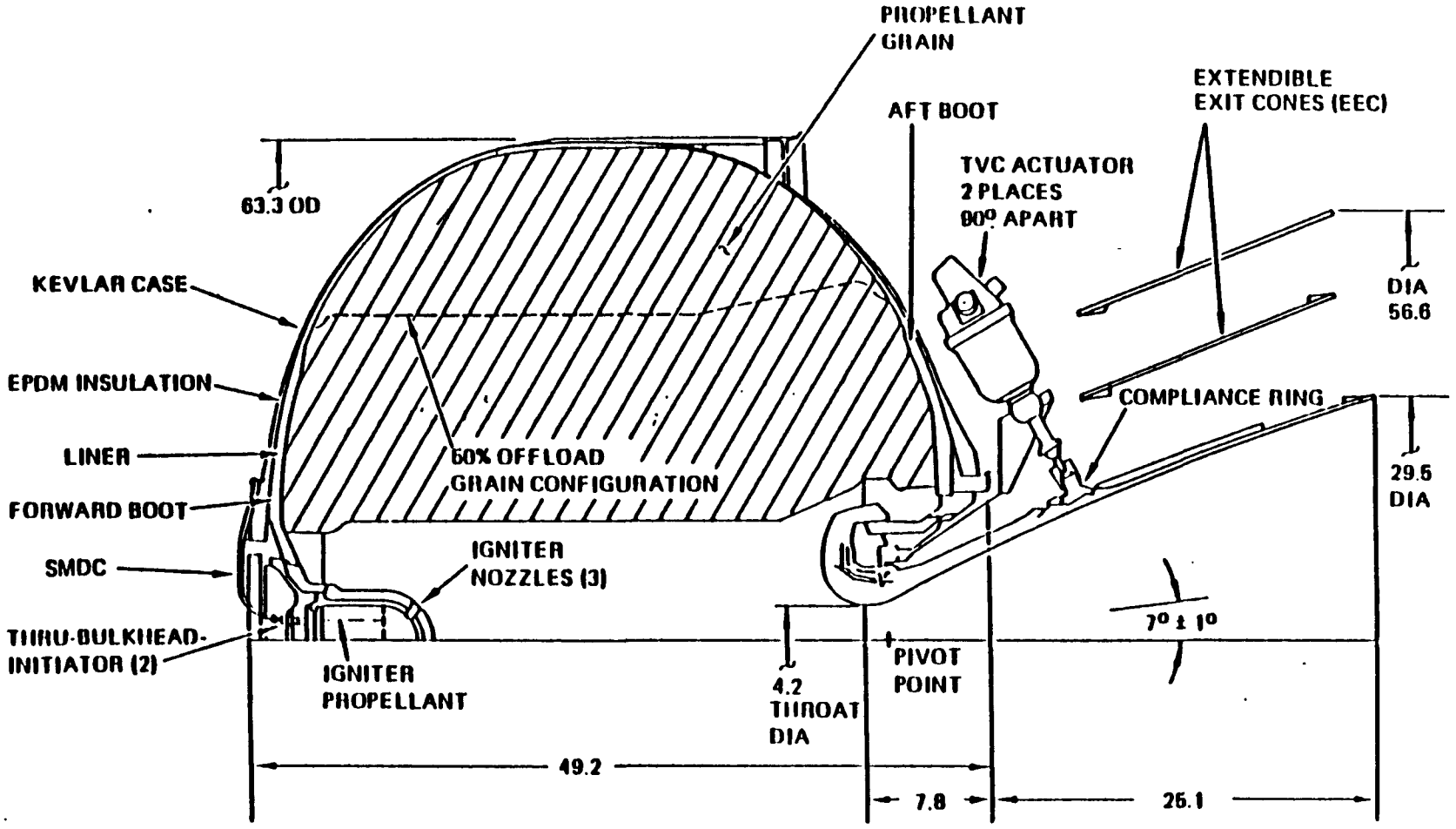

ALL DIMENSIONS ARE IN INCHES

EXTENDIBLE EXIT CONE DEPLOYMENT MECHANISM NOT SHOWN

Figure 4-6. Solid Rocket Motor SRM-2

for SRM-2 motors. It also is an option available on certain SRM-1 motors that have adequate case insulation thickness and suitable burn rate characteristics. All SRMs used for the planetary missions will be "onloaded" motors. A "full load" motor is machined to a standard weight and contains slightly less propellant than does an onload motor. In order to accommodate wide variations in mission requirements and payload weights, all motors are capable of being offloaded up to 50 percent of the full propellant load. Offloading is accomplished by machining propellant from the center of the propellant grain and tailoring the nozzle throat diameter. An insulation blanket comprised of multiple layers of aluminized kapton is fitted around each motor to prevent temperature gradients between the motor case and the propellant grain. The cylindrical sides of the SRM-1 motor case also carry IUS vehicle structural loads, and integral skirts are provided at the forward and aft end for bolt attachment to the vehicle structural sections. SRM-1 motor case thickness varies from a minimum of 0.173 inch, in the forward and aft domes adjacent to the shirt Y-joints, to approximately 0.56 inch at the midpoint of the cylindrical sides. SRM-2 motors are attached to the IUS vehicle through a single aft attachment ring.

Motors SRM-1 and SRM-2 utilize a partially submerged vectorable nozzle to provide directional control during motor burn. The nozzle pivots at the forward end, and cone deflection is controlled by two motor-driven, ballscrew actuators located 90 degrees apart. A potentiometer unit mounted opposite each actuator is electrically coupled with a potentiometer element within the actuator to close the servo loop and provide position instrumentation. Nozzle vector control is provided by either of the two independent, redundant TVC controllers located in the ESS. A staging command from the SCU switches controller outputs from stage 1 actuators to stage 2 actuators. The TVC controllers, actuators and potentiometers are part of the TVC subsystem and are described in Section 4.2.9. The flame-side of the nozzle is fabricated from carbon/carbon composite materials of an axisymmetric three-dimensional structure for the throat and entrance sections and a two-dimensional rossette structure for the exit cone. A closure is fitted to the nozzle to seal the motor interior until ignition occurs. The closure will fail at ignition and leave the nozzle contour unrestricted. Nozzles installed on baseline SRM-2 motors are equipped with a two-segment, extendible exit cone (EEC) which is deployed prior to motor ignition to improve motor performance. SRM-2 motors without EEC are available as an option. SRM-2 motors without EEC utilize the same TVC system and are identical to motors with EEC except that the two extendible cone segments and their deployment mechanisms and control circuit are not installed. The Galileo mission utilizes an EEC.

4.2.4 REACTION CONTROL SUBSYSTEM

The IUS reaction control subsystem (RCS) includes the following components:

Propellant Tank Assemblies,
RCS Manifold Assembly,
Rocket Engine Module (REM)

The reaction Control Subsystem (RCS) performs the thrust functions required for coast attitude control, SRM powered flight roll control, vehicle maneuvers, velocity vernier for SRM impulse dispersions, and spacecraft collision avoidance maneuvers. The thrust functions are controlled by commands generated by the guidance and control functions of the operational flight software described in paragraph 4.1.10. These commands are issued through the SCU valve drivers. The RCS propellant remains sealed in the RCS tanks until after the IUS is deployed and is a safe distance away from the Orbiter. The RCS isolation valves are normally automatically actuated by the IUS self-initialization system 10 minutes after separation from the Orbiter. This delay represents the minimum delay assuring a 200 foot safe separation distance. Operation of the RCS is inhibited during stage 1/2 staging and at spacecraft separation. See Figure 4-7 for RCS schematic and Figure 4-8 for RCS component layout.

The RCS is a monopropellant hydrazine, blowdown-pressurized (non-regulated) system. The system uses six rocket engine modules (REM). Each module comprises two identical (except for nozzle orientation) catalytic decomposition thrusters. The distribution manifold delivers propellant from the tanks to the six REMs. Included in the REMs are redundant heater assemblies for each catalyst bed and control valve assembly. The primary thermal concerns are to maintain all the propellant passages above the freezing temperature of hydrazine (+1.7°C) prior to RCS activation. After RCS activation REM heaters are deenergized and temperatures are maintained by periodic thruster pulsing. All line and tank heaters are part of the thermal control subsystem. The basic RCS configuration contains two propellant tanks and a two-tank compatible manifold. One-tank and three-tank RCS configurations are optional and require compatible manifold assemblies. The planetary mission will fly with the one-tank configuration; the one tank will be loaded with only 32 pounds of propellant for Galileo.

The RCS propellant tank assembly (PTA) includes the tank structure, fill valves, thermal control heaters and MLI, and the isolation valve.

The RCS tanks are 21-inch diameter spherical units made of titanium (Ti-6Al-4V) and equipped with an internal elastomeric diaphragm for positive expulsion. See Figure 4-9. The propellant tank is mounted on brackets at the trunnions. One trunnion is secured with a large hex nut that clamps to the support bracket. The other trunnion is a slip fit in its mount to provide for expansion. Each tank is loaded with propellant and pressurized prior to installation in the IUS. The nominal internal volume of each tank is 4646 cubic inches (4570 cubic inch minimum), and the normal propellant load is 122.5 pounds (3370 cubic inches) of hydrazine (N_2H_4). After loading, the pressurant side is charged with nitrogen/helium (85/15 percent) mix to 400 to 405 psia at 21°C (70°F). This pressure decays approximately 3 to 5 psia in the first two weeks after loading as some pressurant migrates through the diaphragm and goes into solution with the hydrazine. The rated tank operating pressure is 430 psia with a design burst pressure of 1720 psia. At propellant depletion, approximately 110 psia pressure remains in the tank. A summary of the propellant budget for a 2-stage STS/IUS GSO mission with two propellant tanks is provided in Table 4-2. To minimize leakage, the tank, propellant fill valve, pressurant valve, isolation valve, pressure switch and the related fittings are welded and are tested as an assembly.

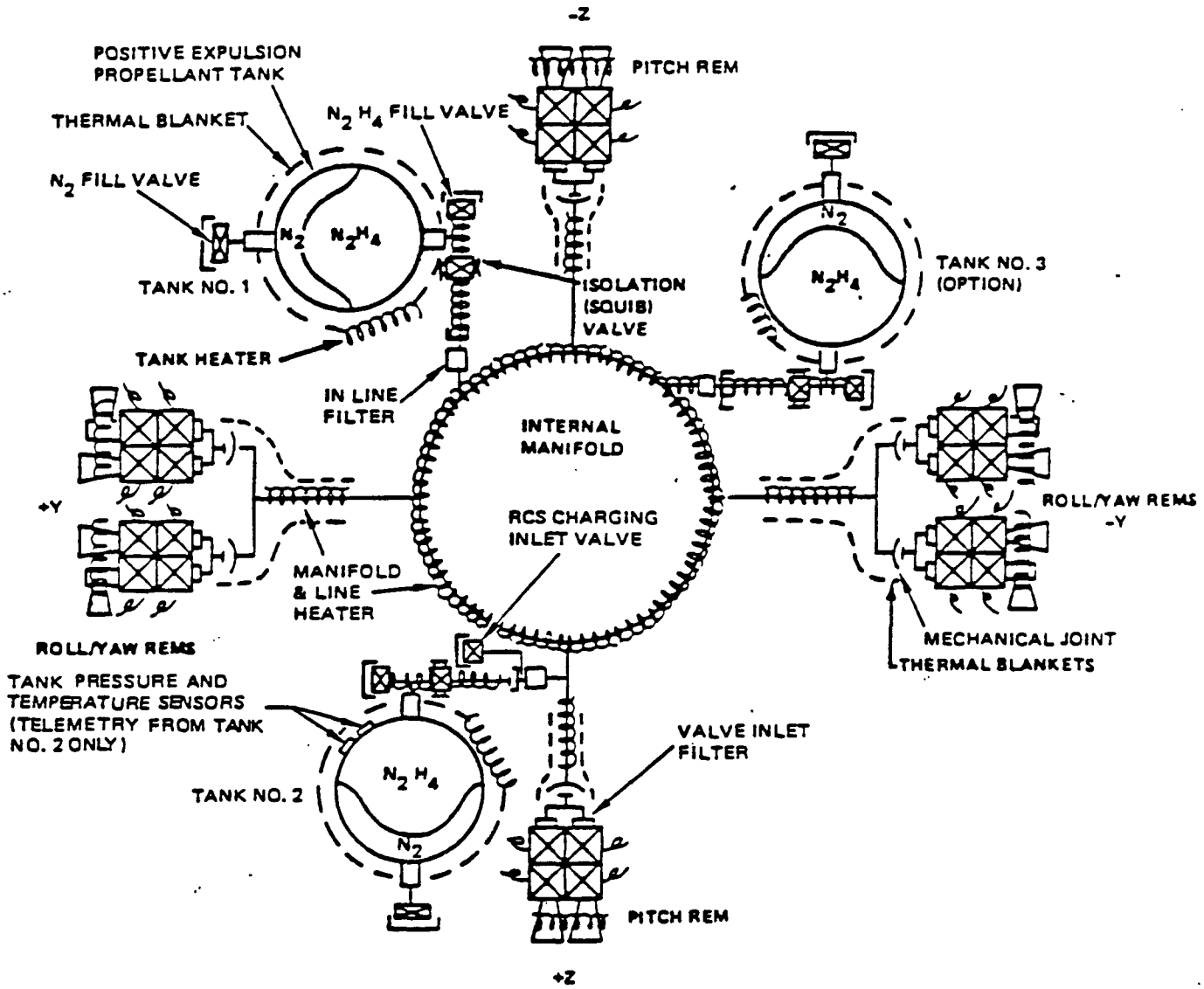

Figure 4-7. Reaction Control System Schematic

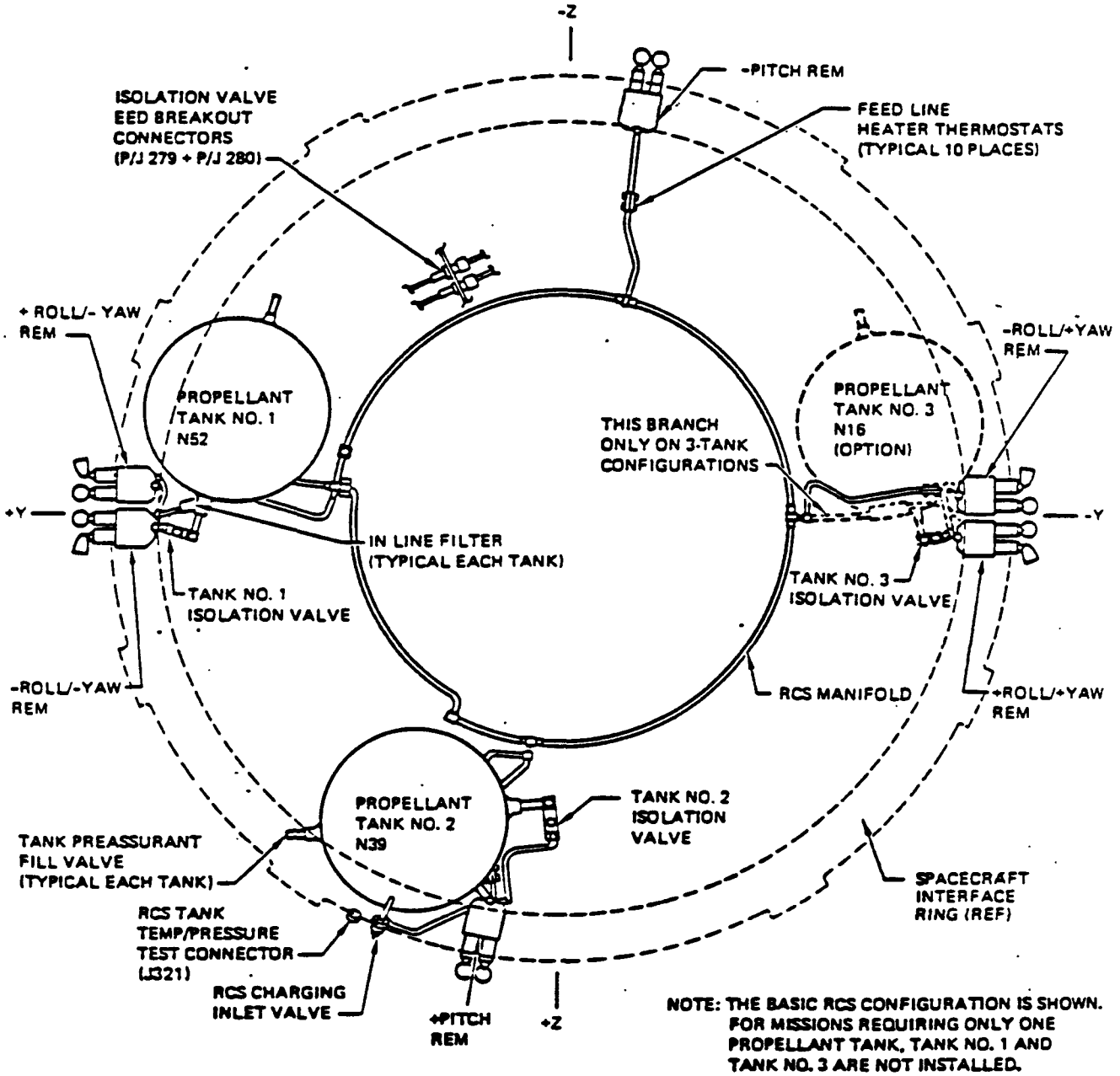

Figure 4-8. Reaction Control System (RCS)

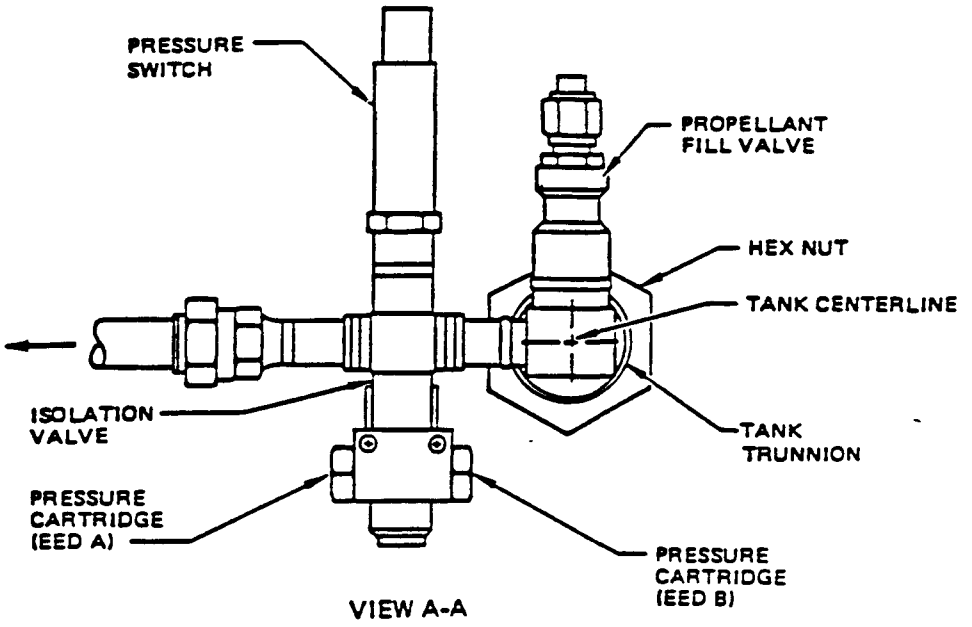

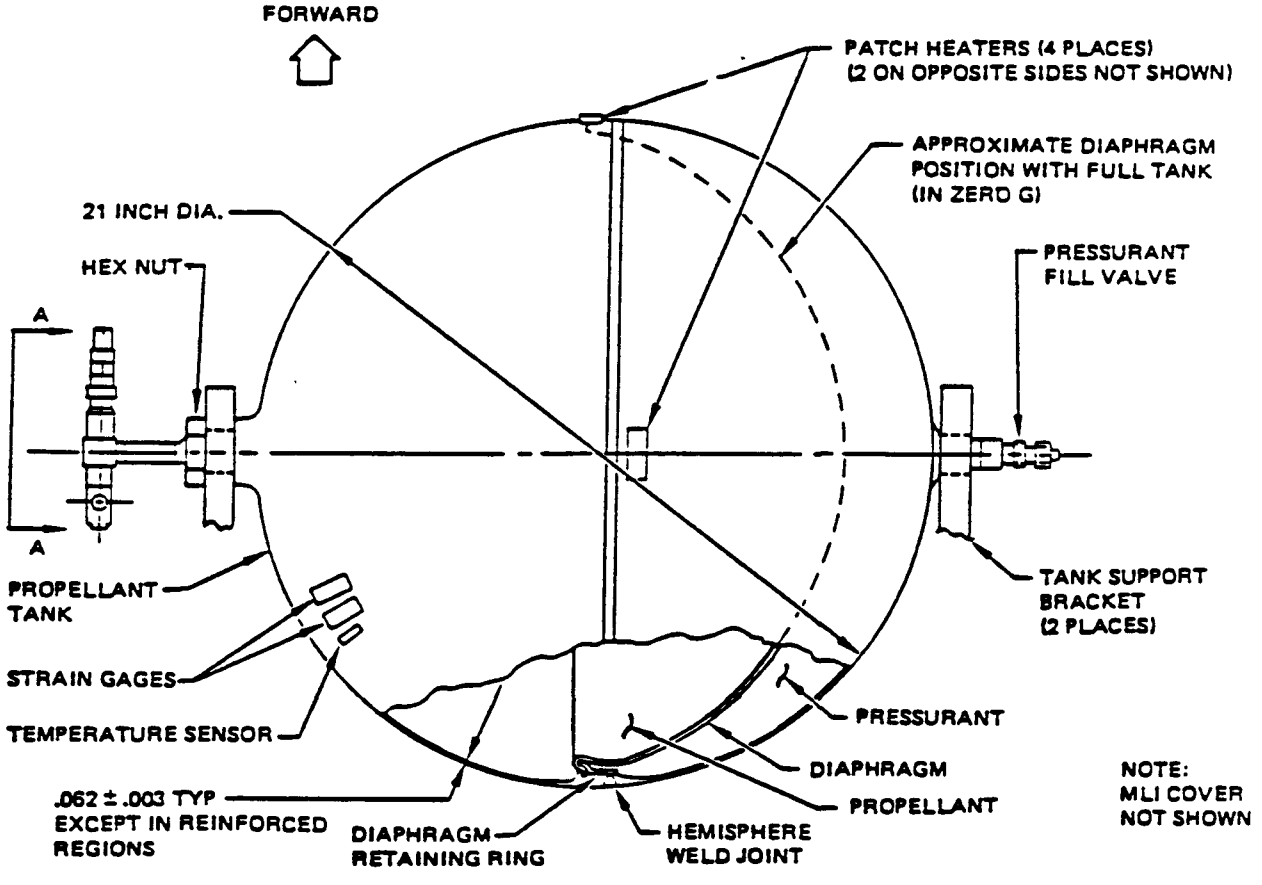

Figure 4-9. RCS Propellant Tank Assembly

Table 4-2. RCS Propellant Budget

FUNCTION	PROPELLANT* (POUNDS)	
	GSO*	GM
ATTITUDE CONTROL PRIOR TO SRM-1 BURN	11.2	11.6
ATTITUDE CONTROL AFTER SRM-1 BURN	1.2	4.6
NOMINAL RCS BURN TO AUGMENT SRM-1 BURN ***	40.0	N/A
ATTITUDE CONTROL DURING TRANSFER **	36.1	N/A
ATTITUDE CONTROL AFTER SRM-2 BURN	1.3	2.2
NOMINAL RCS BURN TO AUGMENT SRM-2***	91.8	N/A
ATTITUDE CONTROL FOLLOWING SRM-2 BURN	2.8	4.2
COLLISION AVOIDANCE MANEUVER	3.6	1.5
FLIGHT PERFORMANCE RESERVES	54.0	7.4
TRAPPED PROPELLANT	3.0	TBD
TOTAL	245.0	31.5

* 2 stage STS/IUS equipped with two propellant tanks on a GSO mission with a single spacecraft.

** RCS usage for thermal control included during transfer orbit.

*** "Nominal RCS burn" is for no SRM dispersions.

The isolation valve is an integral part of the propellant tank assembly and minimizes leakage potential by sealing propellant in the tank until after IUS deployment and system activation. The isolation valve is a dual squib-activated, normally closed isolation valve with a pressure switch welded to the valve body to sense valve actuation. The valve is actuated to the open position by one, or both, of the pyro pressure cartridges. Each pressure cartridge contains an NSI-1 initiator welded to a booster output. The pressure switch senses line pressure when the valve actuates and is used only for telemetry. The switch is set to close when pressure increases above 100 ($\pm$25) psi at RCS activation and will reopen if RCS propellant is depleted and manifold pressure drops to 100 (+25/-50) psi.

4.2.5 GUIDANCE AND NAVIGATION

The guidance and navigation subsystem consists of the redundant inertial measurement unit (RIMU), the star scanner and the associated software. The RIMU is a "strap-down" system using gyroscopes and accelerometers to obtain vehicle inertial attitude rate and acceleration measurements. This data is provided to the flight computers for guidance, navigation and control computations. The star scanner is used to provide attitude initialization prior to deployment to compensate for accumulated drift errors. The star scanner is an option and will not be used on the planetary mission. The IUS vehicle uses an explicit guidance algorithm to generate SRM thrust steering commands, SRM ignition time, and RCS vernier thrust cutoff time. Prior to each SRM ignition and each RCS vernier, the vehicle is oriented to a thrust attitude based on nominal performance of the remaining propulsion stages. During SRM burn, the current state vector determined from the navigation function is compared to the desired state vector, and commanded attitude is adjusted to compensate for the build up of position and velocity errors due to off-nominal SRM performance. The primary purpose of the vernier thrust is to compensate for velocity errors resulting from SRM impulse and cutoff-time dispersions. However, residual position errors remaining from the SRM burn and position errors introduced by impulse and cutoff-time dispersions are also removed by the RCS. Attitude control in response to guidance commands is provided by thrust vector control (TVC) during powered flight and by reaction control subsystem thrusters during coast. Measured attitude from the navigation subsystem is compared with guidance commands to generate error signals. During solid motor burn, these error signals drive the motor nozzle actuators, and the resulting nozzle deflections produce the desired attitude control torques in pitch and yaw. Roll control is maintained by the RCS roll-axis thrusters. During coast flight, the error signals are processed in the computer to generate RCS thruster commands to maintain vehicle attitude or to maneuver the vehicle.

4.2.6 TELEMETRY, TRACKING AND COMMAND

The IUS TT&C subsystem is compatible with the space ground link subsystem (SGLS). During orbital flight, the TT&C subsystem operates in conjunction with the Air Force Satellite Control Facility (AFSCF) remote tracking stations (RTS). The TT&C subsystem also operates with the orbiter while the IUS is in the cargo bay and after deployment at ranges of up to 20 nautical miles.

The IUS TT&C subsystem receives uplink command and ranging signals, demodulates the command data and sends it to the data management subsystem. It transmits a downlink signal consisting of digital telemetry data, analog telemetry data and the turnaround ranging signal. The AFSCF RTSs determine IUS orbital trajectory using the two-way ranging signal and tracking antenna angle information. Range-rate is determined through coherent carrier doppler shift.

4.2.7 ELECTRICAL POWER SUBSYSTEM

The electrical power subsystem supplies and distributes electrical power to the IUS vehicle and the spacecraft. Power sources include ASE power and internal IUS batteries. This power is distributed on several buses with separate buses for the IUS and the spacecraft. The subsystem also provides switching for ordnance events and other control and measurement functions for the data management subsystem (DMS). The majority of the switching functions are controlled by the ASE while the vehicle is in the Orbiter bay.

The IUS receives dc power from the ASE power sources and the IUS stage 1 and stage 2 batteries. ASE power can originate from ground support equipment (during checkout) or from the Orbiter/IUS ASE batteries while the IUS is in the Orbiter bay. Stage 1 batteries include: avionics A, avionics B and a spacecraft battery. Since these batteries have relatively large ampere hour requirements, they are packaged as half batteries, and two of these batteries are connected in series to form a single 28 volt dc battery. The avionics A battery consists of two sets of 100 ampere hour batteries connected in parallel to form a 200 ampere hour supply. The avionics B battery consists of one set of 140 ampere hour batteries, and the spacecraft battery is one set of 100 ampere hour batteries. Stage 2 batteries include avionics A, avionics B, utility A, utility B and spacecraft battery. These batteries are rated at 13 ampere hour and packaged as a single unit. Both stage 1 and 2 battery voltages and temperatures are monitored and included in the digital telemetry. In addition to the generic STS/IUS battery configuration described above, optional 170 ampere hour batteries may be used on stage 1 and the number of batteries used on stage 1 and stage 2 can be varied to support specific mission requirements. The Galileo mission will utilize 100 AH stage 1 avionics batteries and 13 AH stage 2 avionics and utility batteries; no spacecraft batteries are required.

The IUS batteries are a wet silver zinc battery housed in a magnesium case. The case is sealed, and a pressure relief valve operates between 3 to 8 psig. The batteries are manually activated by filling the cells with potassium hydroxide electrolyte. The batteries are designed for a maximum wet life of 35 days. Each battery has two thermostatically controlled heaters.

In addition to the avionics and ASE batteries, the IUS computers use lithium organic primary batteries to supply power required to maintain data stored in the computer memory during periods when primary computer power is removed. The batteries are lithium sulfur dioxide (LiSO2) type, 10AH each, with two batteries per IUS computer (total of four per vehicle). They are located in a compartment on the computer case. The case is sealed with a pressure relief valve which operates at 50 psig.

4.2.8 DATA MANAGEMENT

The Data Management Subsystem (DMS) performs computation, data processing, and signal conditioning associated with guidance, navigation, and control; safing, arming and firing the Solid Rocket Motors (SRMs) and Electro-Explosive Devices (EEDs); command decoding, telemetry formatting; and redundancy management.

The DMS comprises two computers, two signal conditioner units (SCUs) and a Signal Interface Unit (SIU). The two identical computers process data in time interval synchronism. Each computer can exchange data and operating status information with the other computer through a conversation link. The A computer processes data and outputs commands in functional synchronism with computer B. Some functions are implemented by both computers and other functions by the single computer which is currently in control. Each computer executes internal self-test programs to determine the status of the hardware.

Each computer has a 65,536-word memory and an operational capability of at least 550,000 operations per second.

The SCUs perform uplink command decoding, power switching for REM solenoid operation, stage separation devices, and safe-and-arm circuits. They also contain the signal-routing logic for channel switching, required for redundancy management.

4.2.9 THRUST VECTOR CONTROL SUBSYSTEM

The Thrust Vector Control (TVC) consists of:

two TVC controllers
four TVC actuators
four TVC potentiometers

The Thrust Vector Control (TVC) subsystem provides the interface between the Inertial Upper Stage (IUS) Guidance, Navigation and Control System and the Solid Rocket Motor (SRM) gimbaled nozzle to accomplish powered flight attitude control. These functional interfaces are shown in Figure 4-10. Two complete electrically-redundant channels are provided to minimize single-point failures.

Power is supplied from the power distribution unit (PDU) to the TVC controller which controls the actuators. The controller receives analog pitch and yaw commands, proportional to desired nozzle angles, and converts them to pulse-width-modulated voltages to power the actuator motors. The motor drives a ball screw which extends or retracts the actuator to position the SRM nozzle. Potentiometers provide for servo loop closure and for nozzle position instrumentation. Maximum angular nozzle deflection of state 1 and stage 2 is 3.9 and 6.4 degrees, respectively, due to TVC mechanical stop limitations.

Figure 4-11 shows the actuator/potentiometer physical interface to the SRM. A staging command from the SCU allows switching of the controller outputs from actuators on stage one to actuators on the second stage.

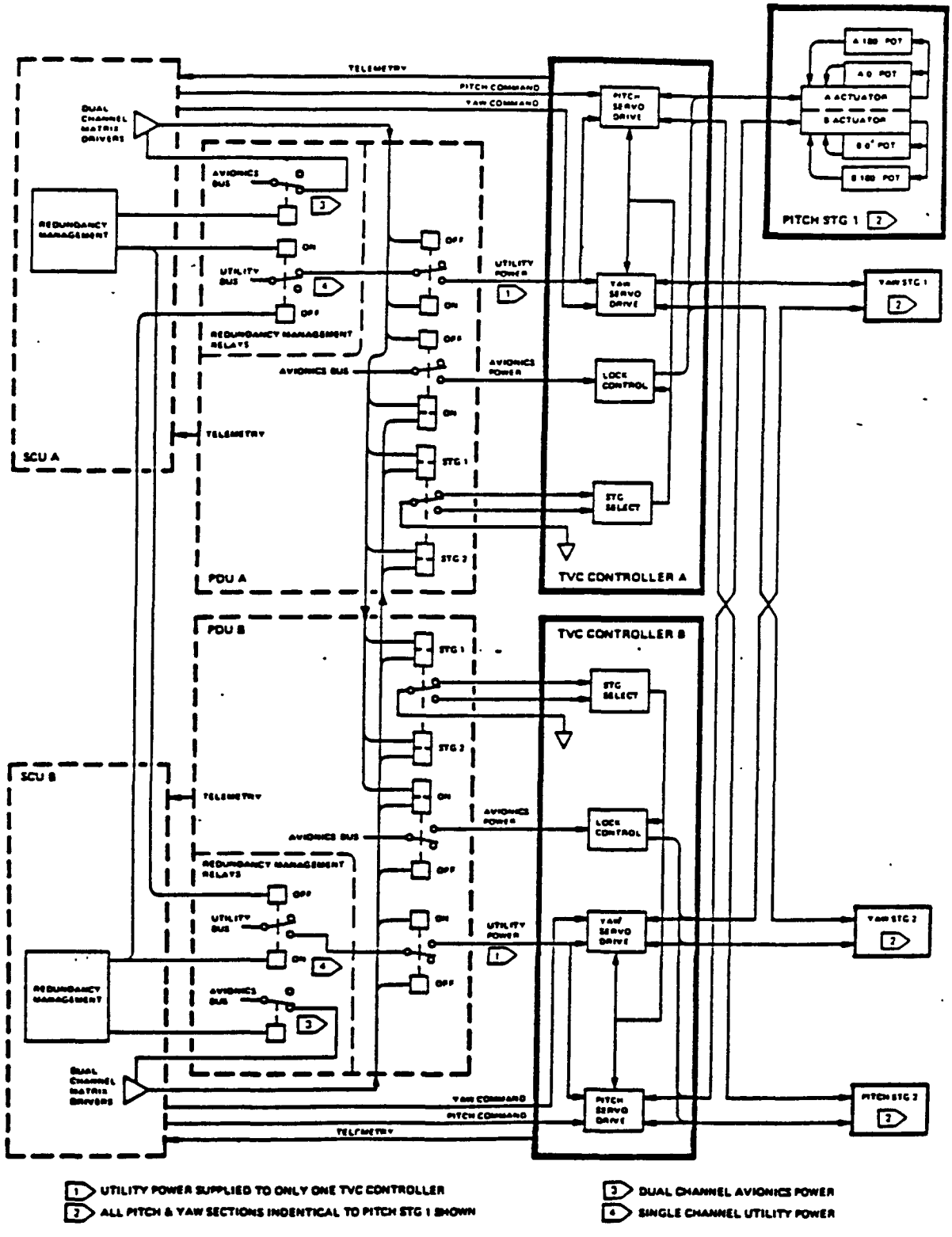

Figure 4-10. Thrust Vector Control System Function Diagram

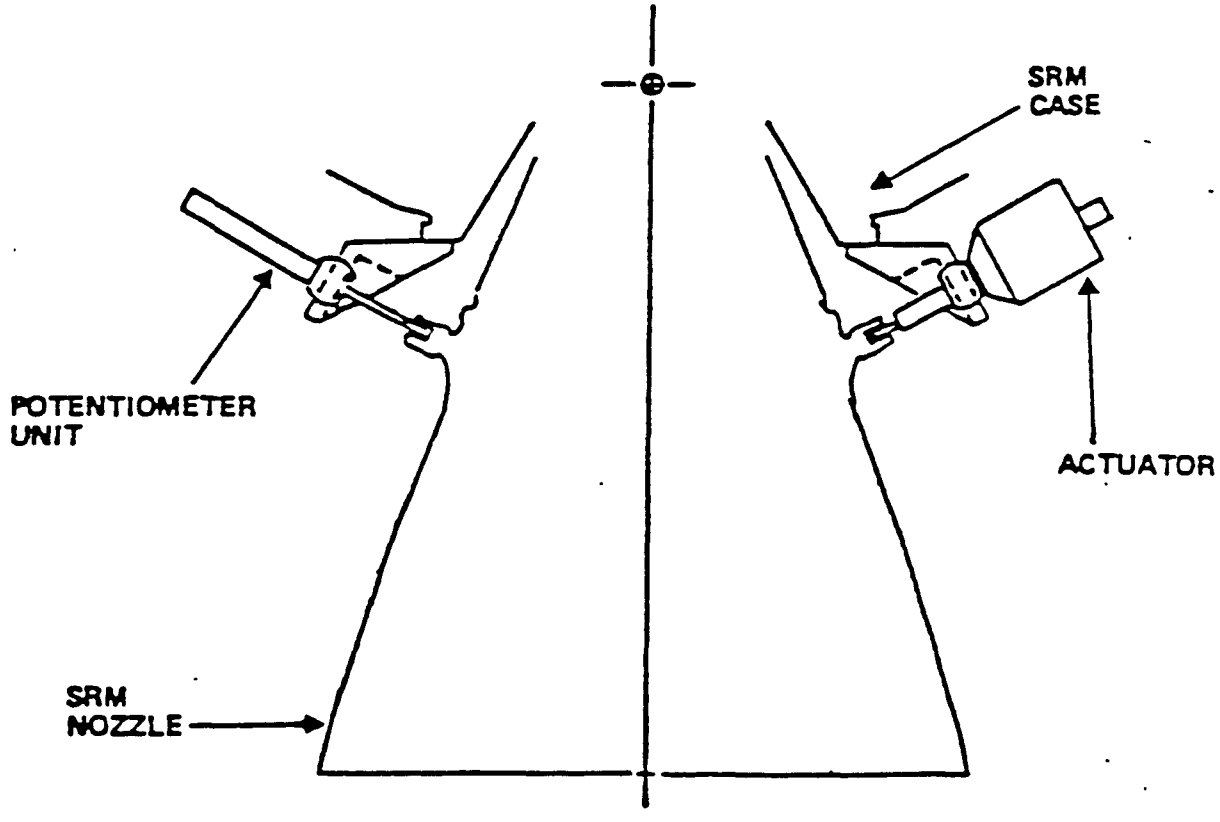

Figure 4-11. Actuator and Potentiometer to SRM Interface

Two potentiometer elements are used to reduce axis cross-coupling errors due to the short coupling between actuator mounting points. One element within the actuator and another within the potentiometer unit (located 180° around the nozzle from the actuator) form a "bridge network" for the closed loop feedback signal. When the nozzle is moved across the plane of actuator motion, the bridge network linearizes the feedback nozzle angle to the command angle relationship and eliminates thermal, pressure and cross-axis errors.

The controller contains damping, error rate limit and current limit circuits as well as position, command, current, temperature and voltage monitor instrumentation.

4.2.10 SOFTWARE

The IUS operational flight software subsystem is organized into eight function areas: executive, mission sequencing, navigation, guidance, attitude control, communications, redundancy management, and checkout. The executive function controls timing synchronization, memory load, input/output, and scheduling of all flight operational software tasks. Mission sequencing controls timing and sequencing of events related to the IUS vehicle. Navigation consists of determining position, velocity and inertial attitude from vehicle linear acceleration and angular velocity (as sensed by the RIMU). This software function includes initialization, alignment, and calibration. The guidance function determines the inertial attitude required to maintain the trajectory that will attain the desired set of end conditions. The guidance function also controls the ignition time of each SRM burn and the start time and duration of RCS vernier burns. Attitude control determines pitch and yaw commands to be sent to the TVC subsystem during SRM burn, and roll, pitch and yaw commands to the RCS during coast periods. Attitude control also generates RCS roll commands to compensate for swirl torques during SRM burn. The communications function processes commands received by the vehicle, processes telemetry data, and controls antenna switching. Redundancy management controls computer self-test and all fault detection, fault isolation and reconfiguration of the computers, RIMU, thrust vector control, TT&C, and signal conditioner unit. The checkout function performs prelaunch and predeployment checkout of the computers, RIMU, TT&C, RCS, and SCU.

4.2.11 REDUNDANCY MANAGEMENT

The function of redundancy management (RM) is to determine the operating status of IUS vehicle avionics autonomously, and to reconfigure, upon detection of failures, to reestablish an operable configuration. The redundancy management function has some unique terms that describe the basic system operation. These unique terms are as follows:

Single channel control -

> Those functions which are implemented by only one channel even though both computers are issuing commands. The channel to implement the commands is determined by the RM control logic in the signal conditioning units (SCUs).

Dual channel control -

Those functions which are implemented in both channels provided no failures exist. If a channel fails, its dual channel control functions are inhibited, as determined by the RM control logic in the SCUs. The good channel is then the only channel to implement the dual channel functions.

4.2.12 AIRBORNE SUPPORT EQUIPMENT

The airborne support equipment (ASE) provides the mechanical and electrical interfaces between the Orbiter and the IUS. See Figure 4-12 and 4-13. The ASE consists of the structure, batteries, electronics, mechanisms and cabling to support the IUS/spacecraft combination, to enable vehicle deployment, to provide and distribute electrical power to the IUS and spacecraft and to provide communication paths between the Orbiter and the IUS and spacecraft. See Figure 4-14 for a functional block diagram.

The ASE installation consists of the forward support frame assembly and the aft support frame assembly, located in the payload (Figure 4-15), and the communications interface unit (CIU) and the power control panel (PCP), located in the crew compartment (Figure 4-13). Additional controls and indicators operated by the crew to support IUS/spacecraft deployment and the interconnecting cabling between the crew compartment and the payload bay are Orbiter provided. Instrumentation is installed on the payload bay ASE to measure dynamic loads and environmental data during the mission. The ASE instrumentation interfaces with Orbiter equipment only and operates independent of the ASE power and the telemetry and command subsystems.

The IUS/ASE can be installed in either of two cargo bay positions which are designated as the IUS aft location and the IUS forward location. Selection of location is based upon the mass properties and dimensional constrains of the IUS payload and other elements manifested on the flight. When installed in the aft location, the IUS SRM-1 nozzle just clears the aft bulkhead. The forward location is approximately 55 inches forward of the aft location.

The following paragraphs provide descriptions of the ASE structure and mechanisms, power, telemetry and command, and instrumentation subsystem.

The Airborne Support Equipment (ASE) Structure and Mechanisms Subsystem in the Orbiter payload bay contain the following components:

Forward Support Frame,
Aft Support Frame (Tilt Table).

The ASE Structure and Mechanisms Subsystem provides for the support of the IUS vehicle/spacecraft combination while in the Orbiter cargo bay. The subsystem also provides for the tilting, release, and deployment of the IUS vehicle/spacecraft combination. Some of the ASE communications and power control equipment is mounted on the aft support frame in the payload bay. See Figure 4-15 for the ASE support frames.

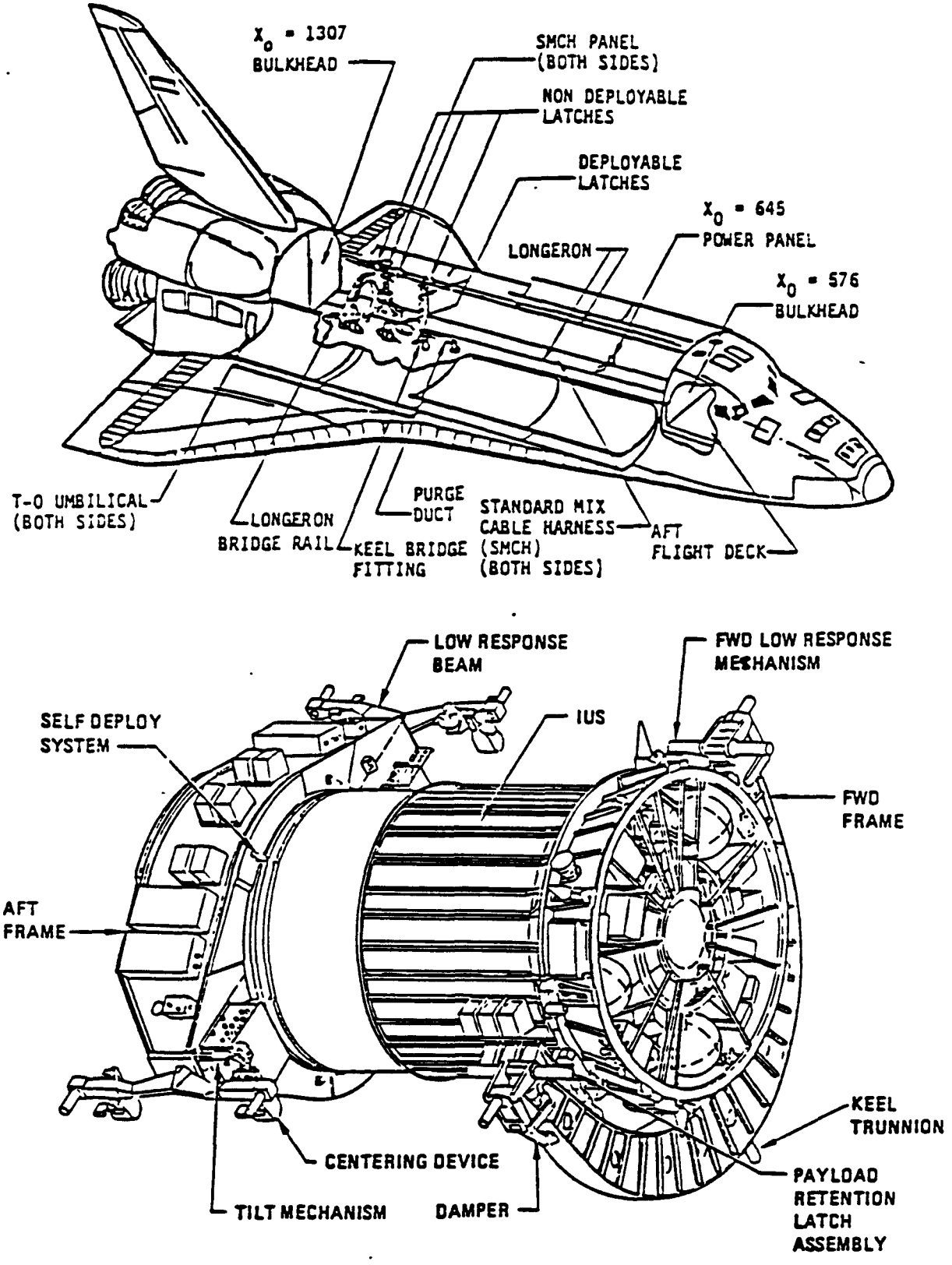

Figure 4-12. Airborne Support Equipment

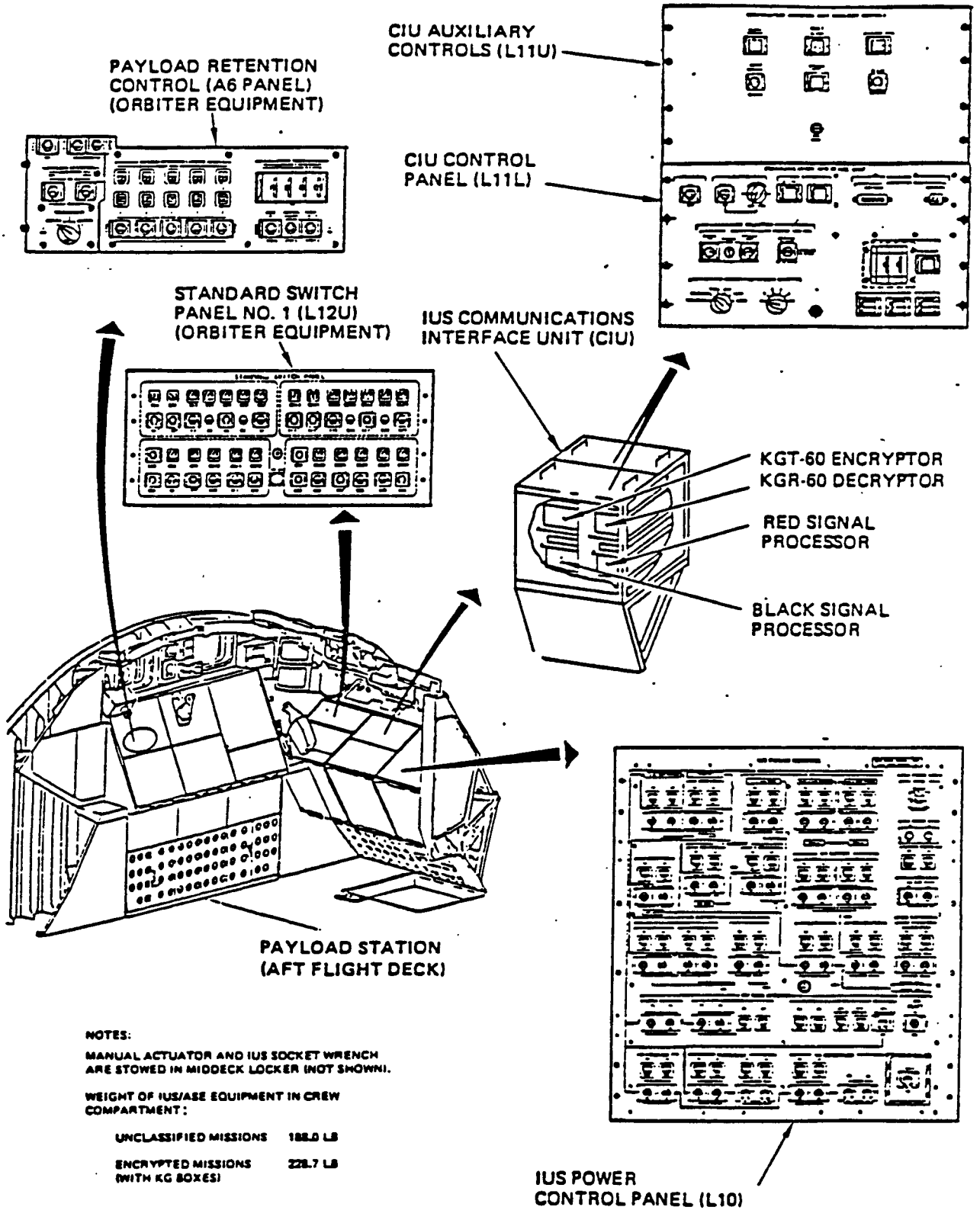

Figure 4-13. IUS/ASE Installations in Orbiter Crew Compartment

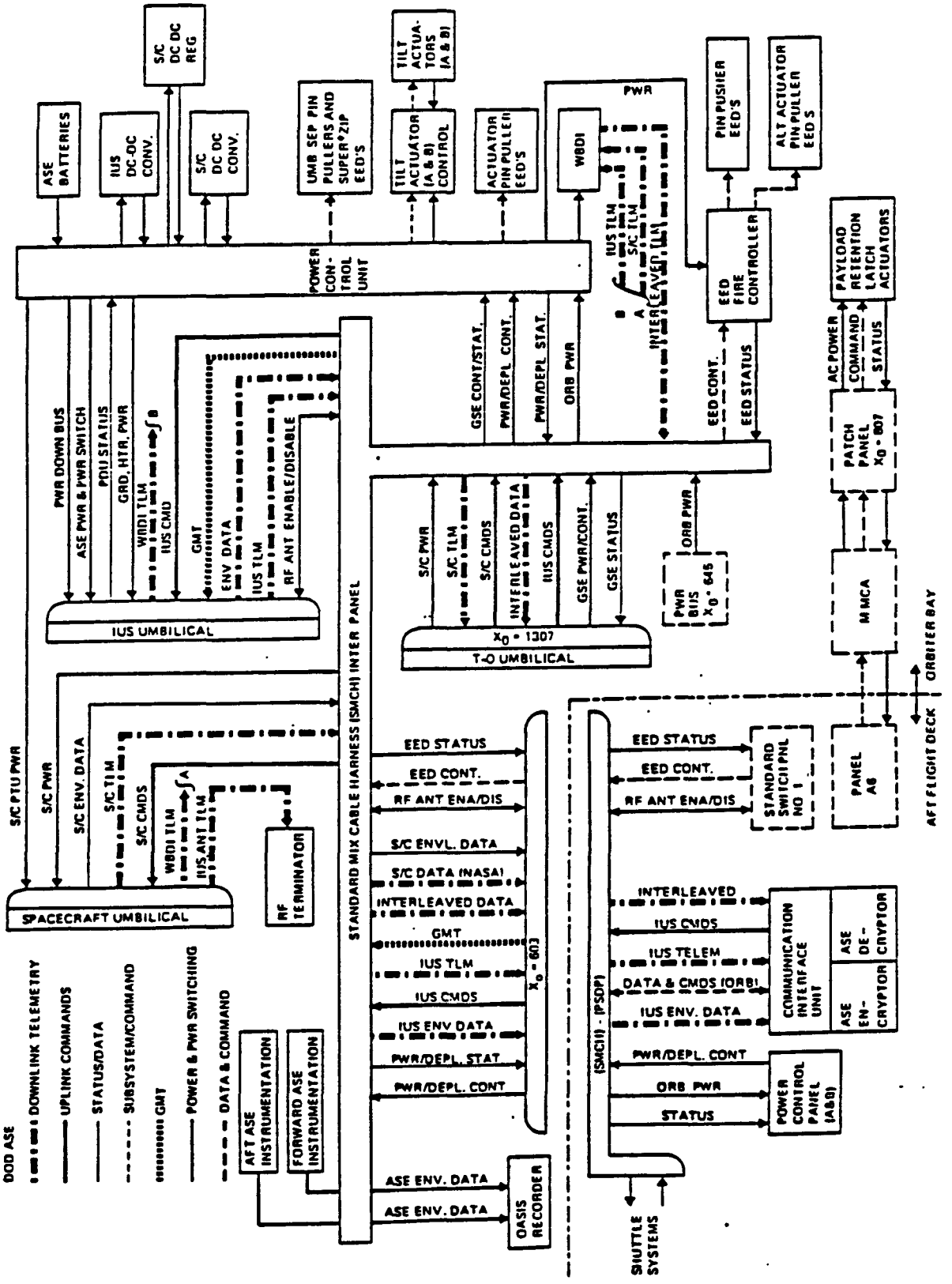

Figure 4-14. ASE Functional Block Diagram

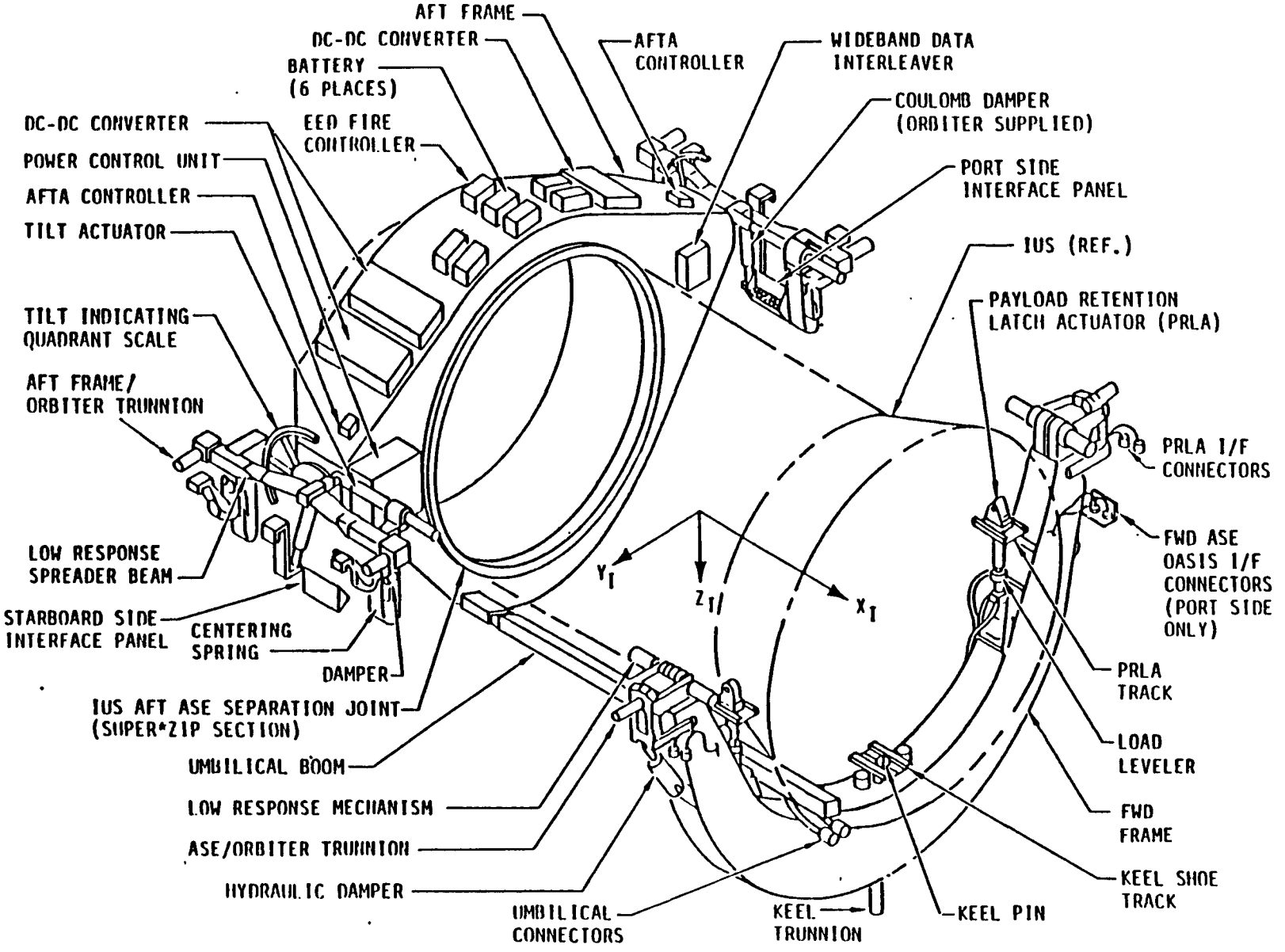

Figure 4-15. ASE Support Frames

The IUS vehicle skirt is structurally attached to the aft ASE frame by the circumferential separation joint. Vehicle trunnions mounted on either side of the forward interstage ring and a recessed socket at the bottom provide the three vehicle hardpoints for attaching the IUS to the forward ASE frame.

The primary Orbiter/ASE structural interface in the payload bay consists of six ASE trunnions, which are mated with standard non-deployable attach fittings mounted on the Orbiter longerons, and a forward ASE keel trunnion, which is mated with an active keel actuator (AKA) mounted on the Orbiter keel. See Figure 4-16. The ASE longeron trunnions are 3.25-inch diameter; the keel trunnion is 3-inch diameter. All longeron attach fittings are pinned to their respective bridge rails except the two fittings that support the aft trunnions on the aft frame. These two fittings are permitted to slide forward and aft on the bridge rails to accommodate dynamic flexing of the ASE low response spreader beams. Payload z-axis loads are reacted by all six longeron trunnions. The keel trunnion on the forward frame reacts the payload lateral (y-axis) loads. The forward trunnions on the aft frame react all payload longitudinal (x-axis) loads except those loads induced by the mass of the forward frame. The IUS vehicle is not constrained by the forward frame in the x-axis, and forward frame generated x-axis loads are independently reacted by the forward frame longeron trunnions and keel trunnion.

In addition to the primary structural load paths through the seven ASE-to-Orbiter trunnions, the mechanical interface includes two centering spring/damper assemblies and an Orbiter - provided coulomb damper attached between each of the aft ASE spreader beams and the Orbiter bridge rails and a purge duct spigot connection located just aft of the forward ASE adjacent to the keel centerline.

4.2.13 RTG COOLING

The RTGs require continuous cooling following installation on the spacecraft until deployment from the Orbiter. Spacecraft GSE (ground support equipment) will precondition the RTG side of the cooling loop during ground operations. Before launch, the coolant lines will be switched over to the Orbiter system. The STS system will maintain RTG cooling until just before payload deployment. At that time, the coolant lines will be vented and purged with nitrogen.

The RTG coolant lines are routed through the IUS ASE and vehicle to the spacecraft interface. Disconnect couplings are provided at the IUS/ASE separation interface, the IUS stage 1-2 separation interface, and the IUS-to-spacecraft separation interface for the Galileo mission.

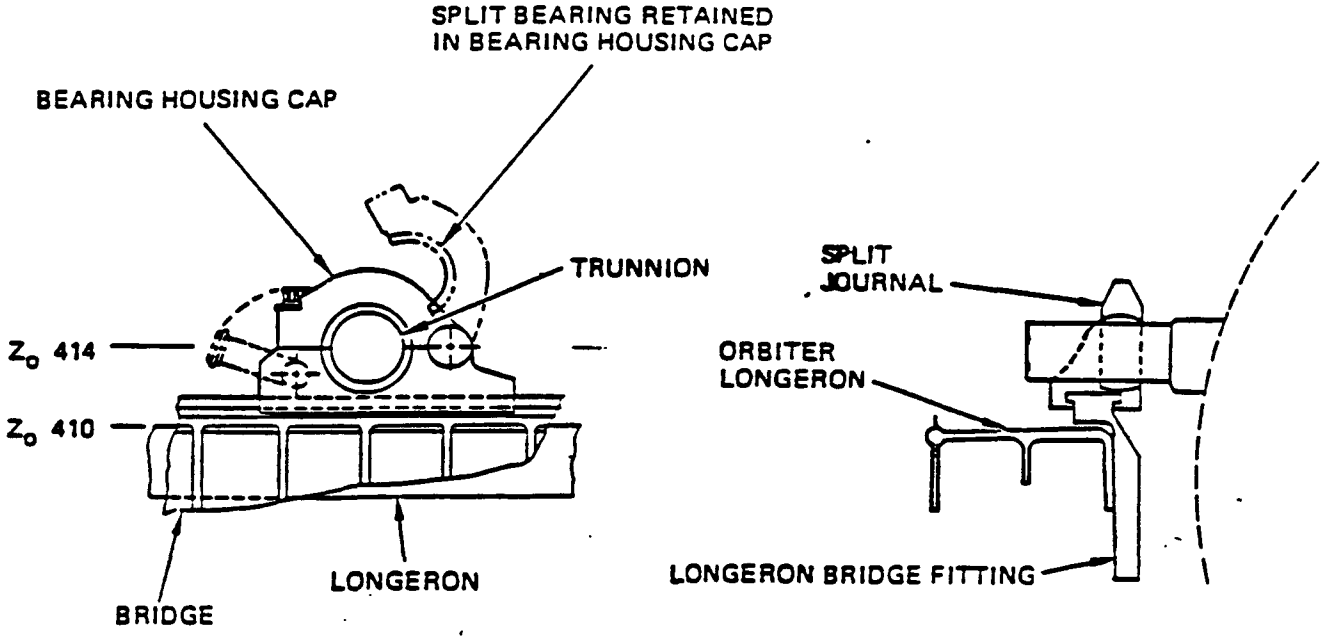

Figure 4-16. ASE Trunnion Interface

4.3 UPPER STAGE/SPACECRAFT WEIGHT SUMMARY

An initial weight estimate for IUS with the Galileo spacecraft appears below.

Spacecraft Separated Weight		5509
GFE Airborne Support Equipment		1504
Boeing Airborne Support Equipment		
Cargo Bay	5529	
Crew Compartment	188	
IUS Flight Vehicle (Stages 1 and 2)		32387
Galileo Adapter		341
Total Loaded Weight (lbs.)		45458

SECTION 5.0

TRAJECTORY AND FLIGHT CHARACTERISTICS

The Galileo mission will commence at the launch of the Space Shuttle from KSC during the November 1989 time period. Specific trajectory details are not finalized, but Table 5-1 presents the sequence of events during the launch and ascent to Earth orbit which are currently representative of those for both missions. The other orbital operations through spacecraft ejection after the hyperbolic escape trajectory is attained are listed also on Table 5-1. These values are taken from the Space Shuttle Data Book (NSTS-08116).

Table 5-1. Mission Sequence

Start propellant loading	T-8.5 hr
Topping	T-6 hr
Crew enters orbiter	T-3 hr
Auto sequencing begins	T-31 sec
Orbiter main engines fire	T-6.6 sec
SRMs fire	T-40 msecs
Vehicle clears tower	T+7 sec
IIP over water 36.6 meters deep (20 fathoms)	T+34 sec
Peak Dyn. pressure	T+50-60 sec
SRMs burnout	T+119 sec
SRMs jettisoned	T+125 sec
MECO	T+514 sec
OMS 1st burn (to orbit) (136 sec burn)	T+634 sec
Begin Ascent Coast	T+802 sec
OMS-2 burn (circularization) (103 sec burn)	T+2770 sec
Payload bay doors opened	T+3615 sec
IUS/SC deployment	T+24000 sec
IUS Burn 1 (TBD sec burn)	T+26400 sec
IUS Burn 2	T+TBD sec
SC Deployment	T+TBD sec

Since the trajectory for the Galileo mission has not been finalized, the Shuttle vehicle flight parameters as a function of time are not available. However, a typical range safety trajectory has been obtained (Reference 5-1) from which typical flight parameters are presented for a 50,000 pound cargo. These parameters are shown on Figures 5-1 through 5-14. Although the Shuttle capacity is 65,000 pounds cargo and the Galileo mission will be at or close to the maximum capacity, the flight parameters are not expected to vary greatly from the "typical" values given here.

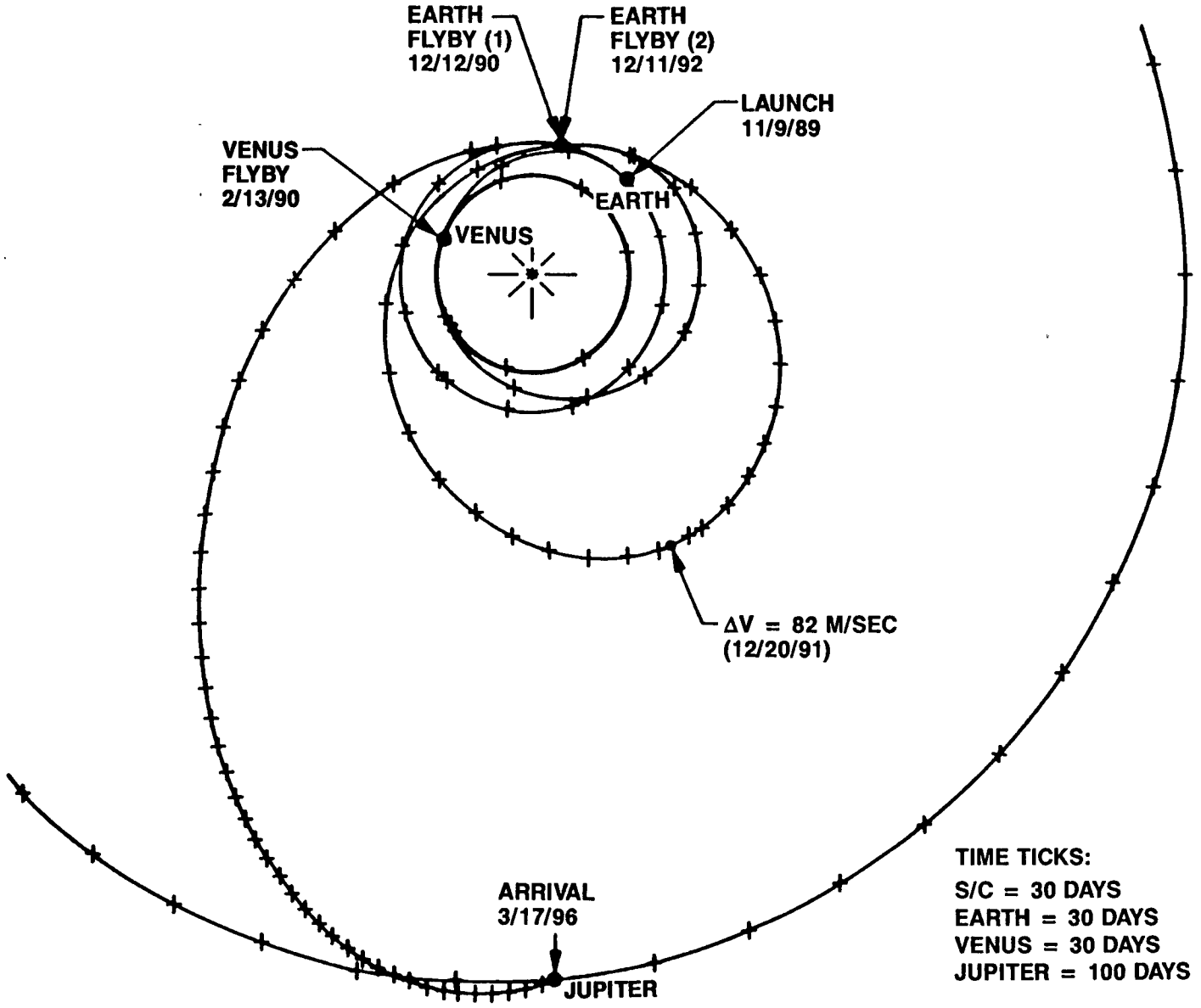

Figure 5-1. Interplanetary Trajectory for November 1989 VEEGA (Preliminary)

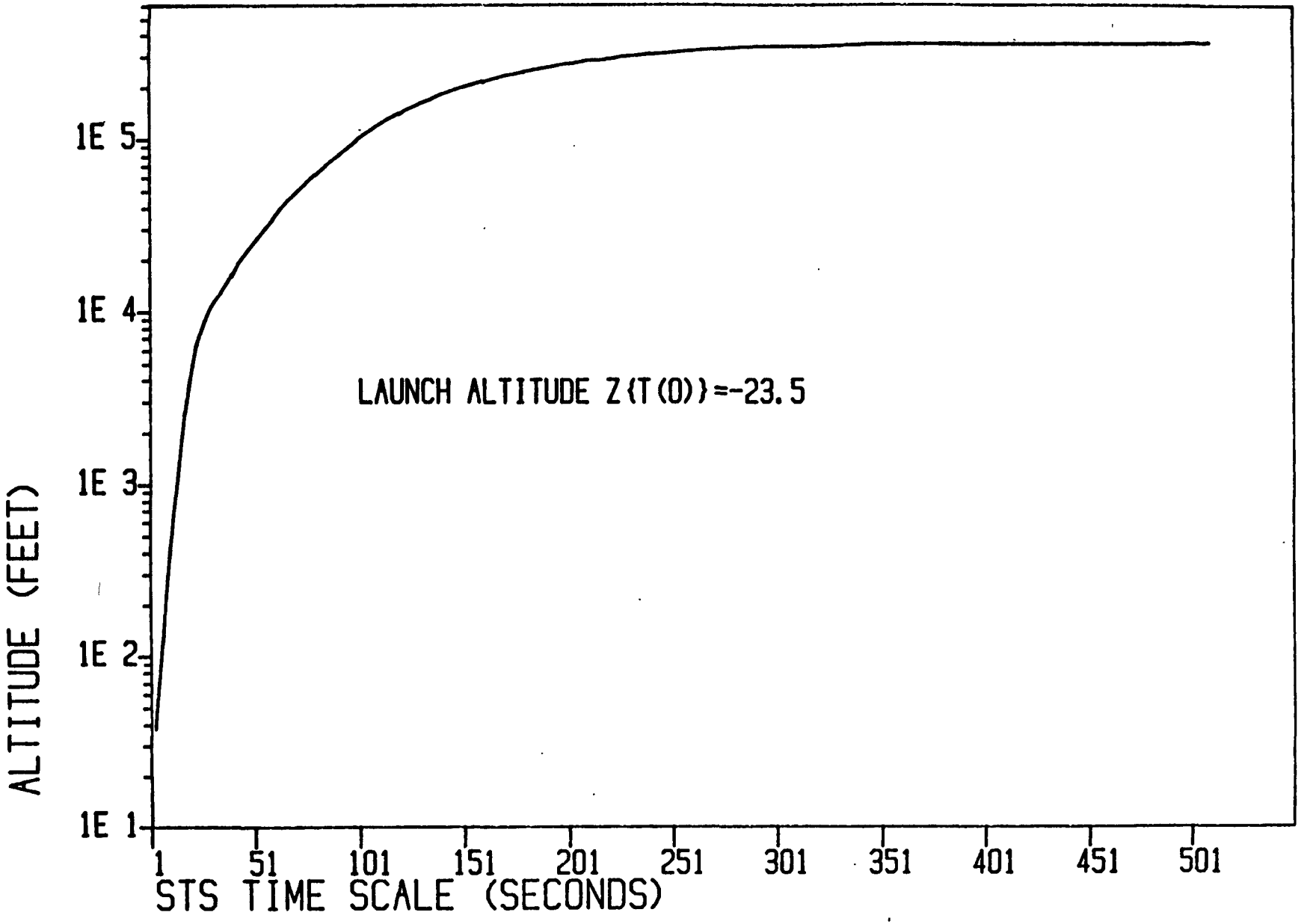

Figure 5-2. STS Trajectory - Altitude as F (Time)

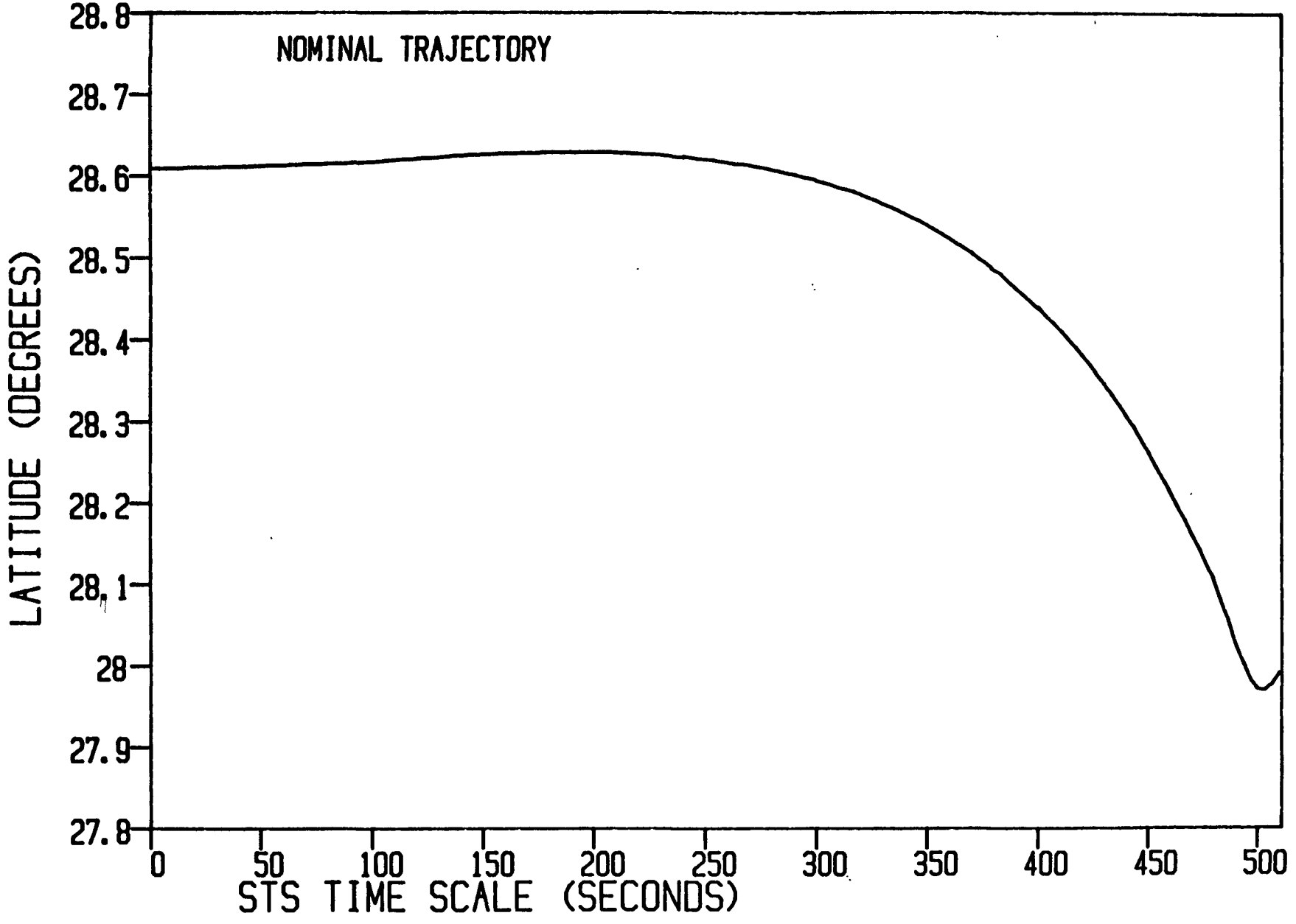

Figure 5-3. STS Trajectory - Latitude as F (Time)

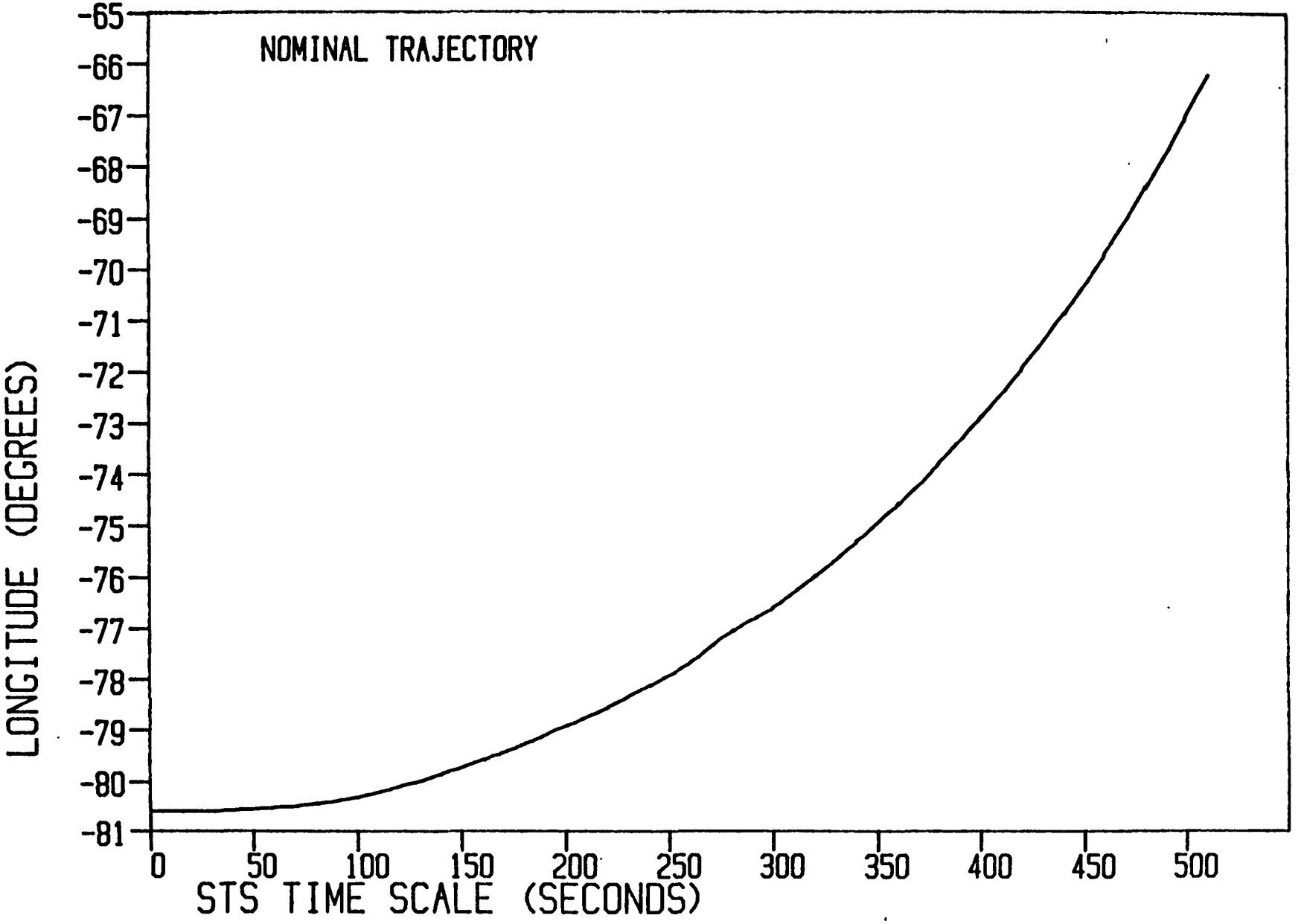

Figure 5-4. STS Trajectory - Longitude as F (Time)

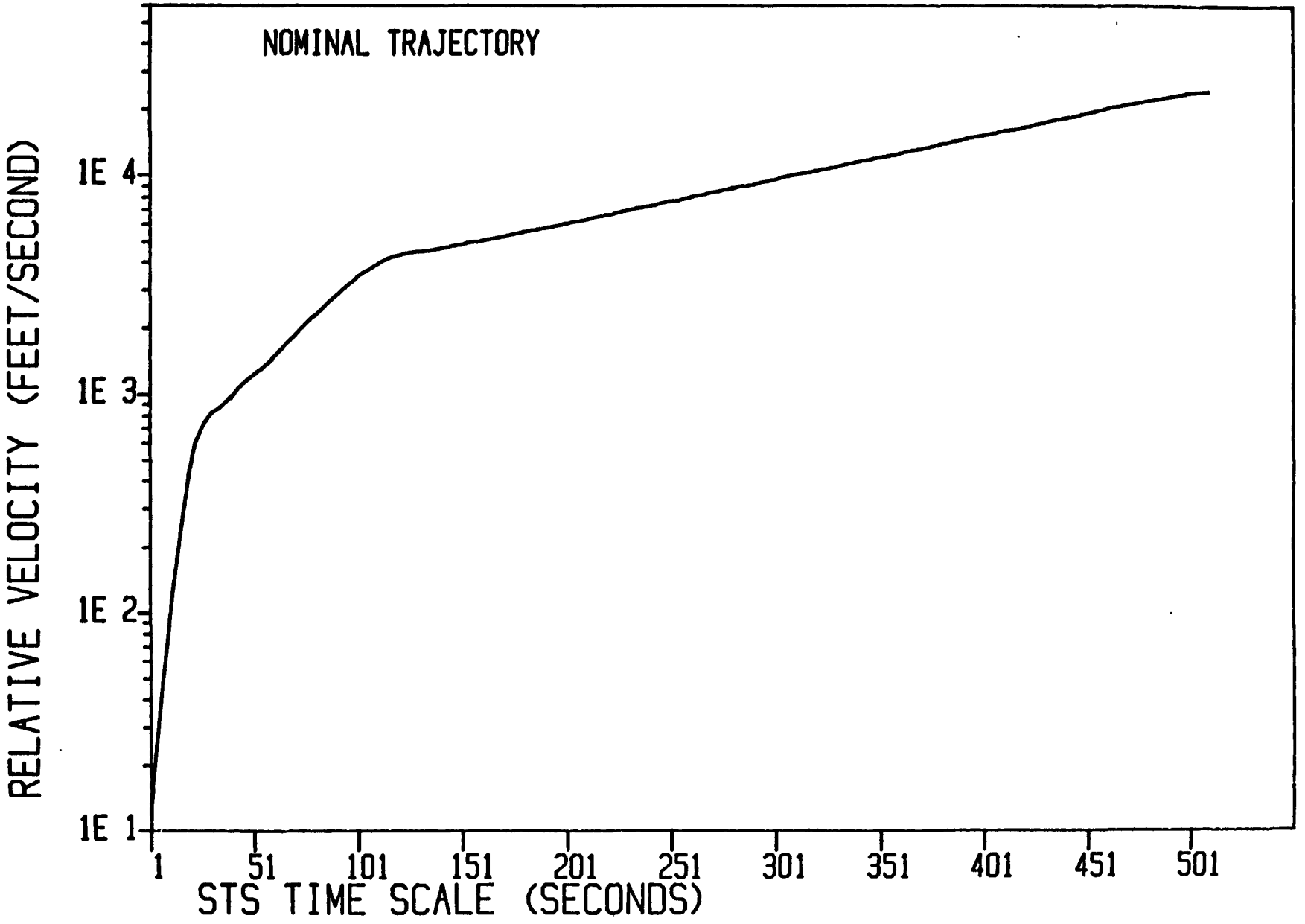

Figure 5-5. STS Trajectory - Shuttle Relative Velocity

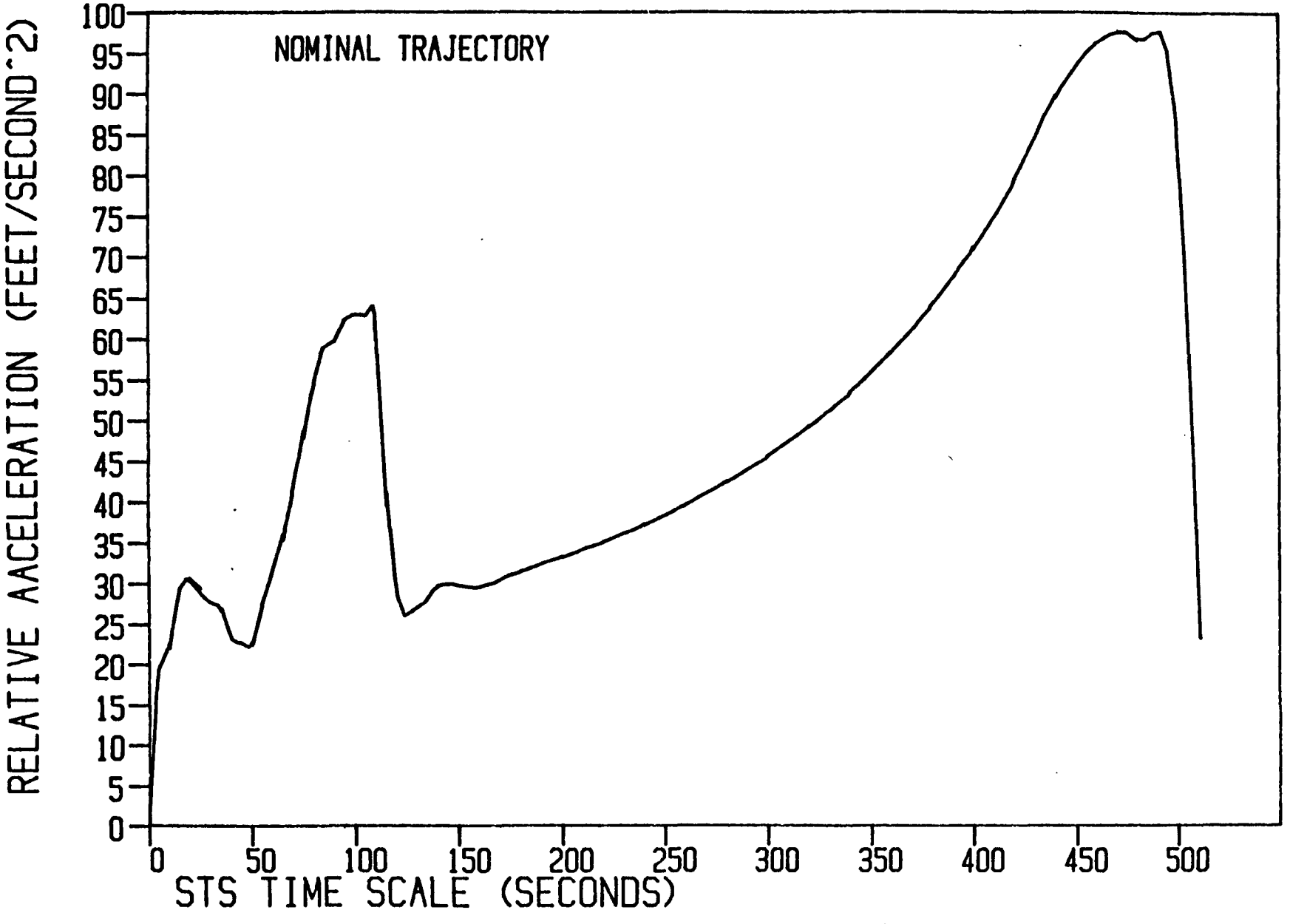

Figure 5-6. STS Trajectory - Shuttle Relative Acceleration

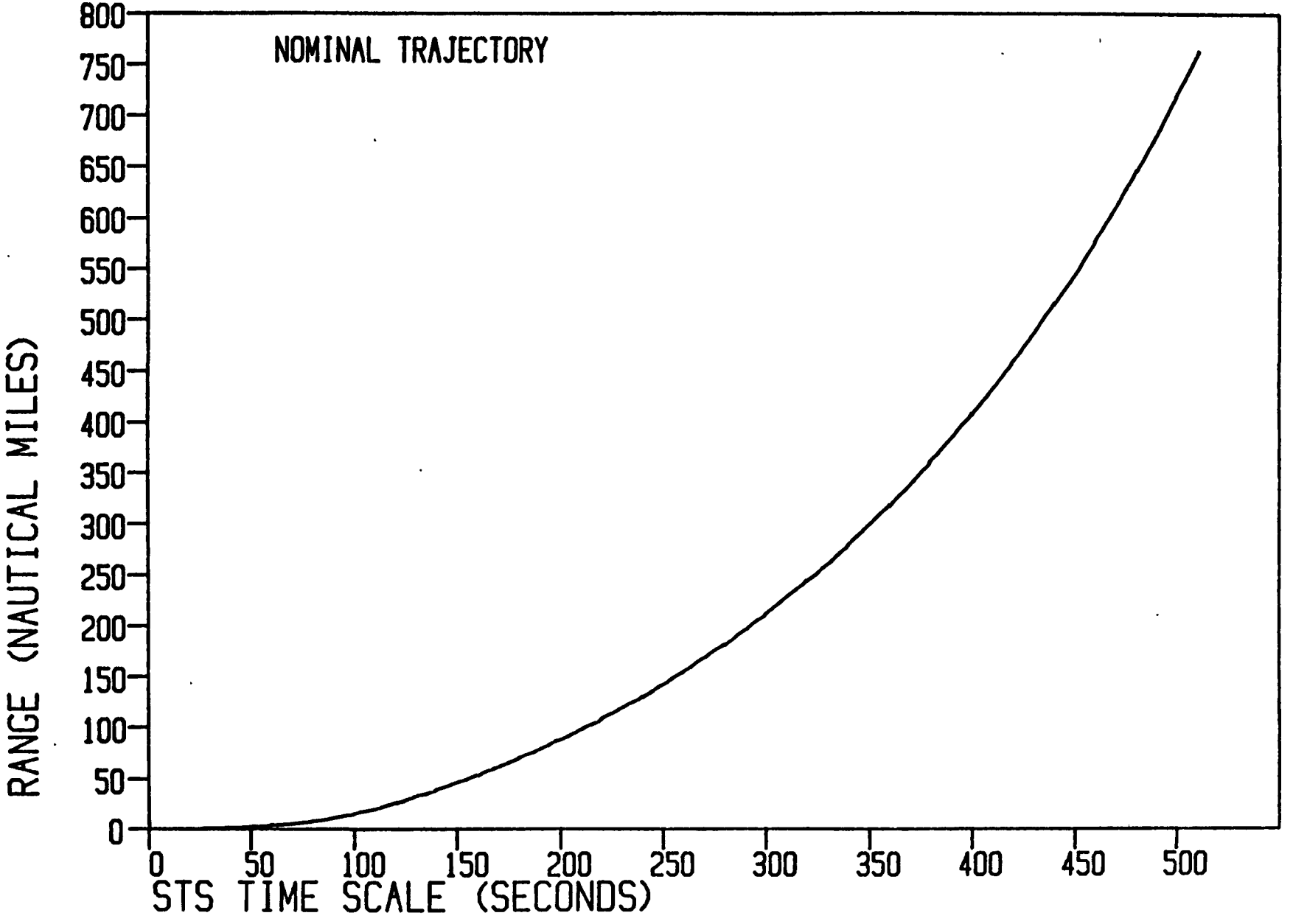

Figure 5-7. STS Trajectory - Shuttle Range

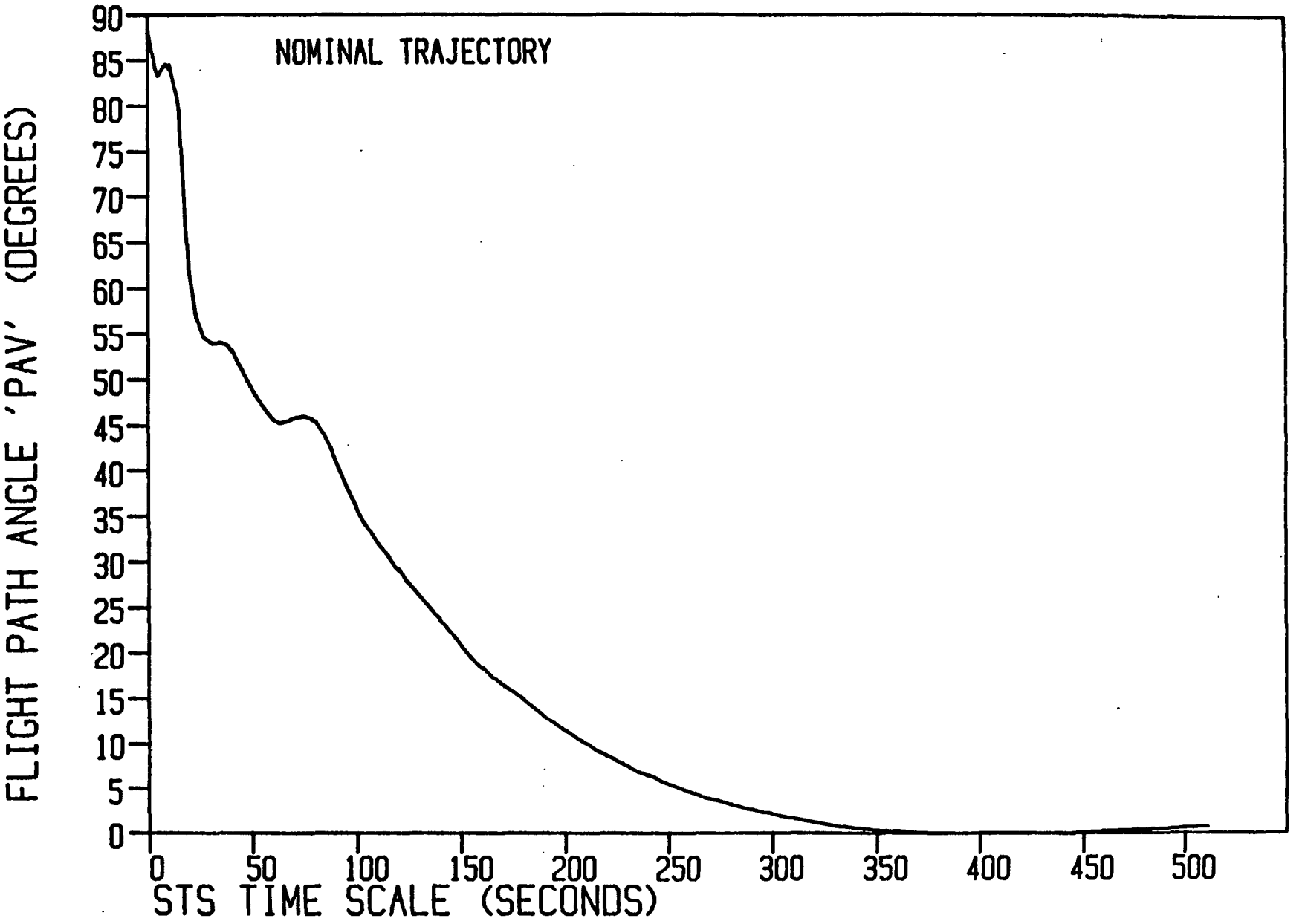

Figure 5-8. STS Trajectory - Flight Path Angle

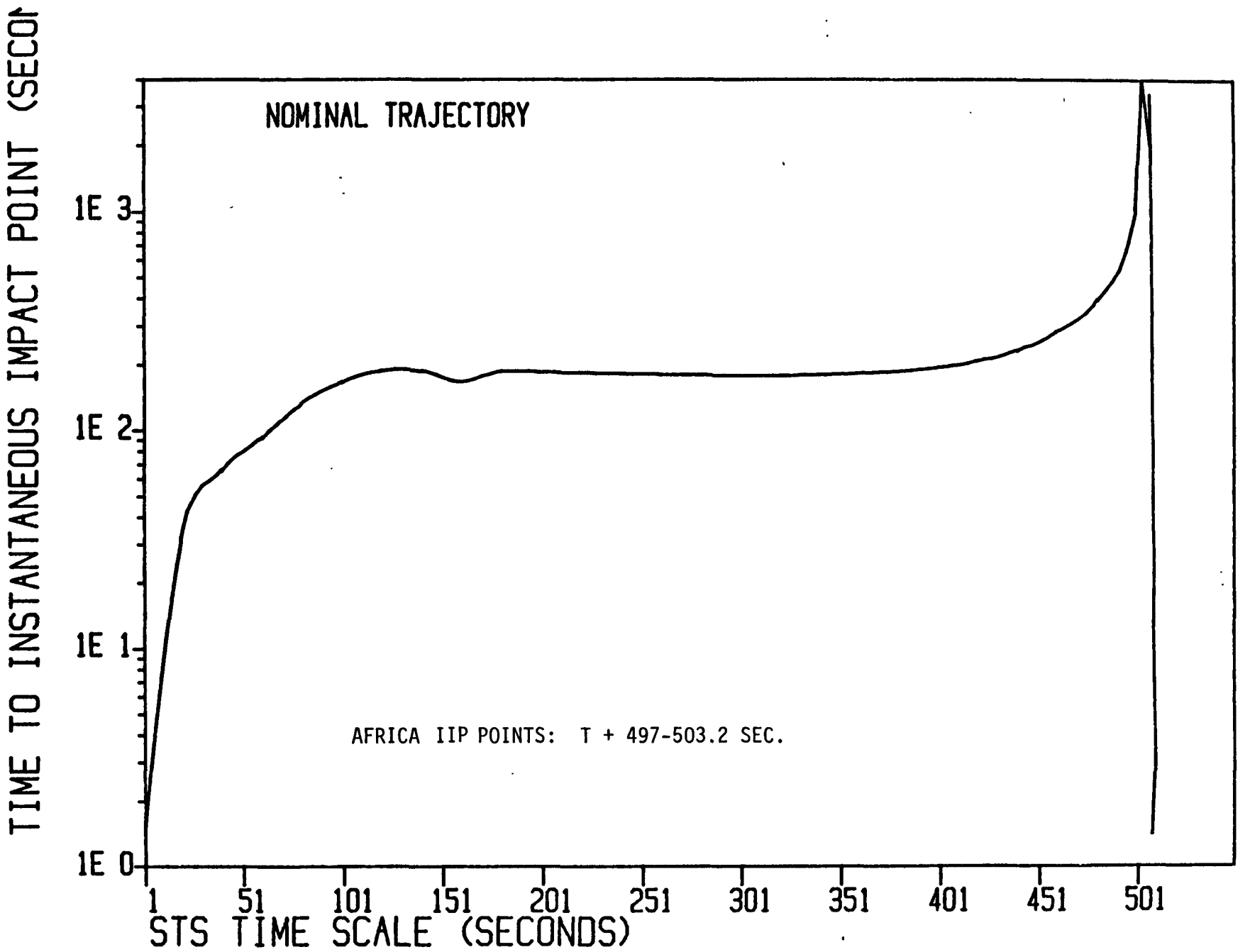

Figure 5-9. STS Trajectory - Time to Instantaneous Impact Point

Figure 5-10. STS Trajectory - Range of Instantanous Impact

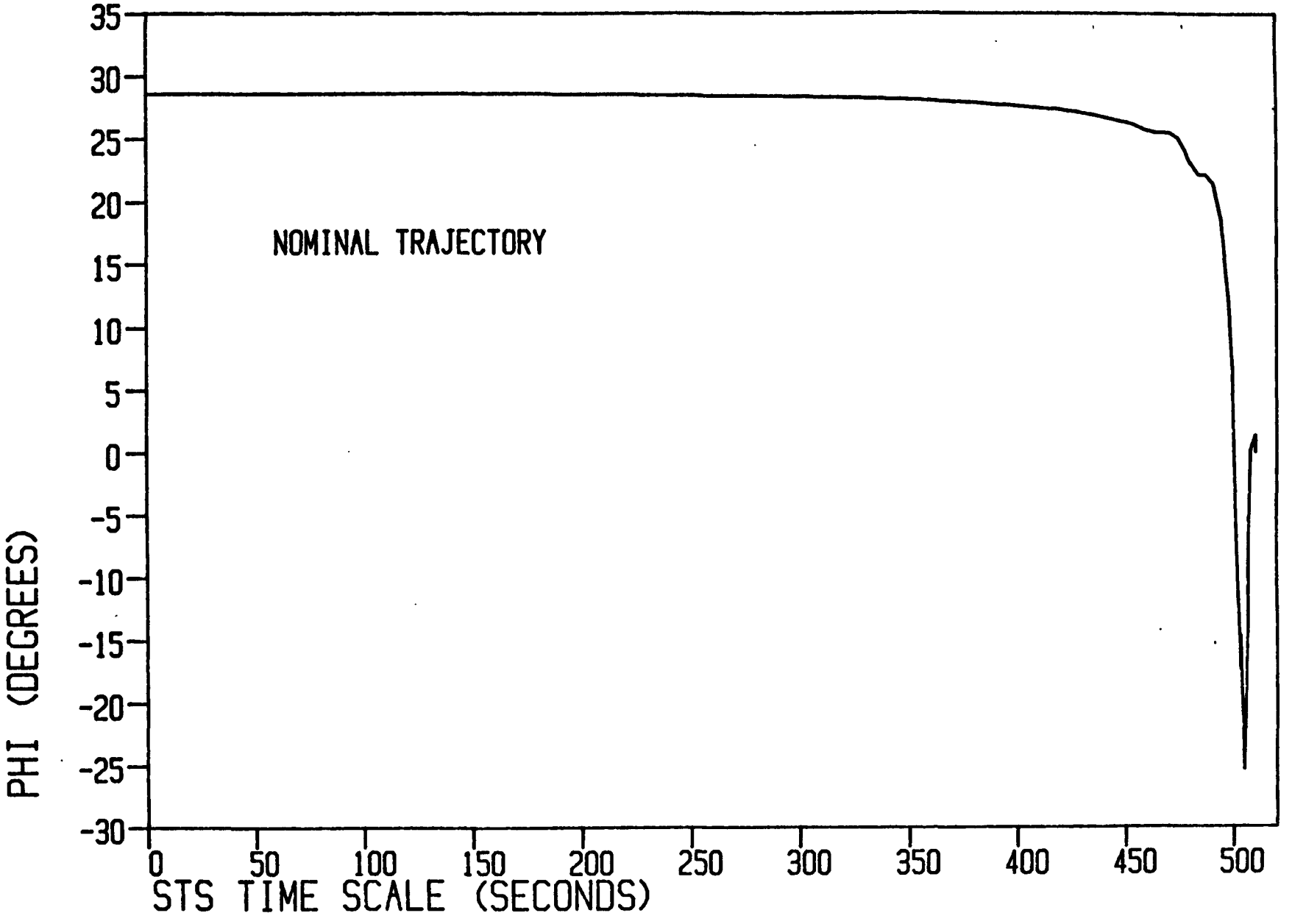

* Latitude of IIP

Figure 5-11. STS Trajectory - PHI as F (Time)*

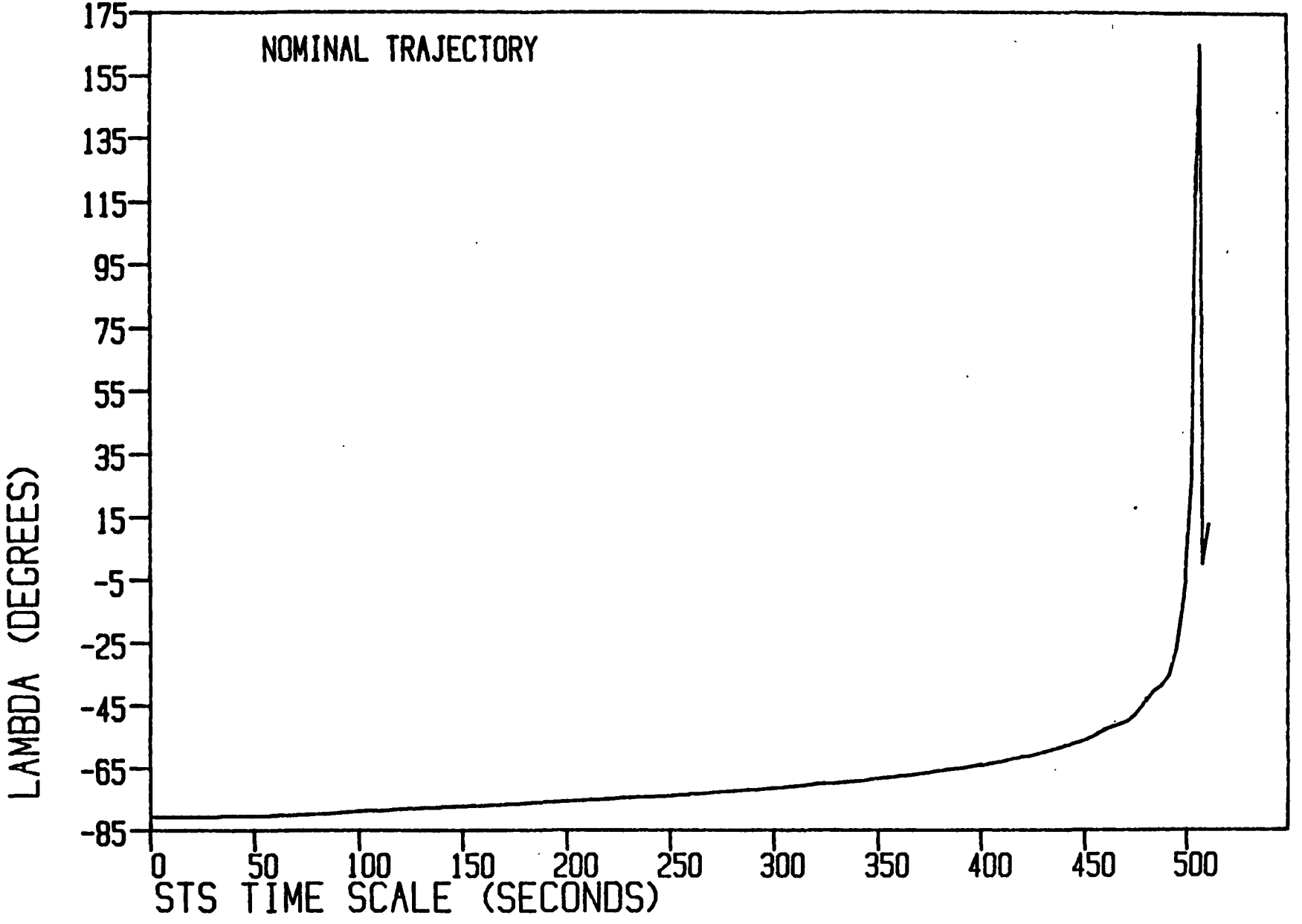

* Longitude of IIP

Figure 5-12. STS Trajectory - Lambda as F (Time)*

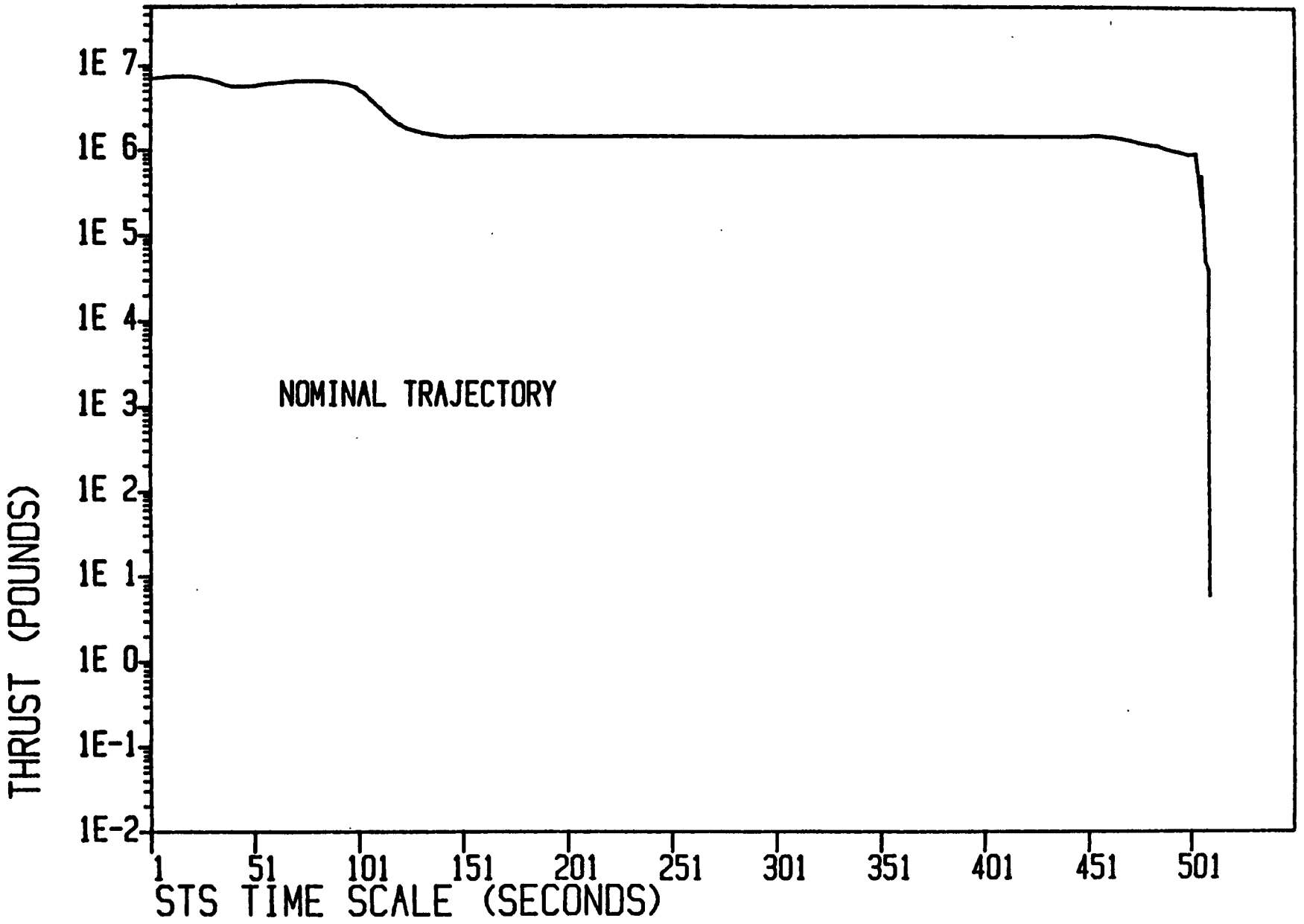

Figure 5-13. STS Trajectory - Thrust as F (Time)

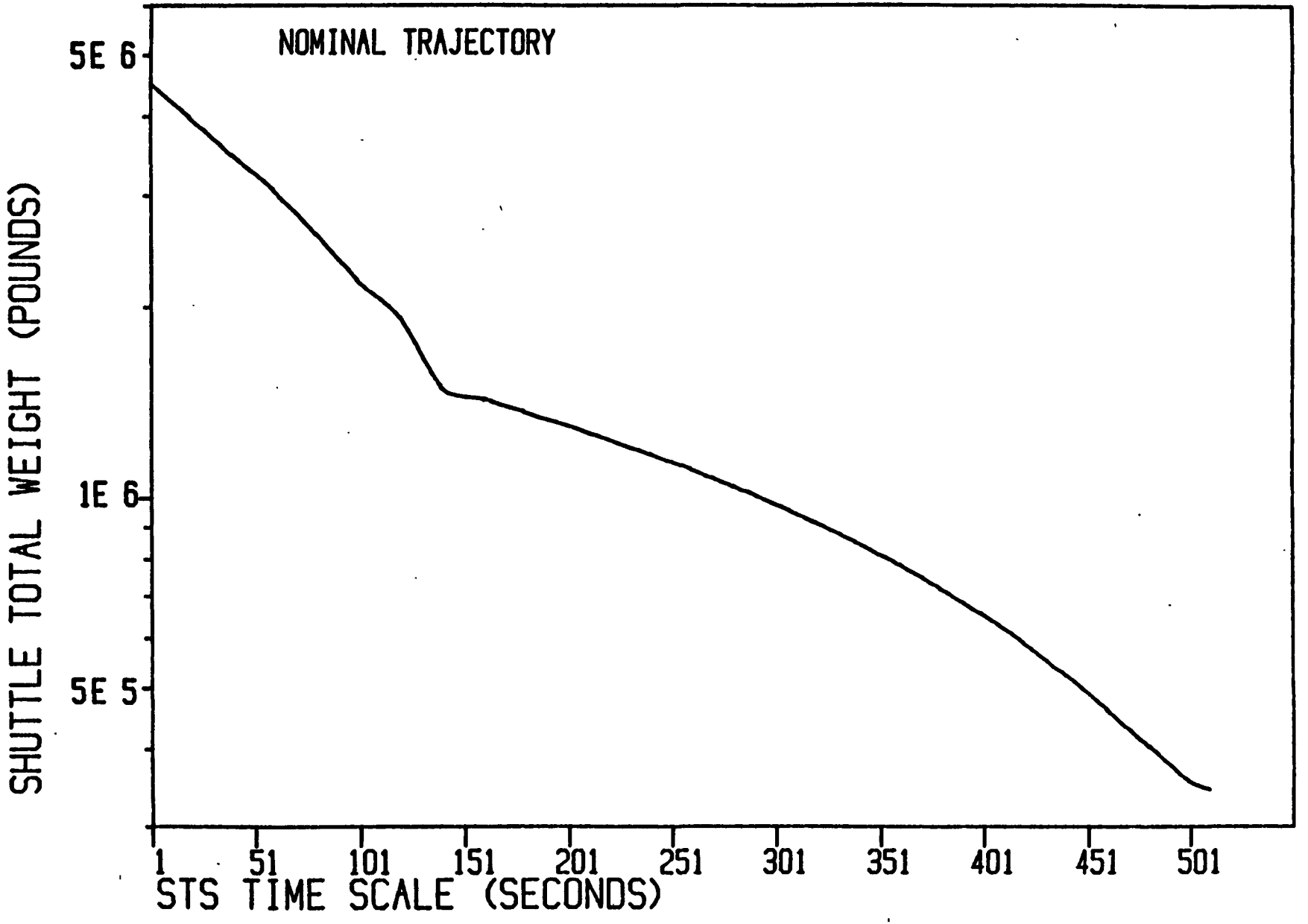

Figure 5-14. STS Trajectory - Shuttle Total Weight

After the Orbiter has attained a low Earth orbit, the IUS and spacecraft will be separated during the sixth Shuttle orbit, at about nine (9) hours after launch. At approximately 45 minutes after Orbiter - IUS separation, the IUS first stage engine, SRM-1, will burn for approximately three (3) minutes and the second stage engine, SRM-2, for approximately two (2) minutes. After SRM-2 burnout, the IUS will go through reorientation maneuvers, the Galileo spacecraft will start deployment of the RTG, science, and magnetometer booms, and the spacecraft will be spun-up to 2.9 rpm and then separated from the IUS.

When the Galileo spacecraft is separated from the IUS, it will be traveling along a trajectory that will include three planetary flybys in order to attain the necessary energy and direction to reach Jupiter by the use of these gravity assist maneuvers. These complicated maneuvers, known as the Venus-Earth-Earth Gravity Assist (i.e., VEEGA), have been chosen to optimize the use of the propellants available in the IUS plus additional propellant on the Galileo spacecraft. Figure 5-1 illustrates the trajectory for the VEEGA maneuvers and the subsequent travel to Jupiter.

After three (3) months in space, the Galileo spacecraft will fly past Venus at a distance of around 19,400 kilometers (12,050 miles) in February, 1990. After continuing on this orbit around the sun, the spacecraft will fly by Earth (Earth flyby 1) at an altitude of around 3,700 kilometers (2,298 miles) in December 1990. This will result also in a trajectory around the sun, and the Galileo's thrusters will add 82 meters/second (269 feet/second) to the speed of the spacecraft at about a year after the first Earth flyby. This velocity change is called the deep space maneuver and is performed to adjust the encounter conditions for the second Earth flyby. In December 1992, the Galileo spacecraft will make the second and final Earth flyby at a speed of around 14.1 kilometers/second (46,250 feet/second) and will pass at a distance of approximately 300 kilometers (186 miles) above the Earth's surface. The arrival at Jupiter will occur in March 1996.

The Jet Propulsion Laboratory/NASA has made a preliminary study of the VEEGA maneuvers to determine the probability of Earth re-entry (Reference 5-2). The results of this study indicate that typical errors in the final aim point (i.e., at Earth flyby 2) range from a few kilometers up to around ten (10) kilometers. At the 300 kilometer target altitude, an error greater than 20σ is required for re-entry to occur. Thus, the report concludes that no statistical error will lead to re-entry and that only a failure can do so. The probability of re-entry is reported to be conservatively less than 10^{-6}.

The end of a successful mission has been addressed for the Galileo mission and the following has been concluded. The Galileo spacecraft will be placed in orbit about Jupiter. There is no known mechanism by which any portion of the RTGs could be ejected from Jupiter orbit and return to Earth, and thereby constitute a hazard to the Earth's population.

SECTION 6.0

FLIGHT CONTINGENCY MODES

During the normal operations, the basic mission of the Space Shuttle is to carry the spacecraft and IUS into space, release this payload into orbit, and then return to Earth for another mission. However, in the case of abnormal events, there are also several contingency operational modes that are intended to maintain orbiter and cargo safety.

The Shuttle Orbiter has been designed to recover safely from many failures. The crew can fly the Orbiter back to Earth after certain types of failures which would result in the destruction of a conventional, expendable launch vehicle. A basic requirement for the Shuttle has been for it to withstand a failure and yet be as operational as if the failure had not occurred. It is also required to tolerate a second failure in a flight critical system and still return safely to Earth. There are exceptions to this requirement as noted in the Orbiter Critical Items List (CIL). The following description of Orbiter safety plans covers three exigencies: intact aborts, contingency aborts, and loss of critical functions.

6.1 INTACT ABORTS

The Space Shuttle Vehicle is required to have an intact abort capability for contingencies arising from certain specific failures which might occur during the powered ascent flight phase (lift-off to post MECO OMS insertion). Intact abort is defined as safely returning the Orbiter, crew, and cargo to a suitable landing site. The specific failures which will result in an intact abort are as listed below. These are considered singly without combination.

1. Complete or partial loss of thrust from one SSME
2. Loss of thrust from one OMS engine
3. Loss of two electrical power buses
4. Failure of two auxiliary power units
5. Failure of some life support equipment

Four basic abort modes have been developed to provide continuous intact abort capability for Shuttle missions during the ascent phase: Return-To-Launch-Site (RTLS), Transatlantic Abort Landing (TAL), Abort-Once-Around (AOA), and Abort-To-Orbit (ATO). The four modes are available during different segments of the ascent flight to provide intact abort capability. Two modes, AOA and ATO, are available after MECO in the event of an OMS engine failure. Figure 6-1 is an altitude/range profile showing the relationship between RTLS, TAL, and AOA aborts. Figures 6-2 and 6-3 show the flight profile of an AOA and ATO, respectively. Figure 6-4 shows the overlapping abort regions for a typical Shuttle mission with an SSME failure.

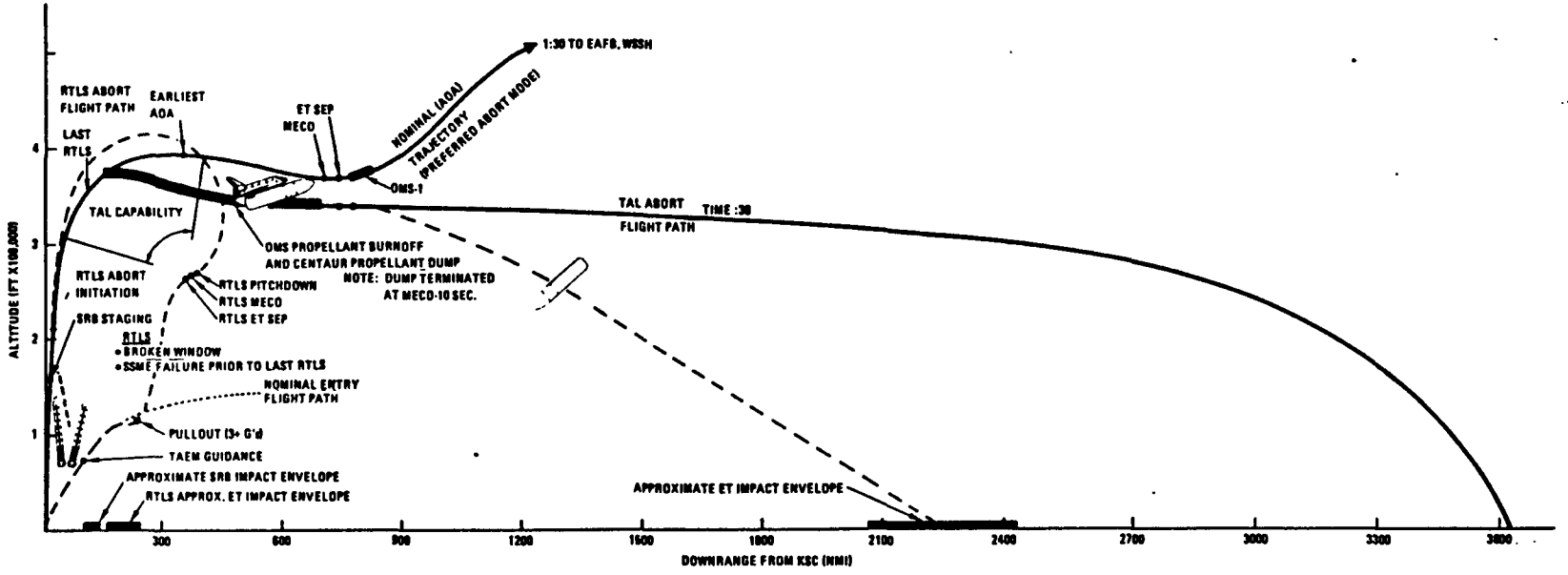

Figure 6-1. Relationship Between RTLS, TAL and AOA Aborts - Altitude vs. Range.

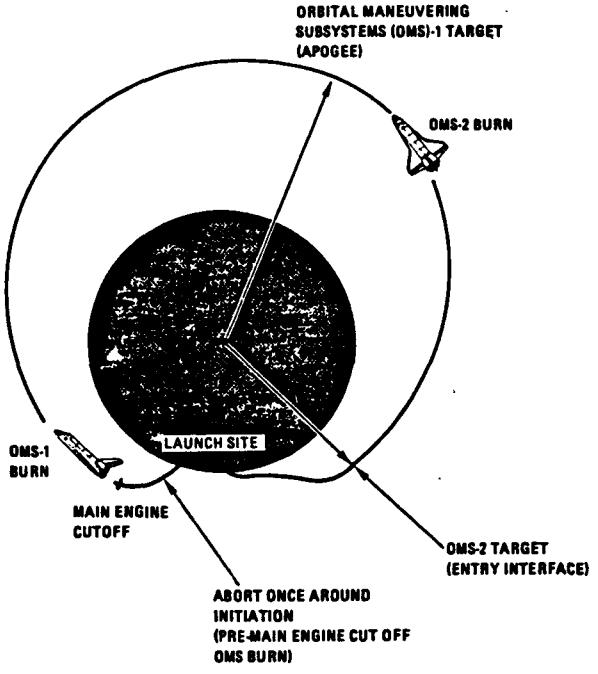

Figure 6-2. Profile of AOA

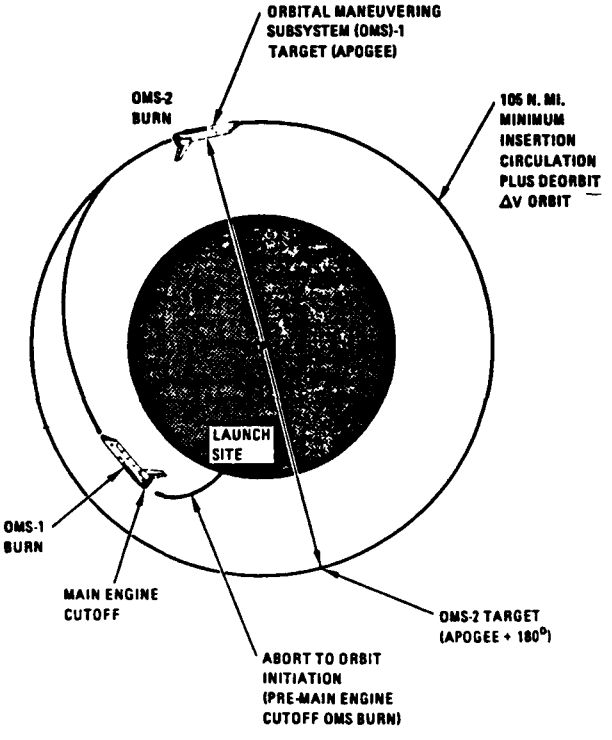

Figure 6-3. Profile of ATO

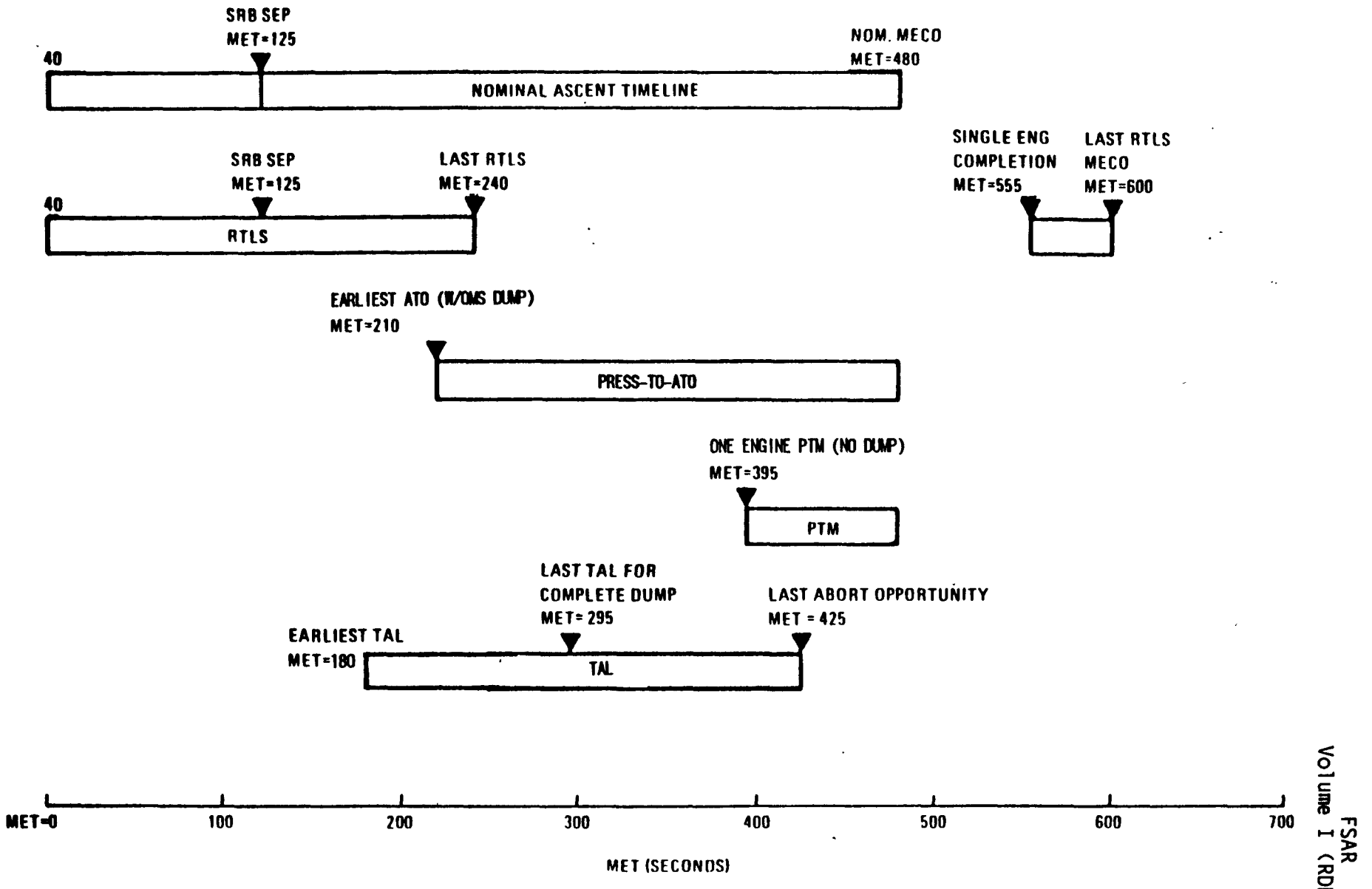

Figure 6-4. Intact Abort Regions for Shuttle Missions

The following paragraphs describe brief summaries of each intact abort made and the choices between modes. Additional information on these abort modes is provided in NSTS-08116, Rev. A.

6.1.1 RTLS

The RTLS abort mode will be used in the event of an SSME failure occurring between lift-off and the end of the predetermined RTLS interval. However, when an overlap occurs between successive abort mode intervals, either abort mode could be selected depending upon abort failure conditions. The RTLS abort mode is selected after separation from the SRBs (second stage flight) even though the SSME failure might have occurred in first stage flight; the vehicle will continue accelerating downrange with the two remaining SSMEs until the MPS propellant equals the amount required to reverse the direction of flight and propel the vehicle to the RTLS MECO target. The RTLS MECO target is selected to provide acceptable Orbiter/ET separation conditions, acceptable ET impact location, and acceptable range to permit gliding safely back to the selected landing site. A typical earliest (liftoff) and latest RTLS abort sequence of events are defined in Table 6-1. Figure 6-5 is an altitude/time profile for RTLS-type aborts. Figure 6-6 is an altitude/range profile for RTLS-type aborts.

6.1.2 TAL

The TAL abort mode will be used for an SSME failure between two engine TAL capability and press-to-MECO. During the RTLS/TAL overlap, TAL is preferred because it is more tolerant of a second SSME failure. After selection of the TAL abort mode, the vehicle will accelerate downrange to the TAL MECO target. At abort select, the OMS propellant dump is initiated to achieve the correct landing weight and center-of-gravity for entry. At an I-loaded velocity (VI=15,400 ft/s) the vehicle rolls heads-up, which decreases ET heating and places the Orbiter in entry attitude prior to MECO (VI=23,800 ft/s). After ET separation, the onboard computers are loaded with the entry flight software, and the Orbiter glides to the landing site. Landing sites change as a function of intended orbit inclination. For example, for orbit inclinations near 28 degrees, Dakar, Senegal (on the west coast of Africa) is the in-plane landing site. The primary site is Ben Guerir, Morocco. For inclinations near 57 degrees, Zaragoza, Spain, is currently the primary landing site. The weather alternate landing site for both of these inclinations is Moron, Spain. There is a possibility of installing runway overrun barriers at some of the TAL/Emergency landing sites; the barrier being considered is a net, which would cause minimal damage to the Orbiter. A typical TAL abort sequence of events is defined in Table 6-2.

6.1.3 PRESS-TO-MECO (AOA or ATO)

If an SSME fails after Press-to-MECO, the Orbiter continues to the nominal MECO target. On some flights, a predetermined amount of OMS propellant will be dumped during powered flight by declaring ATO shortly after the SSME failure. This weight decrease, accompanied by a small increase in thrust from the OMS engines, will increase powered flight performance. After MECO, the

Table 6-1. RTLS Abort Sequence of Events for an Earliest and Latest SSME Failure

Mission Elapsed Time (sec)		Event
Earliest	Latest	
0	0	Liftoff of the Space Shuttle Vehicle
1	240	SSME Failure
125	125	SRB Separation
150	255	RTLS Abort Selected
312	255	OMS Propellant Dump Initiated
424	255	Power Pitch Around Initiated
586	425	OMS Propellant Dump Completed
704	579	Power Pitch Down
721	594	MECO
734	608	ET Separation
745	620	MPS Dump Initiation
765	640	Aft RCS Propellant Dump Initiation
900	775	Aft RCS Propellant Dump Completed
865	740	MPS Dump Completed
940	800	Mach 3.5
1400	1260	Landing

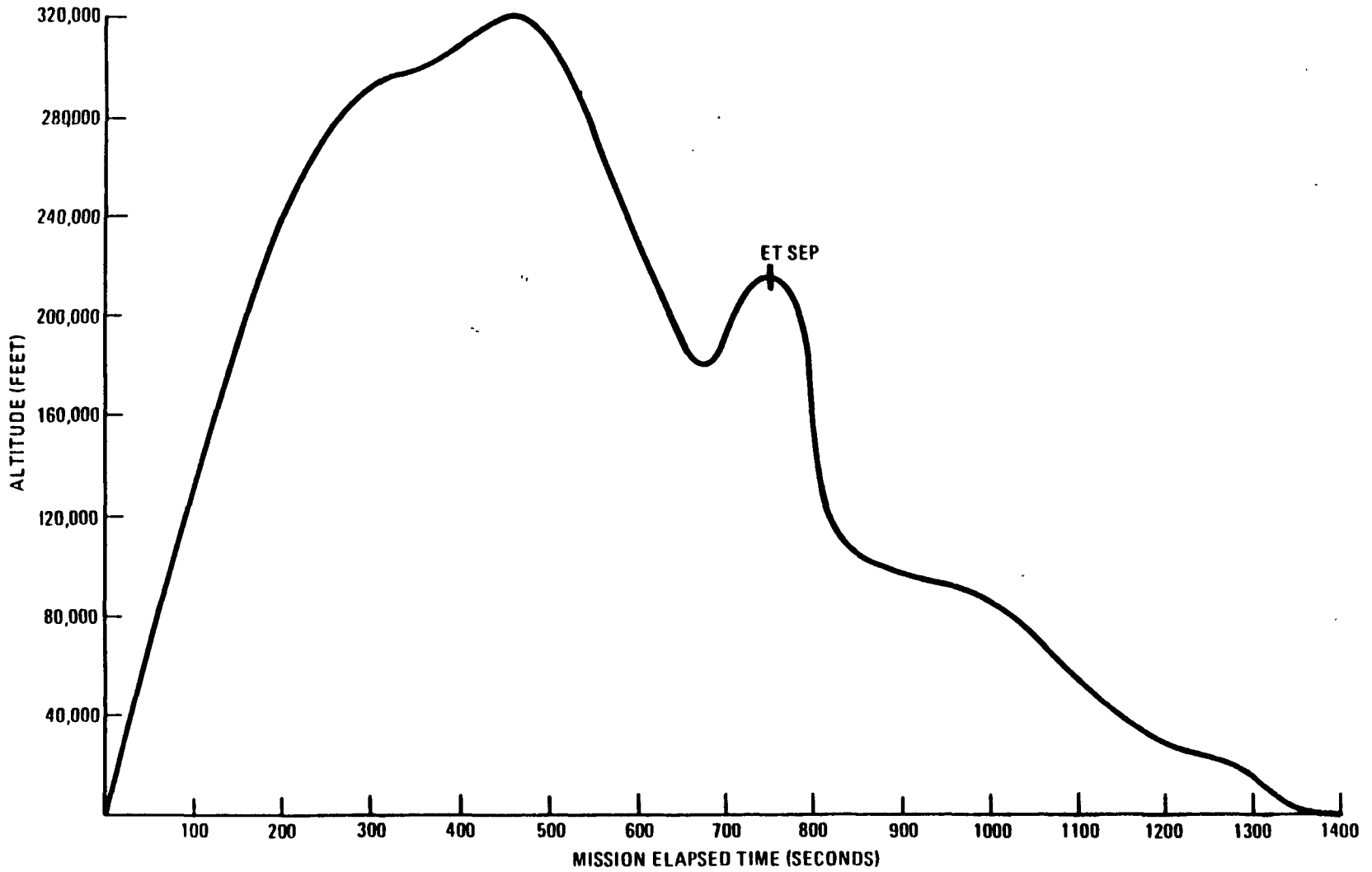

Figure 6-5. Altitude vs. Time for Typical RTLS Type Abort

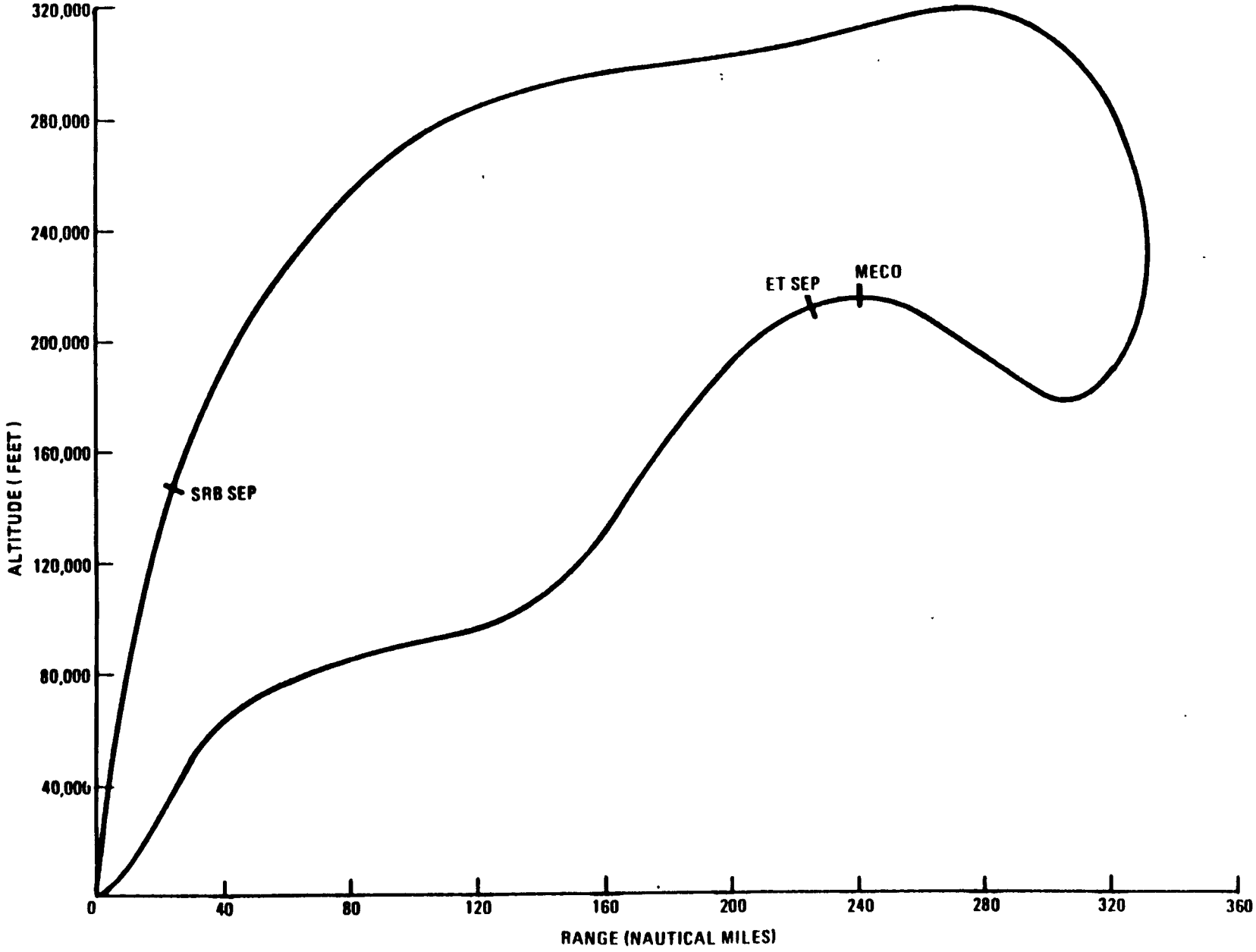

Figure 6-6. Typical RTLS Abort Altitude vs. Range

Table 6-2. TAL Abort Sequence of Events for an Earliest and Latest TAL Abort

Mission Elapsed Time (sec)		Event
Earliest	Latest	
0	0	Liftoff of the Space Shuttle Vehicle
125	125	SRB Separation
240	355	TAL Abort Selected
240	355	OMS Propellant Dump Initiated
480	415	Vehicle Roll-To-Heads Up Attitude
435	510	OMS Propellant Dump Completed
570	520	MECO
588	538	ET Separation
600	550	+X ARCS Thruster Firing Initiated (Manual)
605	555	+X ARCS Stop, MPS Dump Initiated (Manual)
635	585	MPS Dump Stop (Auto)
685	610	Entry Flight Software Memory Load
1650	1600	Mach 3.5
2100	2050	Landing

energy, the OMS delta-V remaining, and the OMS delta-V required for orbit are evaluated. If the OMS delta-V is insufficient for orbit insertion and a subsequent deorbit, an Abort-Once-Around (AOA) will be performed with the OMS engines.

6.2 CONTINGENCY ABORTS

A contingency abort will result if two SSMEs fail prior to single engine TAL capability or if three SSMEs fail prior to AOA capability. There is a possibility of performing a Split-S abort to the KSC runway if two or three SSMEs fail in the first 20 seconds. If three SSMEs fail during the last 30 seconds of an ascent, there is sufficient energy to glide to a runway in Africa. All emergency landing sites being considered are longer than 10,000 feet. During the remainder of the ascent, a contingency abort will result with the crew bailing out at 20,000 feet and the Orbiter impacting the water at about 180 kts with an alpha of about 15 degrees; the corresponding vertical descent rate is about 80 ft/s.

6.3 LOSS OF CRITICAL FUNCTION

This section lists certain types of failures that would preclude either an intact or a contingency abort. These are the failures that lead to the accidents discussed in Volume II, the Accident Model Document.

The types of failures that lead to a loss of critical function are: aft compartment explosion, rupture or explosion of the ET, burnthrough of an SRB, failure of major structure, complete loss of guidance or control, failure of one SRB to ignite, loss of thrust from either SRB, hardover condition of a main engine or an SRB, failure to separate the Orbiter from the ET, failure of the nozzle of an SRB, or premature separation of an SRB from the ET.

6.4 FAST SEPARATION

Fast ET separation will be used during a contingency abort following failure of two SSMEs and prior to single engine TAL capability, or following the failure of three SSMEs during the first stage. It can only be selected manually by the crew when software is in Major Mode (MM) 102, 103, or 601. Here MM102 is first stage ascent, MM103 is second stage ascent, and MM601 is powered RTLS. The fast separation sequence will be entered if ET separation is initiated manually in MM102 and MM601, but in MM103 it will be entered only if a second SSME failure has been confirmed in addition.

The fast sequence shortens the time between MECO and Structural Release (SR) by eliminating some of the timed intervals between commands which allows the first function to be completed before a succeeding function is commanded. Intervals are eliminated in both the SSME Operations (OPS) and separation sequence. The SSME OPS eliminates the interval between MECO and MECO Confirmed. At the latter event, the Separation Sequencer is initiated. The time from MECO to the command ALL PREVALVES COMMANDED CLOSED is shortened from nominal six seconds (approximately) to about 3.75 seconds. The Separation Sequencer is shortened by elimination of delays for PIC arm and fire, for feedline disconnect closure, and for umbilical door closure.

Small differences exist in the fast separation sequencer depending on the MM in effect when it is entered: if in MM103, the MPS gimbals are moved to the dump position after shutdown; otherwise they are moved to the stow position. Also, if in MM103, the -Z Cmd is issued one cycle prior to structural separation; otherwise the -Z jets are fired at structural separation. Finally, if the fast sequence is entered from MM102, the umbilical doors remain open and latched, and a contingency propellant dump is declared. Otherwise, the umbilical doors are closed in a normal sequence requiring about 66 seconds.

The fast separation sequence will not be selected in MM102 while the SRBs are burning because the Orbiter will hang up on the aft attach points and break up aerodynamically. The only planned use in MM102 is when the SRB chamber pressure has decayed to less than 50 psi for three SSMEs failed.

BLANK

SECTION 7.0

LAUNCH SITE

7.1 LOCATION AND SITE DESCRIPTION

The Space Shuttle will be launched from launch pad 39A at the John F. Kennedy Space Center, Cape Canaveral, Florida for the Galileo mission. Figure 7-1 is a map of the Kennedy Space Center (KSC) and Cape Canaveral Air Force Station (CCAFS). The map shows the runway for Orbiter landings, the vehicle assembly building (where the Shuttle will be mated on a mobile launch platform), the Solid Motor Assembly Building (SMAB), the Vertical Processing Facility, (VPF), (where the spacecraft will be mated to the IUS), and launch pad 39A (from which the Shuttle carrying the Galileo payload will be launched). Figure 7-2 is an expanded map of the launch site. Figures 7-3 and 7-4 show a photograph and dimensional details of the Space Shuttle in relation to the fixed and rotating service structures.

A paved roadway borders the launch area. The roadway is roughly circular and located approximately 1200 feet from the center of the launch pad. The Space Shuttle Crawlerway enters Launch Pad 39A from the South and continues to the launch service structures. The crawlerway consists of concrete and packed gravel. The launch pad structure consists of concrete elevated approximately 48 feet from ground (sea) level. The launch service structures are west of the Orbiter in its prelaunch configuration and are primarily constructed of steel. Under the Orbiter is an approximately 14,000 sq. ft. launch platform constructed of steel. A series of concrete roads and buildings extend radially from the pad center. The greatest concentration of concrete structures lies west of the launch pad center. Steel LOX and LH_2 facilities lie respectively to the northwest and northeast of the pad center near the boundary roadway. The majority of the launch pad area consists of sand.

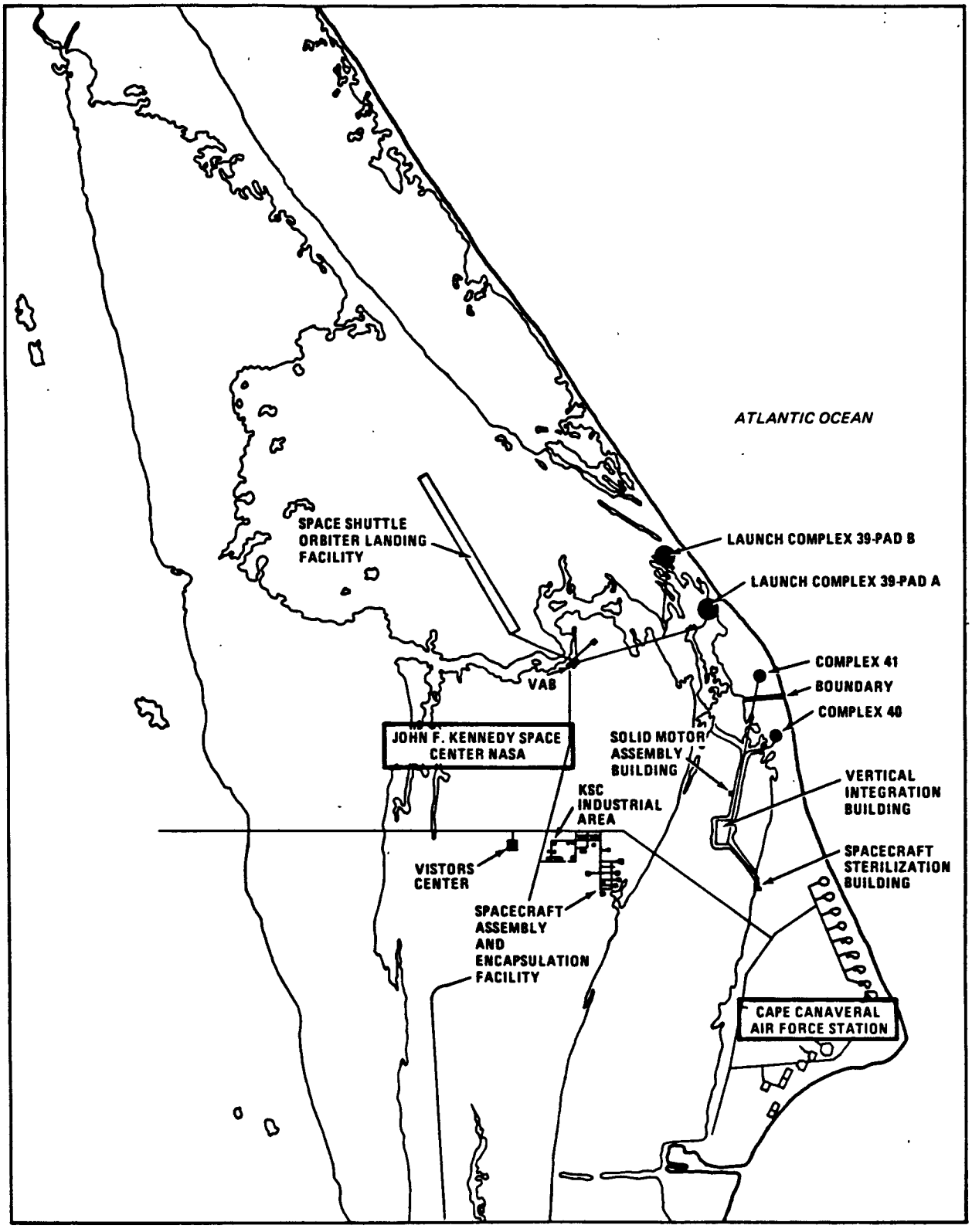

Figure 7-1. Map of Kennedy Space Center and Cape Canaveral Air Force Base

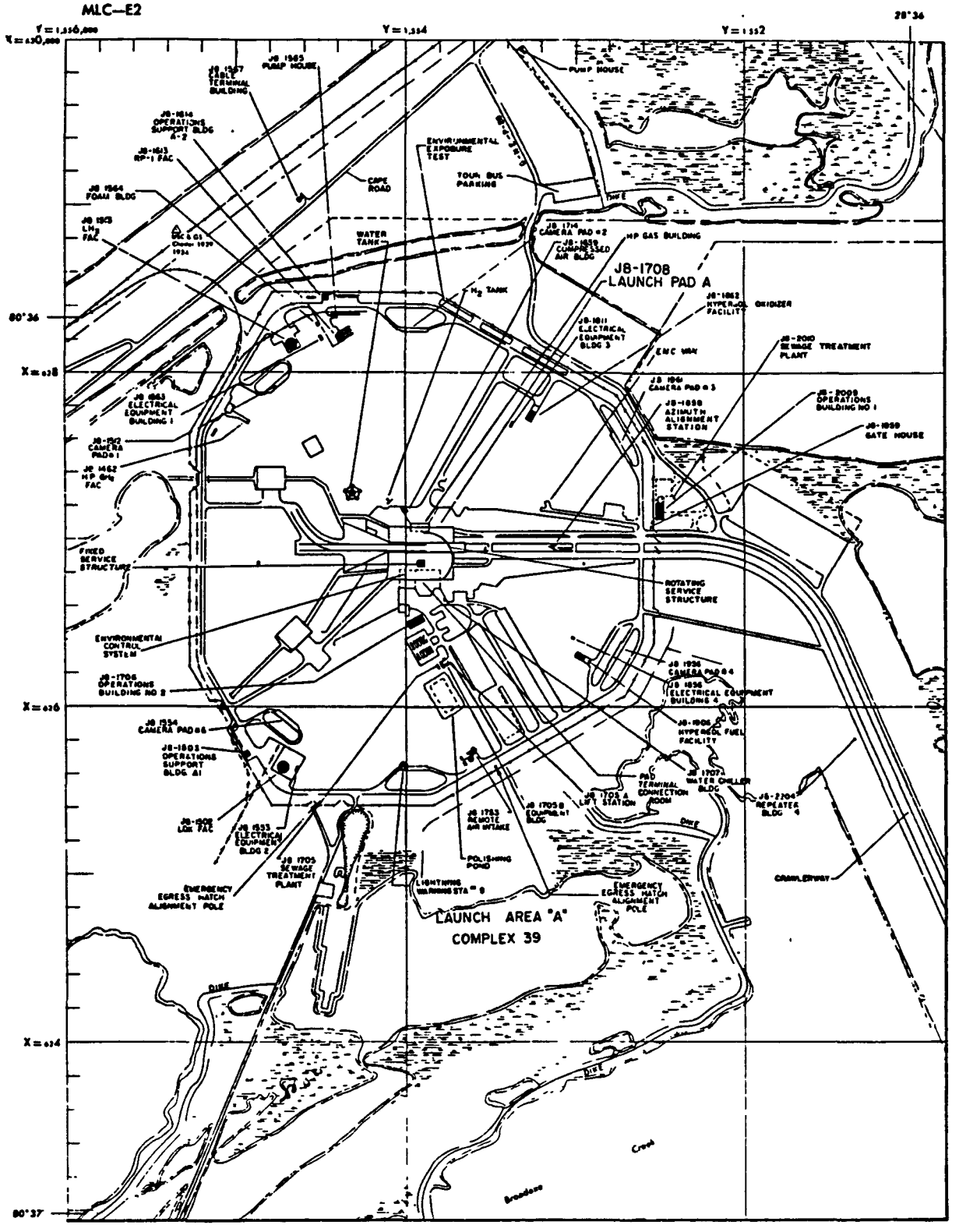

Figure 7-2. Launch Pad 39A at KSC

BLANK

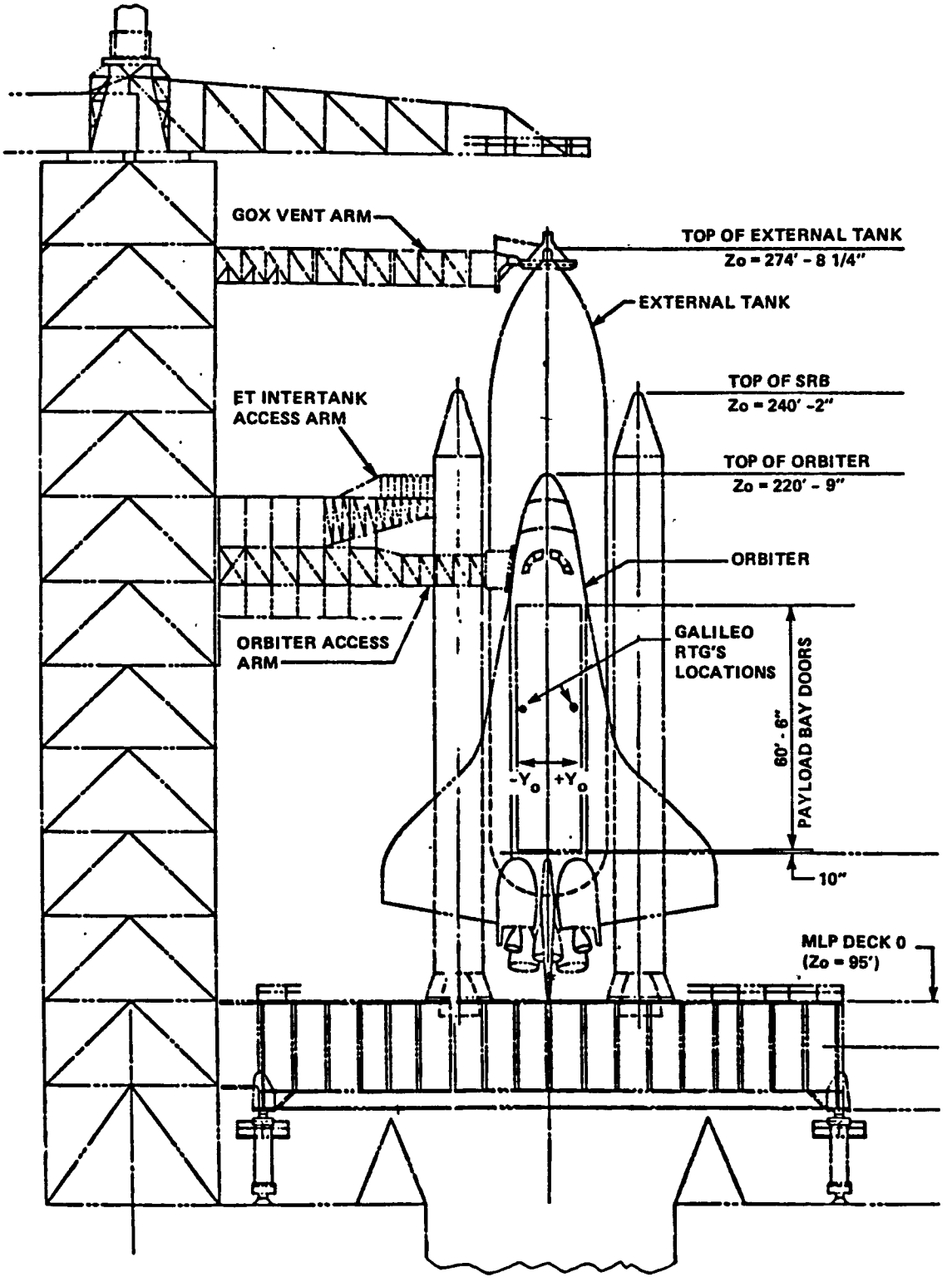

Figure 7-4. Launch Complex Reference Elevations Showing Location of the RTG's for the Galileo Mission

BLANK

SECTION 8.0

REFERENCES

1-1 Feldman, L. "Final Report on Wallops Island Drop Tests." GE Report PIR U-7143-RTG-6235, 14 August 1980.

2-1 Space Shuttle Data for Planetary Mission Radioisotope Thermoelectric Generator (RTG) Safety Analysis Rev. A (Draft) NSTS-08116. No date. (Received 5 June 1987).

5-1 Printout from Magnetic Tape STS51EC1T01 Issued December 1984. Nominal Range Safety Trajectory Data for the Space Transportation System Mission 51E Ascent. Through JSC Project Office by J. W. Nolley/FM3.

5-2 Mitchell, R. and D'Amario, L. "Galileo Earth Avoidance Study Plan and Preliminary Assessment." JPL D-4246, 15 April 1987.

BLANK

APPENDIX A
PLUTONIUM FUEL PROPERTIES/CHARACTERISTICS

Included in this appendix are the currently known properties and characteristics of the plutonium dioxide (PuO_2) fuel. Several of the properties listed are referenced to plutonium-239 since the corresponding data for plutonium-238 is not available. Information indicated by an asterisk (*) has been taken directly from Document MLM-1691, "Plutonium-238 Isotope Fuel Form Data Sheets," Monsanto Research Corporation - Mound Laboratory, October 31, 1969. Document MLM-1691 is the currently accepted reference for this information.

A.1 PRODUCTION PROCESS

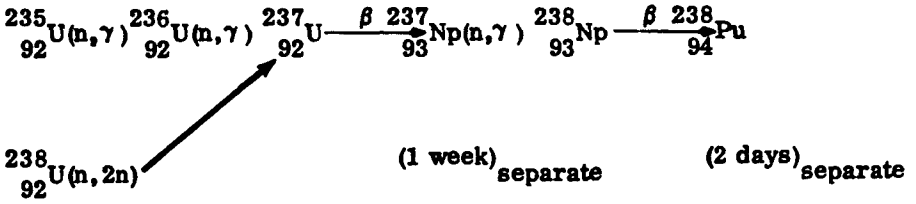

A.2 COMPOSITION OF PRODUCTION GRADE FUEL*

1. Oxygen

   11.8 wt %

2. Plutonium

   88.2 wt %

Isotope	Concentration (wt %)
^{236}Pu	< 0.0001
^{238}Pu	83.5
^{239}Pu, ^{240}Pu, ^{241}Pu, ^{242}Pu	16.3

3.

Actinide Impurities	Concentration (wt %)
^{241}Am	0.0033
^{237}Np	0.130
^{234}U	0.140, increases at the rate of decay of ^{238}Pu

The total of other isotopic impurities including ^{231}Pa ^{232}Th, ^{233}U, ^{235}U, ^{236}U, and ^{227}Ac does not exceed 1 wt % of the fuel.

4. Nonactinide Cationic Impurities (Reference A-9). The total of all nonactinide cationic impurities shall not exceed 2550 ppm (sintered shard weight). Iron, aluminum and silicon shall not exceed the values specified in the following table, while it will be reported if the other individual elements exceed the guide values listed. Values are to be analyzed at SRP 772-F Laboratory (or equivalent).

Element	Sintered Shards ppm by Shard Weight
Al	150
B	1
Ca	300
Cd	50
Cr	250
Cu	100
Fe	800
Mg	50
Mn	50
Mo	250
Na	250
Ni	150
Pb	100
Si	200
Sn	50
Zn	50

A.3 NUCLEAR CHARACTERISTICS

1. Decay Scheme: See Figure A-1
2. Decay Chain: See Figure A-2
3. Gamma Spectrum: See Figure A-3 and A-4

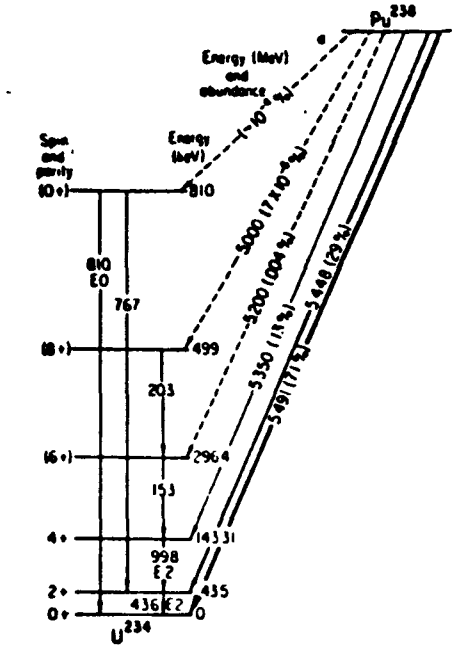

FIGURE A-1 DECAY SCHEME OF Pu^{238}

TABLE A-1
INITIAL ASSAY OF RADIONUCLIDES IN THE FLIGHT RTGs

Nuclide	Half-lives* (years)	F-1 amount on 15-Sep-82 (grams)**	F-1 amount on 15-Sep-82 (curies)	F-3 amount on 08-Apr-83 (grams)	F-3 amount on 08-Apr-83 (curies)	F-5 amount on 20-Sep-82 (grams)	F-5 amount on 20-Sep-82 (curies)
Pu-236	2.85	4.620E-05	2.46E-02	5.000E-05	2.66E-02	4.820E-05	2.56E-02
Pu-238	87.7	8019.831	1.37E+05	8060.992	1.38E+05	8015.569	1.37E+05
Pu-239	2.41E+04	1289.918	8.01E+01	1217.907	7.56E+01	1296.579	8.05E+01
Pu-240	6560	181.685	4.13E+01	161.342	3.66E+01	180.843	4.11E+01
Pu-241	14.4	36.236	3.73E+03	32.761	3.36E+03	36.611	3.77E+03
Pu-242	3.76E-05	11.831	4.65E-02	7.664	3.01E-02	10.839	4.26E-02
Am-241	432.2	0.954	3.27E+00	0.948	3.25E+00	0.954	3.27E+00
Np-237	2.14E+06	7.989	5.63E-03	8.138	5.74E-03	6.586	4.64E-03
U-234	2.45E+05	4.425	2.76E-02	3.213	2.00E-02	4.903	3.06E-02
Th-232	1.41E+10	8.466	9.25E-07	11.324	1.24E-06	8.149	8.91E-07

* The values of the half-lives are from Atomic Data and Nuclear Data Tables, Volume 29, Number 2, September 1983.

* The radionuclide quantities listed for the flight RTGs (F-1, F-3, and F-5) are calculated mean values of the sum of all the pellets in each RTG. These values are valid on the date listed for each RTG.

TABLE A-2

F-1 ASSEMBLY

ACTIVITY OF PARENT AND DAUGHTERS ON 15 MAY 1986

Nuclide——>	Pu-236	U-232	Th-228	Ra-224	Rn-220	Po-216	Pb-212	Bi-212	Tl-208	Po-212
T(1/2) yr.—>	2.85E+00	6.89E+01	1.91E+00	1.00E-02	1.76E-06	4.75E-09	1.21E-03	1.15E-04	5.84E-06	9.44E-15
curies——>	1.01E-02	5.87E-04	2.94E-04	2.93E-04	2.93E-04	2.93E-04	2.92E-04	2.92E-04	1.05E-04	1.87E-04

Nuclide——>	Pu-238	U-234	Th-230	Ra-226	Rn-222	Po-218	Pb-214	Bi-214	Po-214	Pb-210	Bi-210	Po-210
T(1/2) yr.—>	8.77E+01	2.45E+05	7.54E+04	1.60E+03	1.05E-02	5.91E-06	5.10E-05	3.78E-05	5.20E-12	2.23E+01	1.37E-02	3.79E-01
curies——>	1.33E+05	1.40E+00	2.37E-05	1.26E-08	1.24E-08	1.24E-08	1.24E-08	1.24E-08	1.24E-08	3.45E-10	3.38E-10	2.03E-10

Nuclide——>	Pu-239	U-235	Th-231	Pa-231	Ac-227	Th-227	Ra-223	Rn-219	Po-215	Pb-211	Bi-211	Tl-207
T(1/2) yr.—>	2.41E+04	7.04E+08	2.91E-03	3.28E+04	2.18E+01	5.13E-02	3.13E-02	1.25E-07	5.48E-11	6.86E-05	4.58E-06	9.07E-06
curies——>	8.01E+01	2.89E-07	2.88E-07	1.12E-11	4.21E-13	3.97E-13	3.82E-13	3.82E-13	3.82E-13	3.82E-13	3.82E-13	3.82E-13

Nuclide——>	Pu-240	U-236	Th-232	Ra-228	Ac-228	Th-228	Ra-224	Rn-220	Po-216	Pb-212	Bi-212	Tl-208	Po-212
T(1/2) yr.—>	6.56E+03	2.34E+07	1.41E+10	5.75E+00	6.99E-04	1.91E+00	1.00E-02	1.76E-06	4.75E-09	1.21E-03	1.15E-04	5.84E-06	9.44E-15
curies——>	4.12E+01	4.48E-06	4.03E-16	5.33E-17	5.33E-17	1.41E-17	1.39E-17	1.39E-17	1.39E-17	1.39E-17	1.39E-17	5.00E-18	8.89E-18

Nuclide——>	Pu-241	Am-241	Np-237	Pa-233	U-233	Th-229	Ra-225	Ac-225	Fr-221	At-217	Bi-213	Po-213	Pb-209
T(1/2) yr.—>	1.44E+01	4.32E+02	2.14E+06	7.39E-02	1.59E+05	7.34E+03	4.05E-02	2.74E-02	9.32E-06	1.02E-09	8.67E-05	1.33E-13	3.71E-04
curies——>	3.13E+03	2.00E+01	1.23E-05	1.16E-05	6.08E-11	5.17E-15	4.84E-15	4.64E-15	4.64E-15	4.64E-15	4.64E-15	4.64E-15	4.63E-15

Nuclide——>	Pu-242	U-238	Th-234	Pa-234	U-234	Th-230	Ra-226	Rn-222	Po-218	Pb-214	Bi-214	Po-214	Pb-210	Bi-210
T(1/2) yr.—>	3.76E+05	4.47E+09	6.60E-02	2.22E-06	2.45E+05	7.54E+04	1.60E+03	1.05E-02	5.91E-06	5.10E-05	3.78E-05	5.20E-12	2.23E+01	1.37E-02
curies——>	4.65E-02	2.64E-11	2.57E-11	2.57E-11	1.30E-16	8.82E-22	<1E-22	1.22E-21	<1E-22	7.03E-22	9.50E-22	<1E-22	<1E-22	<1E-22

Nuclide——>	Am-241	Np-237	Pa-233	U-233	Th-229	Ra-225	Ac-225	Fr-221	At-217	Bi-213	Po-213	Pb-209
T(1/2) yr.—>	4.32E+02	2.14E+06	7.39E-02	1.59E+05	7.33E+03	4.05E-02	2.74E-02	9.32E-06	1.02E-09	8.67E-05	1.33E-13	3.71E-04
curies——>	3.26E+00	3.87E-06	3.76E-06	2.92E-11	3.27E-15	3.12E-15	3.02E-15	3.02E-15	3.02E-15	3.02E-15	3.02E-15	3.01E-15

Nuclide——>	Np-237	Pa-233	U-233	Th-229	Ra-225	Ac-225	Fr-221	At-217	Bi-213	Po-213	Pb-209
T(1/2) yr.—>	2.14E+06	7.39E-02	1.59E+05	7.33E+03	4.05E-02	2.74E-02	9.13E-06	8.84E-05	8.67E-05	1.33E-13	3.71E-04
curies——>	5.63E-03	5.63E-03	8.73E-08	1.47E-11	1.42E-11	1.39E-11	1.39E-11	1.39E-11	1.39E-11	1.39E-11	1.39E-11

Nuclide——>	U-234	Th-230	Ra-226	Rn-222	Po-218	Pb-214	Bi-214	Po-214	Pb-210	Bi-210	Po-210
T(1/2) yr.—>	2.45E+05	7.54E+04	1.60E+03	1.05E-02	5.91E-06	5.10E-05	3.78E-05	5.20E-12	2.23E+01	1.37E-02	3.79E-01
curies——>	2.76E-02	9.29E-07	7.37E-10	7.31E-10	7.31E-10	7.31E-10	7.31E-10	7.31E-10	2.69E-11	2.64E-11	1.76E-11

Nuclide——>	Th-232	Ra-228	Ac-228	Th-228	Ra-224	Rn-220	Po-216	Pb-216	Bi-212	Tl-208	Po-212
T(1/2) yr.—>	1.41E+10	5.75E+00	6.99E-04	1.91E+00	1.00E-02	1.76E-06	4.75E-09	1.21E-03	1.15E-04	5.84E-06	9.44E-15
curies——>	9.25E-07	3.30E-07	3.30E-07	1.56E-07	1.53E-07	1.53E-07	1.53E-07	1.53E-07	1.53E-07	5.58E-08	9.93E-08

TABLE A-3

F-3 ASSEMBLY

ACTIVITY OF PARENT AND DAUGHTERS ON 15 MAY 1986

Nuclide——>	Pu-236	U-232	Th-228	Ra-224	Rn-220	Po-216	Pb-212	Bi-212	Tl-208	Po-212
T(1/2) yr.—>	2.85E+00	6.89E+01	1.91E+00	1.00E-02	1.76E-06	4.75E-09	1.21E-03	1.15E-04	5.84E-06	9.44E-15
curies——>	1.25E-02	5.72E-04	2.53E-04	2.52E-04	2.52E-04	2.52E-04	2.52E-04	2.52E-04	9.06E-05	1.61E-04

Nuclide——>	Pu-238	U-234	Th-230	Ra-226	Rn-222	Po-218	Pb-214	Bi-214	Po-214	Pb-210	Bi-210	Po-210
T(1/2) yr.—>	8.77E+01	2.45E+05	7.54E+04	1.60E+03	1.05E-02	5.91E-06	5.10E-05	3.78E-05	5.20E-12	2.23E+01	1.37E-02	3.79E-01
curies——>	1.35E+05	1.20E+00	1.71E-05	7.69E-09	7.58E-09	7.58E-09	7.58E-09	7.58E-09	7.58E-09	1.79E-10	1.74E-10	9.71E-11

Nuclide——>	Pu-239	U-235	Th-231	Pa-231	Ac-227	Th-227	Ra-223	Rn-219	Po-215	Pb-211	Bi-211	Tl-207
T(1/2) yr.—>	2.41E+04	7.04E+08	2.91E-03	3.26E+04	2.18E+01	5.13E-02	3.13E-02	1.25E-07	5.48E-11	6.86E-05	4.58E-06	9.07E-06
curies——>	7.56E+01	2.31E-07	2.31E-07	7.55E-12	2.42E-13	2.26E-13	2.16E-13	2.16E-13	2.16E-13	2.16E-13	2.16E-13	2.16E-13

Nuclide——>	Pu-240	U-236	Th-232	Ra-228	Ac-228	Th-228	Ra-224	Rn-220	Po-216	Pb-212	Bi-212	Tl-208	Po-212
T(1/2) yr.—>	6.56E+03	2.34E+07	1.41E+10	5.75E+00	6.99E-04	1.91E+00	1.00E-02	1.76E-06	4.75E-09	1.21E-03	1.15E-04	5.84E-06	9.44E-15
curies——>	3.66E+01	3.37E-06	2.57E-16	2.92E-17	2.92E-17	6.77E-18	6.65E-18	6.65E-18	6.65E-18	6.64E-18	6.64E-18	2.39E-18	4.25E-18

Nuclide——>	Pu-241	Am-241	Np-237	Pa-233	U-233	Th-229	Ra-225	Ac-225	Fr-221	At-217	Bi-213	Po-213	Pb-209
T(1/2) yr.—>	1.44E+01	4.32E+02	2.14E+06	7.39E-02	1.59E+05	7.34E+03	4.05E-02	2.74E-02	9.32E-06	1.02E-09	8.67E-05	1.33E-13	3.71E-04
curies——>	2.91E+03	1.56E+01	8.02E-06	7.50E-06	3.31E-11	2.37E-15	2.19E-15	2.08E-15	2.08E-15	2.08E-15	2.08E-15	2.08E-15	2.08E-15

Nuclide——>	Pu-242	U-238	Th-234	Pa-234	U-234	Th-230	Ra-226	Rn-222	Po-218	Pb-214	Bi-214	Po-214	Pb-210	Bi-210
T(1/2) yr.—>	3.76E+05	4.47E+09	6.60E-02	2.22E-06	2.45E+05	7.54E+04	1.60E+03	1.05E-02	5.91E-06	5.10E-05	3.78E-05	5.20E-12	2.23E+01	1.37E-02
curies——>	3.01E-02	1.45E-11	1.40E-11	1.40E-11	5.98E-17	2.01E-22	<1E-22	7.90E-22	<1E-22	4.55E-22	6.14E-22	<1E-22	<1E-22	<1E-22

Nuclide——>	Am-241	Np-237	Pa-233	U-233	Th-229	Ra-225	Ac-225	Fr-221	At-217	Bi-213	Po-213	Pb-209
T(1/2) yr.—>	4.32E+02	2.14E+06	7.39E-02	1.59E+05	7.33E+03	4.05E-02	2.74E-02	9.32E-06	1.02E-09	8.67E-05	1.33E-13	3.71E-04
curies——>	3.24E+00	3.26E-06	3.15E-06	2.06E-11	1.95E-15	1.84E-15	1.77E-15	1.77E-15	1.77E-15	1.76E-15	1.76E-15	1.76E-15

Nuclide——>	Np-237	Pa-233	U-233	Th-229	Ra-225	Ac-225	Fr-221	At-217	Bi-213	Po-213	Pb-209
T(1/2) yr.—>	2.14E+06	7.39E-02	1.59E+05	7.33E+03	4.05E-02	2.74E-02	9.13E-06	8.84E-05	8.67E-05	1.33E-13	3.71E-04
curies——>	5.74E-03	5.74E-03	7.49E-08	1.06E-11	1.02E-11	9.92E-12	9.92E-12	9.92E-12	9.92E-12	9.92E-12	9.92E-12

Nuclide——>	U-234	Th-230	Ra-226	Rn-222	Po-218	Pb-214	Bi-214	Po-214	Pb-210	Bi-210	Po-210
T(1/2) yr.—>	2.45E+05	7.54E+04	1.60E+03	1.05E-02	5.91E-06	5.10E-05	3.78E-05	5.20E-12	2.23E+01	1.37E-02	3.79E-01
curies——>	2.00E-02	5.71E-07	3.84E-10	3.80E-10	3.80E-10	3.80E-10	3.80E-10	3.80E-10	1.19E-11	1.16E-11	7.26E-12

Nuclide——>	Th-232	Ra-228	Ac-228	Th-228	Ra-224	Rn-220	Po-216	Pb-216	Bi-212	Tl-208	Po-212
T(1/2) yr.—>	1.41E+10	5.75E+00	6.99E-04	1.91E+00	1.00E-02	1.76E-06	4.75E-09	1.21E-03	1.15E-04	5.84E-06	9.44E-15
curies——>	1.24E-06	3.86E-07	3.86E-07	1.62E-07	1.61E-07	1.61E-07	1.61E-07	1.61E-07	1.61E-07	5.79E-08	1.03E-07

TABLE A-4

F-5 ASSEMBLY

ACTIVITY OF PARENT AND DAUGHTERS ON 15 MAY 1986

Nuclide——>	Pu-236	U-232	Th-228	Ra-224	Rn-220	Po-216	Pb-212	Bi-212	Tl-208	Po-212
T(1/2) yr.—>	2.85E+00	6.89E+01	1.91E+00	1.00E-02	1.76E-06	4.75E-09	1.21E-03	1.15E-04	5.84E-06	9.44E-15
curies——>	1.05E-02	6.11E-04	3.05E-04	3.04E-04	3.04E-04	3.04E-04	3.04E-04	3.04E-04	1.09E-04	1.94E-04

Nuclide——>	Pu-238	U-234	Th-230	Ra-226	Rn-222	Po-218	Pb-214	Bi-214	Po-214	Pb-210	Bi-210	Po-210
T(1/2) yr.—>	8.77E+01	2.45E+05	7.54E+04	1.60E+03	1.05E-02	5.91E-06	5.10E-05	3.78E-05	5.20E-12	2.23E+01	1.37E-02	3.79E-01
curies——>	1.33E+05	1.40E+00	2.35E-05	1.24E-08	1.23E-08	1.23E-08	1.23E-08	1.23E-08	1.23E-08	3.40E-10	3.32E-10	2.00E-10

Nuclide——>	Pu-239	U-235	Th-231	Pa-231	Ac-227	Th-227	Ra-223	Rn-219	Po-215	Pb-211	Bi-211	Tl-207
T(1/2) yr.—>	2.41E+04	7.04E+08	2.91E-03	3.28E+04	2.18E+01	5.13E-02	3.13E-02	1.25E-07	5.48E-11	6.88E-05	4.58E-06	9.07E-06
curies——>	8.05E+01	2.89E-07	2.89E-07	1.11E-11	4.18E-13	3.94E-13	3.80E-13	3.80E-13	3.80E-13	3.80E-13	3.80E-13	3.80E-13

Nuclide——>	Pu-240	U-236	Th-232	Ra-228	Ac-228	Th-228	Ra-224	Rn-220	Po-216	Pb-212	Bi-212	Tl-208	Po-212
T(1/2) yr.—>	6.56E+03	2.34E+07	1.41E+10	5.75E+00	6.99E-04	1.91E+00	1.00E-02	1.76E-06	4.75E-09	1.21E-03	1.15E-04	5.84E-06	9.44E-15
curies——>	4.11E+01	4.44E-06	3.98E-16	5.25E-17	5.25E-17	1.39E-17	1.37E-17	1.37E-17	1.37E-17	1.36E-17	1.36E-17	4.91E-18	8.73E-18

Nuclide——>	Pu-241	Am-241	Np-237	Pa-233	U-233	Th-229	Ra-225	Ac-225	Fr-221	At-217	Bi-213	Po-213	Pb-209
T(1/2) yr.—>	1.44E+01	4.32E+02	2.14E+06	7.39E-02	1.59E+05	7.34E+03	4.05E-02	2.74E-02	9.32E-06	1.02E-09	8.67E-05	1.33E-13	3.71E-04
curies——>	3.16E+03	2.02E+01	1.23E-05	1.16E-05	6.08E-11	5.14E-15	4.82E-15	4.61E-15	4.61E-15	4.61E-15	4.61E-15	4.61E-15	4.61E-15

Nuclide——>	Pu-242	U-238	Th-234	Pa-234	U-234	Th-230	Ra-226	Rn-222	Po-218	Pb-214	Bi-214	Po-214	Pb-210	Bi-210
T(1/2) yr.—>	3.76E+05	4.47E+09	6.60E-02	2.22E-06	2.45E+05	7.54E+04	1.60E+03	1.05E-02	5.91E-06	5.10E-05	3.78E-05	5.20E-12	2.23E+01	1.37E-02
curies——>	4.26E-02	2.41E-11	2.35E-11	2.35E-11	1.18E-16	7.94E-22	<1E-22	1.12E-21	<1E-22	6.46E-22	8.70E-22	<1E-22	<1E-22	<1E-22

Nuclide——>	Am-241	Np-237	Pa-233	U-233	Th-229	Ra-225	Ac-225	Fr-221	At-217	Bi-213	Po-213	Pb-209
T(1/2) yr.—>	4.32E+02	2.14E+06	7.39E-02	1.59E+05	7.35E+03	4.05E-02	2.74E-02	9.32E-06	1.02E-09	8.67E-05	1.33E-13	3.71E-04
curies——>	3.26E+00	3.86E-06	3.75E-06	2.90E-11	3.24E-15	3.08E-15	2.98E-15	2.98E-15	2.98E-15	2.98E-15	2.98E-15	2.98E-15

Nuclide——>	Np-237	Pa-233	U-233	Th-229	Ra-225	Ac-225	Fr-221	At-217	Bi-213	Po-213	Pb-209
T(1/2) yr.—>	2.14E+06	7.39E-02	1.59E+05	7.35E+03	4.05E-02	2.74E-02	9.13E-06	8.84E-05	8.67E-05	1.33E-13	3.71E-04
curies——>	4.64E-03	4.64E-03	7.17E-08	1.20E-11	1.16E-11	1.13E-11	1.13E-11	1.13E-11	1.13E-11	1.13E-11	1.13E-11

Nuclide——>	U-234	Th-230	Ra-226	Rn-222	Po-218	Pb-214	Bi-214	Po-214	Pb-210	Bi-210	Po-210
T(1/2) yr.—>	2.45E+05	7.54E+04	1.60E+03	1.05E-02	5.91E-06	5.10E-05	3.78E-05	5.20E-12	2.23E+01	1.37E-02	3.79E-01
curies——>	3.06E-02	1.03E-06	8.11E-10	8.04E-10	8.04E-10	8.04E-10	8.04E-10	8.04E-10	2.94E-11	2.90E-11	1.93E-11

Nuclide——>	Th-232	Ra-228	Ac-228	Th-228	Ra-224	Rn-220	Po-216	Pb-216	Bi-212	Tl-208	Po-212
T(1/2) yr.—>	1.41E+10	5.75E+00	6.99E-04	1.91E+00	1.00E-02	1.76E-06	4.75E-09	1.21E-03	1.15E-04	5.84E-06	9.44E-15
curies——>	8.91E-07	3.17E-07	3.17E-07	1.49E-07	1.49E-07	1.49E-07	1.49E-07	1.48E-07	1.48E-07	5.34E-08	9.50E-08

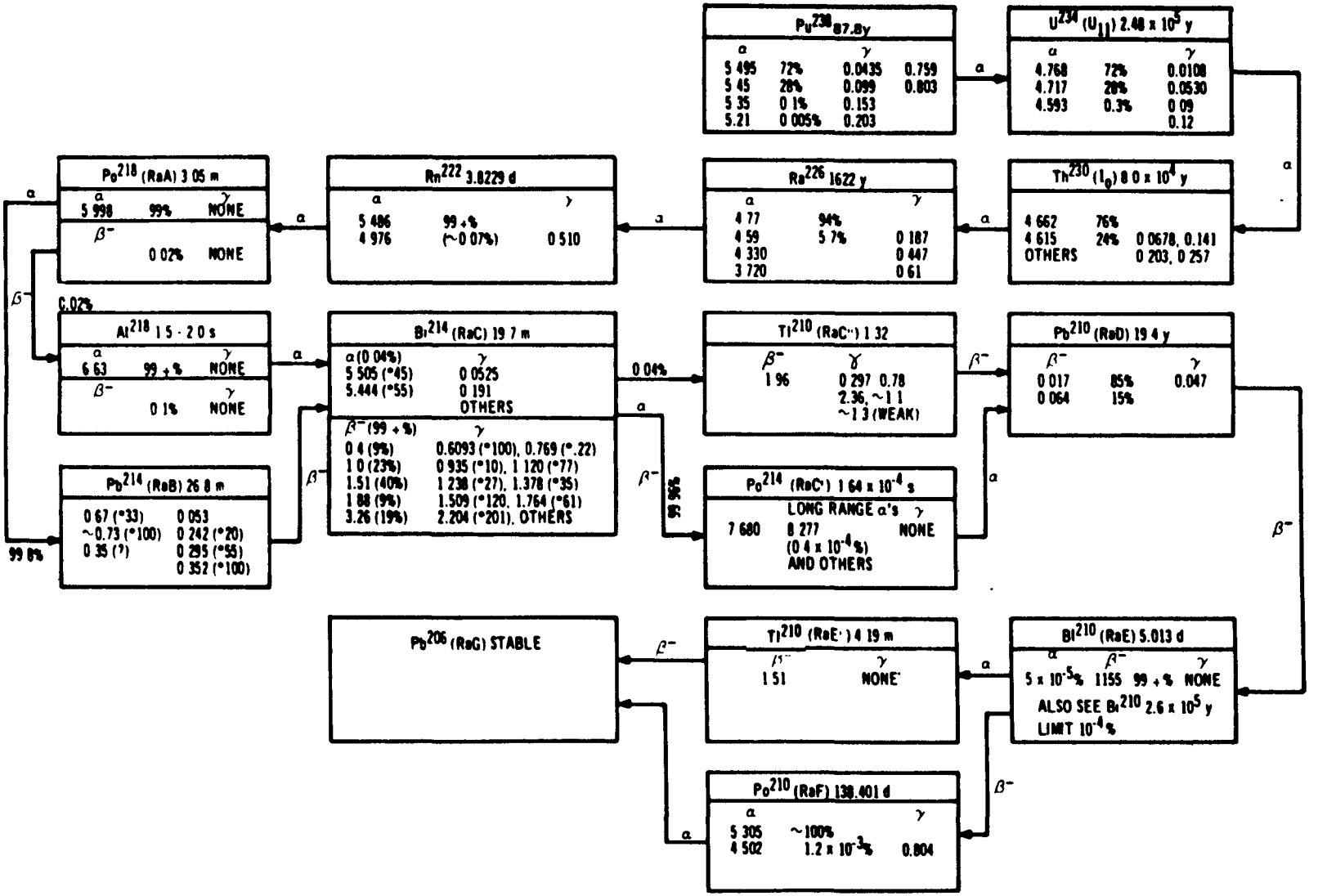

FIGURE A-2 DECAY CHAIN OF Pu-238

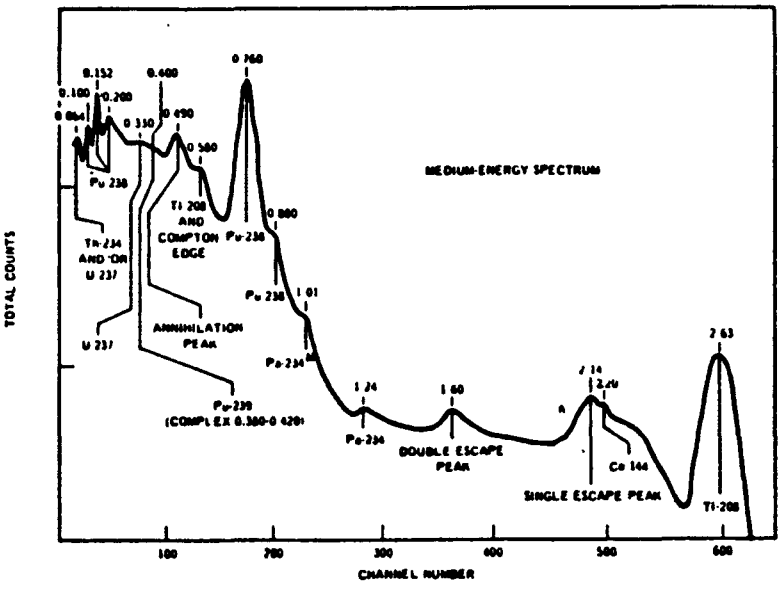

FIGURE A-3 GAMMA SPECTRUM FOR Pu-238 HEAT SOURCE (7.25 WATTS, 3" x 3" NaI (TI) DETECTOR, 10 MINUTE COUNT)

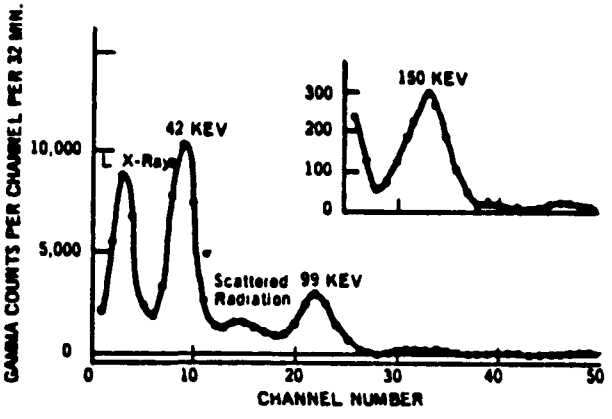

(NOTE: ABSORBERS USED TO REDUCE 18 KEV PEAK BY ~ 10:1)

FIGURE A-4 Pu^{238} GAMMA SPECTRUM

4. **Neutron Emission:** See Figures A-5, A-6, A-7

   Spontaneous Fission*: rate = 2.8×10^{3} n sec^{-1} g^{-1} ^{238}Pu

   $\overline{\nu} = 2.33 \pm 0.08$ n fis^{-1}

5. **Cross Sections:** See Figure A-8

   σth = 18 barns
   σa = 480 barns
   } ^{238}Pu

6. **Half Life*:**

   Alpha 87.8 ± 0.02 years

   Spontaneous Fission 5.0 (±0.6) x 10^{10} years

7. **Criticality** See Table A-5

A.4 PHYSICAL CHARACTERISTICS

1. **Density**

   Theoretical* 11.46 $g\text{-}cm^{-3}$

   Pellets 9.60 $g\text{-}cm^{-3}$ (84% T.D.)

TABLE A-5 MINIMUM CRITICAL MASSES FOR ^{238}Pu

Form	Critical Mass-Bare		Critical Mass-Reflected		Density $g\text{-}cm^{-3}$	Specific Power $w\text{-}g^{-1}$
	Kg	KW(t)	Kg	KW(t)		
^{238}Pu (metal)	8.9	4.1	7.2	3.3	19.6	0.461
$^{238}PuO_2$	23.1	9.3	8.6	3.4	11.46	0.4

Based on data in References A-3, A-4, and A-8

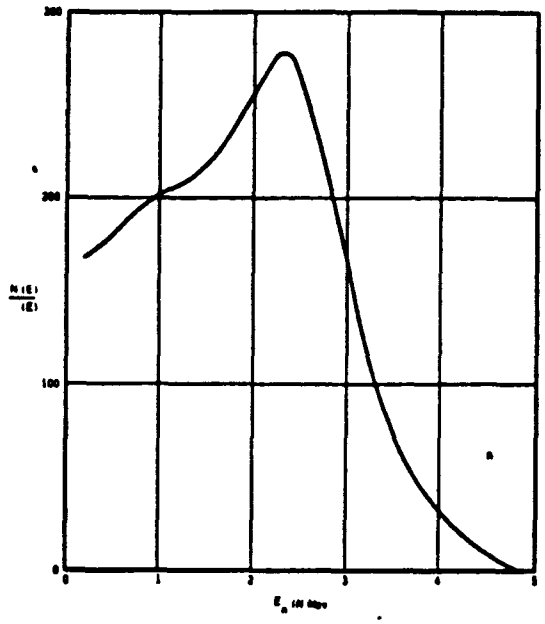

FIGURE A-5. NEUTRON SPECTRUM OF $^{238}PuO_2$ SOURCE

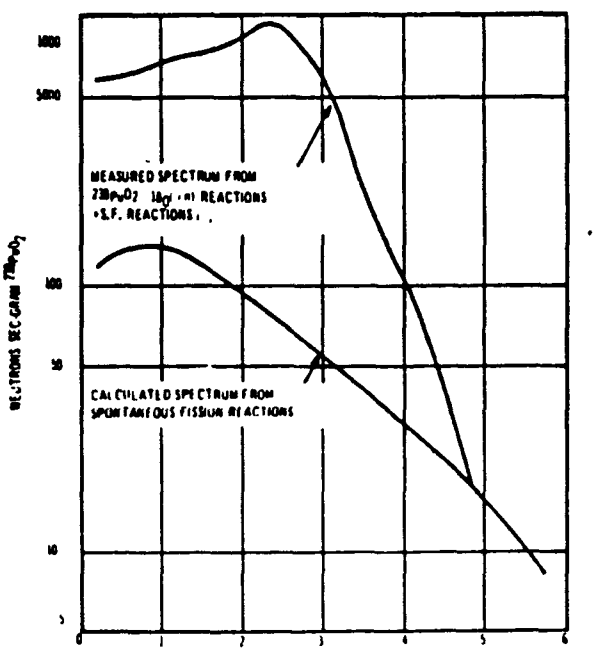

FIGURE A-6. $^{238}PuO_2$ NEUTRON SPECTRUM COMPONENTS

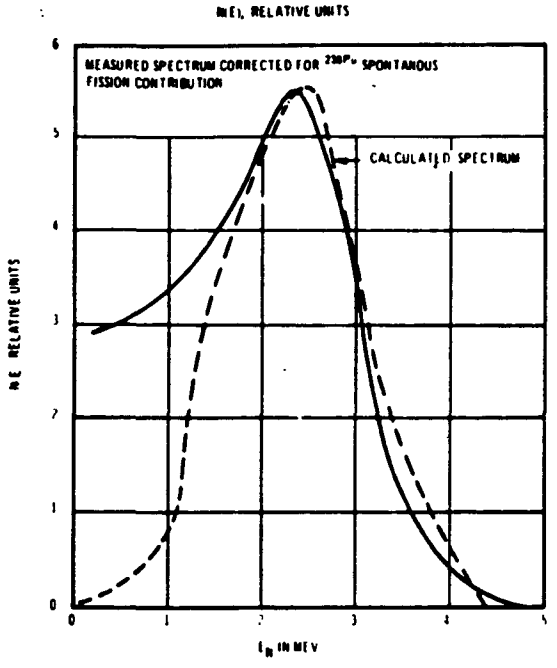

FIGURE A-7. NEUTRON SPECTRUM PRODUCED BY ^{238}Pu ALPHAS IN $^{18}O(\alpha,n)\ ^{21}Ne$ REACTIONS

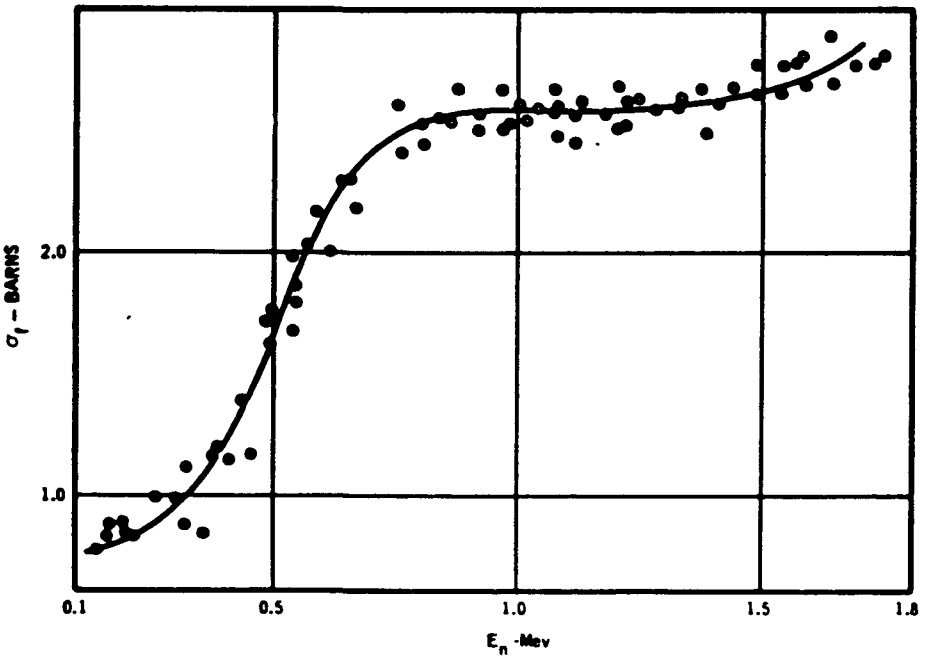

FIGURE A-8 FAST FISSION CROSS SECTIONS FOR ^{238}Pu (REF. A-2)

2. Melting Temperature

Composition (Oxygen to Plutonium Ratio)	Temperature °C (±30°C)
2.00	2400
1.85	2420
1.78	2430
1.73	2490
1.61	2360
1.50	2085

3. Boiling Temperature

3870°C (calculated from vapor pressure)

4. Vapor Pressure*

$\log P = 7.5 - \frac{29260}{T}$ where P is in atmospheres and T is the temperature in K (Reference A-11)

5. Viscosity*

32 centipoise (±25%) at melting point (calculated)

6. Surface Tension* ($^{239}PuO_2$)

525 dynes-cm^{-1} (±15%) at melting point

7. Crystallography:

FCC structure

Space group Fm3m

Lattice constant 5.400 ±.003 Å O/Pu = 2.00

Ionic radius 0.93 Å

8. Solubility

*Data given for $^{238}PuO_2$ microspheres. See Table A-6

PuO_2 pellet 5.1×10^{-4} μg Pu mm^{-2} - day^{-1} @ 464 days (Referenced A-5)

A.5 THERMOPHYSICAL DATA

1. Specific Power * 0.40 W g^{-1}
   12.6 Ci g^{-1}

2. Power Density* 4.58 W cm^{-3}
   (based on 80% ^{238}Pu and theoretical density)

3. Latent Heats of Phase Transformation*

   ΔH_{fus} for $^{239}PuO_2$ = 16.8 ± 1.3 Kcal $mole^{-1}$ (calculated)

   ΔH_{sub} for $^{239}PuO_2$ = 130.2 ± 2.3 Kcal $mole^{-1}$

TABLE A-6 SUMMARY OF Pu RELEASE RATE FROM PPO IN AQUATIC ENVIRONMENTS (REFERENCE A-10)

Sample	Power (W)	Immersion (days)	Water	Temperature (C)	Release Data (nCi/m^2-s)
HPZ-60-2	2.5	2130	Fresh	10	130
HPZ-111-1	25	1829	Fresh	10	370
HPZ-59-4	25	1923	Sea	10	14
HPZ-174	18	818	Sea	10	6
HPZ-186-4	19	814	Sea (Tidal)	10	56

4. THERMAL EXPANSION OF STOICHIOMETRIC $^{238}PuO_2$ RECOMMENDED VALUES

Temp. (°C)	$\Delta L/L_o$ ($\times 10^3$)	Temp. (°C)	$\Delta L/L_o$ ($\times 10^3$)
25	0.00	1000	9.19
50	0.23	1100	10.36
100	0.67	1200	11.61
200	1.55	1300	12.94
300	2.42	1400	14.37
400	3.30	1500	15.91
500	4.19	1600	17.56
600	5.11	1700	(19.33)[a]
700	6.09	1800	(21.24)
800	6.99	1900	(23.29)
900	7.89	2000	(25.49)

[a] Values in parenthesis are extrapolated.

5. Heat Capacity*

Temperature (°K)	Heat Capacity (cal g^{-1} $°K^{-1}$)
300	0.0611
400	0.0693
500	0.0749
600	0.0782
700	0.0800
800	0.0806
900	0.0808
1000	0.0810
1100	0.0817

6. Enthalpy* — See Table A-7

7. Thermal Conductivity — See Table A-8

8. Thermal Diffusivity — See Table A-9

A.6 CHEMICAL PROPERTIES

1. Heat of Formation* — See Table A-7

2. Free Energy of Formation* — See Table A-7

3. Entropy - Absolute* — See Table A-7

4. Entropy of Formation* — See Table A-7

5. Free Energy Change*

	Δ F Kcal		
	1273°K	1773°K	2273°K
$Ir + 4\ PuO_2 \longrightarrow IrO_2 + 2\ Pu_2O_3$	+162	+157	~+134

A.7 ELECTRICAL PROPERTIES

1. Resistivity of $^{239}PuO_2$* See Figure A-10

   800 ohm-cm @ 1250°K

   4×10^{10} ohm-cm @ 298°K (by extrapolation)

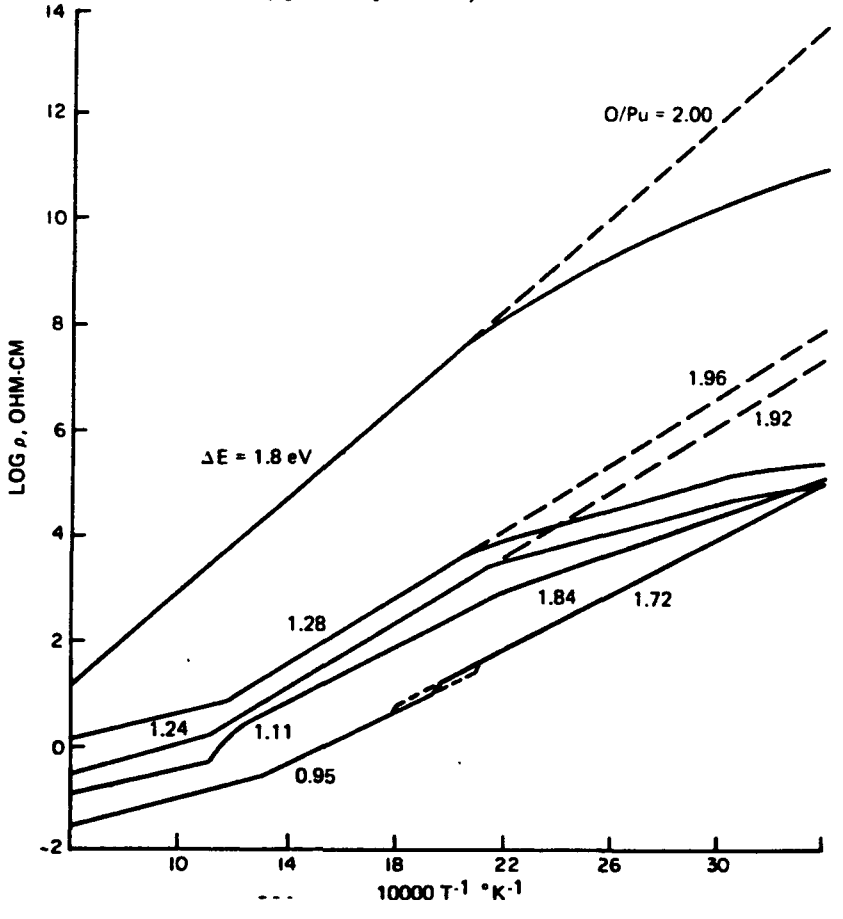

FIGURE A-10 ELECTRICAL RESISTIVITY OF $^{239}PuO_2$ AS A FUNCTION OF TEMPERATURE FOR OXYGEN: PLUTONIUM RATIOS OF 2.00, 1.96, 1.92, 1.84, AND 1.72. ACTIVATION ENERGIES FOR ELECTRONIC CONDUCTION ΔE ARE ALSO GIVEN.

TABLE A-7 SELECTED THERMODYNAMIC FUNCTIONS FOR $^{239}PuO_2$ (MOL WT 271.058) CRYSTAL

Temp. (°K)	cal mole^{-1} deg^{-1}			kcal mole^{-1}		
	(C_p°)	(S°_T)	$[-(G^\circ_T - H^\circ_{298})/T]$	$(H^\circ_T - H^\circ_{298})$	$-(\Delta H_f^\circ)$	$-(\Delta G_f^\circ)$
298	16.400	19.700	19.700	0.000	252.870	240.203
300	16.500	19.802	19.700	0.030	252.867	240.125
400	18.250	24.807	20.371	1.774	253.447	235.893
500	19.230	28.990	21.688	3.651	253.292	231.532
600	19.910	32.558	23.210	5.609	253.096	227.207
700	20.450	35.669	24.772	7.628	252.755	222.918
800	20.880	38.428	26.310	9.695	252.870	218.649
900	21.280	40.911	27.797	11.803	252.416	214.398
1000	21.650	43.172	29.223	13.950	252.638	210.130
1100	22.000	45.253	30.587	16.133	252.144	205.905
1200	22.280	47.179	31.690	18.347	251.628	201.723
1300	22.550	48.974	33.136	20.589	251.093	197.587
1400	22.760	50.562	34.328	22.854	250.542	193.490
1500	22.970	52.230	35.469	25.141	249.976	189.434
1600	23.150	53.718	36.564	27.447	249.397	185.418
1700	23.320	55.127	37.615	29.771	248.805	181.438
1800	23.470	56.464	38.625	32.110	248.205	177.492
1900	23.610	57.737	39.598	34.465	247.595	173.579
2000	23.730	58.951	40.535	36.832	246.978	169.700
2100	23.850	60.112	41.440	39.211	246.354	165.851
2200	23.940	61.223	42.314	41.600	245.727	162.032
2300	24.040	62.290	43.160	43.999	245.094	158.243
2400	24.130	63.315	43.978	46.408	244.457	154.479
2500	24.220	64.302	44.772	48.825	243.818	150.745
2675	24.380	65.945	46.105	53.078	242.688	144.270

TABLE A-8 THERMAL CONDUCTIVITY* OF TWO DENSITIES OF $Pu^{239}O_2$ (REFERENCE A-7)

Temperature (° C)	Thermal Conductivity [cal-sec^{-1} - cm^{-1} °C^{-1}]	
	96.5% of Theoretical Density	81.85% of Theoretical Density
300	14.3×10^{-3}	10.4×10^{-3}
400	12.0×10^{-3}	9.1×10^{-3}
500	10.0×10^{-3}	8.0×10^{-3}
600	8.3×10^{-3}	7.0×10^{-3}
700	7.2×10^{-3}	6.2×10^{-3}
800	6.4×10^{-3}	5.7×10^{-3}
900	5.9×10^{-3}	5.3×10^{-3}
1000	5.7×10^{-3}	5.0×10^{-3}
1100	5.6×10^{-3}	4.8×10^{-3}
1200	5.6×10^{-3}	4.6×10^{-3}

*Table gives thermal conductivity values as calculated from experimentally determined thermal diffusivity of pressed and sintered $Pu^{239}O_2$. The density of the PuO_2 was corrected with temperatures using reported coefficients of linear thermal expansion. The specific heat of PuO_2 was assumed to be the same as UO_2.

TABLE A-9 THERMAL DIFFUSIVITY* OF TWO DENSITIES OF $Pu^{239}O_2$ (REFERENCE A-7)

Temperature (° C)	Thermal Diffusivity (cm^2 / sec)	
	96.5% of Theoretical Density	81.85% of Theoretical Density
300	18.8×10^{-3}	16.8×10^{-3}
400	15.2×10^{-3}	13.7×10^{-3}
500	12.4×10^{-3}	11.6×10^{-3}
600	10.3×10^{-3}	10.6×10^{-3}
700	8.7×10^{-3}	9.0×10^{-3}
800	7.8×10^{-3}	8.1×10^{-3}
900	7.2×10^{-3}	7.5×10^{-3}
1000	6.9×10^{-3}	7.1×10^{-3}
1100	6.6×10^{-3}	6.8×10^{-3}
1200	6.6×10^{-3}	6.5×10^{-3}

A.8 REFERENCES

A-1 Hyde, E. H., The Nuclear Properties of Heavy Elements, Vol. 1, 2, 3, Fission Phenomena. Engelwood Cliffs, N. J.: Prentice Hall, Inc., 1964, pp. 49-85, 211-253.

A-2 Butler, D. K., and Sjoblom, R. K. "Fission Cross Sections of Pu^{238}." APS Meeting Paper RA-7, April, 1963. (Also WASH-1049) Bull. APS, Vol. 8, 1963, p. 369.

A-3 Prince, A., "Cross Sections of Pu-238 and Cm-244, "Appendix C in "Preliminary Design and Safety Studies of a Large Radioisotope Heat Source for Space Power." GEMS-3526-2, General Electric Co., Missile and Space Division, Philadelphia, PA., October, 1965.

A-4 Prince, A., "Neutron Cross Sections for Cm^{244} and Pu^{238}." GEMP-411, General Electric Co., Atomic Products Div., Nuclear Materials and Propulsion Operation, Cincinnati, Ohio, 22 February 1966.

A-5 CMB-2032 Monthly Report for December, 1973, Los Alamos Scientific Laboratory, 18 January 1974.

A-6 Andrew, J.F., Zocher, R.W. and Kent, R.A. "Thermal Expansion of $^{238}PuO_2$". LA-6232-MS, Los Alamos Scientific Laboratory, February 1976.

A-7 Lagedrost, J. F., Askey, D. F., Storhok, V. W., and Gates, J. E., "Thermal Conductivity of PuO_2 as Determined from Thermal Diffusivity Measurements." Nucl. Applns., Vol. 4, January, 1968.

A-8 HW-84369 "Physics Research Quarterly Report. July, August, September, 1964." Hanford Atomic Products Operation (General Electric Co.), October 15, 1964.

A-9 DPSP-79-1076, "Specifications for General Purpose Heat Source Fuel Pellet Acceptance," Savannah River Plant, January 2, 1980.

A-10 Maraman, W. J. (compiled), "General-Purpose Heat Source Project and Space Nuclear Safety and Fuels Program," LA-8311-PR, Los Alamos Scientific Laboratory, January, 1980.

A-11 Williams, David C., "Vaporization of Radioisotope Fuels in Launch Vehicle Abort Fires", SC-RR-71 0118, December 1971.

APPENDIX B

PROPERTIES OF HEAT SOURCE AND CONVERTER MATERIALS

This appendix is a compilation of the material properties that are used both in the design analyses and the safety evaluation of the General Purpose Heat Source and Converter. Some of the information has been obtained directly in support of the GPHS-RTG engineering development program and represents test data under conditions representative of the induced environments resulting from mission operation and aborts.

B.1 IRIDIUM

The iridium to be used for the production of fueled clads is DOP-26 Ir which has been developed by Oak Ridge National Laboratories. A very significant characteristic of the DOP 26 Ir that affects its ability to withstand impacts is the number of grains present in a clad thickness. This grain structure is affected by the thermal environments encountered during operation and a postulated re-entry. This grain growth phenomena has been investigated and is described in the following figures.

Figures B-1 and B-2 show the effect of operating temperatures and re-entry heat pulse temperatures on the number of grains present in a clad thickness. Figure B-3 then relates these temperatures to a minimum impact temperature using the uniform and local strain data. Figures B-1 through B-3 are taken from Reference B-1. Figure B-4 (presented at the December 13, 1979 Task Force on MHW FSA Meeting) presents the effect of the surrounding environment on the grain size while Figure B-5 relates this to the minimum impact temperature using the 20% local strain condition. Figures B-6 and B-7 (from Reference B-1) shows the impact response of the iridium as a function of grain size and impact temperature. A comparison of the impact ductility of DOP-26 Ir-base metal and welds is shown in Figure B-8.

Figure B-9 shows the curve of linear thermal expansion to 1400°C. This curve was determined from tests conducted at GE-Evendale, Ohio (Reference B-2) and shows a comparison with data from References B-3 and B-4. Table B-1 (from Reference B-5) provides the total hemispherical emittance of six iridium strips treated in various ways as functions of temperature.

B.2 CBCF-3 CARBON INSULATOR

The properties of CBCF-3 are determined in two directions, the "C" direction and the "A" direction. The thermal conductivity of this insulating material in these two directions are shown in Figures B-10 and B-11 where these are for the experimental samples as defined in Table B-2. Figure B-12 provides a graph of the linear thermal expansion of the CBCF-3. These figures were taken from Reference B-6. Table B-3 provides the hemispherical total emittance of the CBCF-3 and Table B-4 provides the crush strength. This information was previously presented in Reference B-7.

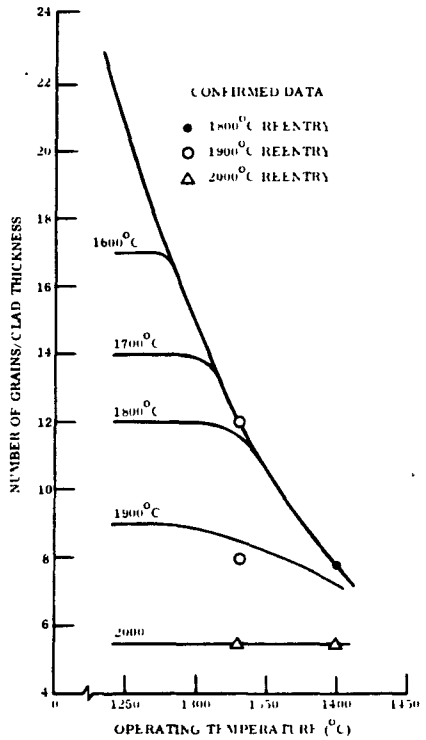

FIGURE B-1 DOP-26 GRAIN SIZE AFTER 6 MO. AT OPERATING TEMPERATURE AND A 2 MIN. REENTRY HEAT PULSE

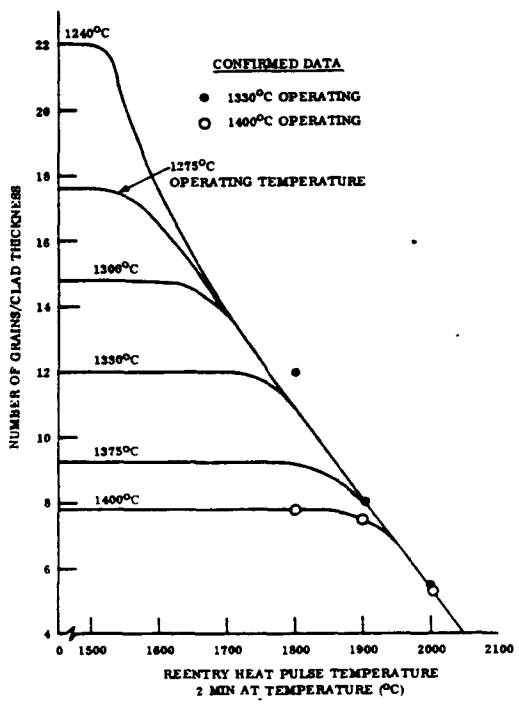

FIGURE B-2 EFFECT OF REENTRY HEAT PULSE ON DOP-26 GRAIN SIZE AFTER 6 MO. AT VARIOUS OPERATING TEMPERATURES

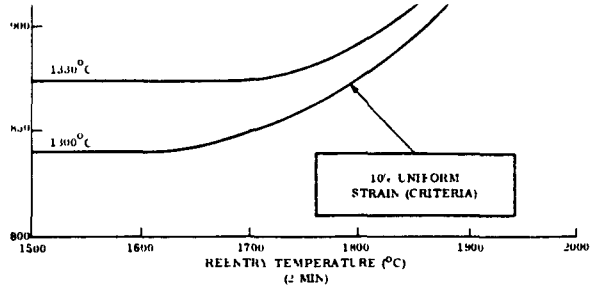

FIGURE B-3 MINIMUM IMPACT TEMPERATURE OF DOP-26 IRIDIUM AS A FUNCTION OF OPERATING AND REENTRY TEMPERATURE USING UNIFORM AND LOCAL STRAIN DATA

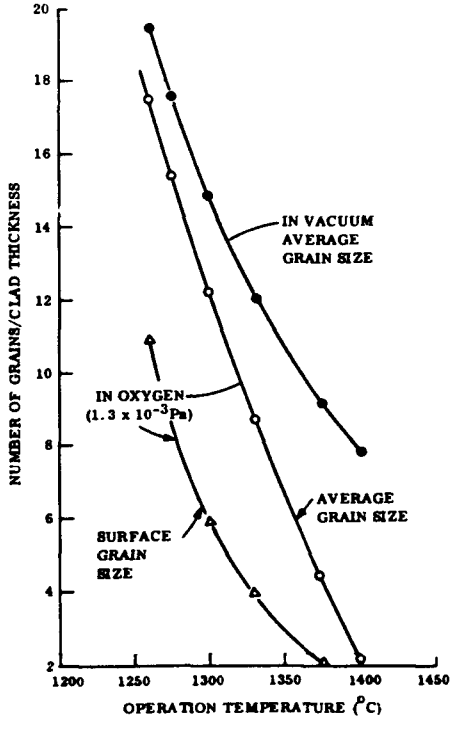

FIGURE B-4 DOP-26 GRAIN SIZE AFTER 6 MO. HEAT TREATMENT IN VACUUM AND OXYGEN ENVIRONMENTS

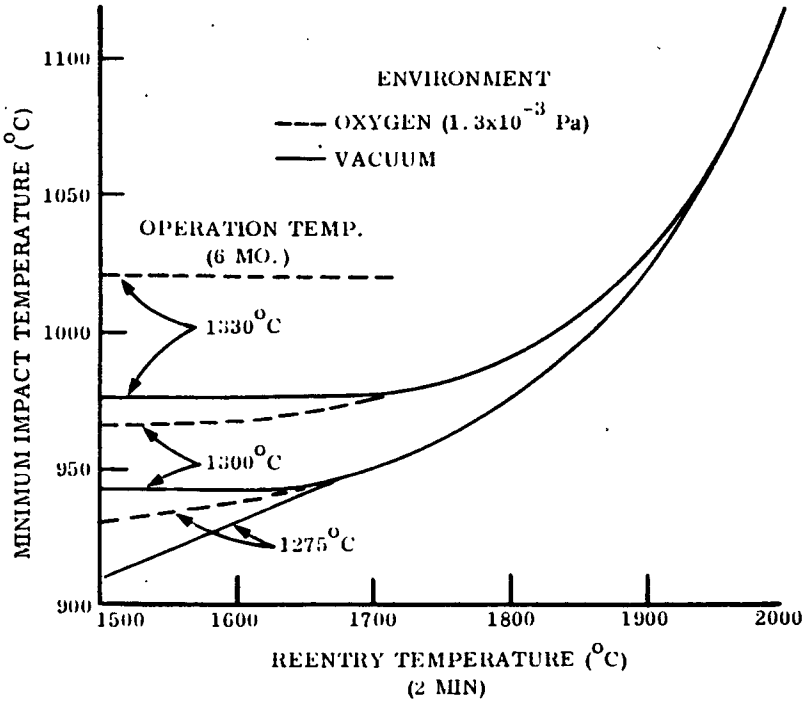

FIGURE B-5 MINIMUM IMPACT TEMPERATURE OF DOP-26 IRIDIUM AS A FUNCTION OF OPERATION AND REENTRY TEMPERATURE USING 20% LOCAL STRAIN CONDITION

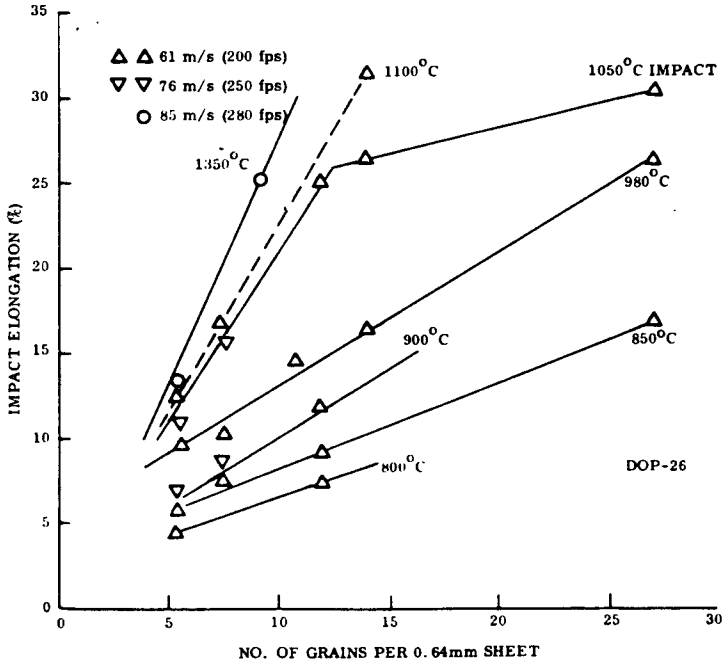

FIGURE B-6 TENSILE IMPACT ELONGATION OF DOP-26 IRIDIUM AS A FUNCTION OF GRAIN SIZE AND IMPACT TEMPERATURE

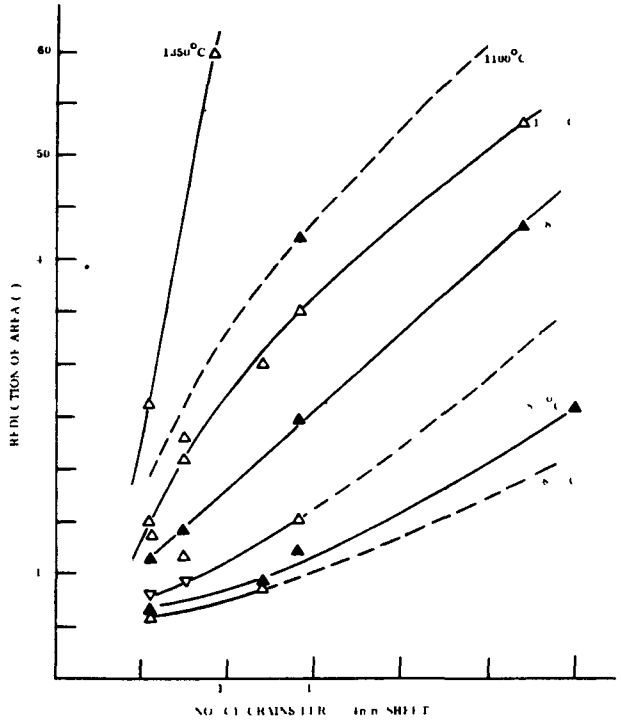

FIGURE B-7 REDUCTION OF AREA IN TENSILE IMPACT TESTS OF DOP-26 IRIDIUM AS A FUNCTION OF GRAIN SIZE AND IMPACT TEMPERATURE

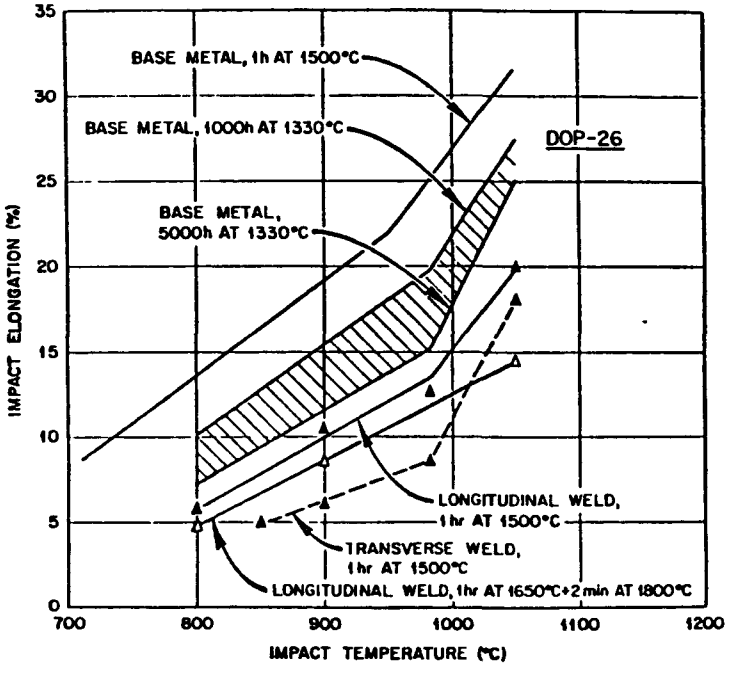

FIGURE B-8 COMPARISON OF THE IMPACT DUCTILITY OF DOP-26 Ir-BASE METAL AND WELDS

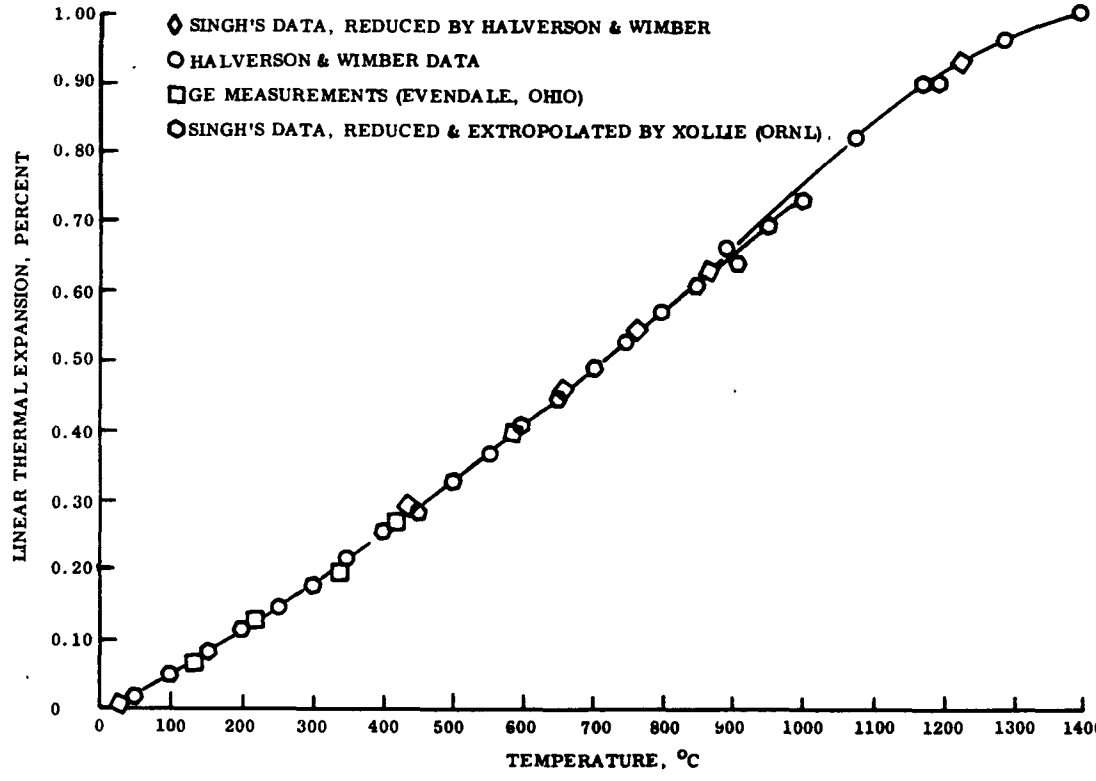

FIGURE B-9 LINEAR THERMAL EXPANSION OF Ir

TABLE B-1 IRIDIUM SMOOTHED VALUES FOR ϵ

Temperature (K)	As Rolled	As Rolled (Annealed)	Grit Blasted	Grit Blasted (Annealed)	Graphite Coated	Graphite Coated (Annealed)
600	0.087	0.076	0.245	0.117	0.663	0.615
700	0.094	0.083	0.253	0.127	0.666	0.628
800	0.101	0.090	0.262	0.136	0.670	0.640
900	0.108	0.097	0.271	0.146	0.673	0.652
1000	0.116	0.105	0.279	0.156	0.676	0.664
1100	0.123	0.112	0.287	0.165	0.680	0.677
1200	0.130	0.119	0.296	0.175	0.683	0.689
1300	0.137	0.126	0.304	0.185	0.686	0.701
1400	0.144	0.133	0.313	0.194	0.689	0.713
1500	0.151	0.141	0.321	0.204	0.693	0.726
1600	0.159	0.148	0.330	0.214	0.696	0 738

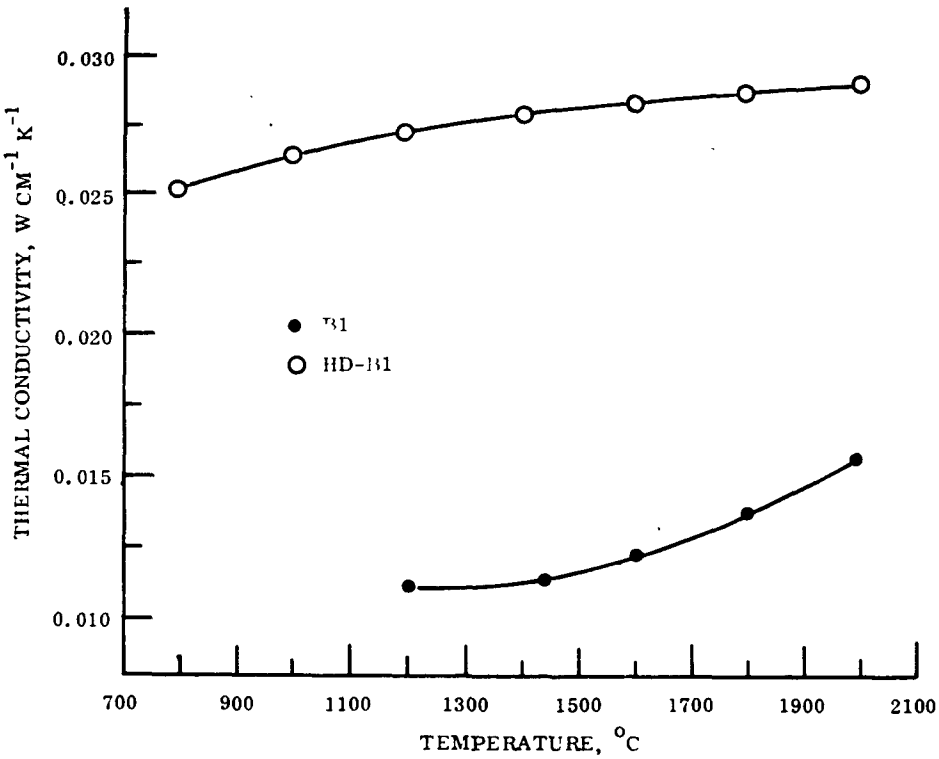

FIGURE B-10 CBCF THERMAL CONDUCTIVITY RESULTS IN THE "A" DIRECTION

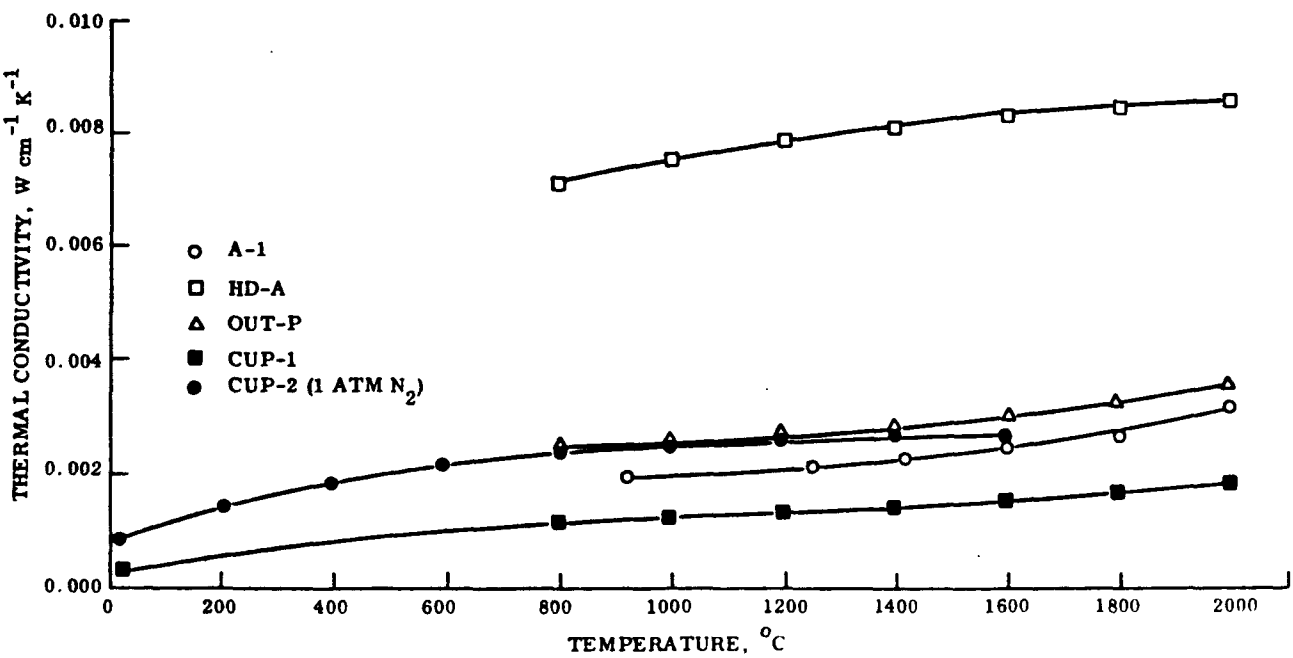

FIGURE B-11 CBCF THERMAL CONDUCTIVITY IN "C" DIRECTION

TABLE B-2 CBCF3 THERMAL DIFFUSIVITY SAMPLES

Group (No.)	Sample Designation	Sample Description	Heat Flow Direction	Density (gm-cm-3)
1	A-1	Virgin Plate	C	0.272
1	A-2	Virgin Plate	C	0.272
1	B-1	Virgin Plate	A	0.281
2	HD-A1	High Density Plate	C	0.5917
2	HD-B1	High Density Plate	A	0.6436
3	Out-P	Outgassed Plate	C	0.2703
3	Cup 1	Outgassed Cup	C	0.1859
4	Cup 2	Outgassed Cup	(in N_2)	0.1857

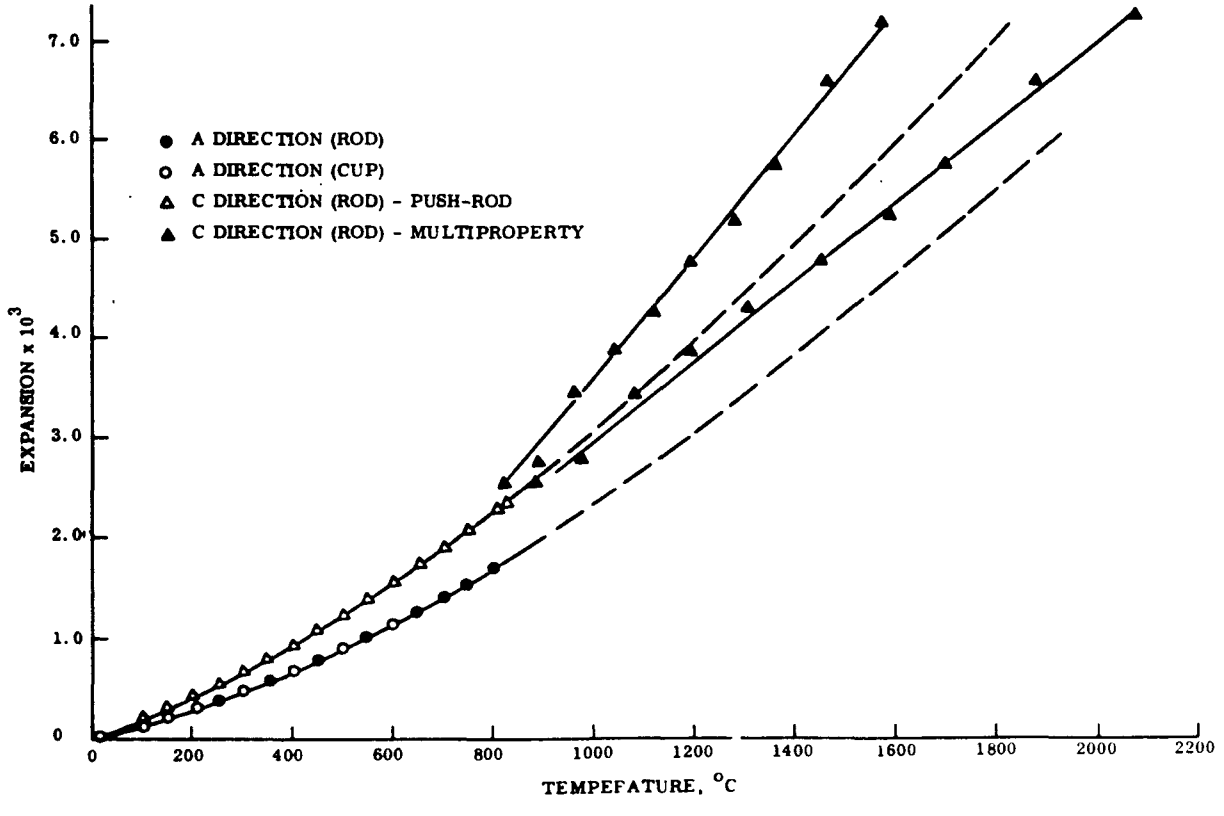

FIGURE B-12 THERMAL EXPANSION RESULTS FOR CBCF3

TABLE B-3 HEMISPHERICAL TOTAL EMITTANCE (ϵ_H) OF AS-MADE CBCF-3 PLATE ($0.275\ gm\text{-}cm^{-3}$)

Interior Temp	Surface Temp		ϵ_H
K	K	°C	
1455	1270	997	0.802
1738	1454	1181	0.797
2014	1608	1335	0.811
2140	1688	1415	0.803
2291	1782	1509	0.807
2481	1900	1627	0.804
2715	2005	1732	0.801

TABLE B-4 CBCF STRENGTH

THE STANDARD GRAPHITE OUTGASSING TREATMENT HAD LITTLE OR NO EFFECT ON THE CRUSH STRENGTH OF CBCF-3, WITH A DENSITY OF 0.28 g/cc.

AS-RECEIVED
YS (0.2%) : 277 psi

36 HR A 1500°C
YS (0.2%) : 268 psi

B.3 FWPF

Figures B-13 and B-14 show the hemispherical total emissivity (as reported in Reference B-8) in both the X-Y and Z plus X-Y directions, respectively. Figures B-15 through B-38 present the thermal and mechanical properties for the FWPF as obtained from Reference B-9.

B.4 ALUMINUM 2219 T-6

The outer shell and pressure domes of the converter are constructed of aluminum 2219 T-6. The properties of this material are shown in Table B-5.

B.5 THERMOCOUPLES

The thermocouple thermal conductivity has been established as .0134 cal/sec-cm-^{o}C (3.23 Btu/hr-ft-^{o}F) by test of the MHW couple configuration.

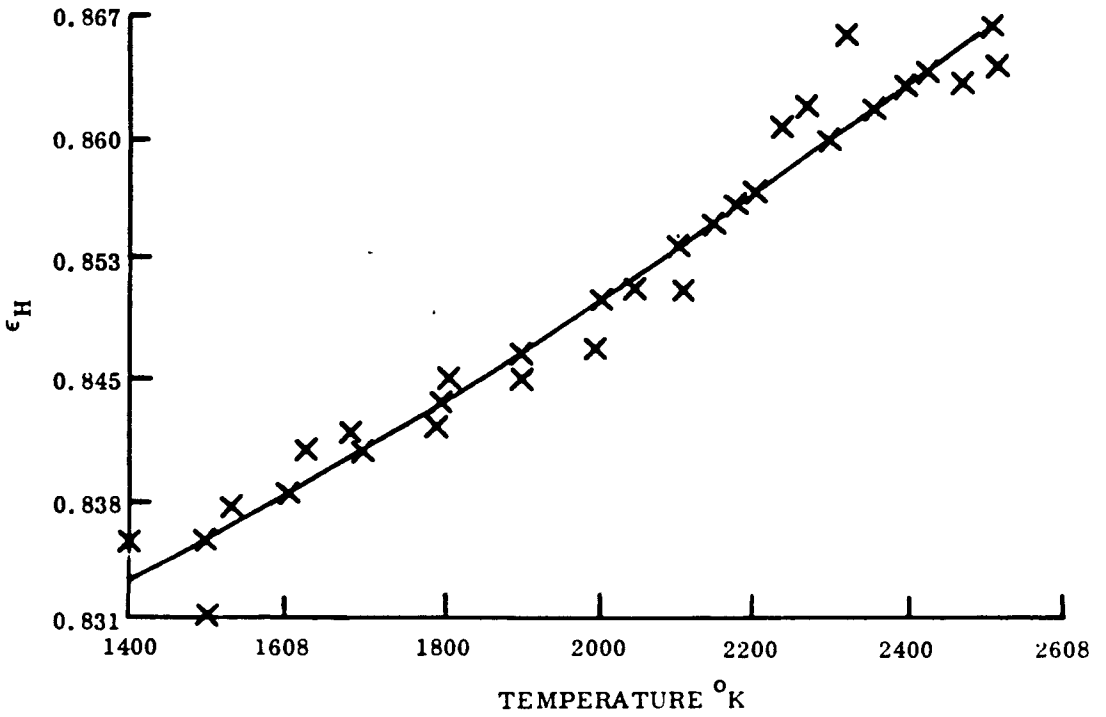

FIGURE B-13 AVCO FWPF HEMISPHERICAL TOTAL EMISSIVITY (X-Y AXIS)

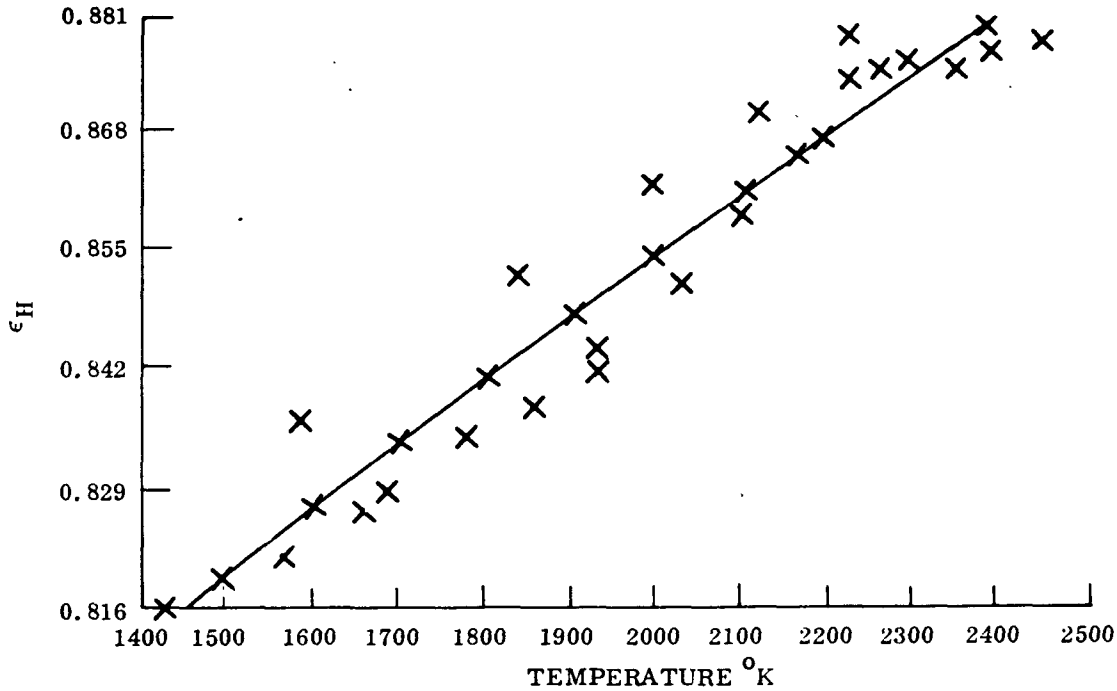

FIGURE B-14 AVCO FWPF HEMISPHERICAL TOTAL EMISSIVITY (Z PLUS X-Y)

TABLE B-5 MATERIAL PROPERTIES FOR RTG OUTER CASE

PROPERTY		ALUMINUM 2219 T-6
DENSITY	$\frac{LB}{IN^3}$	.1
THERMAL CONDUCTIVITY (500°F)	$\frac{BTU\text{-}FT}{HR\text{-}FT^2\text{-}^oF}$	100
MELT TEMPERATURE	°F	1010-1190
COEFFICIENT OF EXPANSION (500°F)	$\frac{IN}{IN\text{-}^oF}$	13.5×10^{-6}
MODULUS OF ELASTICITY (212°F)	PSI	10.5×10^6
YIELD STRENGTH (500°F)	PSI	17,300
ULTIMATE STRENGTH (500°F)	PSI	24,300
YIELD STRENGTH (212°F)	PSI	33,500
ULTIMATE STRENGTH (212°F)	PSI	49,100
CREEP STRENGTH (500°F, .1%, 100 HR)	PSI	7,500

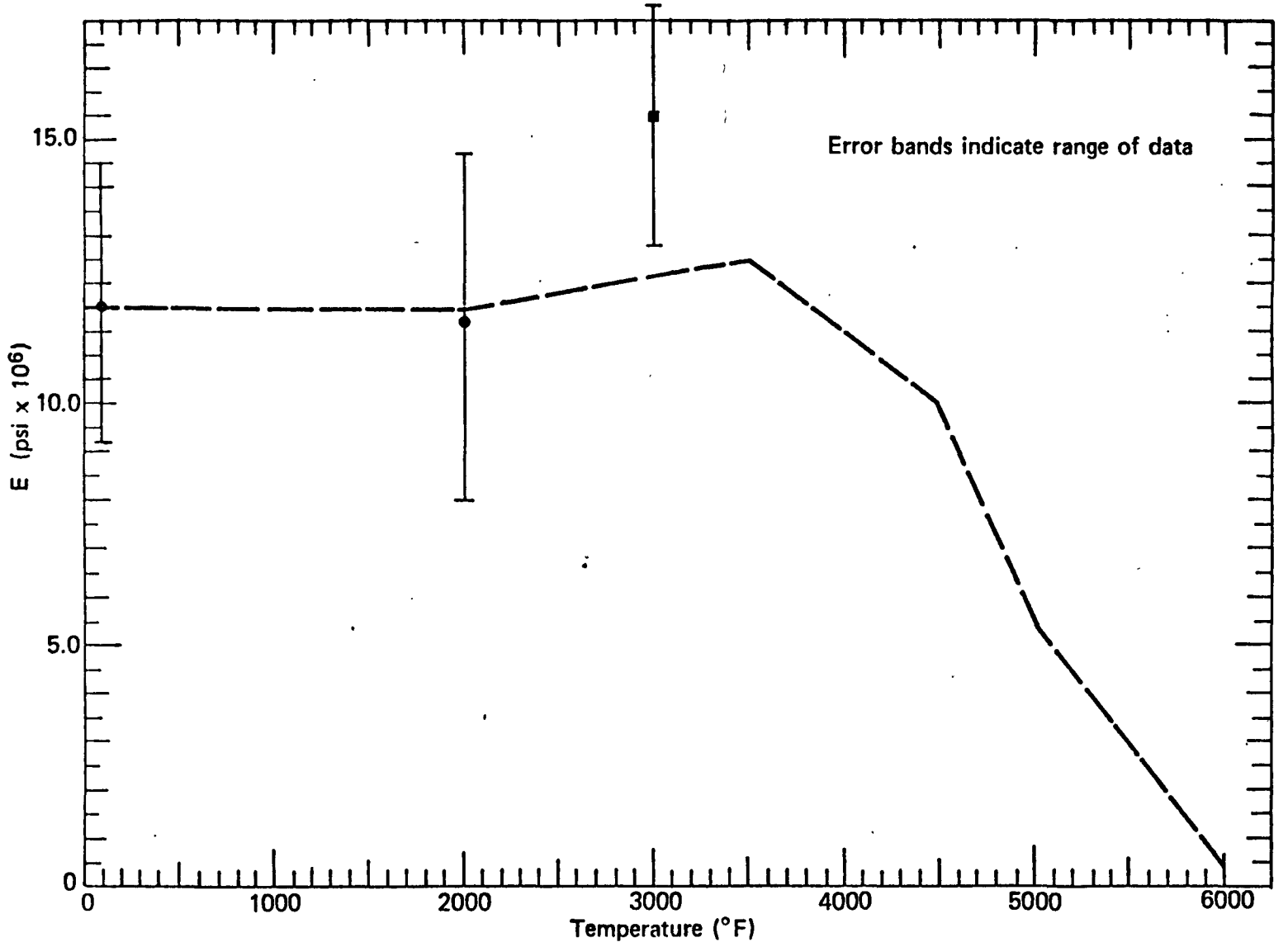

FIGURE B-15 TENSILE ELASTIC MODULUS VS. TEMPERATURE (X) OF FWPF

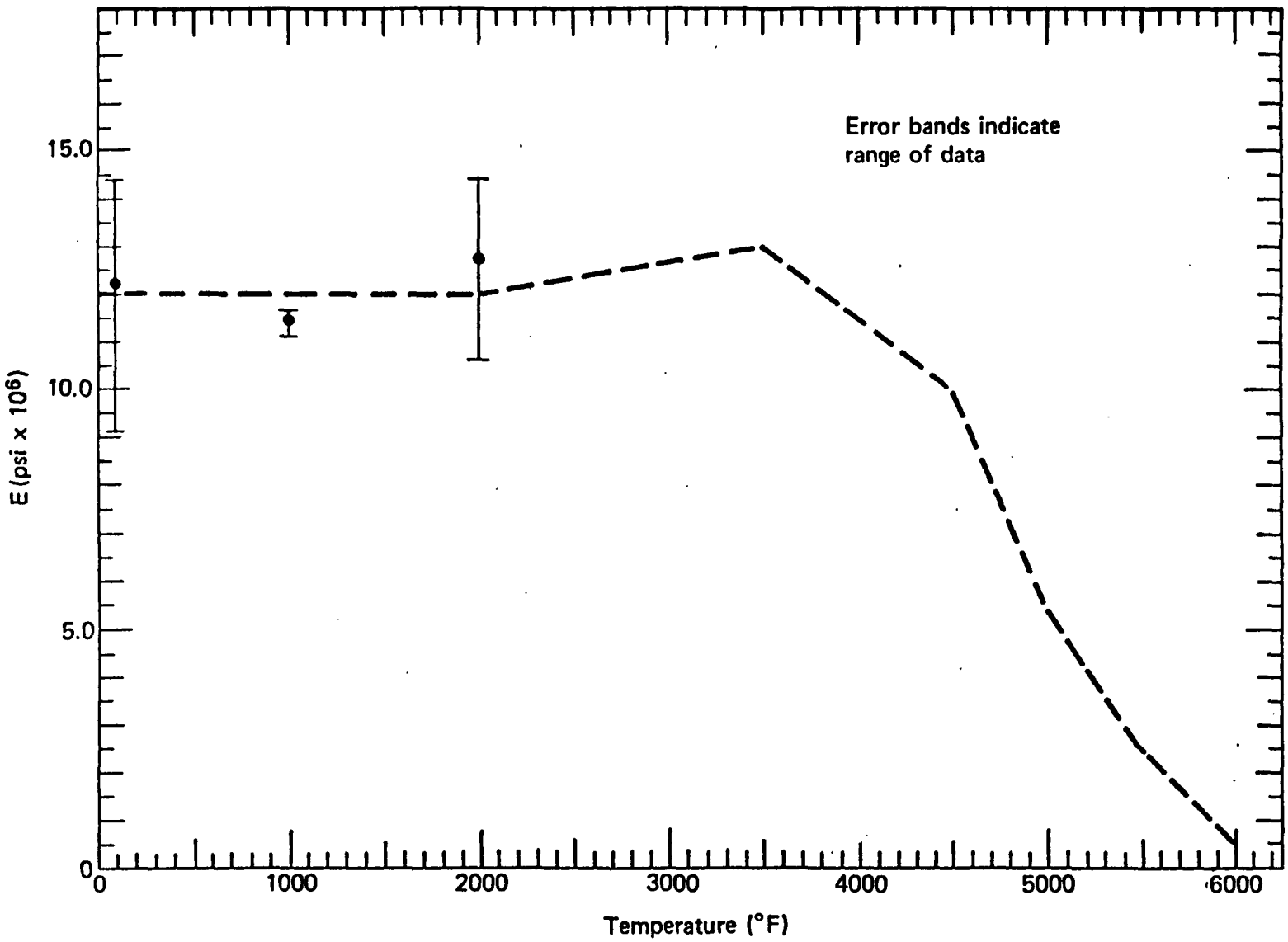

FIGURE B-16 TENSILE ELASTIC MODULUS VS. TEMPERATURE (Z) OF FWPF

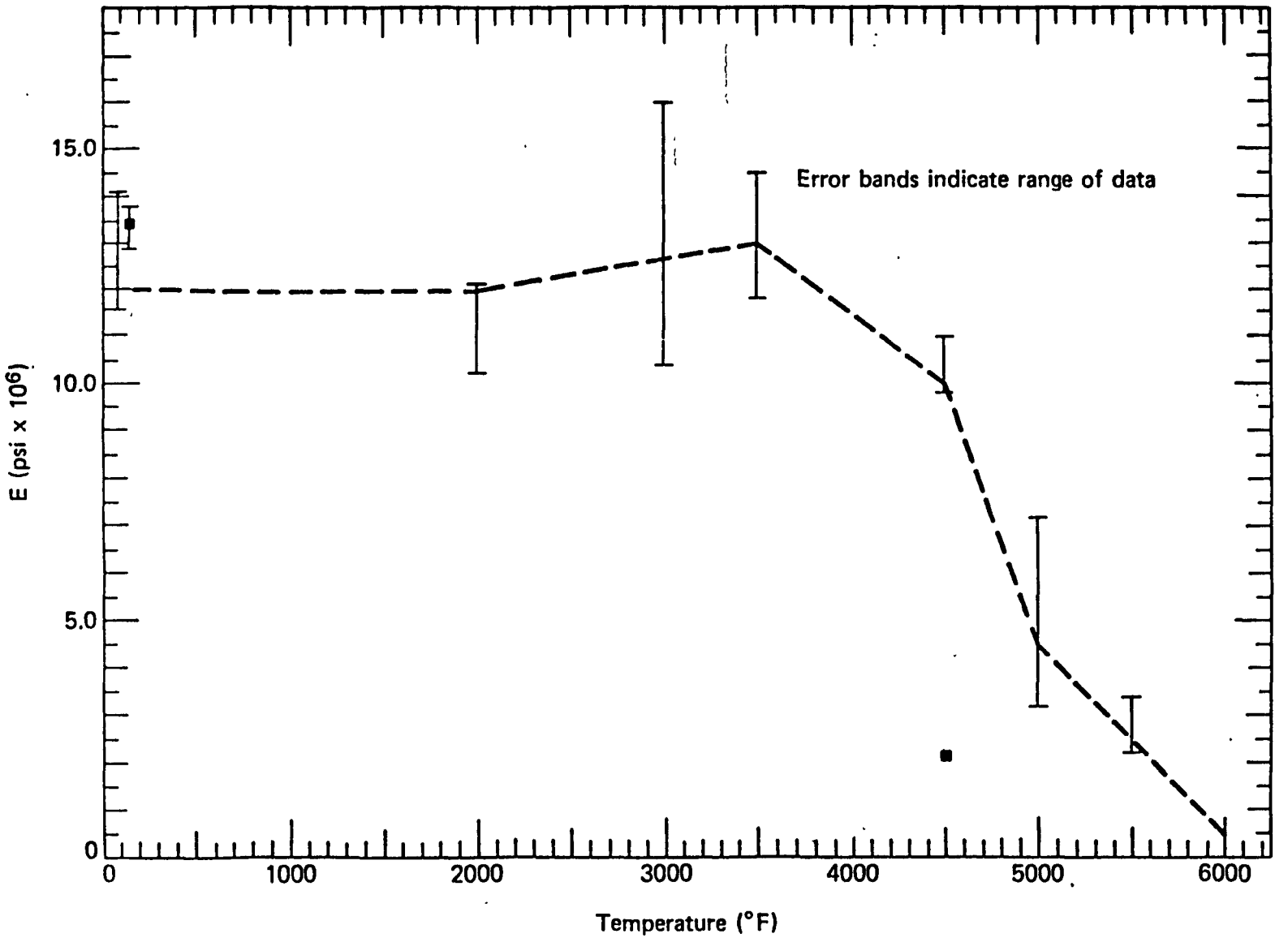

FIGURE B-17 COMPRESSIVE ELASTIC MODULUS VS. TEMPERATURE (X) OF FWPF

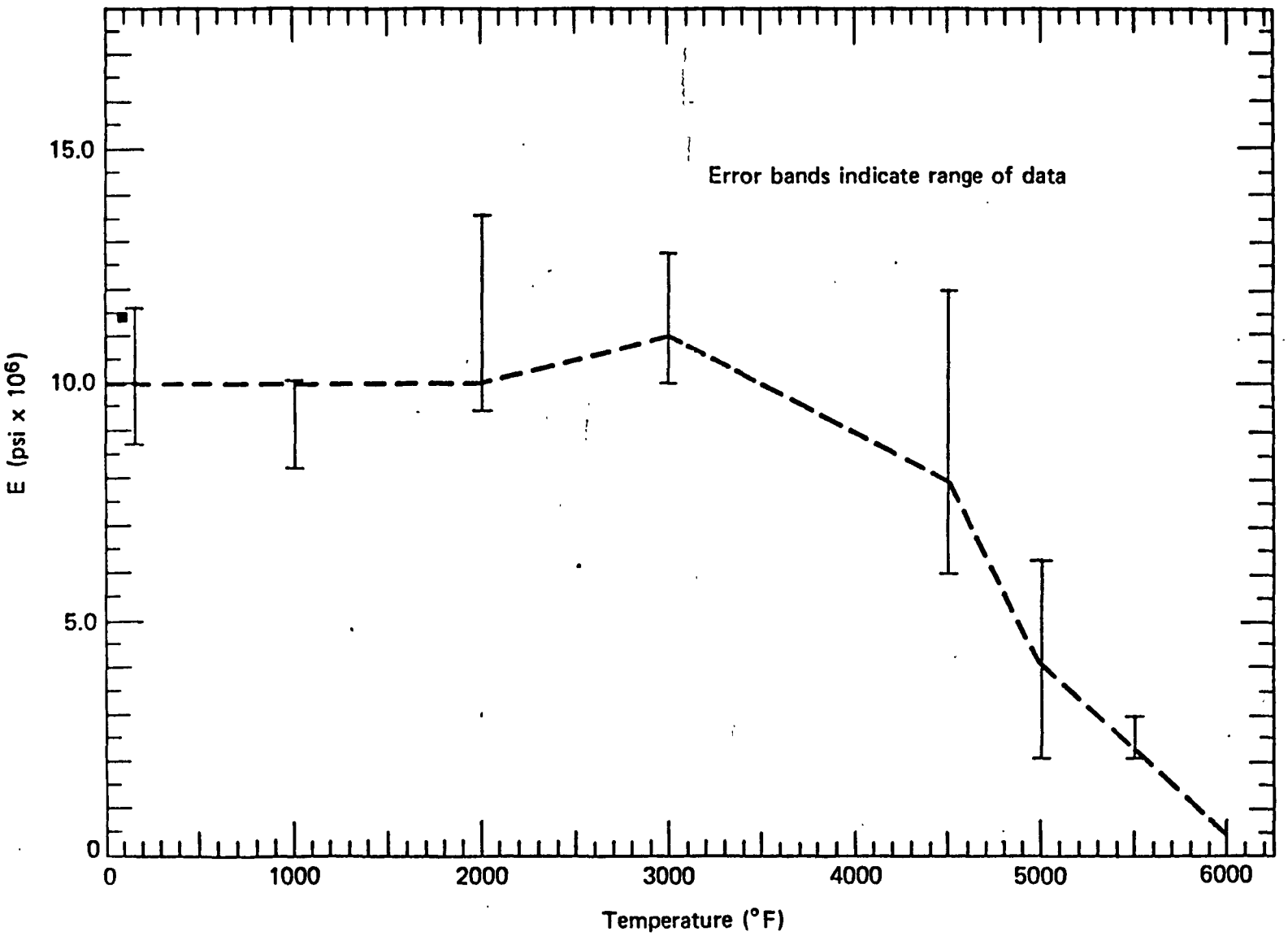

FIGURE B-18 COMPRESSIVE ELASTIC MODULUS VS. TEMPERATURE (Z) OF FWPF

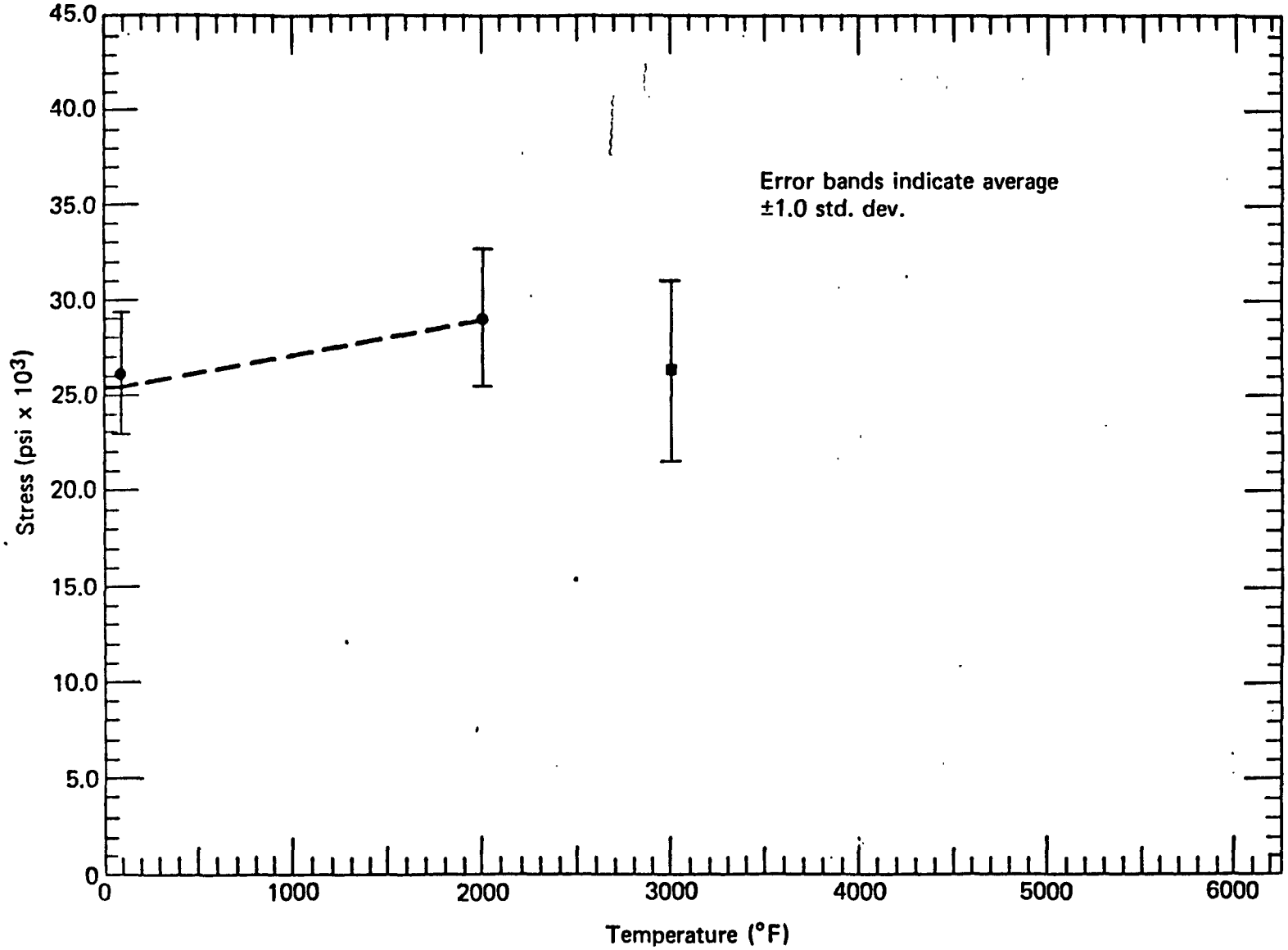

FIGURE B-19 TENSILE STRENGTH VS. TEMPERATURE (X) OF FWPF

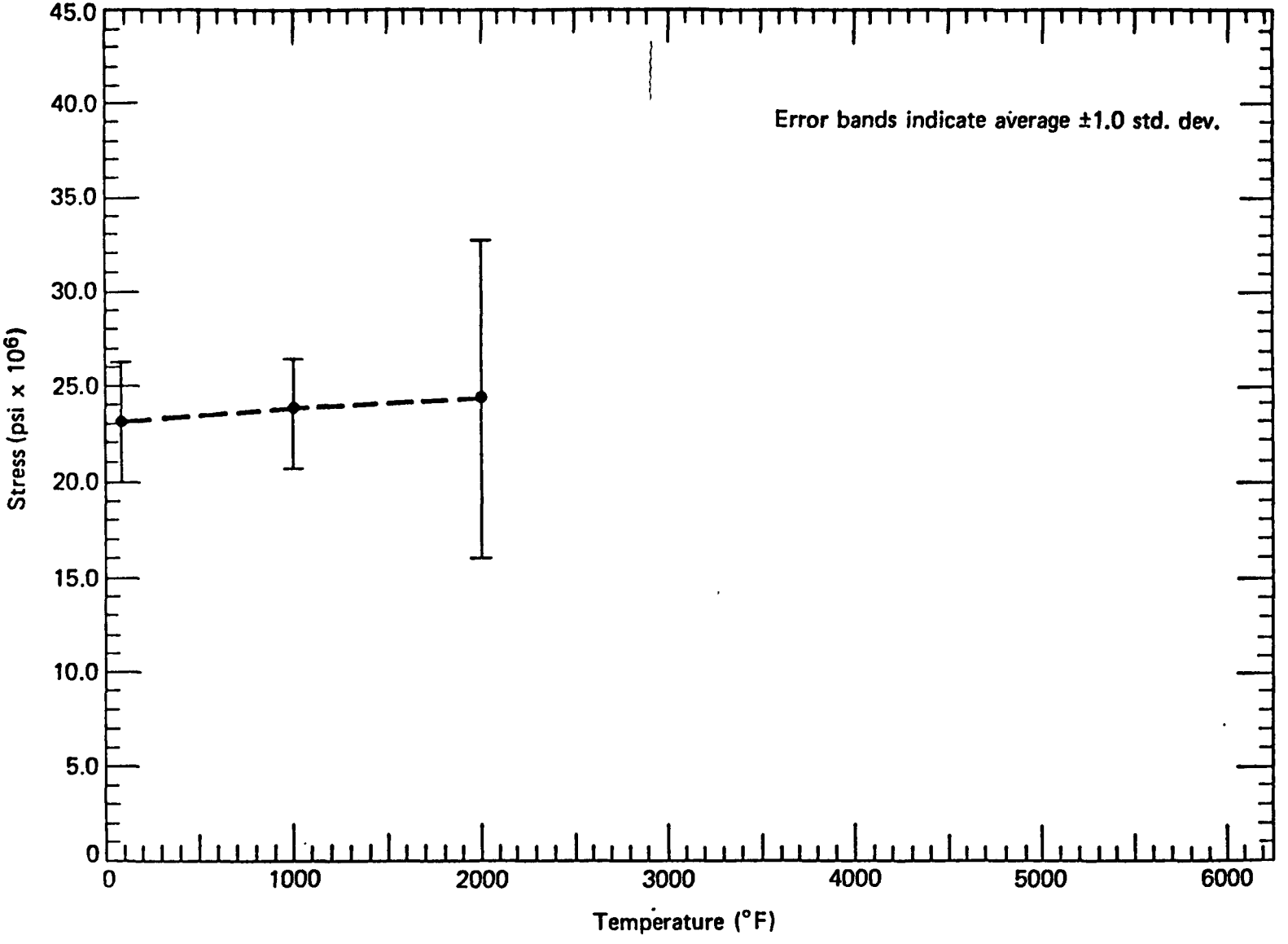

FIGURE B-20 TENSILE STRENGTH VS. TEMPERATURE (Z) OF FWPF

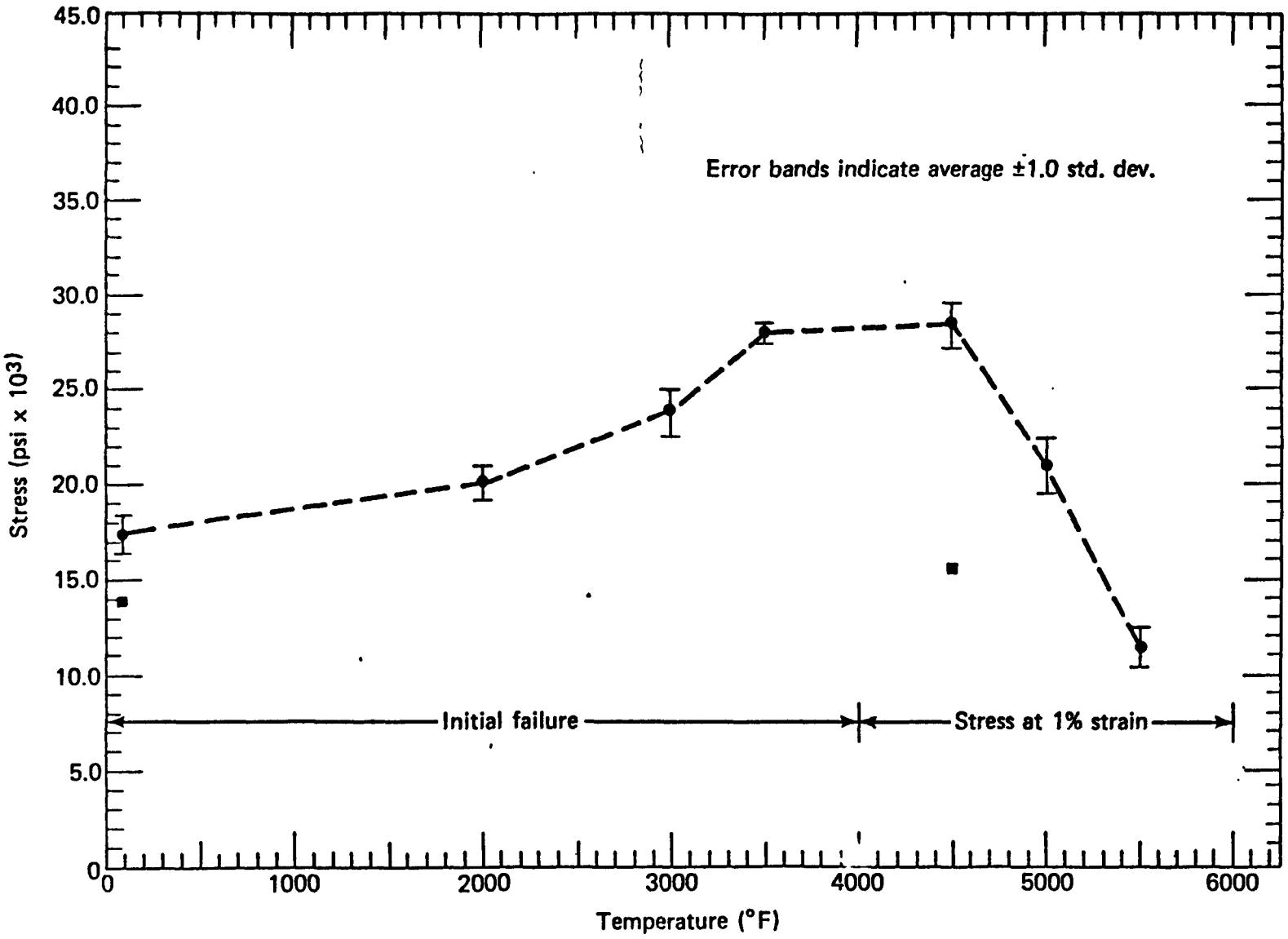

FIGURE B-21 COMPRESSIVE STRENGTH VS. TEMPERATURE (X) OF FWPF

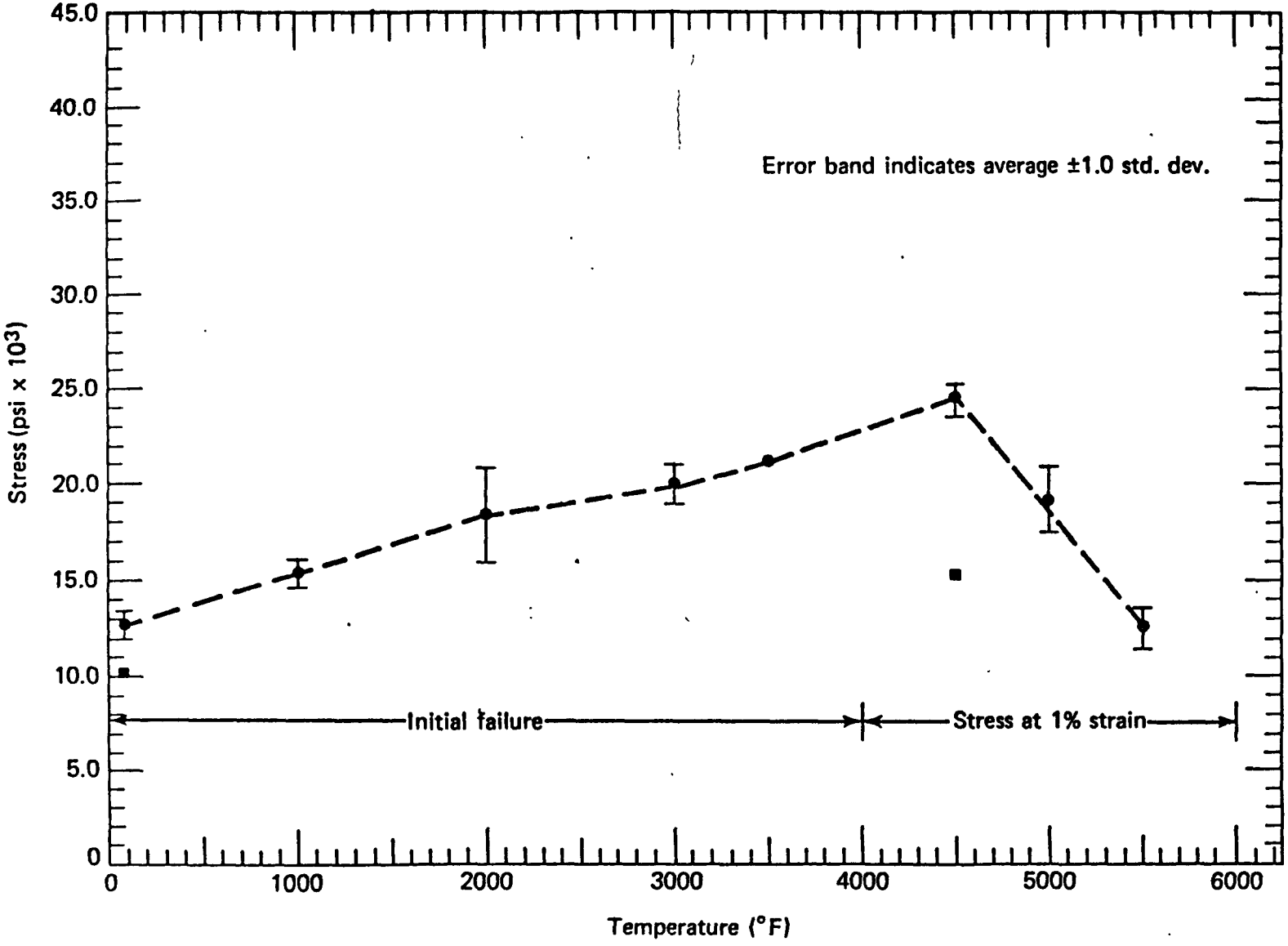

FIGURE B-22 COMPRESSIVE STRENGTH VS. TEMPERATURE (Z) OF FWPF.

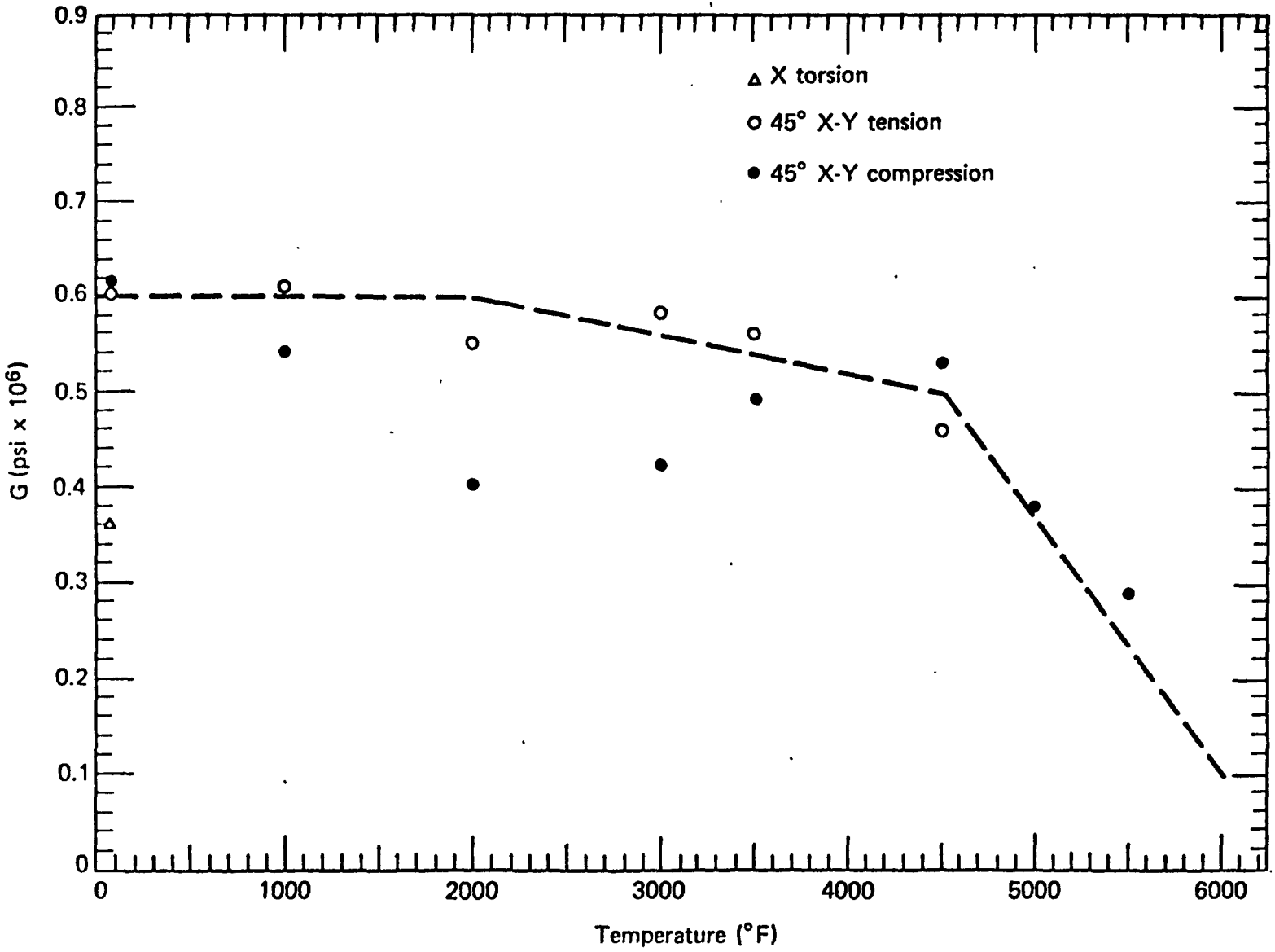

FIGURE B-23 SHEAR MODULUS VS. TEMPERATURE (XY) OF FWPF

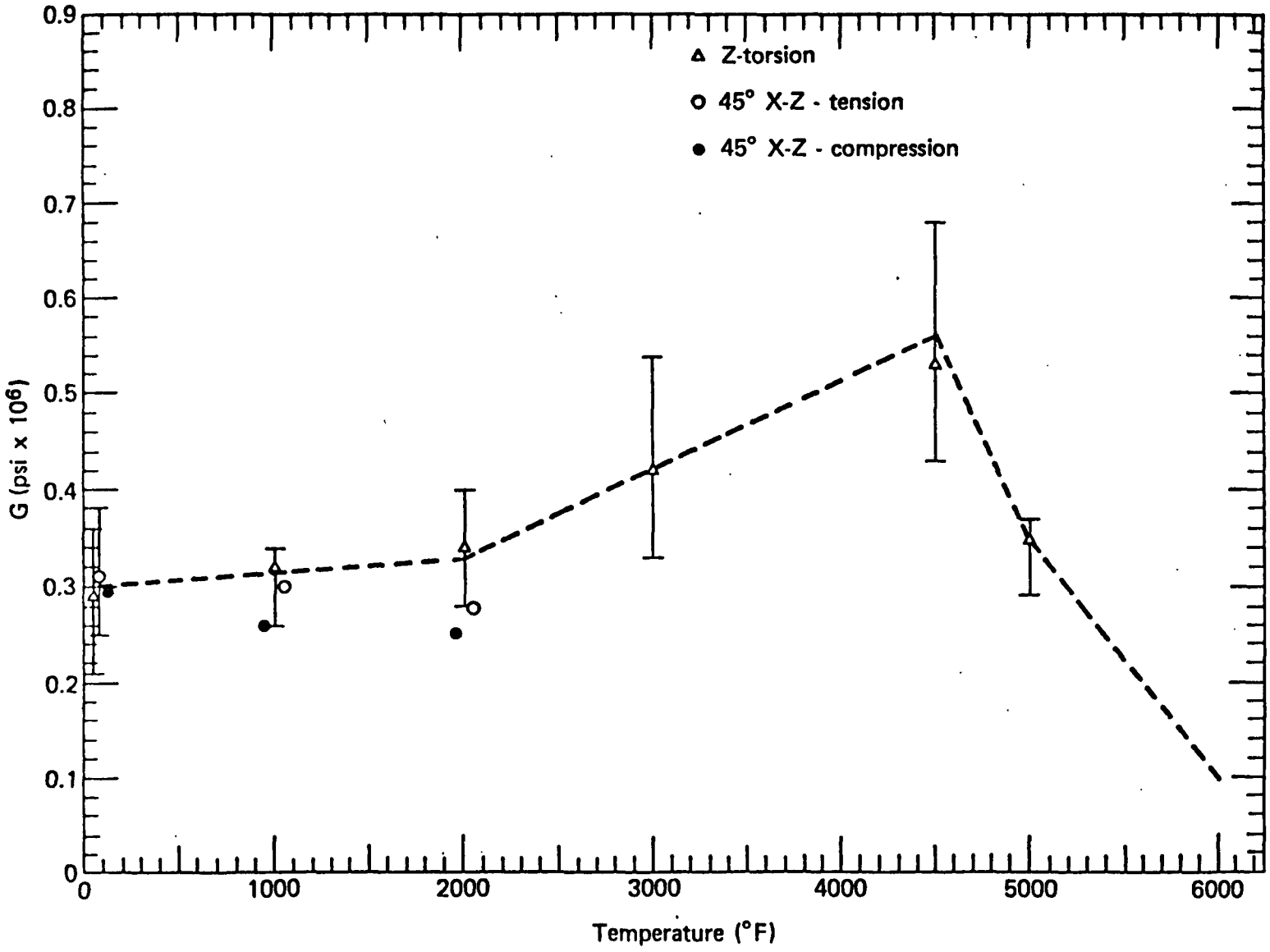

FIGURE B-24 SHEAR MODULUS VS. TEMPERATURE (X-Z) OF FWPF

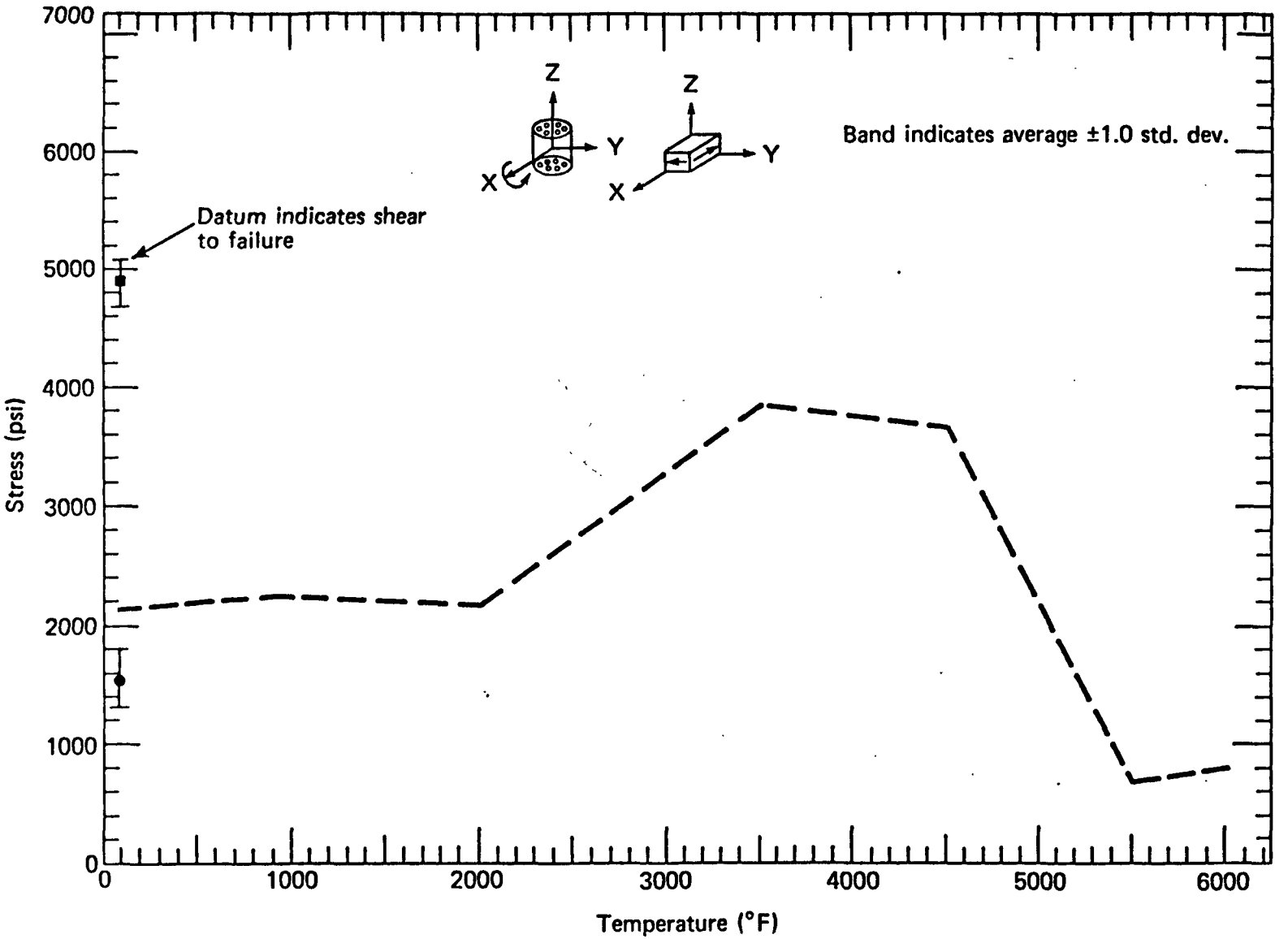

FIGURE B-25 0.2% OFFSET YIELD VS. TEMPERATURE XY SHEAR (SHEAR X FIBERS, FAILURE OCCURS IN YZ PLANE) OF FWPF

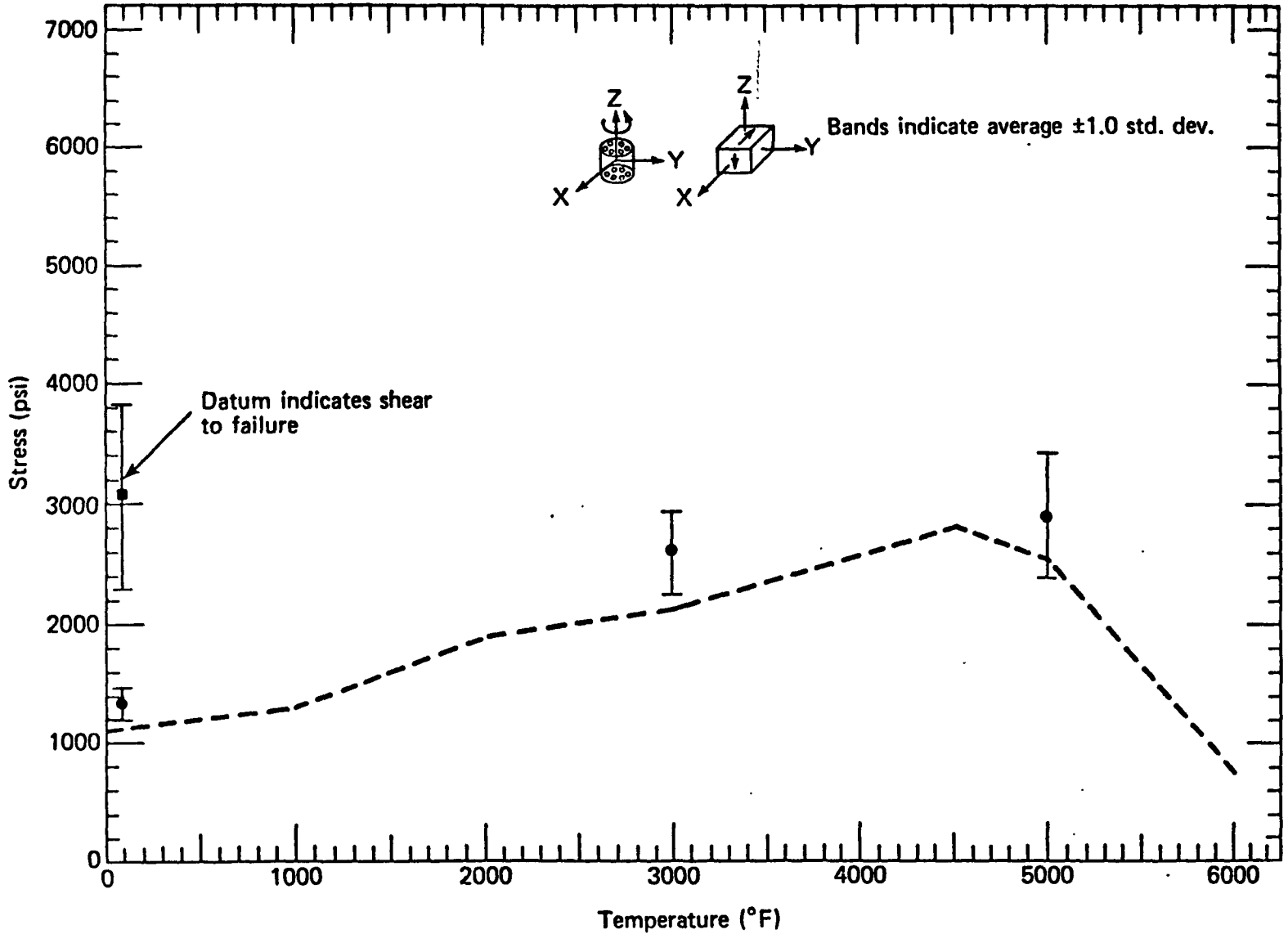

FIGURE B-26 0.2% OFFSET YIELD VS. TEMPERATURE XZ SHEAR
(SHEAR Z FIBERS, FAILURE OCCURS IN XY PLANE) OF FWPF

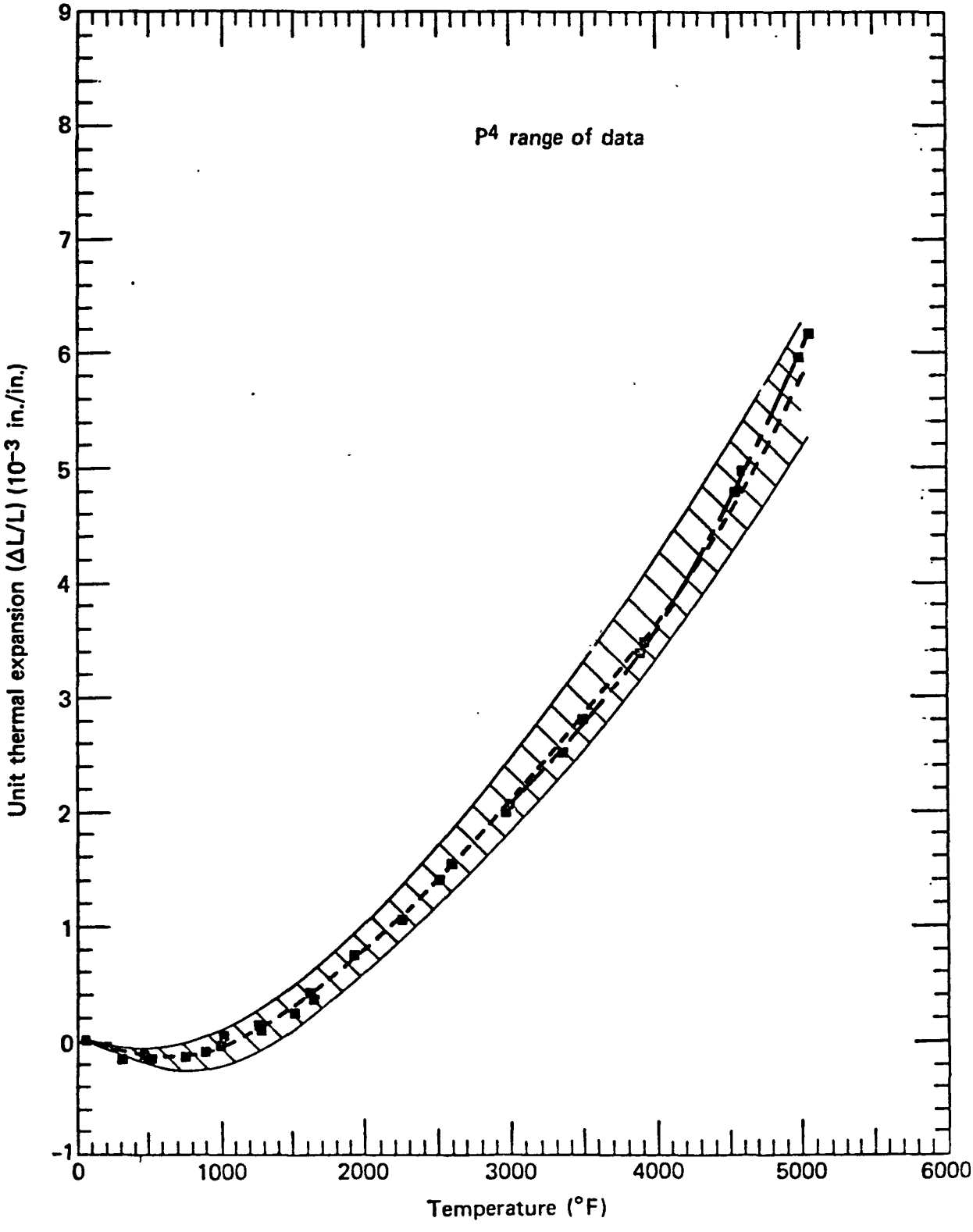

FIGURE B-27 UNIT THERMAL EXPANSION (ΔL/L) VS. TEMPERATURE (X) OF FWPF

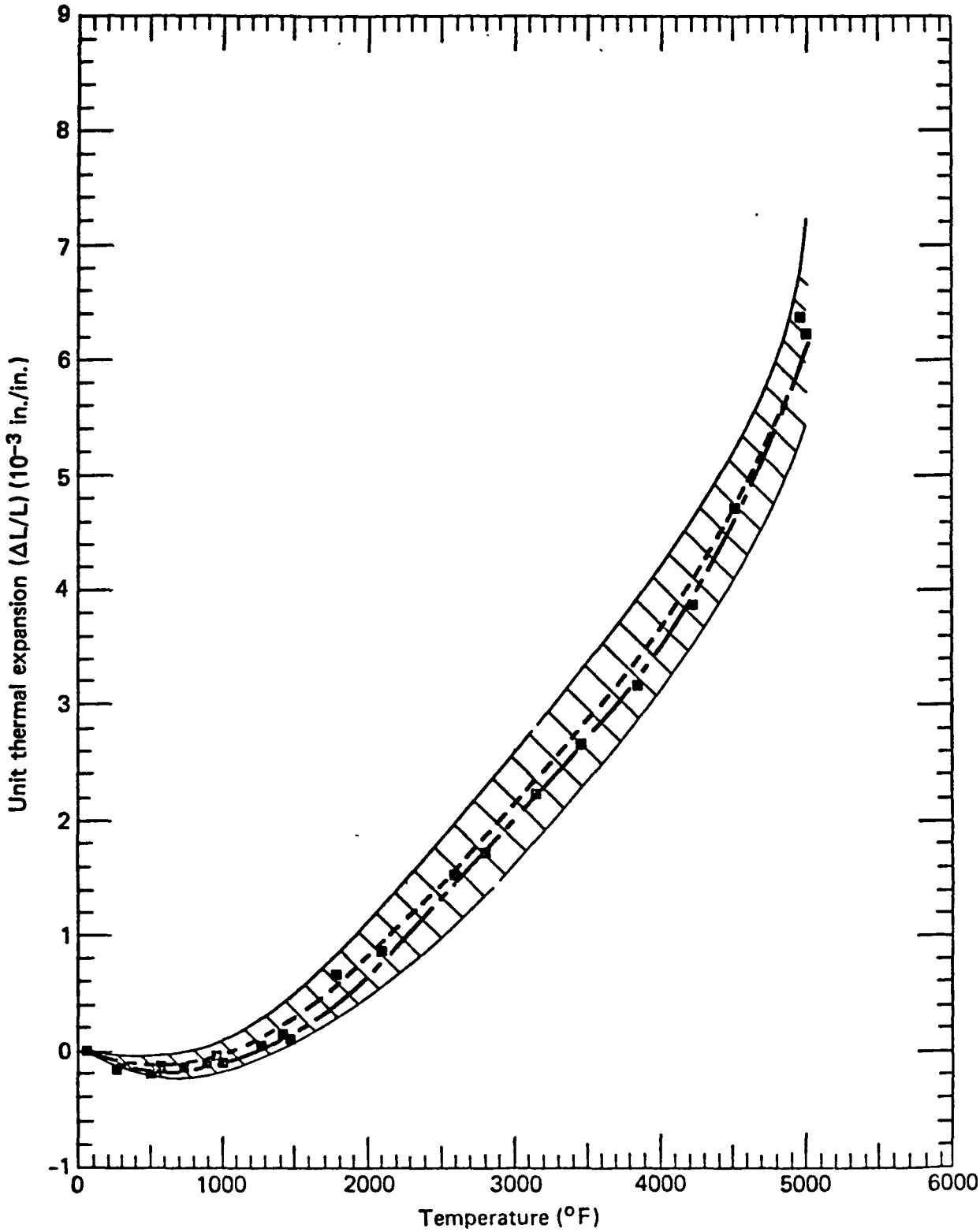

FIGURE B-28 UNIT THERMAL EXPANSION (ΔL/L) VS. TEMPERATURE (Z) OF FWPF

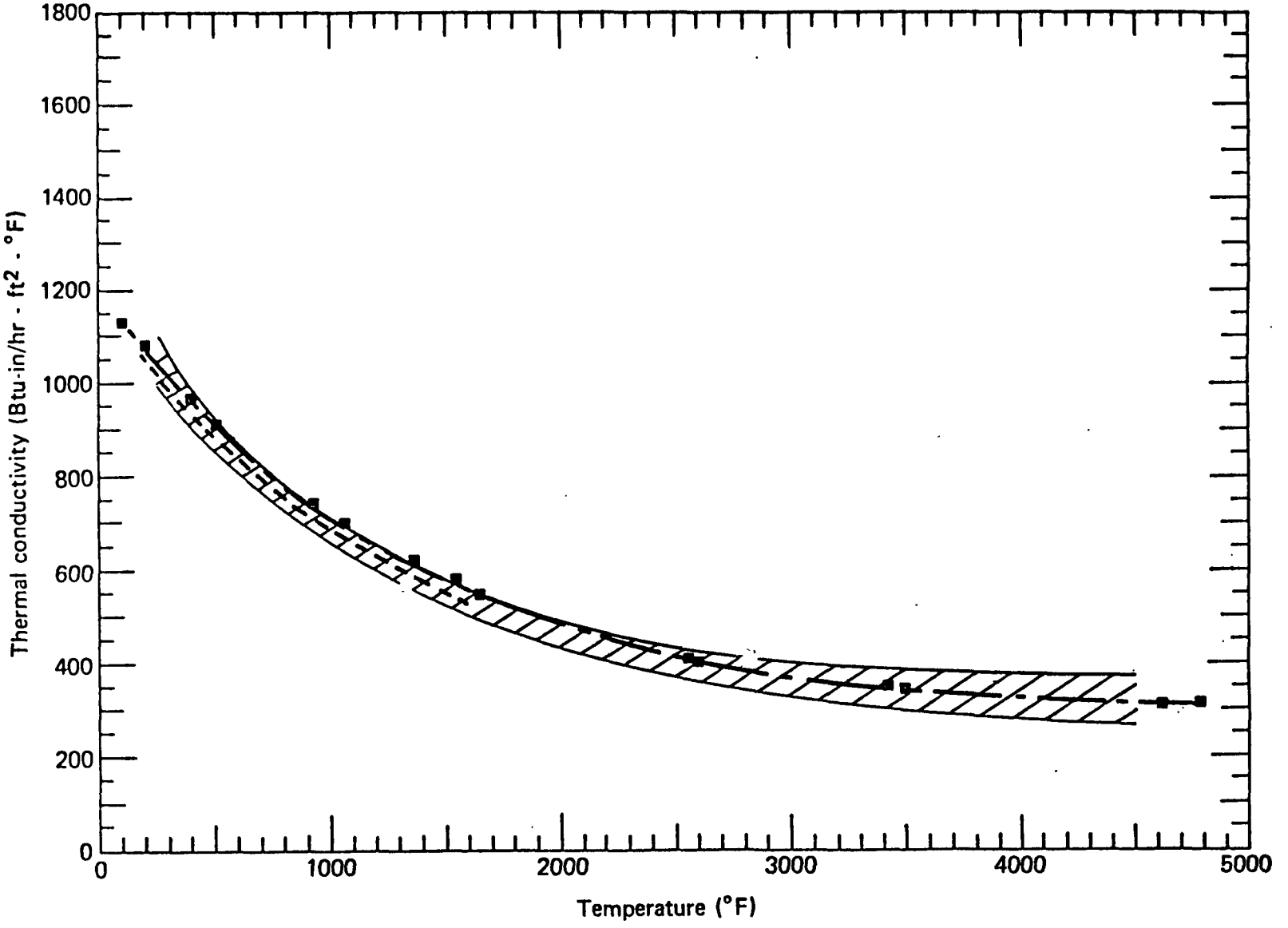

FIGURE B-29 THERMAL CONDUCTIVITY VS. TEMPERATURE (X) OF FWPF

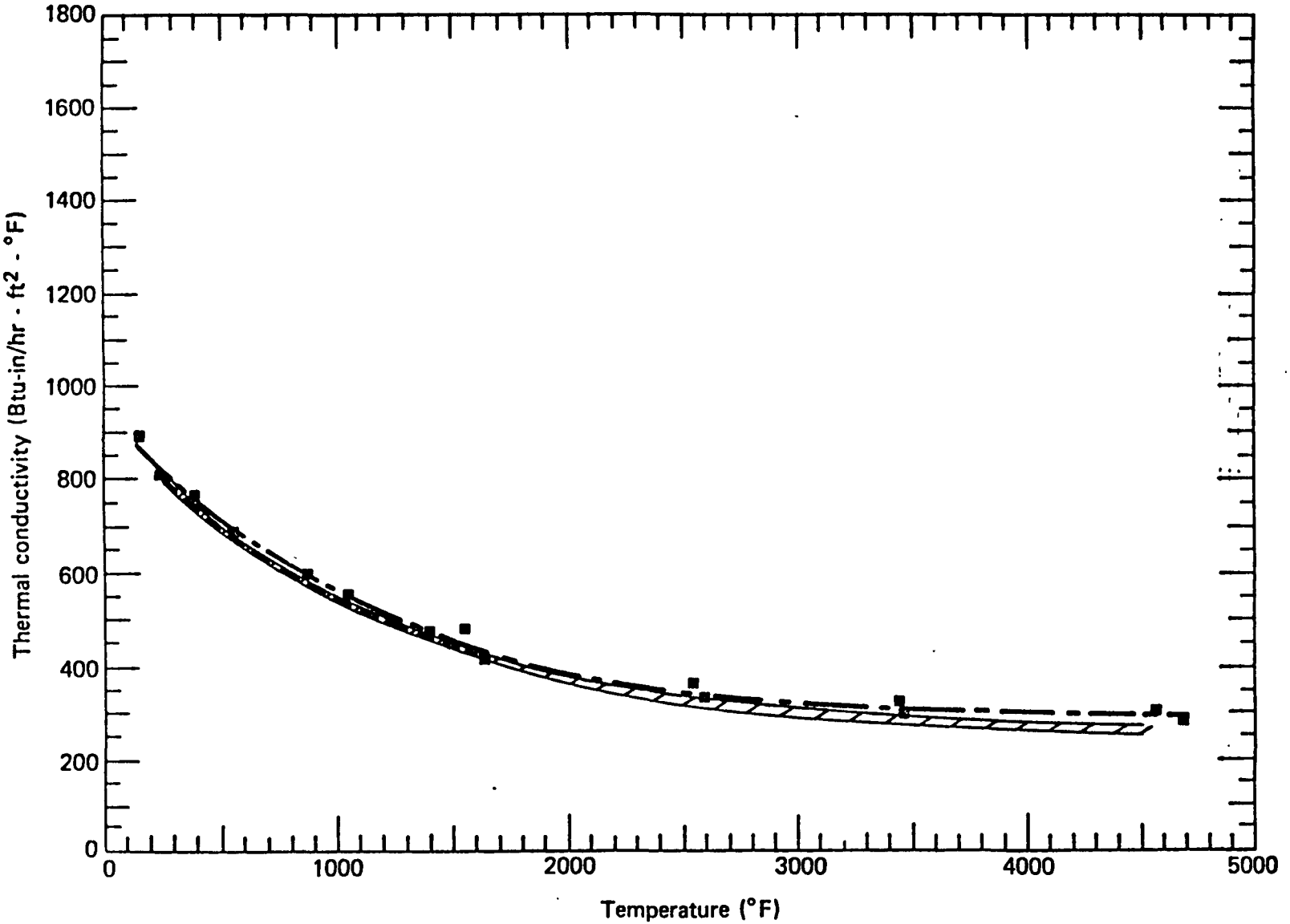

FIGURE B-30 THERMAL CONDUCTIVITY VS. TEMPERATURE (Z) OF FWPF

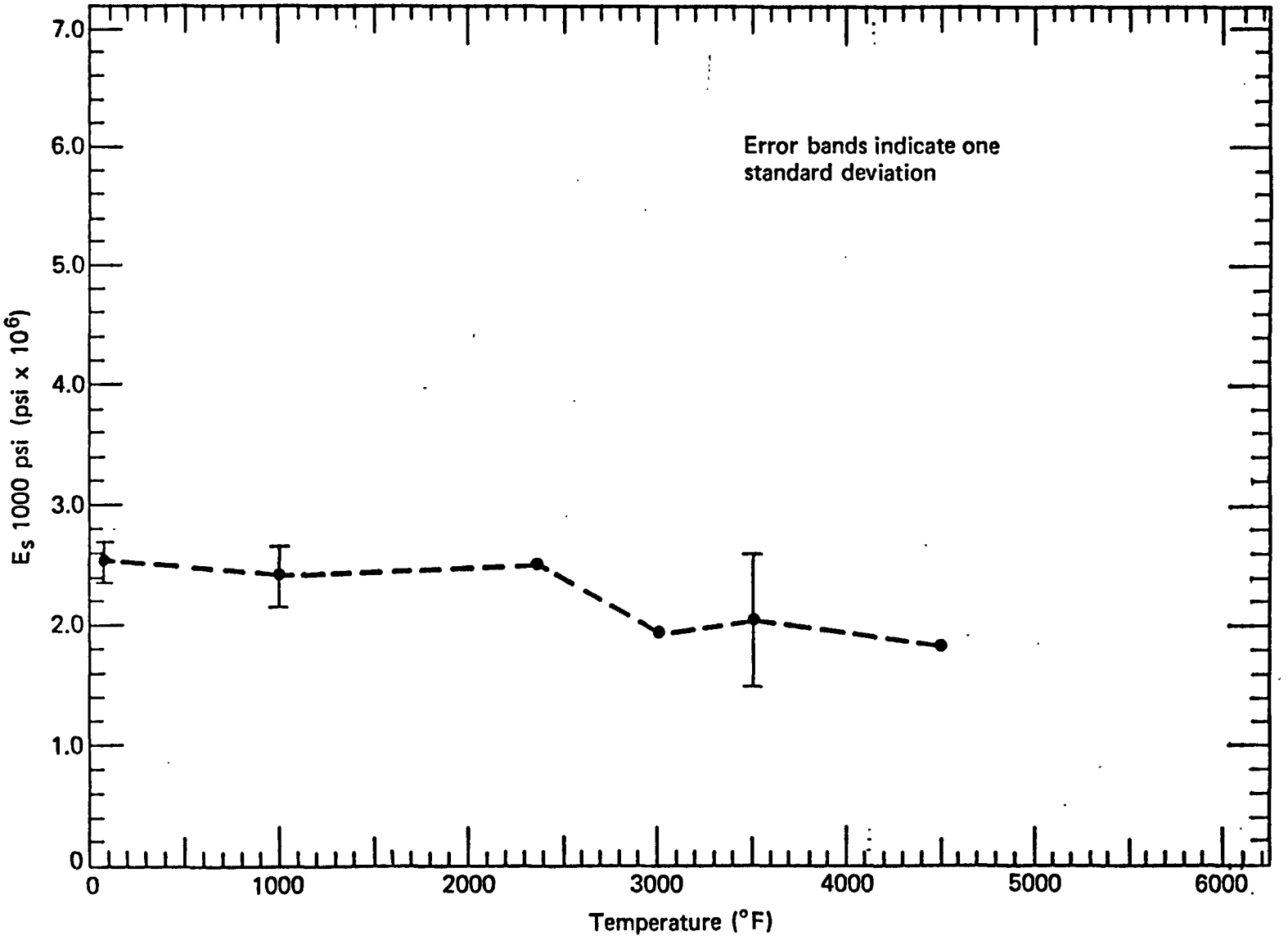

FIGURE B-31 1000 psi SECANT TENSILE ELASTIC MODULUS VS. TEMPERATURE (45 XY) OF FWPF

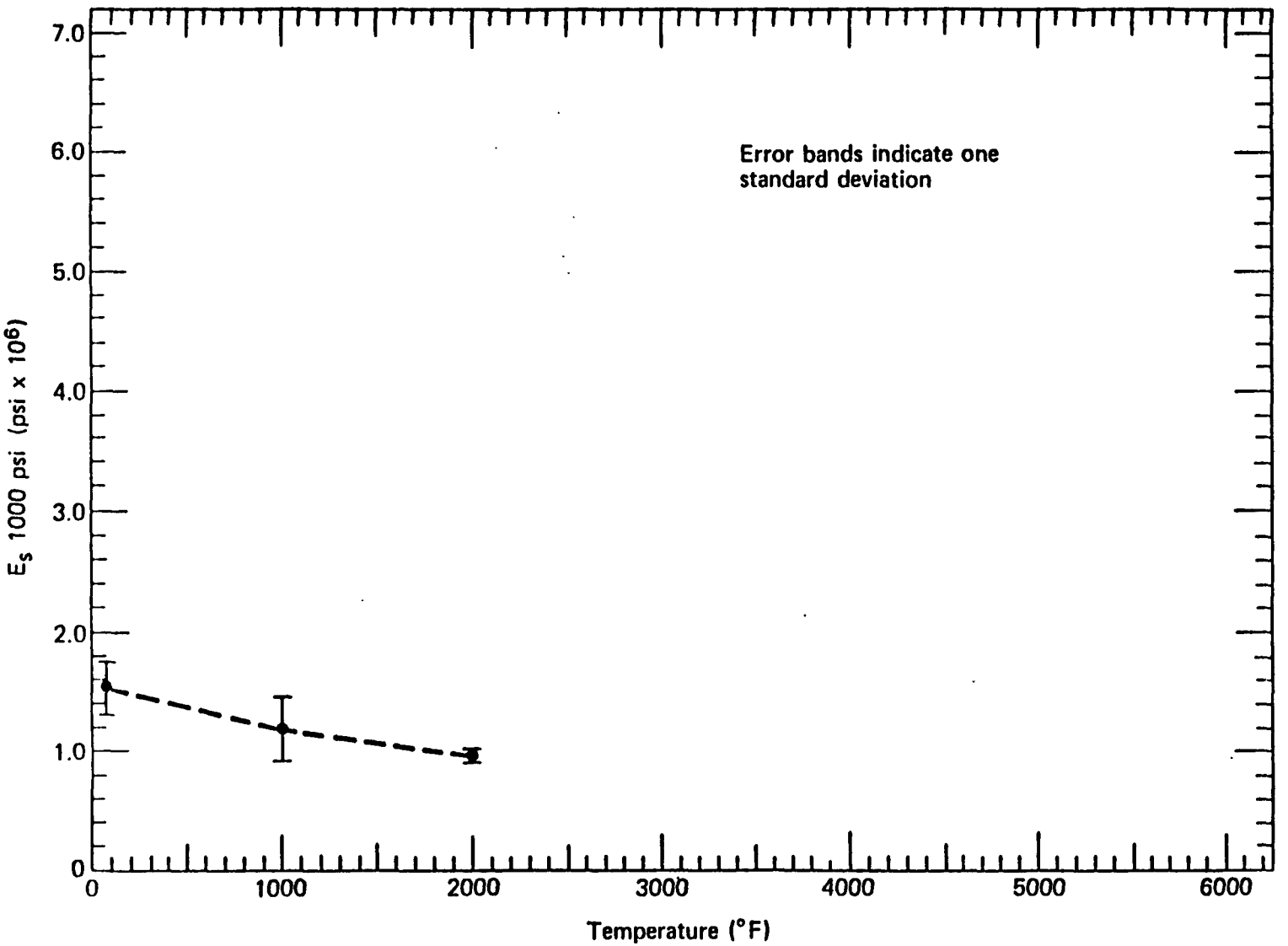

FIGURE B-32 1000 psi SECANT TENSILE ELASTIC MODULUS VS. TEMPERATURE (45 XZ) OF FWPF

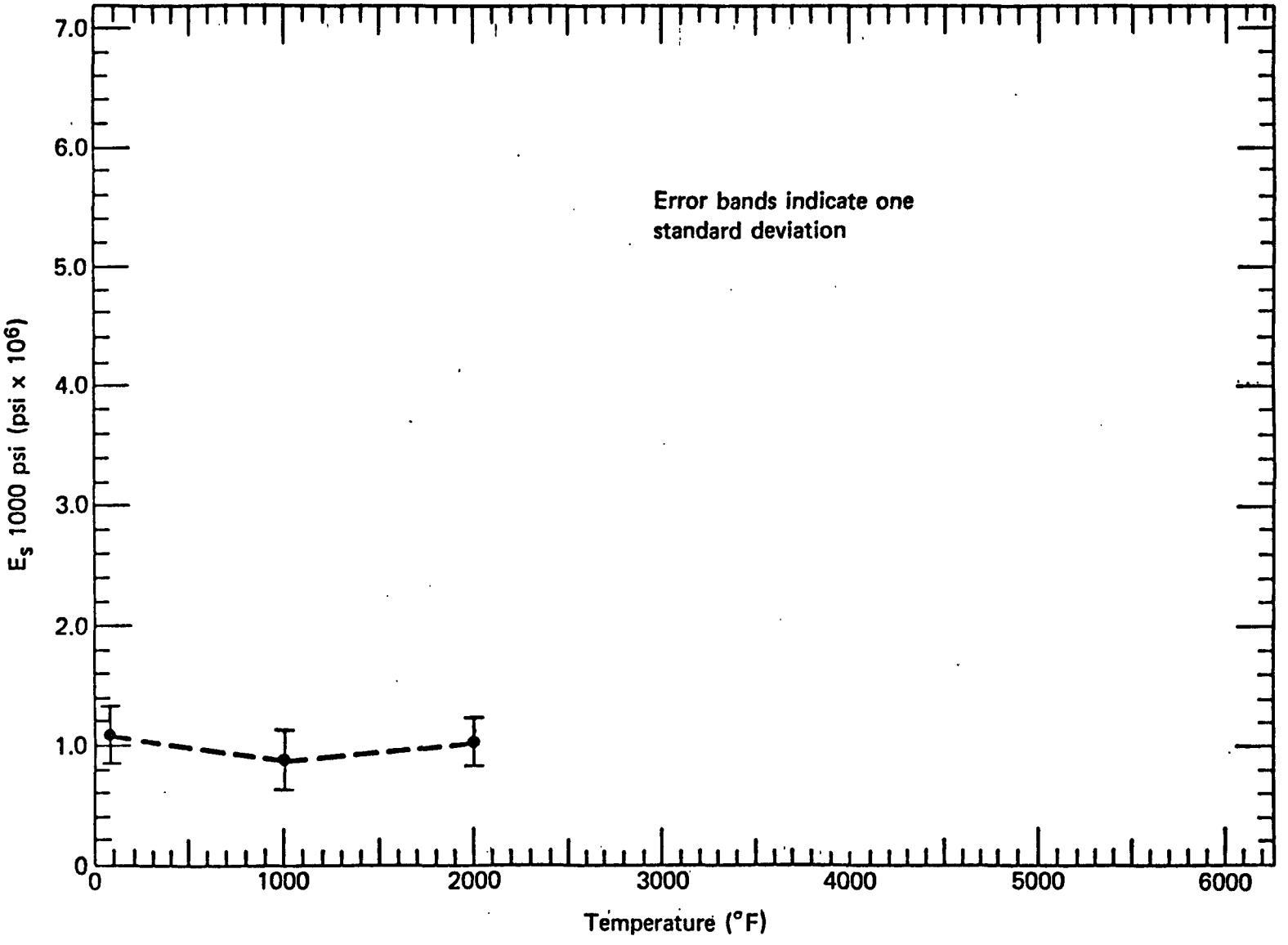

FIGURE B-33 1000 psi SECANT COMPRESSIVE MODULUS VS. TEMPERATURE (45 XY) OF FWPF

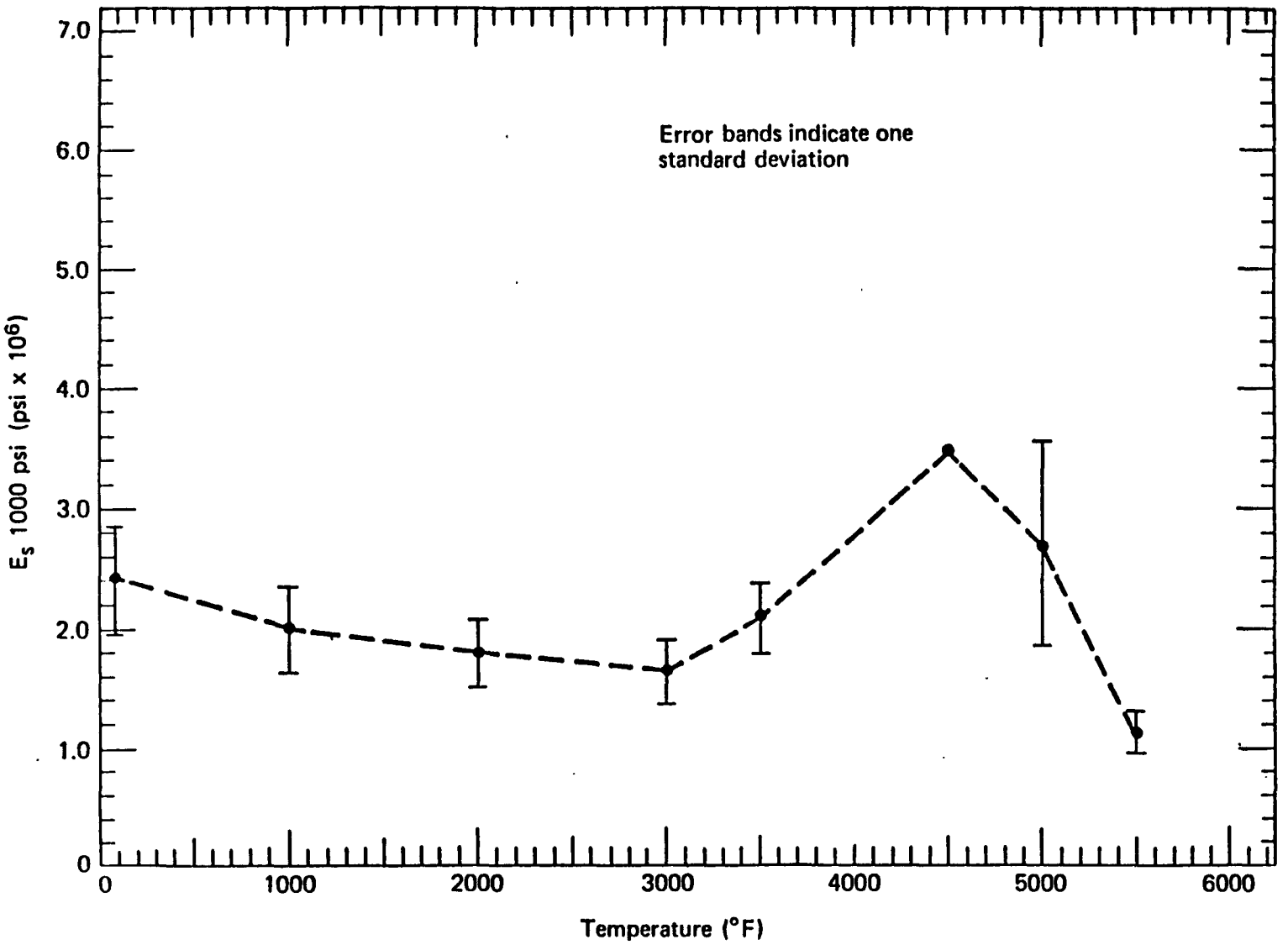

FIGURE B-34 1000 psi SECANT COMPRESSIVE MOLULUS VS. TEMPERATURE (45 XZ) OF FWPF

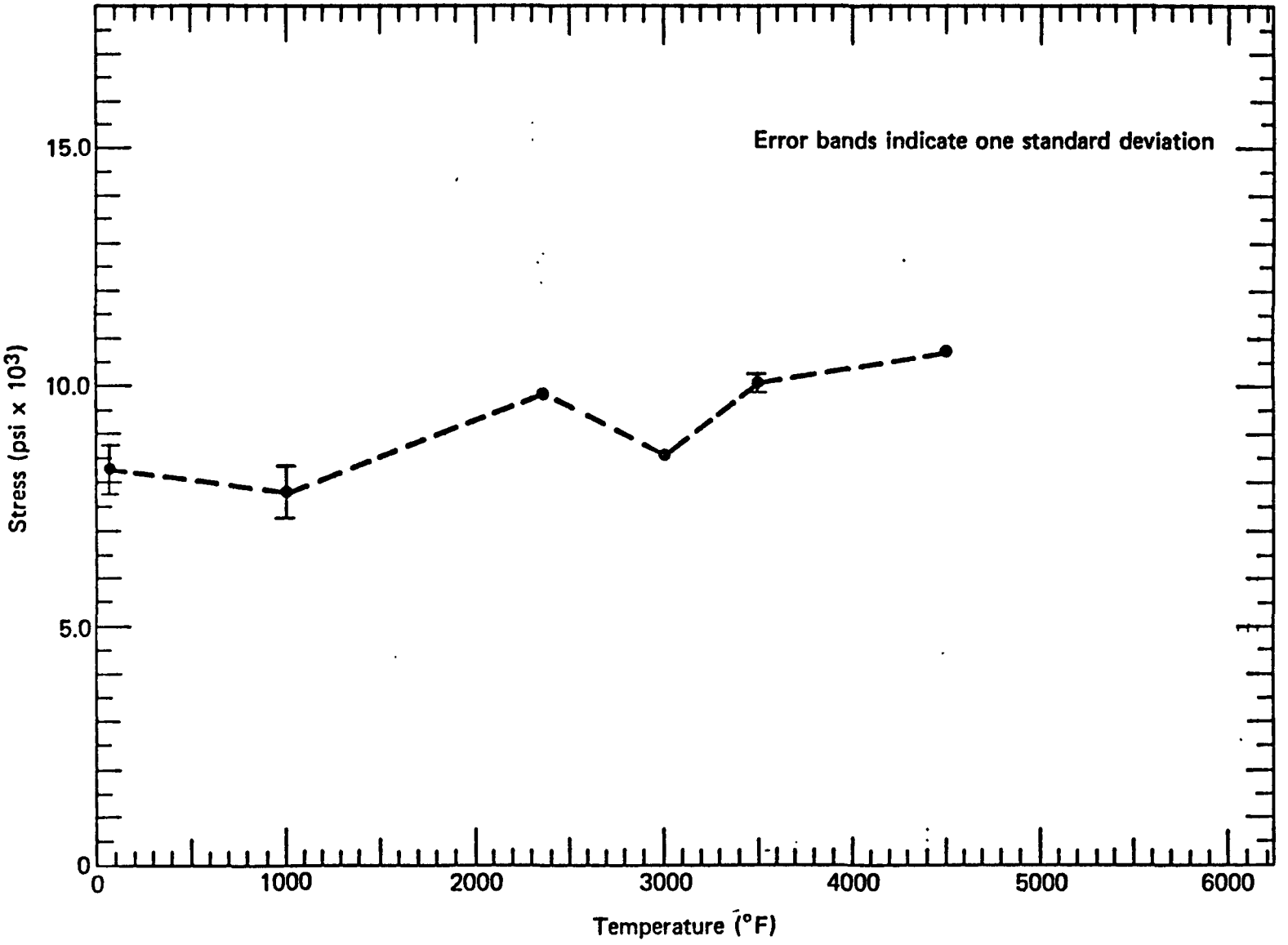

FIGURE B-35 TENSILE ULTIMATE STRENGTH VS. TEMPERATURE (45 XY) OF FWPF

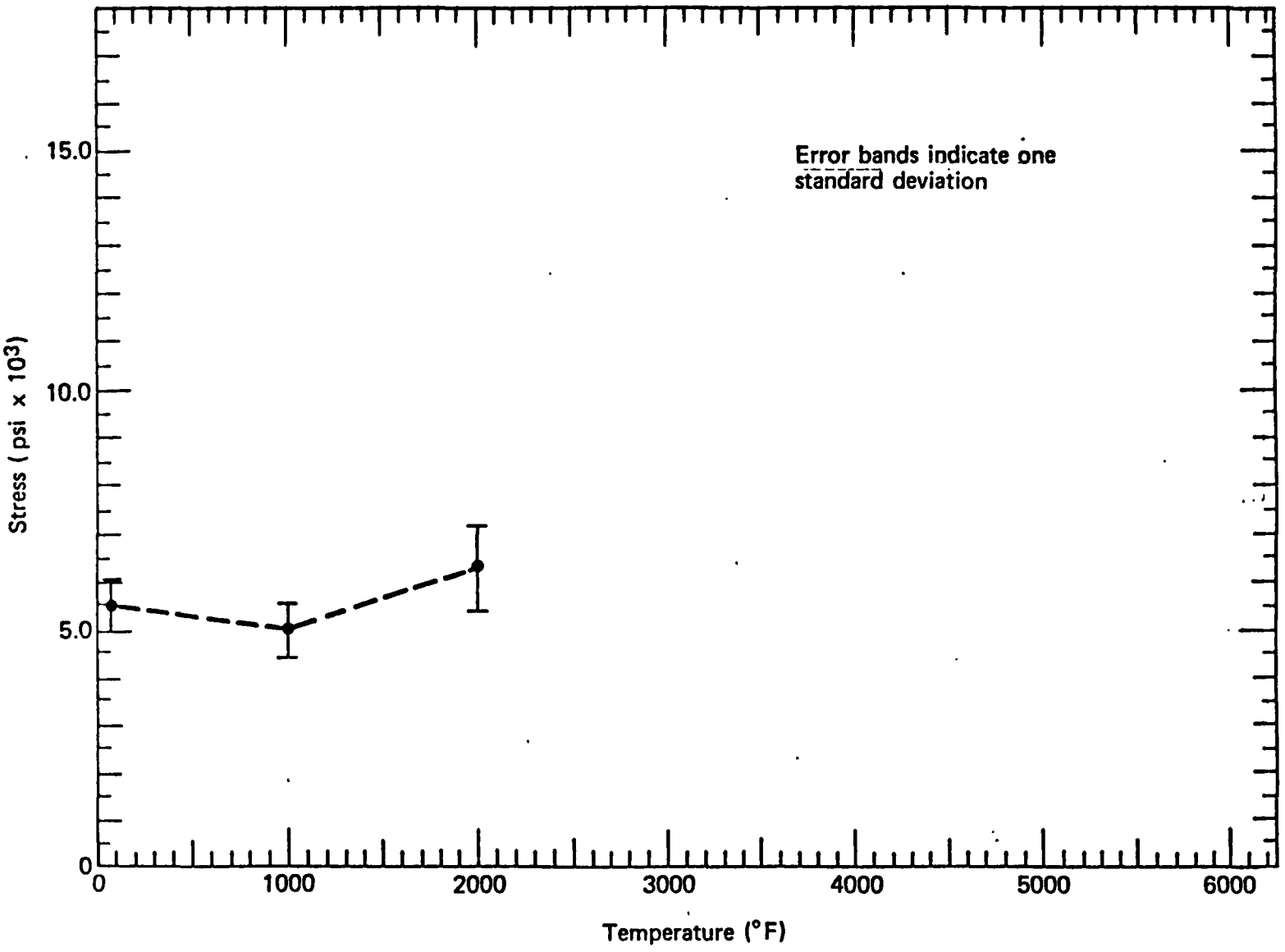

FIGURE B-36 TENSILE ULTIMATE STRENGTH VS. TEMPERATURE (45 XZ) OF FWPF

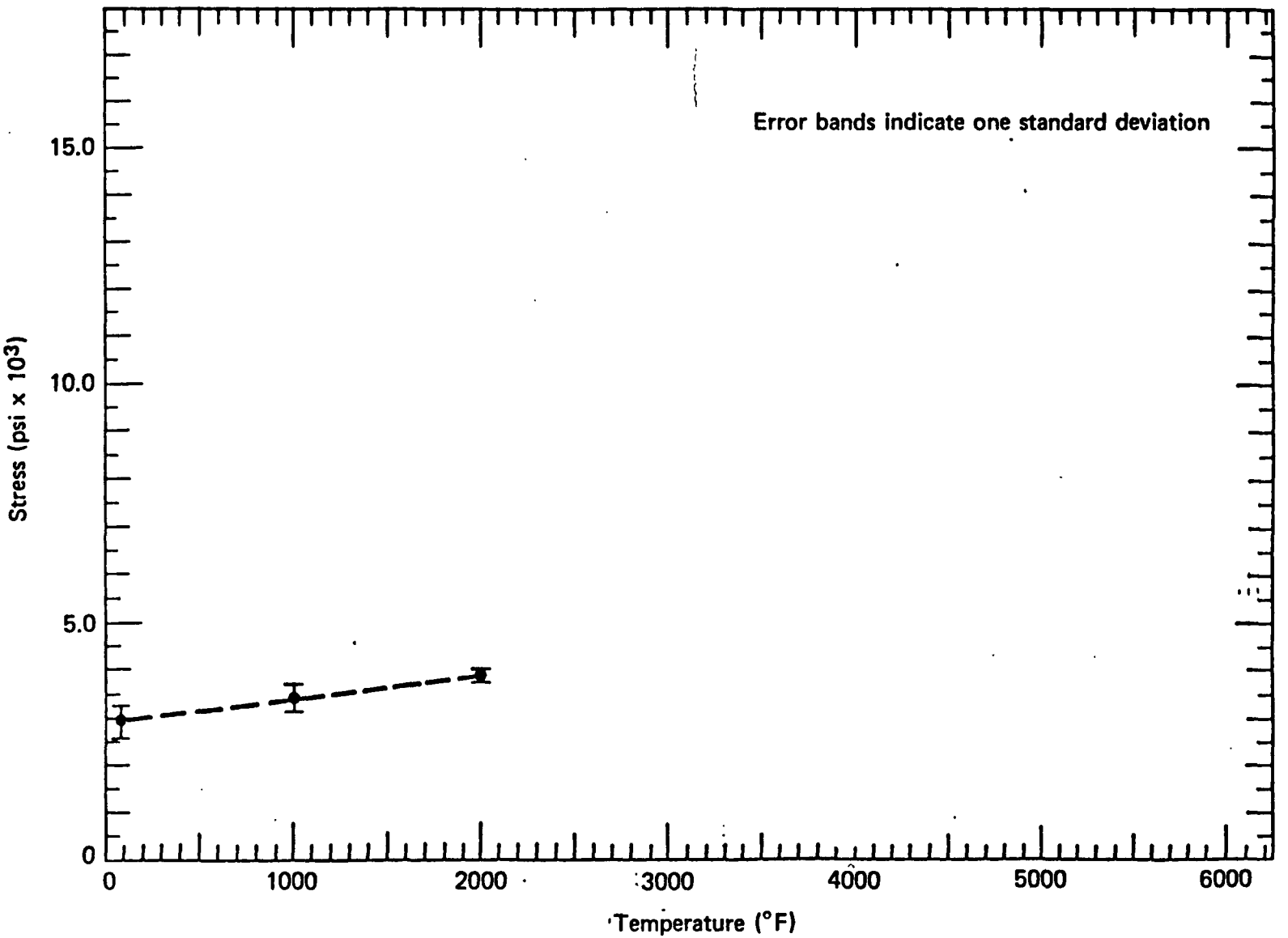

FIGURE B-37 COMPRESSIVE STRENGTH AT 1% STRAIN VS. TEMPERATURE (45 XY) OF FWPF

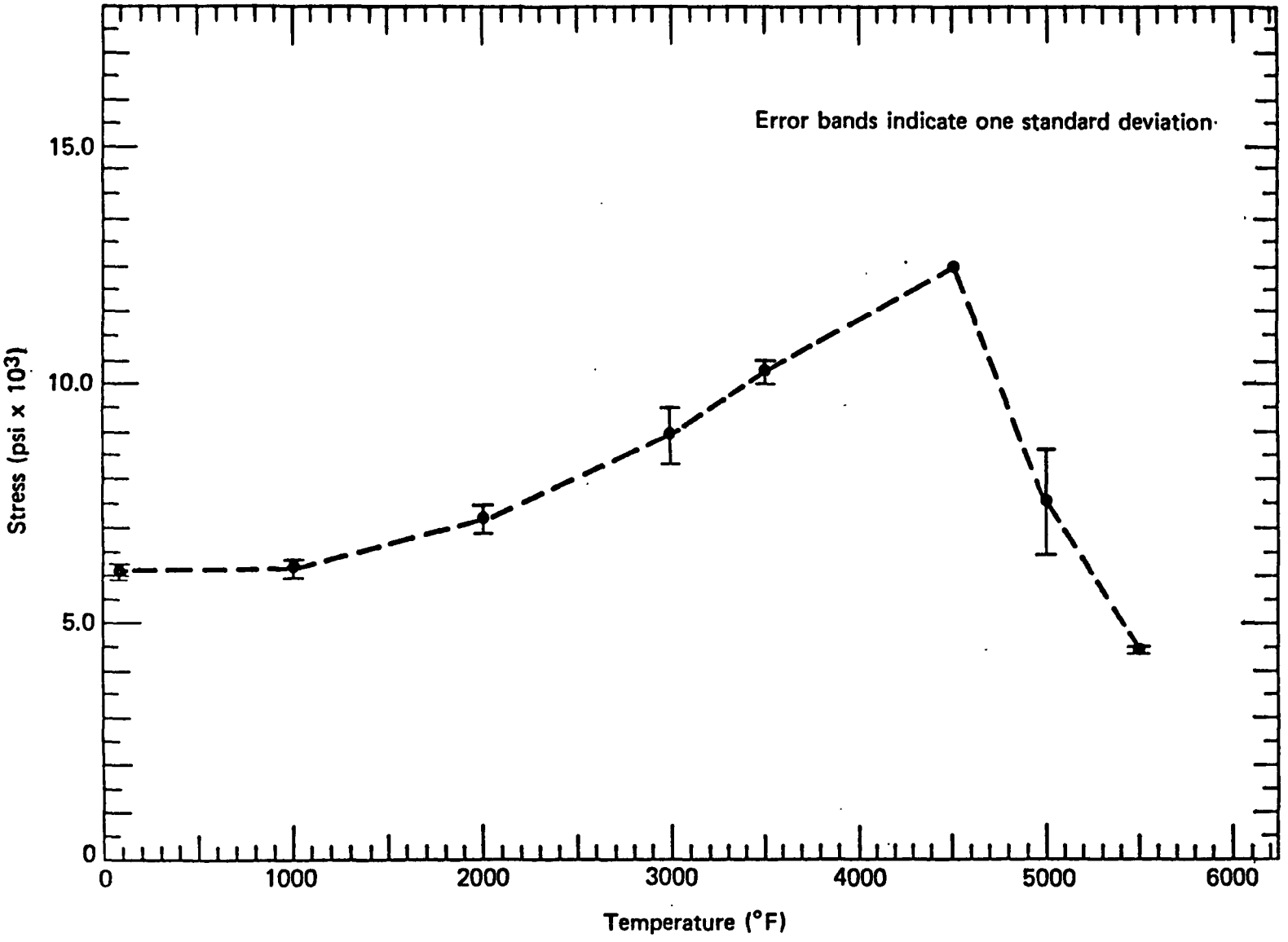

FIGURE B-38 COMPRESSIVE STRENGTH AT 1 % STRAIN VS. TEMPERATURE (45 XZ) OF FWPF

B.6 MULTIFOIL INSULATION

The total weight per unit area of the 0.70 inch thick insulation is 1.034 grams/square centimeter (0.0147 pounds/square inch), and the effective conductivity has been established by measurement as 2.39 x 10^{-5} cal/sec-cm-^{o}C (0.00578 Btu/hr-ft-^{o}F).

B.7 MISCELLANEOUS MATERIALS

The materials listed below are standard alloys having well defined properties and characteristics which may be found in the applicable standard of specification.

Material	Reference Specification
Titanium S-2-4-2	AMS 4976
Titanium 6 Al-4V	MIL-T-9047
Inconel X-750	AMS-5668
SST Type 304	QQS-763
SST Type A286	AMS-5735

B.8 REFERENCES

B-1 Letter from A.C. Schaffhauser (ORNL) to GPHS Task Force, "Update on Iridium Grain Growth and Impact Data", dated September 5, 1979.

B-2 Donnelly, R.G., Editor "Isotope Power Materials Development Progress Report." Monthly Reports for March 1973 through June, 1975. Oak Ridge National Laboratory. (ORNL-TM series).

B-3 Halvorson, J.J., and Wimber, R.T. "Thermal Expansion of Iridium at High Temperatures." Journal of Applied Physics, Vol. 43, No. 6, June, 1972.

B-4 Singh, H.P. "Determination of Thermal Expansion of Germanium, Rhodium, and Iridium by X-rays." Acta Cryst. , A24, 469, 1968.

B-5 Letter from R.L. Heestand (ORNL) to R.F. Hartman (GE), dated January 28, 1980.

B-6 Taylor, R.E., Groot, H., and Shoemaker, R.L. "Thermophysical Properties of Carbon Insulation", TPRL-196, December, 1979.

B-7 "Preliminary Design Review - International Solar Polar Mission Radioisotope Thermoelectric Generator", GE/SD, November, 1979.

B-8 Taylor, R.E., and Groot, H. "Thermophysical Properties of Carbon Insulation", TPRL-196A, December, 1979.

B-9 Letter to Dr. Gary L. Bennett, DOE, from James C. Hagan, Applied Physics Laboratory/Johns Hopkins University, Subject: Transmittal of Summary of Thermal and Mechanical Property Information of Fineweave Pierced Fabric, ANSP-L-550, July 21, 1980.

BLANK